U.PORTO

DOUTORAMENTO

BIOTECNOLOGIA MOLECULAR E CELULAR APLICADA ÀS CIÊNCIAS DA SAÚDE

# Engineered platforms with site-specific immobilized laminin for neural applications

Daniela Filipa dos Santos Barros

**D**

**2019**

U.PORTO

**Daniela Filipa dos Santos Barros.** Engineered platforms with site-specific immobilized laminin for neural applications

**D**.ICBAS **2019**

**Engineered platforms with site-specific immobilized laminin for neural applications**

Daniela Filipa dos Santos Barros

SEDE ADMINISTRATIVA **INSTITUTO DE CIÊNCIAS BIOMÉDICAS ABEL SALAZAR**
**FACULDADE DE FARMÁCIA**

Daniela Filipa dos Santos Barros

# Engineered platforms with site-specific immobilized laminin for neural applications

Tese de Candidatura ao grau de Doutor em Biotecnologia Molecular e Celular Aplicada às Ciências da Saúde;

Programa Doutoral da Universidade do Porto (Instituto de Ciências Biomédicas de Abel Salazar e Faculdade de Farmácia)

Orientadora – Professora Doutora Ana Paula Gomes Moreira Pêgo
Categoria – Investigadora Principal, Professora Associada Convidada
Afiliação – Instituto de Investigação e Inovação em Saúde (i3S), Universidade do Porto (UP); Instituto Nacional de Engenharia Biomédica (INEB), UP; Faculdade de Engenharia (FEUP), UP; Instituto de Ciências Biomédicas Abel Salazar (ICBAS), UP.

Co-orientadora – Doutora Isabel Maria Santana Ramos de Freitas Amaral
Categoria – Investigadora Auxiliar
Afiliação – Instituto de Investigação e Inovação em Saúde, Universidade do Porto (i3S, UP); Instituto Nacional de Engenharia Biomédica (INEB), UP; Faculdade de Engenharia (FEUP), UP.

The work presented in this thesis was developed at:

nBTT - nanoBiomaterials for Targeted Therapies Group
i3S – Instituto de Investigação e Inovação em Saúde
INEB – Instituto Nacional de Engenharia Biomédica
Universidade do Porto, Portugal



García Lab
Parker H. Petit Institute for Bioengineering and Bioscience
George W. Woodruff School of Mechanical Engineering
Georgia Institute of Technology, Atlanta, GA, USA

The work presented in this thesis was funded by projects NORTE-01-0145-FEDER-000008 and NORTE-01-0145-FEDER-000012, supported by Norte Portugal Regional Operational Programme (NORTE 2020), under the PORTUGAL 2020 Partnership Agreement, through the European Regional Development Fund (ERDF) and FEDER - Fundo Europeu de Desenvolvimento Regional funds through the COMPETE 2020 - Operacional Programme for Competitiveness and Internationalisation (POCI), Portugal 2020; by Portuguese funds through FCT/MCTES in the framework of the project "Institute for Research and Innovation in Health Sciences" (POCI-01-0145-FEDER-007274) and Santa Casa da Misericórdia de Lisboa through project COMBINE (Prémio Neurociências Melo e Castro-MC-1068-2015).
D. Barros was supported by FCT PhD Programs (PD/BD/105953/2014) and Programa Operacional Potencial Humano (POCH), in the scope of the BiotechHealth Program (Doctoral Program on Cellular and Molecular Biotechnology Applied to Health Sciences), Programa FLAD Healthcare 2020 and the project PARES (Prémio Albino Aroso).

***Remember what they say***
***There's no shortcut to a dream***
***It's all about blood and sweat***
***And life is what you manage in-between***

October, Broken Bells

# ACKNOWLEDGMENTS

E 5 anos depois, eis que esta longa e desafiante jornada está prestes a terminar! O doutoramento foi sem dúvida uma etapa durante a qual vivi algumas das melhores e também piores experiências da minha vida, e que me fez crescer não só cientificamente, mas também a nível pessoal. Felizmente não fiz este caminho sozinha, tive pessoas espetaculares a apoiar-me e a fazer-me querer ir sempre um bocadinho mais além, e é a todas elas que quero agradecer e também dedicar esta tese.

Às minhas orientadoras Ana Paula e Isabel, obrigada por me terem recebido e me terem dado a oportunidade de explorar uma área que estava totalmente fora da minha zona de conforto...aprendi imenso nestes últimos anos. Uma das coisas mais importantes que aprendi foi que muitas vezes (ou quase sempre) temos de desligar o "descomplicómetro" e olhar para aquilo que vemos como perdido/mau de forma mais positiva. Obrigada pelo vosso entusiasmo, apoio e pelas palavras de incentivo. A vossa orientação e apoio foi fundamental para o meu crescimento científico nestes últimos anos.

To Andrés, thank you for the opportunity to work in your laboratory and for being such an enthusiastic and positive mentor. I had a really great time in your lab. Thank you also, to all the members from García Lab who welcomed me so well, and specially to Woojin and Ricardo, my coffee buddies, for the friendship and support, making my journey at GeorgiaTech, a really happy journey.

Ao Professor Mário Barbosa, pela oportunidade de frequentar o BiotechHealth e pelo esforço em tornar este, um programa doutoral de excelência. À Helena Martins, Catarina Pereira, Daniel Vasconcelos e João Cortez por estarem sempre disponíveis para ajudar e tornar a nossa vida um bocadinho mais fácil. Aos meus colegas do BiotechHealth que fizeram este caminho comigo, foi muito bom contar com o vosso apoio e companheirismo.

À Paula Parreira e Cristina Martins, pela ajuda e apoio numa fase crucial desta tese. Obrigada pela vossa persistência e pelas palavras de incentivo...a vossa ajuda foi fundamental para o meu trabalho.

A todas as pessoas dos serviços do i3S, Frederico, Fátima, Maria, Dalila, Ricardo, Eduardo, Tânia, Paula, Hugo e André, muito obrigada por partilharem o vosso conhecimento e me ajudarem nos momentos mais críticos. Um obrigada especial à Joana, que foi essencial na fase inicial do meu doutoramento. A tua paciência e apoio fizeram toda a diferença.

Ao grupo nBTT/Lab214.S3, obrigada pela amizade, apoio, por todos os momentos de diversão, pelas palavras de incentivo e acima de tudo por aguentarem tão bem todo o meu

drama (#dramaqueen)...vocês são espetaculares e vou guardar-vos para sempre no coração.

Um muito obrigada a todos os colegas e amigos do INEB/IBMC/i3S...sinto-me uma sortuda pela quantidade enorme de pessoas que tive oportunidade de conhecer e manter na minha vida ao longo destes 5 anos (e não só). Foi muito bom poder contar com o vosso apoio e amizade!!

À Catarina e ao Philippe, os novos "bosses", por todo o apoio e compreensão nesta fase de transição. A todos os colegas do ICB Lab e do iBiMED por me acolherem tão bem no laboratório e em Aveiro.

À minha família do coração, àqueles que são as "minhas pessoas" Beta, Jorginho, Pedro e Tânia, e ao mais recente elemento, Tiago, obrigada pelo apoio, pelo carinho, pelos serões passados a estupidificar (sempre com o belo do copo de vinho a acompanhar)...obrigada por fazerem parte da minha vida e me deixarem fazer parte da vossa.

À pessoa que durante muitos anos partilhou comigo as angústias, alegrias e que nunca me impediu de sonhar... apesar dos nossos caminhos já não se cruzarem, obrigada Ricardo por nunca teres desistido de mim!

Aos meus pais, não há palavras para lhes agradecer o apoio e amor incondicional. Muito do que sou hoje devo-o a vocês, que me ensinaram a não baixar os braços e a nunca desistir de ir atrás dos meus sonhos. OBRIGADA POR TUDO!!!

À minha irmã, pelo apoio, pelo amor, por mostrar tanto entusiasmo e orgulho pelas minhas conquistas, por nunca me deixar desistir, pelas palavras certas nos momentos mais complicados,...POR TUDO!!! Obrigada ao André pelos conselhos e apoio. E obrigada ao meu Guigas, que é uma das pessoas que eu mais amo neste mundo e que nos seus pequenos gestos me faz sentir tão amada e feliz.

# LIST OF MAIN OUTPUTS

The main outputs of the work conducted during the period of this thesis are listed below:

### *Papers in peer-reviewed scientific journals*

D. Barros, P. Parreira, J. Furtado, F. Ferreira-da-Silva, E. Conde-Sousa, A.J. Garcia, M.C.L. Martins, I.F. Amaral, A.P. Pêgo, An affinity-based approach to engineer laminin-presenting cell instructive microenvironments, Biomaterials 192 (2019) 601-611

W. M. Han, S. E. Anderson, M. Mohiuddin, D. Barros, S. A. Nakhai, E. Shin, I. F. Amaral, A. P. Pêgo, A. J. García, Y. C. Jang, Synthetic matrix enhances transplanted satellite cell engraftment in dystrophic and aged skeletal muscle with comorbid trauma, Science Advances, 4 (2018).

J. Silva, A. R. Bento, D. Barros, T. L. Laundos, S. R. Sousa, P. Quelhas, M. M. Sousa, A. P. Pêgo, I. F. Amaral, Fibrin functionalization with synthetic adhesive ligands interacting with $\alpha 6\beta 1$ integrin receptor enhances neurite outgrowth of embryonic stem cell-derived neural stem/progenitors, Acta Biomaterialia, 59 (2017) 243-256.

D. Barros, I. F. Amaral, A. P. Pêgo, Biomimetic Synthetic Self-Assembled Hydrogels for Cell Transplantation. Current Topics in Medicinal Chemistry, 15(13) (2015) 1209-26.

### *Manuscripts in preparation for submission*

D. Barros, I. F. Amaral, A. P. Pêgo, Laminin-inspired cell instructive microenvironments for neural tissue engineering. (Literature Review).

D. Barros, A. J. García, I. F. Amaral, A. P. Pêgo, Engineering hydrogels with affinity-bound laminin as 3D neural stem cell culture systems. (Original Research).

### *Book Chapter*

J. Caldeira, F. Sousa, D. Sousa, D. Barros (2018). Extracelular matrix constitution and function for tissue regeneration and repair, in *Peptides and Proteins as Biomaterials for Tissue Regeneration and Repair*, M.A. Barbosa and M.C.L. Martins, Editors. Woodhead Publishing – Elsevier.

### *Patents*

D. Barros, I.F. Amaral, A.P. Pêgo, Laminin immobilization, methods and uses thereof, Portuguese Provisional Patent Application no. 20181000074673, filled 2018/11/30.

*Published articles were herein reproduced with permission from editors*.

# ABSTRACT

Neural stem cells (NSCs) hold great potential for application in the treatment of central nervous system (CNS) disorders. These multipotent cells reside within a dynamic and complex microenvironment, the NSC niche, where cell-cell interactions and local microenvironmental cues are key to regulate stem cell behavior. Therefore, the development of new platforms allowing a better understanding of niche properties and how they regulate NSC behavior and function is highly desirable. These are expected to provide valuable insight into cell physiology and interactions with the surrounding microenvironment, and ultimately be used for the development of more effective NSC-based regenerative therapies.

Laminin has a key role in the modulation of NSC function and fate within neurogenic niches. Indeed, different studies already explored the immobilization of full-length laminin and its peptide analogues into diverse biological and synthetic matrices, to recapitulate the microenvironment of stem cell niches and/or gain insight into the role of ECM on stem cell behavior. However, the strategies currently explored for laminin immobilization within three-dimensional (3D) matrices do not address a critical aspect influencing laminin bioactivity, which is the control over the exposure of laminin crucial bioactive epitopes.

In this thesis, we propose the design of biologically relevant matrices able to recapitulate the laminin-rich microenvironment of NSC niches. For that, we explored the modification of a degradable synthetic hydrogel with full-length laminin or with a laminin-derived peptide interacting with syndecans - AG73.

One of the specific aims of this thesis was the establishment of an affinity-based approach that takes advantage of the high affinity interaction between laminin and the human N-terminal agrin (hNtA) domain. A recombinant human NtA (rhNtA) domain was produced and successfully conjugated at its N-terminal with a thiol-terminated poly(ethylene glycol) (PEG) – mono-PEGylated rhNtA. Mono-PEGylated rhNtA showed ability to act as an effective natural binding partner for the site-selective immobilization of laminin, while preserving the exposure of laminin key bioactive domains. This translated into an enhanced ability of laminin to polymerize and mediate hNSC adhesion and spreading. Aiming at the establishment of a chemically-defined cell-instructive microenvironment, the proposed affinity-based approach was explored to promote the site-selective immobilization of different laminin isoforms (in the context of this thesis assessed for mouse laminin-111 and recombinant human laminin-521) into a degradable synthetic hydrogel. A four-arm maleimide-end functionalized poly(ethylene glycol) (PEG-

4MAL) macromer based hydrogel was selected as the base material, due to its modular nature, good biocompatibility and well characterized biochemical and biophysical properties. The PEG-4MAL macromer was functionalized with the thiol-terminated mono-PEGylated rhNtA domain to mediate the site-selective incorporation of laminin into PEG-4MAL. The developed hydrogels revealed mechanical properties (complex modulus (G*) = 251 Pa) within the range of values preferred for NSC proliferation (100 – 1000 Pa) and neurite branching and extension (200 – 400 Pa). Moreover, the affinity-bound laminin PEG-4MAL hydrogels showed an enhanced ability to mediate hNSC proliferation and neurite outgrowth, when compared to unmodified hydrogels, and most importantly, in contrast to hydrogels containing equal amount of physically entrapped laminin.

In alternative to the incorporation of full-length laminin, a laminin-derived peptide interacting with syndecan receptors (AG73) was explored to confer bioactivity to 3D matrices. The modular nature of the synthetic matrix used, allowed us to explore the effect of AG73 peptide density on cell behavior, independently of other hydrogel biophysical and biochemical properties. The tethering of AG73 peptide to PEG-4MAL hydrogels led to a significant improvement of cell viability after 7 days in culture, independently of the input peptide concentration. In addition, we demonstrated that a higher input AG73 concentration (1 mM) better supports hNSC proliferation and neurite outgrowth, as well as the establishment of a neuronal network.

Overall, the work presented in this thesis contributed to: (i) the development of an affinity-based strategy for site-selective immobilization of laminin, suitable for use as an alternative to conventional immobilization approaches (physical entrapment and non-selective covalent immobilization) in a wide range of applications (*e.g.* engineered coatings for neuroelectrodes, 2D substrates for cell culture, and biofunctionalization of 3D matrices); (ii) development of engineered matrices for use as defined 3D platforms for the establishment of artificial NSC niches and as temporary mimetic microenvironments to support hNSC transplantation in the context of nervous system regeneration/disorders.

In summary, we strongly believe this work opens new avenues in the design of more efficient hydrogel matrices for application in NSC-based regenerative approaches for the treatment of traumatic CNS disorders or neurodegenerative diseases.

# RESUMO

As células estaminais neurais (CENs) apresentam um grande potencial para aplicação no tratamento de doenças do sistema nervoso central (SNC). Estas células multipotentes residem num microambiente dinâmico e complexo, o nicho das CEN, onde as interações célula-célula e os sinais do microambiente local são essenciais para regular o comportamento das células estaminais. Deste modo, o desenvolvimento de novas plataformas que permitam compreender melhor as propriedades do nicho e a forma como estas regulam o comportamento e a função das CENs é altamente vantajoso. É expectável que estas plataformas permitam uma melhor compreensão da fisiologia celular das CENs e das suas interações com o ambiente circundante, e que contribuam para o desenvolvimento de terapias regenerativas baseadas no transplante de CENs mais efetivas.

A laminina tem um papel crucial na modulação da função e diferenciação das CENs nos nichos neurogénicos. De facto, já vários estudos exploraram a imobilização da molécula da laminina e de péptidos derivados da laminina em matrizes biológicas e sintéticas, de forma a recapitular o microambiente do nicho e/ou a compreender melhor o papel da matriz extracelular no comportamento das células estaminais. Contudo, as estratégias exploradas atualmente para a imobilização da laminina em matrizes tridimensionais (3D) não contemplam um aspeto crítico para a bioatividade da laminina, e que é o controlo sobre a exposição dos epítopos bioativos mais importantes.

Nesta tese, propomos o desenvolvimento de matrizes biologicamente relevantes capazes de recapitular o microambiente rico em laminina dos nichos neurogénicos. Para isso, explorámos a modificação de um hidrogel sintético degradável com a molécula da laminina ou com um péptido derivado da laminina capaz de interagir com recetores sindecano – AG73.

Um dos objetivos específicos desta tese foi o desenvolvimento de uma estratégia de imobilização por afinidade, baseada na interação de elevada afinidade entre a laminina e o domínio N-terminal da agrina (NtA). O domínio recombinate humano NtA (rhNtA) foi produzido e conjugado eficazmente no seu N-terminal com um polietilenoglicol (PEG) contendo um grupo tiol numa das suas extremidades – rhNtA mono-PEGilado. O rhNtA mono-PEGilado demonstrou capacidade para atuar como um ligando natural para a imobilização seletiva da laminina, sem comprometer a exposição dos domínios bioativos desta proteína. A eficiência do ligando proposto traduziu-se numa maior capacidade da laminina para polimerizar e para mediar a adesão das CENs humanas, assim como a organização do seu citoesqueleto. Com o objetivo de estabelecer um microambiente

quimicamente definido e capaz de modular o comportamento celular, explorámos a estratégia de imobilização por afinidade proposta para a imobilização controlada de diferentes isoformas da laminina (no contexto desta tese avaliámos a laminina-111 derivada de ratinho e a laminina-521 recombinante humana) num hidrogel sintético e degradável. Para o efeito selecionámos um hidrogel de PEG com quatro braços funcionalizados nas extremidades com maleimida (PEG-4MAL) devido à sua natureza modular, biocompatibilidade e propriedades bioquímicas e biofísicas bem caracterizadas. O PEG-4MAL foi inicialmente funcionalizado com o domínio rhNtA mono-PEGilado para lhe permitir mediar a incorporação selectiva da laminina. Os hidrogéis desenvolvidos apresentaram propriedades mecânicas (módulo complexo (G*) = 251 Pa) no gama de valores preferidos para a proliferação das CEN (100 – 1000 Pa) e extensão de neurites (200 – 400 Pa). Os hidrogéis com laminina imobilizada seletivamente revelaram modular de forma mais eficaz a proliferação das CENs e a extensão de neurites, quando comparados com hidrogéis não modificados, e sobretudo em contraste com hidrogéis sem o domínio rhNtA mono-PEGilado, mas contendo a mesma quantidade de laminina fisicamente incorporada.

Alternativamente à imobilização da molécula da laminina, também explorámos um péptido derivado da laminina que interage com os recetores sindecano (AG73), para conferir bioatividade às matrizes 3D. A natureza modular da matriz sintética utilizada, permitiu-nos explorar o efeito da densidade do péptido AG73 no comportamento celular, independentemente de outras propriedades bioquímicas e biofísicas do hidrogel. Os hidrogéis de PEG-4MAL modificados com o péptido levaram a um aumento significativo da viabilidade celular após 7 dias em cultura, independentemente da concentração de péptido. Além disso, a concentração máxima de AG73 testada (1 mM) revelou suportar melhor a proliferação das CENs e a extensão de neurites, tal como favorecer o estabelecimento de uma rede neuronal.

No geral, o trabalho apresentado nesta tese contribuiu para: (i) o desenvolvimento de uma estratégia de afinidade para a imobilização seletiva da laminina, com potencial para ser utilizada em alternativa às estratégias de imobilização convencionais (incorporação física e imobilização covalente não seletiva) em diversas aplicações (*p.e.* revestimentos para neuro-elétrodos, substratos para cultura celular, e biofuncionalização de matrizes 3D); (ii) desenvolvimento de plataformas 3D definidas com potencial de utilização no estabelecimento de nichos neurogénicos artificiais e como microambientes temporários biomiméticos, para transplante de CENs no contexto da regeneração do sistema nervoso.

Em resumo, acreditamos que este trabalho abre novas perspetivas para o desenvolvimento de matrizes mais eficazes para aplicação em terapias regenerativas baseadas no transplante de CENs para o tratamento de doenças traumáticas ou degenerativas do SNC.

# TABLE OF CONTENTS

# LIST OF ABBREVIATIONS

## A

**A** – Avogadro's constant

**Ac-PEG-NHS** – Acrylate - Poly(ethylene glycol) - N-hydroxysuccinimide

**ACN** – Acetonitrile

**ATDPC** – Adipose tissue-derived progenitor cell(s)

## B

**BDNF** – Brain-derived neurotrophic factor

**bFGF** – Basic fibroblast growth factor

**BM** – Basement membrane

**BMEC** – Brain microvascular endothelial cell(s)

**BMP** - Bone morphogenic protein

**BMHP** - Bone-marrow homing peptide

**BMSC** - Bone marrow stromal cell(s)

**BSA** - Bovine serum albumin

## C

**CBD** - Collagen-binding domain

**CHCA** - *alpha-Cyano-4-hydroxycinnamic acid*

**CLSM** - Confocal laser scanning microscopy

**CNS** - Central Nervous System

**CS** – Chondroitin sulfate

## D

**DAPI** - 4',6-diamidino-2-phenylindole

**DGR** - Osteopontin cell-adhesion motif

**DIBO** – Dibenzocyclooctyne

**Dibutyril cAMP** - $N^6$, 2'-O-Dibutyryladenosine 3', 5'-cyclic monophosphate sodium salt

**DRG** - Dorsal root ganglia

**ΔD** - Dissipation shift

## E

***E*** - Elastic moduli

**ECM** - Extracellular matrix

**EDC -** 3-(N,N-dimethylamino) propyl-N-ethylcarbodiimide

**EGF** – Epidermal growth factor

**EG4** - (11-mercaptoundecyl) tetraethylene glycol

**ELISA** - Enzyme-linked immunosorbent assay

**ELP** - Elastin-like polypeptide

**ESC** - Embryonic stem cell(s)

## F

**Δf** - Frequency shift

**FBS** – Fetal bovine serum

**FI** - Fluorescence intensity

**Fmoc** - Fluoren-9-ylmethyloxycarbonyl

**Fmoc-FF -** Fluoren-9-ylmethyloxycarbonyl-diphenylalanine

**FOV** – Field of view

## G

**G'** – Storage modulus

**G''** – Loss modulus

**G*** - Complex modulus

**GAG** – Glycosaminoglycan

**GMEM** - Glasgow Minimum Essential Medium

## H

**HA** - Hyaluronic acid

**hECFC-EC** – Human endothelial colony-forming cell-derived endothelial cell(s)

**HEPES -** 4-(2-hydroxyethyl)-1-piperazineethanesulfonic acid

**hiPSC-EC** – Human induced pluripotent stem cell-derived endothelial cell(s)

**HRP** - Horseradish peroxidase

**HS** - Heparan sulfate

**HSPG** - Heparan sulfate proteoglycan

**HUVEC** - Human umbilical vein endothelial cell(s)

## I

**IPN** - Interpenetrating polymer network

**iPSC** - Induced pluripotent stem cell(s)

**IPTG** - Isopropyl β-D-1-thiogalactopyranoside

**IRRAS** - Infrared reflection absorption spectroscopy

## K

$\mathbf{k_a}$ - Association rate constant

$\mathbf{K_D}$ - Dissociation constant

$\mathbf{k_d}$ - Dissociation rate constant

## L

**LE** – Laminin-type epidermal growth factor like

**LG** - Laminin globular

**LN** - Laminin N-terminal

**LVR** – Linear viscoelastic region

## M

**MC** - Methylcellulose

**MMP** - Matrix metalloproteinase

**mPEG** - mono-PEGylated

**MS** - Mass spectrometry

**MSC** - Mesenchymal stem cell(s)

**msLn-111** - Laminin-111 from mouse Engelbreth-Holm-Swarm sarcoma

**MWCO** - Molecular weight cut-off

## N

**Nap** - Naphthalene

**NHS** - N-hydroxysuccinimide

**NSC** - Neural stem cell

**NPC** – Neural progenitor cell

**NSPC** – Neural stem progenitor cell

**NT** - Neurotrophin

**NtA** - N-terminal agrin

## O

**ON** - Overnight

**OXMC** - Oxidized methylcellulose

## P

δ - Phase angle

**PA** - Peptide amphiphile

**PBS** - Phosphate buffered saline

**PCLM** - Poly(caprolactone methacryloyloxyethyl ester)

**PCR** - Polymerase chain reaction

**PDL** – poly(D-lysine)

**PEG** - Poly(ethylene glycol)

**PEG-4Ac -** Four-arm acrylate-end functionalized poly(ethylene glycol)

**PEG-4MAL -** Four-arm maleimide-end functionalized poly(ethylene glycol)

**PEG-DA** - Poly(ethylene glycol) diacrylate

**PEGDVS -** Poly(ethylene glycol) divinyl sulfone

**PFA** - Paraformaldeyde

**PGR** - 2-unit RGD motifs

**pHPMA**-poly(N-(2-hydroxypropyl) methacrylamide)

**PI** – Propidium iodide

**PMF** - Peptide mass fingerprint

## Q

**QCM-D** - Quartz crystal microbalance with dissipation monitoring

## R

**R** – Gas constant

**rhLn-521** - Recombinant human Laminin-521

**RIA** - Radioimmunoassay

**RT** - Room temperature

## S

**SAM** - Self-assembled monolayer

**SANPAH** - sulfosuccinimidyl 6-(4'-azido-2'-nitrophenylamino)hexanoate

**SC** – Schwann cell

**Sca-1** – Stem cells antigen-1

**SCI** - Spinal cord injury

**SD** - Standard deviation

**SDS-PAGE** - Sodium dodecyl sulfate–polyacrylamide gel electrophoresis

**SDF-1α** - Stromal cell-derived factor-1α

**SELP** - Silk-elastin-like polypeptide

**SEM** - Standard error of the mean

**SFM** - StemPro® NSC serum-free medium

**SGZ** - Subgranular zone

**SH-PEG-SGA** - thiol-poly(ethylene glycol) -succinimidyl glutaramide

**SH-PEG-SH** – poly(ethylene glycol)-dithiol

**SLIC** - Sequence and ligation independent cloning

**SPR** - Surface Plasmon Resonance

**SVZ** - Subventricular zone

## T

**3D** - Three-dimensional

**2D** - Two-dimensional

**T** - Temperature

**$T_t$** - Transition temperature

**TBS-T** - Tris-buffered saline – 0.1% Tween® 20

**TCPS** - Tissue culture polystyrene

**TFA** - Trifluoroacetic acid

**TMB** - 3,3',5,5' tetramethyl benzidine

**Trx-$His_6$** - Thioredoxin-poly-$His_6$ (6x Histidine residues)

## U

**uPA** - urokinase plasminogen activator

**UV** - Ultraviolet

## V

**VEGF** - Vascular endothelial growth factor

**VZ** - Ventricular zone

# PART 1

# CHAPTER I

General Introduction

Central nervous system (CNS) neurological disorders, which may be induced by physical trauma (*e.g.* spinal cord or traumatic brain injury), or by chronic neural degeneration in the case of neurodegenerative diseases (*e.g.* Parkinson's and Alzheimer's disease and Amyotrophic Lateral Sclerosis)), affect millions worldwide and are commonly characterized by the loss of neurons and glial cells [1, 2]. After an injury/trauma, a physical and chemical barrier to axonal regeneration is created within CNS. This leads to the destruction of neural and vasculature structures; recruitment of inflammatory cells and reactive astrocytes, which favor the formation of a glial scar; and to the release of inhibitory molecules associated with myelin, fibrotic tissue or glial scar that will contribute to the failure of axonal regrowth [3, 4]. Ultimately, the complexity and hostility of the CNS microenvironment established after injury/trauma, limits its ability to repair and regenerate [5].

The treatments currently available for CNS disorders, which include physical therapy, pharmacological intervention and functional electrical stimulation [6, 7], although able to alleviate the symptoms of the disease or injury, do not evidence ability to efficiently promote the regrowth and restoration of damaged central nerve cells, neither the creation of new neurons. Therefore, continuous research to better understand the pathophysiology of CNS disorders and provide new therapeutic strategies is highly needed. In this context, stem cell therapies are being extensively explored, as they allow the targeting of multiple therapeutic mechanisms in a controlled fashion [4, 5, 8]. These therapies rely upon the neuroprotective, trophic and replacement potential of stem cells [4, 9], which may contribute to create a permissive microenvironment for the processes of repair and regeneration to occur. Among the different stem cells being currently investigated in the context of neurologic disorders, neural stem cells (NSCs) constitute one of the most attractive choices [4, 9, 10].

NSCs are multipotent stem cells that differentiate into the main cell phenotypes of the CNS - neurons, oligodendrocytes and astrocytes - and can thus, be used for the replacement of lost neurons or oligodendrocytes [9]. Moreover, through the production and secretion of neurotrophic and immunomodulatory factors, either naturally or through genetic modification, transplanted NSCs have shown to have a neuroprotective effect on endogenous neural cells [9] and are able to promote the regrowth of disrupted axons *in vivo* [11]. Ultimately, NSC transplantation is expected to support the regeneration of the damaged CNS, through the reestablishment of a relay neuronal circuitry and restoration of the neurological function. NSCs can be isolated from developing or adult CNS, where they reside within distinct and specific microenvironments; differentiated from pluripotent stem cells, including embryonic stem (ES) or induced pluripotent stem (iPS) cells; or directly converted from somatic cells, such as skin fibroblasts, urine cells and blood cells, easily harvested in the clinic [9].

Different CNS disorders have already shown promise as targets for NSC transplantation, both in pre-clinical and clinical studies [9, 12, 13]. Nevertheless, and despite the significant advances made in the last few years, towards the clinical implementation of NSC-based therapies [9, 14], these still present limited success. This is mainly related to the rapid clearance and minimal engraftment observed within the host tissue after transplantation. Indeed, different studies showed that less than 5% of transplanted cells remain at the site of injection within days of transplantation [15]. The lack of stable engraftment is thought to be mainly related with the complexity and hostility of the CNS microenvironment established after injury, which adversely impacts stem cell fate and function. In this regard, and to achieve long-term functional integration of transplanted NSCs into the host CNS and better support their survival and differentiation along the neuronal lineage, a better understanding of the surrounding microenvironment, both under physiological and pathological conditions, as well as the underlying mechanisms controlling the NSC fate is highly desirable.

NSCs reside within a dynamic and complex microenvironment, the stem cell niche, where cell-cell interactions and local microenvironmental cues, including those from neighboring cells, humoral factors and extracellular matrix (ECM), are key to regulate stem cell behavior [16-18]. However, the intrinsic regulatory mechanisms allowing NSCs to integrate this complex array of signals remain poorly understood, as the traditional culture systems are unable to recapitulate several important features of these microenvironments [19]. Consequently, in the last few years, emphasis was put on the development of well-defined and tunable three-dimensional (3D) platforms that replicate the physical and chemical elements of the native neurogenic niches. These are expected to provide more accurate insights into *in vivo* cell physiological function and interactions with the surrounding microenvironment, and ultimately, contribute to the design of more effective NSC-based therapies. Different standard approaches for the 3D culture of cells, including spheroids, porous scaffolds and hydrogels, have been explored in this regard [20, 21]. Among these, hydrogels still constitute the most widespread option, as they are well-defined and tunable matrices that share many key physical properties with native ECM [19]. These include high-water content, good permeability and elasticity, resembling the nature of soft tissue microenvironments [22, 23]. Moreover, the structural, mechanical and chemical properties of hydrogels can be easily tuned to mimic the tissue-specific ECM microenvironment [22, 23]. Natural and synthetic polymer-based hydrogels have been already explored in different studies to mimic critical aspects of the NSC niches [24-27]. Natural polymers constitute an attractive option for the design of biomimetic hydrogels, due to their inherent bioactivity and mechanical properties similar to those of the native ECM. Nevertheless, their use is very often hindered by batch-to-batch variability and limited range of mechanical properties [28, 29]. Synthetic polymers, in turn, have been

receiving more attention for such applications, as they are able to overcome many of the inherent limitations of natural-based hydrogels. These are chemically-defined materials, which can be easily tuned to present the desired mechanical properties [23]. Moreover, although synthetic polymers, usually, may not intrinsically offer biological information (*e.g.* adhesive cues, growth factors and protease-sensitive sequences), they can be easily engineered to include biological signals [23].

Poly(ethylene glycol) (PEG), the starting material explored in this thesis, is a synthetic hydrophilic polymer widely used in clinic, with low risk of immunogenicity, which has been extensively explored for the development of cell-instructive microenvironments, with application in the framework of regenerative medicine and tissue engineering [30-32]. PEG has linear and branched (multi-arm or star) basic structure that can be easily modified with different functional groups, including acrylate, maleimide, vinyl sulfone, among others [33], to allow hydrogel formation or conjugation with biomolecules. Different crosslinking methods can be explored for PEG hydrogel formation, including free radical polymerization and covalent reaction of PEG macromers with reactive chain ends (*e.g*. Michael-type addition, click chemistry, enzymatic reaction, *etc*; for a more comprehensive review see [30]). Michael-type addition, the polymerization approach used in this thesis, is one of the most commonly explored, as it allows the easy and fast incorporation of cysteine-containing peptides within appropriately functionalized PEG macromers, at physiological pH conditions [34, 35]. As previously mentioned, the chemical and mechanical properties of synthetic hydrogels can be easily tuned and optimized to create a favorable cell microenvironment to maximize the survival and function of encapsulated cells and promote interaction with the host microenvironment. Matrix adhesiveness and degradability are two critical factors to take into consideration, when designing cell-instructive microenvironments, as they will be key for the modulation of NSC function (*e.g.* viability, proliferation, outgrowth and differentiation) and matrix remodeling [27, 36, 37]. Therefore, and despite the bioinert nature of PEG, this polymer can be synthesized to include reactive functional groups enabling the tethering of bioactive cues, such as cell adhesive domains and protease-sensitive sequences. The structural and viscoelastic properties of these hydrogels, can also be tailored by varying the polymer concentration, chain length, chain configuration (*e.g.* linear, multi-arm, *etc.*) and cross-linking density [38, 39]. The modulation of these properties will ultimately impact different cellular functions, including NSC survival, proliferation and differentiation [34, 36, 37]. In addition, the fine control over hydrogel mechanical and structural properties will be crucial to direct neural stem cell fate [40-43].

Within the neurogenic niche, laminin constitutes one of the most important and best described ECM factors [44, 45]. This heterotrimeric glycoprotein comprises several bioactive domains

contributing for basement membrane assembly and stability, and involved on the modulation of NSC behavior (*e.g.* cell adhesion, viability and neuronal outgrowth and migration) [46-49]. Indeed, different studies have already explored the immobilization of full-length laminin and their peptide analogues, for the design of 3D NSC niche microenvironments (for a more comprehensive review see [50]). The developed 3D matrices have shown ability to create a permissive microenvironment for cell growth and differentiation *in vitro*, and some of these matrices evidenced promising *in vivo* biological performance, when explored as vehicles for cell transplantation in the context of neurological disorders.

The tethering of bioactive factors, such as proteins and peptides, onto hydrogels requires appropriate synthetic techniques for the preservation of biological function. Nevertheless, the selection of the most appropriate chemistry is not trivial, as it should assure control over peptide/ protein orientation and conformation, which in turn will impact their bioactivity and ability to modulate cellular behavior [51-53]. Specifically, strategies explored, to date, for full-length laminin immobilization, have relied either on its transient non-covalent incorporation or physical entrapment or, alternatively, on its non-selective covalent immobilization by taking advantage of functional groups present in multiple sites of the laminin structure, such as amines and thiols [50] (Fig. 1). Despite widely used, one of the main limitations presented by these strategies is the inability to control the conformation and orientation of bioactive molecules upon immobilization. In this regard, in recent years, immobilization strategies have shifted towards site-specific conjugation, with special focus on biorthogonal chemical reactions (click chemistry), enzymatic ligation and affinity binding, using either unnatural amino acids or engineered site-selective amino acid sequences (for a more comprehensive review see [54]). These strategies are expected to provide a higher retention of bioactivity, by favoring the access to the active sites of immobilized proteins.

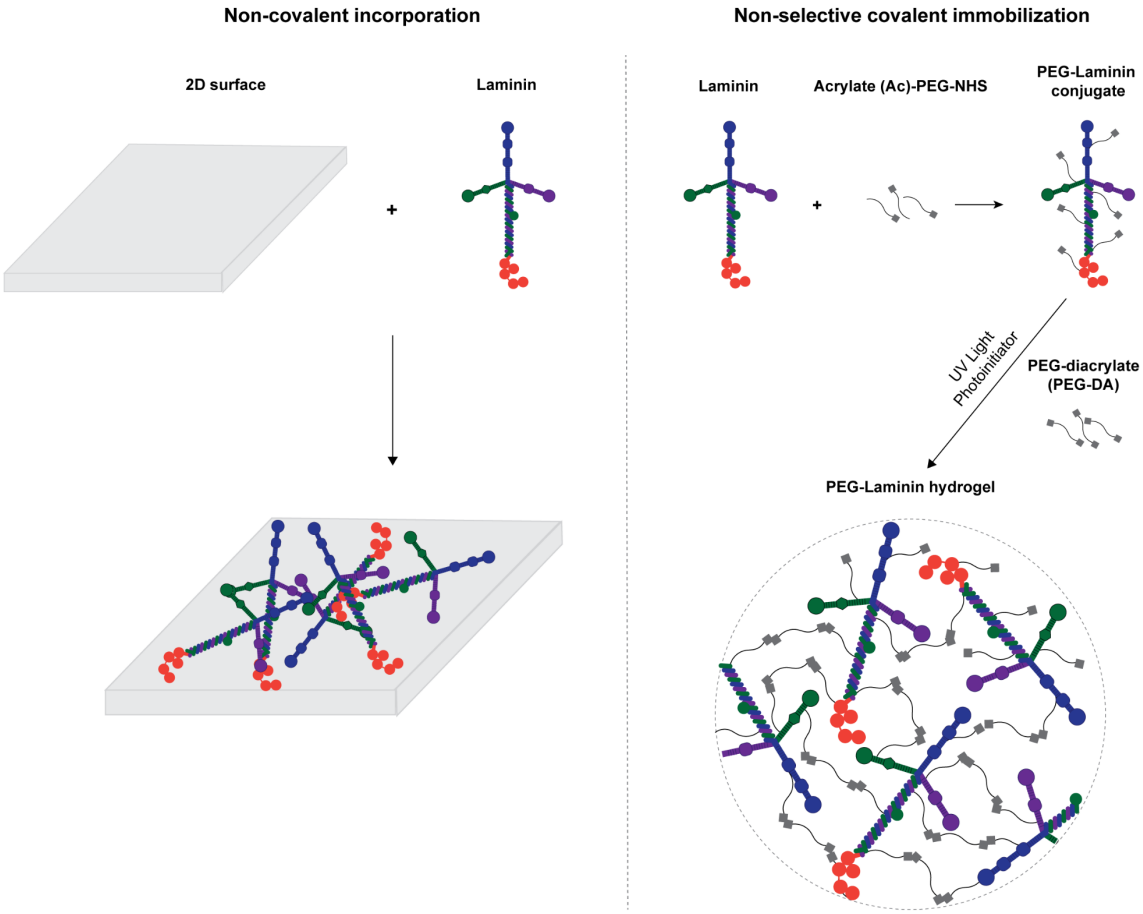


**Figure 1**. **Strategies currently explored for laminin immobilization into 2D and 3D cell instructive microenvironments.** Non-covalent incorporation approaches are used under the assumption the adsorbed protein layer forms a molecular network, retaining the overall properties of laminin matrices *in vivo*. Non-selective covalent immobilization, in turn, takes advantage of functional groups (*e.g.* amines and thiols) present in multiple sites on the laminin structure. Both strategies lack the ability to control the orientation and conformation of laminin upon immobilization, which may compromise the exposure of key laminin bioactive epitopes.

Affinity-binding has been increasingly explored, as it allows the design of dynamic biomimetic systems, favoring the site-specific and reversible conjugation of proteins and peptides, and, as a result, resembling more closely what happens *in vivo*. However, its successful implementation is highly dependent on the appropriate selection of the binding pairs. With this in mind, and in alternative to the “artificial” binding systems, such as streptavidin and biotin, which require the protein of interest to be either recombinantly or chemically modified, natural binding partners are being explored. By taking advantage of the native high affinity interaction

between proteins and peptides, strong non-covalent interactions can be established without the need for protein modification.

The N-terminal agrin (NtA) domain, which comprises the first 135 amino acids of agrin, mediates a high affinity interaction with laminin (dissociation constant $K_D \cong 5nM$) [55], required for the integration of agrin into synaptic basal lamina and other basement membranes [56]. The amino acid sequence of this domain is highly conserved, with > 90% of the residues being identical, among chick, mouse and human [57] (Fig. 2). The agrin-binding site in laminin was shown to be localized in the central region of the coiled-coil domain of laminin and maps to a sequence of 20 surface-exposed and conserved residues within the $\gamma$1 chain [58, 59]. This represents more than 50% of the isoforms identified to date [60], with variations in affinity imposed by $\alpha$ and $\beta$ chains. Interestingly, this interaction requires a coiled-coil conformation of the agrin-binding site [59]. To better understand the interaction of agrin with laminin, the crystal structure of chicken NtA domain, in the presence of a synthetic 20-residue peptide corresponding to the agrin-binding site within the laminin $\gamma$1 chain, was described [57]. The NtA core domain comprises five $\beta$-strands that form two orthogonally packed $\beta$-sheets flanked by $\alpha$-helices at both termini, characterized by a high content of charged amino acids (Fig. 2) [57]. Indeed, charged residues account for > 25% of all amino acid residues that constitutes the NtA sequence. Laminin coiled-coil structures, in turn, were shown to exhibit the typical heptad repeat $(abcdefg)_n$, in which solvent exposed positions are generally occupied by polar or charged residues while hydrophobic amino acids tend to be oriented towards the core of the superhelix [61, 62]. In line with these evidences, different studies demonstrated that the high affinity interaction between the coiled-coil domain of laminin and the globular NtA domain was mainly of ionic nature and was mediated by the C-terminal helix 3 as the primary binding site and by the highly conserved charged residues at the open face of the $\beta$-barrel as an auxiliary site [55].

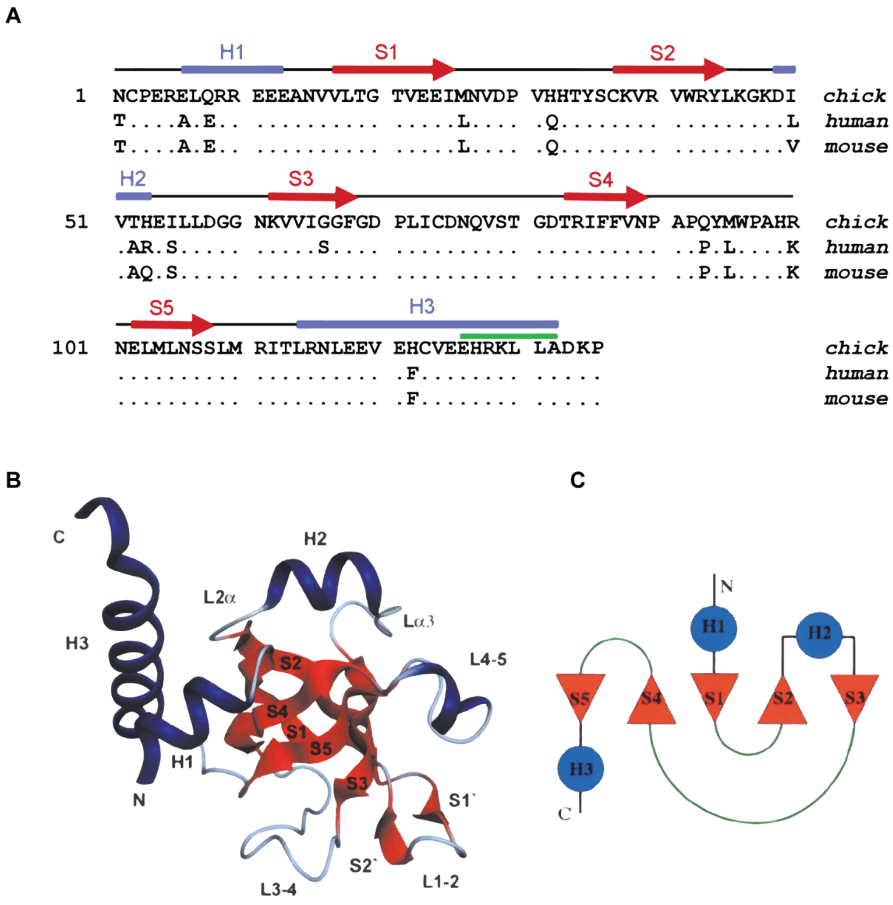


**Figure 2. Structure of the NtA domain. A)** Alignment of agrin NtA domain of chick, human and mouse. The sequences were aligned to the first 135 amino acids of chick agrin, starting after the signal sequence cleavage site. Conserved residues are indicated by dots and the secondary structure elements are indicated above the alignment using correspondent color code in B). **B)** Ribbon and **C)** topology diagrams of the NtA structure secondary elements. β-strands (S1-S5) are represented in red; α-helices (H1-H3) are represented in blue; loop regions (L1-2, L3-4 and L4-5) are oriented to the same surface of the protein in B) and are shown as green lines in C). Adapted from [57], Copyright© 2001, Springer Nature.

The high affinity interaction between the NtA domain and laminin was already explored for the development of different controlled release systems for therapeutic proteins, such as growth factors [63-66] and neuropeptides [67]. For such purpose, fusion proteins consisting of the NtA domain and a growth factor or a neuropeptide moiety were successfully engineered. These were shown to be able to target laminin accumulated in the lesion areas, thus evidencing the potential of NtA to be used as a natural binding ligand, preventing the diffusion

of the growth factors or neuropeptides and hence increase their timely presence at a specific site.

Laminin-derived small adhesive sequences have been increasingly explored, in alternative to the incorporation of the full-length protein, to confer bioactivity to 3D matrices [50]. Most of the works published to date, have explored synthetic adhesive peptides, which mediate cell interaction via integrin receptors [50]. Alternatively, cell binding ligands interacting with transmembrane heparan sulfate proteoglycans (HSPGs), and more specifically syndecans, have gained more attention in the last few years, as attractive alternative to engineer biomimetic matrices, as result of their key role in regulating NSC stemness [68-70]. Syndecans are transmembrane HSPGs, with a key role on the modulation of different biological processes, including neural patterning, angiogenesis, inflammation and wound healing [71]. These cell adhesion receptors are composed by an extracellular domain, comprising glycosaminoglycan (GAG) chains, including heparan sulfate (HS) and chondroitin sulfate (CS) chains, which mediate the interaction with growth factors, ECM proteins, as well as with other receptors (Fig. 3) [71, 72]. Syndecan receptors also present a single transmembrane domain that regulates homo- and hetero-dimerization, and a short cytoplasmic domain, which interact directly with intracellular signaling molecules (Fig. 3) [71, 72]. The extracellular domain of these receptors varies between the four members of the syndecan family identified in mammals (Syndecan-1, -2, -3 and -4), while the transmembrane and cytoplasmic domains,, are highly conserved [71].

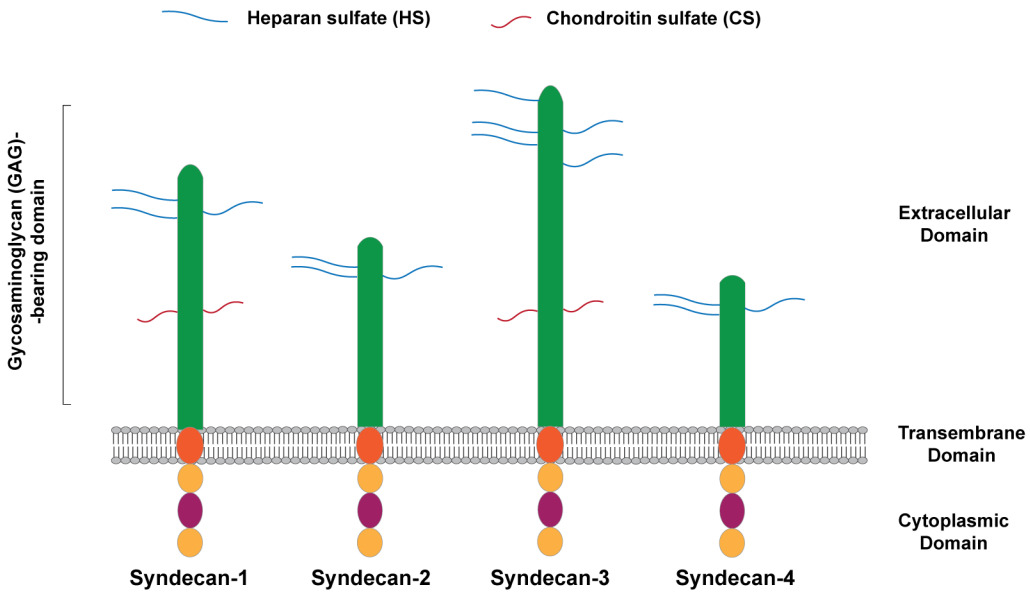


**Figure 3**. **Schematic representation of mammalian syndecan receptors**. Syndecan receptors are composed by an extracellular domain comprising several glycosaminoglycan (GAG) chains – Heparan

sulfate (HS) and Chondroitin sulfate (CS) chains, which mediate several cell-cell and cell-matrix interactions. They also have a single transmembrane domain responsible to promote self-association between core proteins, and a cytoplasmic domain that will mediate downstream signaling. Adapted from [73], Copyright® 2014, John Wiley & Sons.

The four members of the syndecan family (Syndecan-1, -2, -3 and -4) present distinct cell- and tissue-specific expression patterns [74]. More specifically, within the NSC niche, syndecans have a key role on the modulation of all stages of stem cell maintenance and neurogenesis (*e.g.* proliferation, self-renewal, differentiation, migration and maturation), either through independent signaling or by working alongside with other receptors, such as integrins [68-70]. Syndecan-1 is highly expressed during neurogenesis and is key to support NSC proliferation and progenitor cell maintenance [75, 76], while syndecan-4 constitutes a key marker of NSCs differentiation [77]. These evidences are in agreement with previous studies from our lab, showing that human NSCs (hNSCs) derived from the H9 embryonic stem cell line, cultured under basal conditions, express high levels of syndecan-1 (98.6%), whereas syndecan-4 levels were found in much lower amounts (2.62%) [78]. Syndecan-3 is key for the modulation of axon guidance [79, 80] and neurite outgrowth [81, 82], and together with syndecan-4 [83] controls neuronal migration. Lastly, syndecan-2 exerts a remarkable effect in dendritic spine morphogenesis [84].

AG73 (RKRLQVQLSIRT) is a synthetic peptide derived from the laminin globular 4 (LG4) domain of laminin $\alpha$1 chain, which interacts with syndecan-1 [85, 86] and syndecan-4 [87]. This peptide was reported to promote cell adhesion with membrane ruffling [88-90], and showed great potential to enhance neurite outgrowth of PC12 neuronal cells when tethered onto natural-based hydrogels [91-93]. A previous study from our lab, evidenced that functionalization of fibrin hydrogels with AG73 improves cell outgrowth of hNSCs [78]. Despite the promising results, the intrinsic bioactivity presented by natural-based polymers makes difficult to deconvolute the contribution of the syndecan-binding peptide to the final biological outcome. Synthetic-based polymers, in turn, constitute an attractive alternative in this regard, as they are chemically-defined materials that allow a precise and independent control over the biochemical and biophysical properties of the matrix [23]. Additionally, to the best of our knowledge, to date, no study evaluating the functionalization of synthetic hydrogels with the AG73 peptide and assessing its effect on the modulation of NSC fate and function was conducted.

In summary, the design of biologically relevant matrices able to recapitulate the microenvironment of the stem cell niches and modulate the stem cell function and fate, hold

great potential when trying to improve the efficacy of cell-based therapeutic strategies currently under investigation and development.

## References

[1] R.Y. Tam, T. Fuehrmann, N. Mitrousis, M.S. Shoichet, Regenerative therapies for central nervous system diseases: a biomaterials approach, Neuropsychopharmacology 39(1) (2014) 169-88.

[2] L. Binan, A. Ajji, G. De Crescenzo, M. Jolicoeur, Approaches for neural tissue regeneration, Stem Cell Rev 10(1) (2014) 44-59.

[3] G. Yiu, Z. He, Glial inhibition of CNS axon regeneration, Nat Rev Neurosci 7(8) (2006) 617-27.

[4] A.P. Pego, S. Kubinova, D. Cizkova, I. Vanicky, F.M. Mar, M.M. Sousa, E. Sykova, Regenerative medicine for the treatment of spinal cord injury: more than just promises?, J Cell Mol Med 16(11) (2012) 2564-82.

[5] S.A. Goldman, Stem and Progenitor Cell-Based Therapy of the Central Nervous System: Hopes, Hype, and Wishful Thinking, Cell Stem Cell 18(2) (2016) 174-88.

[6] C.H. Ho, R.J. Triolo, A.L. Elias, K.L. Kilgore, A.F. DiMarco, K. Bogie, A.H. Vette, M.L. Audu, R. Kobetic, S.R. Chang, K.M. Chan, S. Dukelow, D.J. Bourbeau, S.W. Brose, K.J. Gustafson, Z.H. Kiss, V.K. Mushahwar, Functional electrical stimulation and spinal cord injury, Phys Med Rehabil Clin N Am 25(3) (2014) 631-54, ix.

[7] I. Vismara, S. Papa, F. Rossi, G. Forloni, P. Veglianese, Current Options for Cell Therapy in Spinal Cord Injury, Trends Mol Med 23(9) (2017) 831-849.

[8] O. Lindvall, Z. Kokaia, Stem cells in human neurodegenerative disorders--time for clinical translation?, J Clin Invest 120(1) (2010) 29-40.

[9] Y. Tang, P. Yu, L. Cheng, Current progress in the derivation and therapeutic application of neural stem cells, Cell Death Dis 8(10) (2017) e3108.

[10] J.A. Steinbeck, L. Studer, Moving stem cells to the clinic: potential and limitations for brain repair, Neuron 86(1) (2015) 187-206.

[11] P. Lu, L.L. Jones, E.Y. Snyder, M.H. Tuszynski, Neural stem cells constitutively secrete neurotrophic factors and promote extensive host axonal growth after spinal cord injury, Exp Neurol 181(2) (2003) 115-29.

[12] K. Reekmans, J. Praet, J. Daans, V. Reumers, P. Pauwels, A. Van der Linden, Z.N. Berneman, P. Ponsaerts, Current challenges for the advancement of neural stem cell biology and transplantation research, Stem Cell Rev 8(1) (2012) 262-78.

[13] D. McLauchlan, N.P. Robertson, Stem cells in the treatment of central nervous system disease, J Neurol 265(4) (2018) 984-986.

[14] A. Trounson, C. McDonald, Stem Cell Therapies in Clinical Trials: Progress and Challenges, Cell Stem Cell 17(1) (2015) 11-22.

[15] M.H. Amer, F. Rose, K.M. Shakesheff, M. Modo, L.J. White, Translational considerations in injectable cell-based therapeutics for neurological applications: concepts, progress and challenges, NPJ Regen Med 2 (2017) 23.
[16] F. Gattazzo, A. Urciuolo, P. Bonaldo, Extracellular matrix: a dynamic microenvironment for stem cell niche, Biochim Biophys Acta 1840(8) (2014) 2506-19.
[17] S.W. Lane, D.A. Williams, F.M. Watt, Modulating the stem cell niche for tissue regeneration, Nat Biotechnol 32(8) (2014) 795-803.
[18] A. Vishwakarma, J. Rouwkema, P.A. Jones, J.M. Karp, The Need to Study, Mimic and Target Stem Cell Niches, in: A. Vishwakarma, J.M. Karp (Eds.), Biology and Engineering of Stem Cell Niches, Elsevier2017.
[19] J.L. Wilson, T.C. McDevitt, Biofunctional Hydrogels for Three-Dimensional Stem Cell Culture, in: A. Vishwakarma, J.M. Karp (Eds.), Biology and Engineering of Stem Cell Niches, Elsevier2017.
[20] F. Ruedinger, A. Lavrentieva, C. Blume, I. Pepelanova, T. Scheper, Hydrogels for 3D mammalian cell culture: a starting guide for laboratory practice, Appl Microbiol Biotechnol 99(2) (2015) 623-36.
[21] Technology Platforms for 3D Cell Culture: A User's Guide, John Wiley & Sons Ltd.2017.
[22] M.W. Tibbitt, K.S. Anseth, Hydrogels as Extracellular Matrix Mimics for 3D Cell Culture, Biotechnol. Bioeng. 103(4) (2009) 655-663.
[23] D. Barros, I.F. Amaral, A.P. Pego, Biomimetic synthetic self-assembled hydrogels for cell transplantation, Curr Top Med Chem 15(13) (2015) 1209-26.
[24] K.J. Lampe, S.C. Heilshorn, Building stem cell niches from the molecule up through engineered peptide materials, Neurosci Lett 519(2) (2012) 138-46.
[25] J. Lam, S.T. Carmichael, W.E. Lowry, T. Segura, Hydrogel design of experiments methodology to optimize hydrogel for iPSC-NPC culture, Adv Healthc Mater 4(4) (2015) 534-9.
[26] C. Regalado-Santiago, E. Juarez-Aguilar, J.D. Olivares-Hernandez, E. Tamariz, Mimicking Neural Stem Cell Niche by Biocompatible Substrates, Stem Cells Int 2016 (2016) 1513285.
[27] C.M. Madl, B.L. LeSavage, R.E. Dewi, C.B. Dinh, R.S. Stowers, M. Khariton, K.J. Lampe, D. Nguyen, O. Chaudhuri, A. Enejder, S.C. Heilshorn, Maintenance of neural progenitor cell stemness in 3D hydrogels requires matrix remodelling, Nat Mater 16(12) (2017) 1233-1242.
[28] J. Zhu, R.E. Marchant, Design properties of hydrogel tissue-engineering scaffolds, Expert Rev. Med. Devices 8(5) (2011) 607-26.
[29] G.A. Saracino, D. Cigognini, D. Silva, A. Caprini, F. Gelain, Nanomaterials design and tests for neural tissue engineering, Chem. Soc. Rev. 42(1) (2013) 225-62.

[30] J. Zhu, Bioactive modification of poly(ethylene glycol) hydrogels for tissue engineering, Biomaterials 31(17) (2010) 4639-56.
[31] Y.H. Tsou, J. Khoneisser, P.C. Huang, X. Xu, Hydrogel as a bioactive material to regulate stem cell fate, Bioact Mater 1(1) (2016) 39-55.
[32] X. Lu, T.H. Perera, A.B. Aria, L.A.S. Callahan, Polyethylene glycol in spinal cord injury repair: a critical review, J Exp Pharmacol 10 (2018) 37-49.
[33] N.A. Peppas, K.B. Keys, M. Torres-Lugo, A.M. Lowman, Poly(ethylene glycol)-containing hydrogels in drug delivery, J Control Release 62(1-2) (1999) 81-7.
[34] E.A. Phelps, N.O. Enemchukwu, V.F. Fiore, J.C. Sy, N. Murthy, T.A. Sulchek, T.H. Barker, A.J. Garcia, Maleimide cross-linked bioactive PEG hydrogel exhibits improved reaction kinetics and cross-linking for cell encapsulation and in situ delivery, Adv Mater 24(1) (2012) 64-70, 2.
[35] J. Yu, F. Chen, X. Wang, N. Dong, C. Lu, G. Yang, Z. Chen, Synthesis and characterization of MMP degradable and maleimide cross-linked PEG hydrogels for tissue engineering scaffolds, Polymer Degradation and Stability 133 (2016) 312-320.
[36] N.O. Enemchukwu, R. Cruz-Acuna, T. Bongiorno, C.T. Johnson, J.R. Garcia, T. Sulchek, A.J. Garcia, Synthetic matrices reveal contributions of ECM biophysical and biochemical properties to epithelial morphogenesis, J Cell Biol 212(1) (2016) 113-24.
[37] W.M. Han, S.E. Anderson, M. Mohiuddin, D. Barros, S.A. Nakhai, E. Shin, I.F. Amaral, A.P. Pego, A.J. Garcia, Y.C. Jang, Synthetic matrix enhances transplanted satellite cell engraftment in dystrophic and aged skeletal muscle with comorbid trauma, Sci Adv 4(8) (2018) eaar4008.
[38] S. Lin, N. Sangaj, T. Razafiarison, C. Zhang, S. Varghese, Influence of physical properties of biomaterials on cellular behavior, Pharm Res 28(6) (2011) 1422-30.
[39] J. Kim, Y.P. Kong, S.M. Niedzielski, R.K. Singh, A.J. Putnam, A. Shikanov, Characterization of the crosslinking kinetics of multi-arm poly(ethylene glycol) hydrogels formed via Michael-type addition, Soft Matter 12(7) (2016) 2076-85.
[40] L.A. Flanagan, Y.E. Ju, B. Marg, M. Osterfield, P.A. Janmey, Neurite branching on deformable substrates, Neuroreport 13(18) (2002) 2411-5.
[41] K. Saha, A.J. Keung, E.F. Irwin, Y. Li, L. Little, D.V. Schaffer, K.E. Healy, Substrate modulus directs neural stem cell behavior, Biophys. J. 95(9) (2008) 4426-38.
[42] A. Banerjee, M. Arha, S. Choudhary, R.S. Ashton, S.R. Bhatia, D.V. Schaffer, R.S. Kane, The influence of hydrogel modulus on the proliferation and differentiation of encapsulated neural stem cells, Biomaterials 30(27) (2009) 4695-9.
[43] S.R. Hynes, M.F. Rauch, J.P. Bertram, E.B. Lavik, A library of tunable poly(ethylene glycol)/poly(L-lysine) hydrogels to investigate the material cues that influence neural stem cell differentiation, J Biomed Mater Res A 89(2) (2009) 499-509.

[44] A. Kerever, J. Schnack, D. Vellinga, N. Ichikawa, C. Moon, E. Arikawa-Hirasawa, J.T. Efird, F. Mercier, Novel extracellular matrix structures in the neural stem cell niche capture the neurogenic factor fibroblast growth factor 2 from the extracellular milieu, Stem Cells 25(9) (2007) 2146-57.
[45] I. Kazanis, J.D. Lathia, T.J. Vadakkan, E. Raborn, R. Wan, M.R. Mughal, D.M. Eckley, T. Sasaki, B. Patton, M.P. Mattson, K.K. Hirschi, M.E. Dickinson, C. ffrench-Constant, Quiescence and activation of stem and precursor cell populations in the subependymal zone of the mammalian brain are associated with distinct cellular and extracellular matrix signals, J Neurosci 30(29) (2010) 9771-81.
[46] A. Hyysalo, M. Ristola, M.E. Makinen, S. Hayrynen, M. Nykter, S. Narkilahti, Laminin alpha5 substrates promote survival, network formation and functional development of human pluripotent stem cell-derived neurons in vitro, Stem Cell Res 24 (2017) 118-127.
[47] L. Luckenbill-Edds, Laminin and the mechanism of neuronal outgrowth, Brain Res Brain Res Rev 23(1-2) (1997) 1-27.
[48] S.K. Powell, H.K. Kleinman, Neuronal laminins and their cellular receptors, Int J Biochem Cell Biol 29(3) (1997) 401-14.
[49] S. Plantman, M. Patarroyo, K. Fried, A. Domogatskaya, K. Tryggvason, H. Hammarberg, S. Cullheim, Integrin-laminin interactions controlling neurite outgrowth from adult DRG neurons in vitro, Mol Cell Neurosci 39(1) (2008) 50-62.
[50] D. Barros, I.F. Amaral, A.P. Pego, Laminin inspired cell instructive microenvironments for neural tissue engineering applications, Manuscript in preparation (2019).
[51] B.G. Keselowsky, D.M. Collard, A.J. Garcia, Surface chemistry modulates fibronectin conformation and directs integrin binding and specificity to control cell adhesion, J Biomed Mater Res A 66(2) (2003) 247-59.
[52] J.C. Rodriguez Hernandez, M. Salmeron Sanchez, J.M. Soria, J.L. Gomez Ribelles, M. Monleon Pradas, Substrate chemistry-dependent conformations of single laminin molecules on polymer surfaces are revealed by the phase signal of atomic force microscopy, Biophys J 93(1) (2007) 202-7.
[53] O.M. Ba, M. Hindie, P. Marmey, O. Gallet, K. Anselme, A. Ponche, A.C. Duncan, Protein covalent immobilization via its scarce thiol versus abundant amine groups: Effect on orientation, cell binding domain exposure and conformational lability, Colloids Surf B Biointerfaces 134 (2015) 73-80.
[54] S.A. Fisher, A.E.G. Baker, M.S. Shoichet, Designing Peptide and Protein Modified Hydrogels: Selecting the Optimal Conjugation Strategy, J Am Chem Soc 139(22) (2017) 7416-7427.
[55] J.B. Mascarenhas, M.A. Ruegg, U. Winzen, W. Halfter, J. Engel, J. Stetefeld, Mapping of the laminin-binding site of the N-terminal agrin domain (NtA), EMBO J 22(3) (2003) 529-36.

[56] M.A. Ruegg, J.L. Bixby, Agrin orchestrates synaptic differentiation at the vertebrate neuromuscular junction, Trends Neurosci 21(1) (1998) 22-7.
[57] J. Stetefeld, M. Jenny, T. Schulthess, R. Landwehr, B. Schumacher, S. Frank, M.A. Ruegg, J. Engel, R.A. Kammerer, The laminin-binding domain of agrin is structurally related to N-TIMP-1, Nat Struct Biol 8(8) (2001) 705-9.
[58] A.J. Denzer, T. Schulthess, C. Fauser, B. Schumacher, R.A. Kammerer, J. Engel, M.A. Ruegg, Electron microscopic structure of agrin and mapping of its binding site in laminin-1, EMBO J 17(2) (1998) 335-43.
[59] R.A. Kammerer, T. Schulthess, R. Landwehr, B. Schumacher, A. Lustig, P.D. Yurchenco, M.A. Ruegg, J. Engel, A.J. Denzer, Interaction of agrin with laminin requires a coiled-coil conformation of the agrin-binding site within the laminin gamma1 chain, EMBO J 18(23) (1999) 6762-70.
[60] M. Aumailley, L. Bruckner-Tuderman, W.G. Carter, R. Deutzmann, D. Edgar, P. Ekblom, J. Engel, E. Engvall, E. Hohenester, J.C. Jones, H.K. Kleinman, M.P. Marinkovich, G.R. Martin, U. Mayer, G. Meneguzzi, J.H. Miner, K. Miyazaki, M. Patarroyo, M. Paulsson, V. Quaranta, J.R. Sanes, T. Sasaki, K. Sekiguchi, L.M. Sorokin, J.F. Talts, K. Tryggvason, J. Uitto, I. Virtanen, K. von der Mark, U.M. Wewer, Y. Yamada, P.D. Yurchenco, A simplified laminin nomenclature, Matrix Biol 24(5) (2005) 326-32.
[61] D.A. Parry, R.D. Fraser, J.M. Squire, Fifty years of coiled-coils and alpha-helical bundles: a close relationship between sequence and structure, J Struct Biol 163(3) (2008) 258-69.
[62] G. Armony, E. Jacob, T. Moran, Y. Levin, T. Mehlman, Y. Levy, D. Fass, Cross-linking reveals laminin coiled-coil architecture, Proc Natl Acad Sci U S A 113(47) (2016) 13384-13389.
[63] W. Sun, C. Sun, H. Zhao, H. Lin, Q. Han, J. Wang, H. Ma, B. Chen, Z. Xiao, J. Dai, Improvement of sciatic nerve regeneration using laminin-binding human NGF-beta, PLoS One 4(7) (2009) e6180.
[64] Q. Han, B. Li, H. Feng, Z. Xiao, B. Chen, Y. Zhao, J. Huang, J. Dai, The promotion of cerebral ischemia recovery in rats by laminin-binding BDNF, Biomaterials 32(22) (2011) 5077-85.
[65] J. Xie, B. Jin, D.W. Li, B. Shen, N. Gong, T.Z. Zhang, P. Dong, Effect of laminin-binding BDNF on induction of recurrent laryngeal nerve regeneration by miR-222 activation of mTOR signal pathway, Am J Transl Res 7(6) (2015) 1071-80.
[66] B. Wang, J. Yuan, X. Chen, J. Xu, Y. Li, P. Dong, Functional regeneration of the transected recurrent laryngeal nerve using a collagen scaffold loaded with laminin and laminin-binding BDNF and GDNF, Sci Rep 6 (2016) 32292.

[67] L. Wu, J. Wang, X. Chen, A. Hong, Expression, identification and biological effects of the novel recombination protein, PACAP38-NtA, with high bioactivity, Int J Mol Med 35(2) (2015) 376-82.
[68] M. Ford-Perriss, K. Turner, S. Guimond, A. Apedaile, H.D. Haubeck, J. Turnbull, M. Murphy, Localisation of specific heparan sulfate proteoglycans during the proliferative phase of brain development, Dev Dyn 227(2) (2003) 170-84.
[69] Y. Choi, H. Chung, H. Jung, J.R. Couchman, E.S. Oh, Syndecans as cell surface receptors: Unique structure equates with functional diversity, Matrix Biol 30(2) (2011) 93-9.
[70] F.E. Poulain, H.J. Yost, Heparan sulfate proteoglycans: a sugar code for vertebrate development?, Development 142(20) (2015) 3456-67.
[71] N.A. Afratis, D. Nikitovic, H.A. Multhaupt, A.D. Theocharis, J.R. Couchman, N.K. Karamanos, Syndecans - key regulators of cell signaling and biological functions, FEBS J 284(1) (2017) 27-41.
[72] H. Chung, H.A. Multhaupt, E.S. Oh, J.R. Couchman, Minireview: Syndecans and their crucial roles during tissue regeneration, FEBS Lett 590(15) (2016) 2408-17.
[73] J.R. Couchman, S. Gopal, H.C. Lim, S. Norgaard, H.A. Multhaupt, Fell-Muir Lecture: Syndecans: from peripheral coreceptors to mainstream regulators of cell behaviour, Int J Exp Pathol 96(1) (2015) 1-10.
[74] X. Xian, S. Gopal, J.R. Couchman, Syndecans as receptors and organizers of the extracellular matrix, Cell Tissue Res 339(1) (2010) 31-46.
[75] Q. Wang, L. Yang, C. Alexander, S. Temple, The niche factor syndecan-1 regulates the maintenance and proliferation of neural progenitor cells during mammalian cortical development, PLoS One 7(8) (2012) e42883.
[76] L. Morizur, A. Chicheportiche, L.R. Gauthier, M. Daynac, F.D. Boussin, M.A. Mouthon, Distinct Molecular Signatures of Quiescent and Activated Adult Neural Stem Cells Reveal Specific Interactions with Their Microenvironment, Stem Cell Reports (2018).
[77] L.E. Oikari, R.K. Okolicsanyi, A. Qin, C. Yu, L.R. Griffiths, L.M. Haupt, Cell surface heparan sulfate proteoglycans as novel markers of human neural stem cell fate determination, Stem Cell Res 16(1) (2016) 92-104.
[78] A.R. Bento, Improving neurite outgrowth in 3D hydrogel matrices by mimicking cell receptor-ECM interactions occurring in neurogenic niches: an engineering approach to develop more efficient neural stem cell hydrogel carriers, Faculdade de Engenharia, Universidade do Porto, 2018.
[79] A. Kinnunen, T. Kinnunen, M. Kaksonen, R. Nolo, P. Panula, H. Rauvala, N-syndecan and HB-GAM (heparin-binding growth-associated molecule) associate with early axonal tracts in the rat brain, Eur J Neurosci 10(2) (1998) 635-48.

[80] A. Kinnunen, M. Niemi, T. Kinnunen, M. Kaksonen, R. Nolo, H. Rauvala, Heparan sulphate and HB-GAM (heparin-binding growth-associated molecule) in the development of the thalamocortical pathway of rat brain, Eur J Neurosci 11(2) (1999) 491-502.
[81] E. Raulo, M.A. Chernousov, D.J. Carey, R. Nolo, H. Rauvala, Isolation of a neuronal cell surface receptor of heparin binding growth-associated molecule (HB-GAM). Identification as N-syndecan (syndecan-3), J Biol Chem 269(17) (1994) 12999-3004.
[82] T. Kinnunen, E. Raulo, R. Nolo, M. Maccarana, U. Lindahl, H. Rauvala, Neurite outgrowth in brain neurons induced by heparin-binding growth-associated molecule (HB-GAM) depends on the specific interaction of HB-GAM with heparan sulfate at the cell surface, J Biol Chem 271(4) (1996) 2243-8.
[83] H.K. Matthews, L. Marchant, C. Carmona-Fontaine, S. Kuriyama, J. Larrain, M.R. Holt, M. Parsons, R. Mayor, Directional migration of neural crest cells in vivo is regulated by Syndecan-4/Rac1 and non-canonical Wnt signaling/RhoA, Development 135(10) (2008) 1771-80.
[84] I.M. Ethell, Y. Yamaguchi, Cell surface heparan sulfate proteoglycan syndecan-2 induces the maturation of dendritic spines in rat hippocampal neurons, J Cell Biol 144(3) (1999) 575-86.
[85] M.P. Hoffman, M. Nomizu, E. Roque, S. Lee, D.W. Jung, Y. Yamada, H.K. Kleinman, Laminin-1 and laminin-2 G-domain synthetic peptides bind syndecan-1 and are involved in acinar formation of a human submandibular gland cell line, J Biol Chem 273(44) (1998) 28633-41.
[86] L.N. Gama-de-Souza, E. Cyreno-Oliveira, V.M. Freitas, E.S. Melo, V.F. Vilas-Boas, A.S. Moriscot, R.G. Jaeger, Adhesion and protease activity in cell lines from human salivary gland tumors are regulated by the laminin-derived peptide AG73, syndecan-1 and beta1 integrin, Matrix Biol 27(5) (2008) 402-19.
[87] N. Suzuki, N. Ichikawa, S. Kasai, M. Yamada, N. Nishi, H. Morioka, H. Yamashita, Y. Kitagawa, A. Utani, M.P. Hoffman, M. Nomizu, Syndecan binding sites in the laminin alpha1 chain G domain, Biochemistry 42(43) (2003) 12625-33.
[88] M. Nomizu, W.H. Kim, K. Yamamura, A. Utani, S.Y. Song, A. Otaka, P.P. Roller, H.K. Kleinman, Y. Yamada, Identification of cell binding sites in the laminin alpha 1 chain carboxyl-terminal globular domain by systematic screening of synthetic peptides, J Biol Chem 270(35) (1995) 20583-90.
[89] K. Hozumi, N. Suzuki, P.K. Nielsen, M. Nomizu, Y. Yamada, Laminin alpha1 chain LG4 module promotes cell attachment through syndecans and cell spreading through integrin alpha2beta1, J Biol Chem 281(43) (2006) 32929-40.

[90] M. Mochizuki, Y. Kadoya, Y. Wakabayashi, K. Kato, I. Okazaki, M. Yamada, T. Sato, N. Sakairi, N. Nishi, M. Nomizu, Laminin-1 peptide-conjugated chitosan membranes as a novel approach for cell engineering, FASEB J 17(8) (2003) 875-7.
[91] Y. Yamada, K. Hozumi, F. Katagiri, Y. Kikkawa, M. Nomizu, Biological activity of laminin peptide-conjugated alginate and chitosan matrices, Biopolymers 94(6) (2010) 711-20.
[92] Y. Yamada, F. Katagiri, K. Hozumi, Y. Kikkawa, M. Nomizu, Cell behavior on protein matrices containing laminin alpha1 peptide AG73, Biomaterials 32(19) (2011) 4327-35.
[93] Y. Yamada, K. Hozumi, A. Aso, A. Hotta, K. Toma, F. Katagiri, Y. Kikkawa, M. Nomizu, Laminin active peptide/agarose matrices as multifunctional biomaterials for tissue engineering, Biomaterials 33(16) (2012) 4118-25.

# CHAPTER II

Aim and Structure of the Thesis

# AIM OF THE THESIS

The main aim of the work presented in this thesis was the design of biologically relevant matrices, able to recapitulate the laminin-rich microenvironment of neural stem cell (NSC) niches. For that, we proposed the biofunctionalization of protease-sensitive synthetic hydrogel matrices, *via* site-selective immobilization of full-length laminin. Additionally, we also explored the modification of such matrices with a syndecan interacting laminin-derived peptide (AG73). The developed hydrogels were designed to support NSC viability, proliferation and neuronal differentiation, which are key features for their application, as dynamic cell-instructive extracellular matrix (ECM) analogs, in *in vitro* three-dimensional (3D) platforms for NSC culture and as vehicles for NSC transplantation into the damaged central nervous system (CNS).

Specific aims of the proposed work included:

- Establishment of an affinity-based approach to promote the site-selective immobilization of laminin, allowing for the subsequent controlled presentation of this ECM protein in cell microenvironments.
- Evaluation of the potential of the proposed strategy for the site-selective immobilization of different laminin isoforms (in the context of this thesis assessed for mouse laminin-111 (msLn-111) and recombinant human laminin-521 (rhLn-521)) into a synthetic hydrogel. As the starting material for the development of the hydrogel, a four-arm maleimide-end functionalized poly(ethylene glycol) (PEG-4MAL) macromer was selected, due to its good biocompatibility, both *in vitro* and *in vivo* [1-3], and well characterized biochemical and biophysical properties [3-5]. By selecting a synthetic polymer as the hydrogel backbone, we aim at assuring reproducibility, while exploring the versatility of synthetic materials in terms of tunable physical properties and biofunctionalization.
- Validation of the developed 3D platform for the culture of human NSCs (hNSCs), in terms of ability to support cell viability, proliferation and neurite outgrowth.
- Biofunctionalization of PEG-4MAL hydrogels with a syndecan-binding laminin-derived peptide (AG73) with neurite-promoting activity, and evaluation of the impact of the input peptide concentration on hNSC viability, proliferation and neurite outgrowth.

# STRUCTURE OF THE THESIS

This thesis is divided into **two parts**, comprising a total of **nine chapters**. In **Part 1**, a general introduction and a literature background is given to contextualize and support the work described in this thesis. In **Part 2**, the explored methodology and obtained results are presented, and an overall discussion of the developed work is provided.

The key role of laminin on the modulation of NSC behavior [6-9], makes this ECM protein highly attractive for the design of NSC niche microenvironments. Indeed, some works already explored laminin immobilization into different biological and synthetic matrices. In **Chapter III** we summarize the structural properties and main functions of laminin and reviewed the most relevant works using full-length laminin and laminin-derived peptides for the design of biomimetic matrices, for application in a neural regenerative context [10].

To better understand NSC physiology and interactions with the surrounding microenvironment, the development of well-defined and tunable 3D platforms able to replicate the physical and chemical elements of the native ECM is highly desirable. Among the several 3D platforms developed to date, biomimetic hydrogels still constitute one of the most attractive options for the design of matrices able to recapitulate the microenvironment of NSC niches, as they share many key physical properties with native ECM/tissues. In **Chapter IV** the most recent work using biomimetic synthetic self-assembled hydrogels for cell transplantation [11] is reviewed, due to their interesting properties for application in the CNS, when compared to covalently-crosslinked hydrogels. Additionally, we discuss some of the main challenges hampering the translation of these systems to the clinic and the issues that need to be addressed for these to progress from bench-to-bedside.

Many of the strategies explored to date for the immobilization of full-length laminin into both two-dimensional (2D) and 3D cell-instructive microenvironments are limited by the inability to control laminin orientation and conformation, upon immobilization, with preservation of protein bioactivity. In this regard, and envisaging the development of a 3D cell-instructive microenvironment, in **Chapter V** we described an affinity-based approach able to promote the site-selective immobilization of laminin to a specific substrate, while preserving the exposure of the protein key bioactive epitopes [12, 13]. The proposed strategy takes advantage of the native high affinity interaction between laminin and the human N-terminal agrin (hNtA) domain, allowing the controlled immobilization of laminin, with preservation of its ability to polymerize and mediate hNSC adhesion and spreading.

The application of the proposed affinity-based approach for the site-selective immobilization of laminin (msLn-111) into a degradable PEG-4MAL hydrogel is reported in **Chapter VI** [14]. This aims the establishment of an artificial niche able to support NSC 3D culture and

hopefully, transplantation. Affinity-bound laminin PEG-4MAL hydrogels showed great potential to be used as defined 3D platforms enabling NSC proliferation and neurite outgrowth, when compared to currently available strategies for laminin immobilization, which include physical entrapment and non-selective covalent immobilization.

Ln-521 has a key role on the modulation of neural cell behavior (*e.g.* adhesion, viability and network formation) [6, 15] and already showed potential to be used as a robust substratum for the culture and renewal of human embryonic [16] and pluripotent [6] stem cells. Consequently, in **Chapter VII** we explored the development of an affinity-bound rhLn-521 PEG-4MAL hydrogel, by taking advantage of the immobilization strategy previously proposed in **Chapter V** [12, 13], with some specific modifications, aiming to improve rhLn-521 binding to NtA and, consequently its impact on hNSC behavior. A significant improvement on neurite outgrowth was observed, compared to unmodified hydrogels, suggesting an impact of such modifications on protein conformation and domain presentation to cells.

Laminin-derived small adhesive sequences (*e.g.* IKVAV, YIGSR, RNIAEIIKDI, RKRLQVQSIRT) have been previously explored as alternative to the incorporation of the full-length laminin, to confer bioactivity to 3D matrices. Most of the works published to date, explored peptides mediating cell interaction *via* integrin receptors. More recently, a different class of receptors, syndecans, have gained more attention as attractive alternative therapeutic targets to engineer biomimetic matrices in a neural regeneration context. In **Chapter VIII**, a syndecan-binding peptide (AG73 – RKRLQVQSIRT) with neurite-promoting activity and previously explored to modify natural hydrogel matrices [17-21], was explored for the functionalization of a degradable PEG-4MAL hydrogel. More specifically, the impact of different input peptide concentrations on cell behavior was assessed. The tethering of AG73 peptide to PEG-4MAL hydrogels led to a significant improvement of cell viability, after 7 days, independently of the input peptide concentration tested. Additionally, a significant improvement in hNSC proliferation and neurite outgrowth, as well as the establishment of a neuronal network were observed, after 14 days, for cells cultured on hydrogels tethered with the higher concentration of peptide tested (1 mM).

Finally, in **Chapter IX** the concluding remarks correlating the overall obtained results and the perspectives for future research are presented.

## References

[1] J.D. Weaver, D.M. Headen, J. Aquart, C.T. Johnson, L.D. Shea, H. Shirwan, A.J. Garcia, Vasculogenic hydrogel enhances islet survival, engraftment, and function in leading extrahepatic sites, Sci Adv 3(6) (2017) e1700184.

[2] R. Cruz-Acuna, M. Quiros, A.E. Farkas, P.H. Dedhia, S. Huang, D. Siuda, V. Garcia-Hernandez, A.J. Miller, J.R. Spence, A. Nusrat, A.J. Garcia, Synthetic hydrogels for human intestinal organoid generation and colonic wound repair, Nat Cell Biol 19(11) (2017) 1326-1335.

[3] W.M. Han, S.E. Anderson, M. Mohiuddin, D. Barros, S.A. Nakhai, E. Shin, I.F. Amaral, A.P. Pego, A.J. Garcia, Y.C. Jang, Synthetic matrix enhances transplanted satellite cell engraftment in dystrophic and aged skeletal muscle with comorbid trauma, Sci Adv 4(8) (2018) eaar4008.

[4] E.A. Phelps, N.O. Enemchukwu, V.F. Fiore, J.C. Sy, N. Murthy, T.A. Sulchek, T.H. Barker, A.J. Garcia, Maleimide cross-linked bioactive PEG hydrogel exhibits improved reaction kinetics and cross-linking for cell encapsulation and in situ delivery, Adv Mater 24(1) (2012) 64-70, 2.

[5] N.O. Enemchukwu, R. Cruz-Acuna, T. Bongiorno, C.T. Johnson, J.R. Garcia, T. Sulchek, A.J. Garcia, Synthetic matrices reveal contributions of ECM biophysical and biochemical properties to epithelial morphogenesis, J Cell Biol 212(1) (2016) 113-24.

[6] A. Hyysalo, M. Ristola, M.E. Makinen, S. Hayrynen, M. Nykter, S. Narkilahti, Laminin alpha5 substrates promote survival, network formation and functional development of human pluripotent stem cell-derived neurons in vitro, Stem Cell Res 24 (2017) 118-127.

[7] L. Luckenbill-Edds, Laminin and the mechanism of neuronal outgrowth, Brain Res Brain Res Rev 23(1-2) (1997) 1-27.

[8] S.K. Powell, H.K. Kleinman, Neuronal laminins and their cellular receptors, Int J Biochem Cell Biol 29(3) (1997) 401-14.

[9] S. Plantman, M. Patarroyo, K. Fried, A. Domogatskaya, K. Tryggvason, H. Hammarberg, S. Cullheim, Integrin-laminin interactions controlling neurite outgrowth from adult DRG neurons in vitro, Mol Cell Neurosci 39(1) (2008) 50-62.

[10] D. Barros, I.F. Amaral, A.P. Pego, Laminin inspired cell instructive microenvironments for neural tissue engineering applications, Manuscript in preparation (2019).

[11] D. Barros, I.F. Amaral, A.P. Pego, Biomimetic synthetic self-assembled hydrogels for cell transplantation, Curr Top Med Chem 15(13) (2015) 1209-26.

[12] D. Barros, P. Parreira, J. Furtado, F. Ferreira-da-Silva, E. Conde-Sousa, A.J. Garcia, M.C.L. Martins, I.F. Amaral, A.P. Pego, An affinity-based approach to engineer laminin-presenting cell instructive microenvironments, Biomaterials 192 (2019) 601-611.

[13] D. Barros, I.F. Amaral, A.P. Pego, Laminin immobilization, methods and uses thereof, Portuguese Provisional Patent Application no. 20181000074673, filled 2018/11/30.
[14] D. Barros, E. Conde-Sousa, A.J. Garcia, I.F. Amaral, A.P. Pego, Engineering hydrogels with affinity-bound laminin as 3D neural stem cell culture systems Manuscript in preparation (2019).
[15] A. Bergeron, H. Sherman, P. Pardo, H. Gitschier, H. Nandivada, D. Saxena, Corning® rLaminin-521 (Human) for Expansion and Differentiation of Human Neural Stem Cells, Corning Incorporated | Application Note (2015).
[16] S. Rodin, L. Antonsson, C. Niaudet, O.E. Simonson, E. Salmela, E.M. Hansson, A. Domogatskaya, Z. Xiao, P. Damdimopoulou, M. Sheikhi, J. Inzunza, A.S. Nilsson, D. Baker, R. Kuiper, Y. Sun, E. Blennow, M. Nordenskjold, K.H. Grinnemo, J. Kere, C. Betsholtz, O. Hovatta, K. Tryggvason, Clonal culturing of human embryonic stem cells on laminin-521/E-cadherin matrix in defined and xeno-free environment, Nat Commun 5 (2014) 3195.
[17] M. Mochizuki, Y. Kadoya, Y. Wakabayashi, K. Kato, I. Okazaki, M. Yamada, T. Sato, N. Sakairi, N. Nishi, M. Nomizu, Laminin-1 peptide-conjugated chitosan membranes as a novel approach for cell engineering, FASEB J 17(8) (2003) 875-7.
[18] Y. Yamada, K. Hozumi, F. Katagiri, Y. Kikkawa, M. Nomizu, Biological activity of laminin peptide-conjugated alginate and chitosan matrices, Biopolymers 94(6) (2010) 711-20.
[19] Y. Yamada, F. Katagiri, K. Hozumi, Y. Kikkawa, M. Nomizu, Cell behavior on protein matrices containing laminin alpha1 peptide AG73, Biomaterials 32(19) (2011) 4327-35.
[20] Y. Yamada, K. Hozumi, A. Aso, A. Hotta, K. Toma, F. Katagiri, Y. Kikkawa, M. Nomizu, Laminin active peptide/agarose matrices as multifunctional biomaterials for tissue engineering, Biomaterials 33(16) (2012) 4118-25.
[21] A.R. Bento, Improving neurite outgrowth in 3D hydrogel matrices by mimicking cell receptor-ECM interactions occurring in neurogenic niches: an engineering approach to develop more efficient neural stem cell hydrogel carriers, Faculdade de Engenharia, Universidade do Porto, 2018.

# CHAPTER III

Laminin-Inspired Cell-Instructive Microenvironments for Neural Tissue Engineering

# Laminin-Inspired Cell-Instructive Microenvironments for Neural Tissue Engineering

Daniela Barros [1,2,3], Isabel F. Amaral [1,2,4], Ana P. Pêgo [1,2,3,4]

[1] i3S - Instituto de Investigação e Inovação em Saúde, Universidade do Porto (UPorto), Portugal

[2] INEB - Instituto de Engenharia Biomédica, UPorto, Portugal

[3] ICBAS - Instituto de Ciências Biomédicas Abel Salazar, UPorto, Portugal

[4] FEUP - Faculdade de Engenharia, UPorto, Portugal

---

**Manuscript (Literature Review) in preparation**

**Abstract**

Laminin is a heterotrimeric glycoprotein with a key role in the formation and maintenance of basement membrane (BM) architecture and properties, as well as on the modulation of several biological functions, including cell adhesion, migration, differentiation and matrix-mediated signaling. Laminin is differentially expressed within central nervous system (CNS) during development and homeostasis, with an impact on the modulation of cell function and fate. Within neurogenic niches, laminin is one of the most important and well described extracellular matrix (ECM) proteins. Therefore, an understanding of laminin assembly, domain architecture and interaction of its different bioactive domains with cell surface receptors, soluble signaling molecules and ECM proteins is essential to better understand the role of this ECM protein and its receptors on the modulation of neurogenesis, both in homeostasis or during repair. This is also expected to provide a rational basis to design biomaterial-based matrices that mimic the biological properties of the BM for neural tissue repair and cell replacement.

In this chapter, a general overview of laminin structure and domain architecture, as well as the main biological functions mediated by this heterotrimeric glycoprotein is provided. The expression and distribution of laminin in the CNS, and more specifically its role within adult neural stem cell niche is summarized. Moreover, a detailed overview on the use of full-length laminin and laminin derived peptides/recombinant laminin fragments for the development of biocompatible hydrogels mimicking the neurogenic niches, and with application for tissue repair and cell replacement in the context of the nervous tissue is given. Finally, the main challenges associated with the development of laminin-inspired hydrogels and the issues that need to be addressed for these to progress from bench-to-bedside are discussed.

## 1. Laminin

### *1.1. Structure and domain architecture*

Laminins are large heterotrimeric glycoproteins (400 – 900 kDa) composed by three polypeptide subunits, α, β, and γ, which assemble into cross-shaped molecules (Fig. 1A). To date 5 α, 3 β, and 3 γ chains have been identified and associated with the formation of 16 different laminin isoforms (Fig. 1B), whose expression pattern differ among different tissue types and developing stages (for a more comprehensive review see [1-3]). Heterotrimers containing laminin α1 (*e.g.* laminin-111) are mainly expressed during embryogenesis, disappearing progressively from most basement membranes (BM) during development, while those comprising the α5 chain (*e.g.* laminin-511 and -521) are the most ubiquitous form in the adult organism [4-7]. Laminin isoforms 211 and 221 are mainly present in the BM of skeletal and cardiac muscles [8-10], while laminin-411 and -421 are abundant in endothelial BM [11-13]. Laminin-332, in turn, is specific for the basal lamina underlying epithelial cells [14, 15]. In addition to the laminin isoforms identified to date, and summarized in Fig. 1B, novel potential laminin chain combinations have been proposed – 212/222 (α2β1γ2 / α2β2γ1) [16]; 312 (α3β1γ2) [17]; 3A33 (α3Aβ3γ3) [18]; 422 (α4β2γ2) [17]; 522 (α5β2γ2) [19], though their expression *in vivo* has not been demonstrated to date.

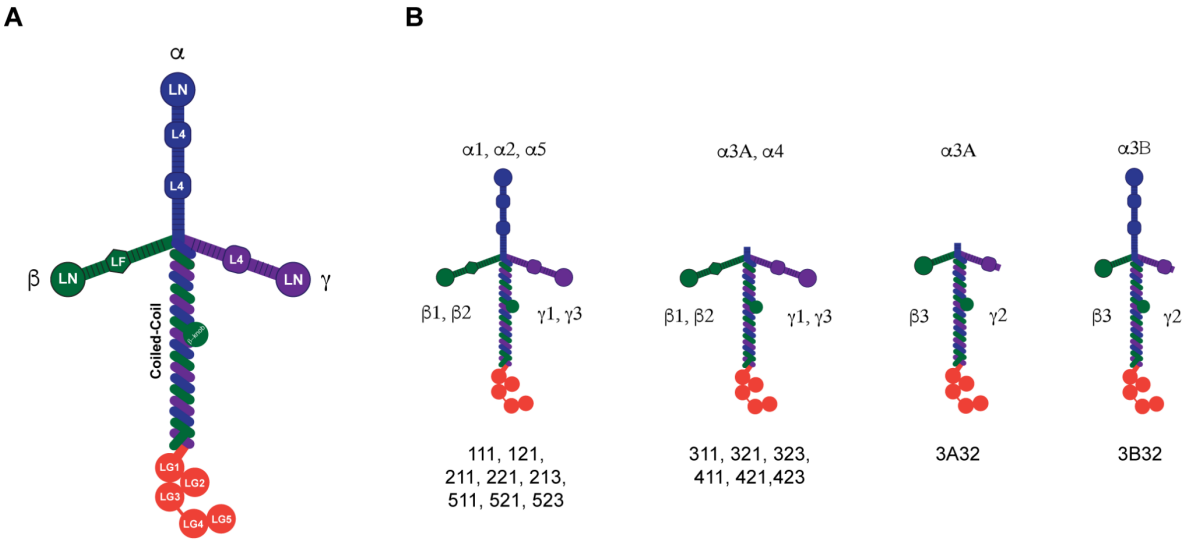


**Figure 1. Laminin structure and domain architecture**. **A)** Representative model of laminin structure composed by three polypeptide subunits, α (blue), β (green) and γ (purple). *LN* laminin N-terminal domain; *LE* laminin-type epidermal growth factor like domains; *L4* laminin 4 and *LF* laminin four domains; *LG* laminin globular domains. **B)** The sixteen different laminin isoforms described to date, grouped according to their domain similarities. The laminin molecules are named according to their chain composition. Thus, laminin-511 contains α5, β1, and γ1 chains, for example. Adapted from [7], Copyright© 2013 Landes Bioscience.

Laminin isoforms are composed by three short arms and a triple $\alpha$ helical coiled-coil domain (long arm), formed by the combination of $\alpha$, $\beta$ and $\gamma$ subunits (Fig. 1A). Short arms, with the exception of the $\alpha$3A, $\alpha$4 and $\gamma$2 chains (Fig. 1B), are composed by a large globular domain at the N-terminus, the laminin N-terminal (LN) domain and by tandem repeats of laminin-type epidermal growth factor like (LE) domains interspersed by globular domains (laminin 4 (L4) and laminin four (LF) domains), whose number vary among laminin subunits, and whose function is still unknown [1]. Long arms present a highly conserved domain structure composed by $\alpha$-helical domains, rich in heptad repeats $(abcdefg)_n$ of charged and non-polar amino acids, folded into a trimeric coiled-coil structure [20-22]. $\beta$-subunits have all a short stretch of amino acids, termed $\beta$-knob, whose function has not yet been unveiled [20]. The long arm coiled-coil domain of the $\alpha$-chain comprises a large globular domain, which is divided into five laminin globular (LG) domains (LG1-LG5) grouped into functional and structural distinct subdomains – LG1-3 and LG4-5 [23]. The coiled-coil is thought to help to orientate the LG domains, so they can be available to interact with cells, via cell surface receptors, including integrins [23-25], syndecans and dystroglycan [23, 26-28], and bind to growth factors [29] and other extracellular matrix (ECM) proteins [23].

### *1.2. Main Functions*

The multiple bioactive domains of laminin are involved in the modulation of a plethora of biological functions, including ECM deposition, cell-ECM and cell-cell interactions (Fig. 2A). More specifically, the laminin short arms (N-terminus) mediate laminin interaction with other ECM proteins (*e.g.* nidogen, netrin 4, heparan sulfate proteoglycans (HSPGs) and collagen IV), playing a key role in the assemble and stability of the BM [7]. These domains are also involved in laminin ability to polymerize [30-32], even in the absence of other BM components, forming the molecular network that will be in contact with the cellular surface [7]. In addition to its structural role, laminin comprises multiple bioactive domains that interact with cell surface receptors (*e.g*. integrins, dystroglycans and syndecans) and growth factors. While the interaction with different laminin receptors is known to be essential for the modulation of different cell functions, including cell adhesion, proliferation, migration and differentiation, as well as for ECM deposition [7, 10, 33], interaction of laminin with growth factors (*e.g.* vascular endothelial growth factor/platelet-derived growth factor; fibroblast growth factor; bone morphogenic protein (BMP); neurotrophin (NT);endothelial growth factor; CXCL chemokines) was only recently described [29], and thus, further studies to assess its potential contribution for cell function still need to be conducted.

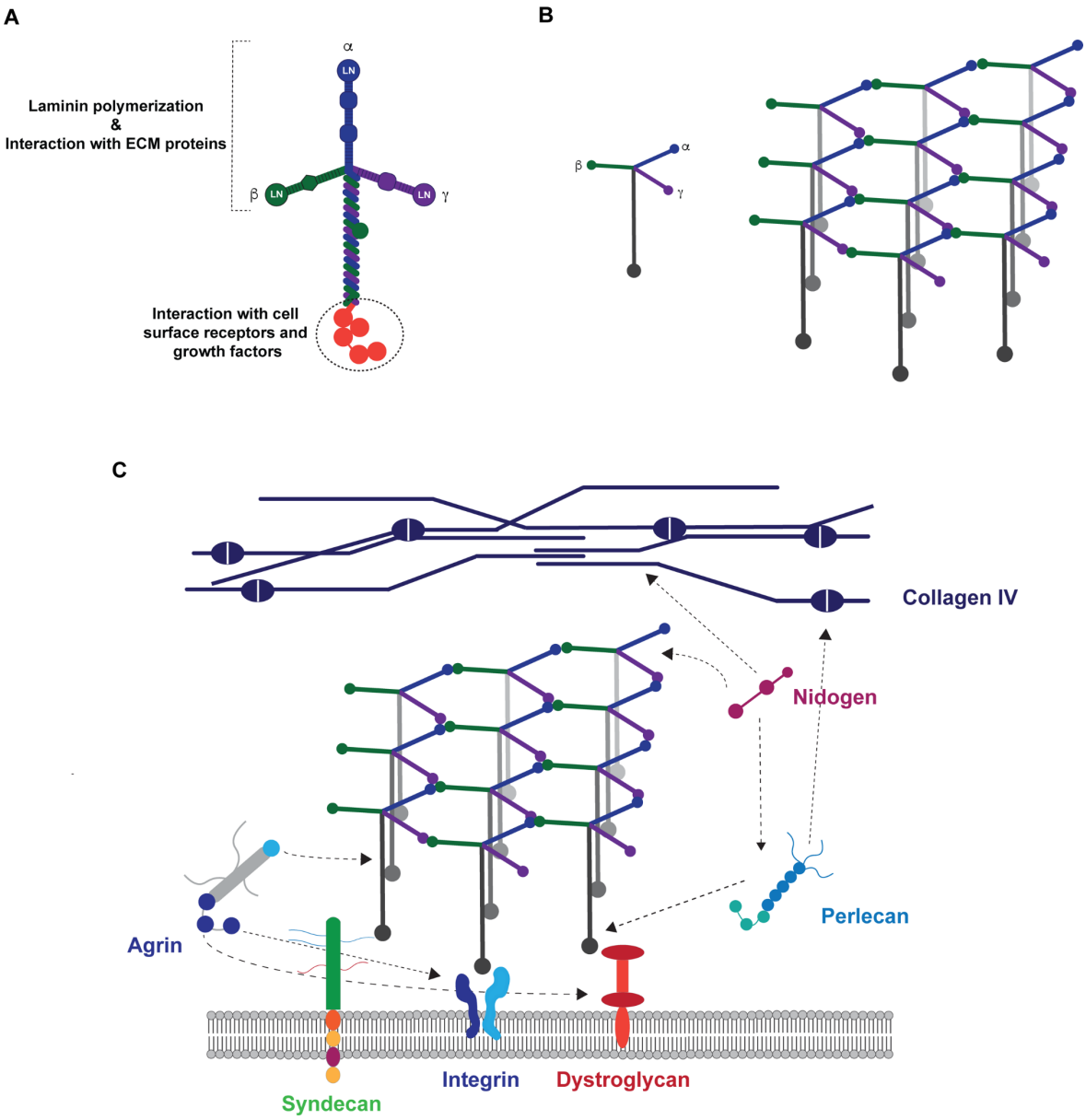


**Figure 2. Main biological functions mediated by laminin (not to scale). A)** Schematic representation of the major functions of laminin. The laminin short arms (N-terminus) mediate the process of laminin polymerization and the interaction with other ECM proteins, contributing to the assembly and stability of BMs. The globular domains within the end of laminin long arm (C-terminus), in turn, mediate laminin interactions with cells and growth factors, being responsible for the modulation of different cell functions (*e.g.* adhesion, proliferation, migration and differentiation). Adapted from [7], Copyright© 2013 Landes Bioscience. **B)** Schematic representation of laminin polymerization. N-terminal domain of α, β and γ chains interact to form a polygonal network. Adapted from [34], Copyright© 2012 Landes Bioscience. **C)** Schematic representation of supramolecular assembly of the BM. Laminin polymeric network interacts with different components of the BM, including nidogen, perlecan, agrin and collagen IV, contributing for the stability and assembly of BM. Nidogen and perlecan mediates laminin-collagen IV binding, whereas agrin binds to laminin through

its N-terminal domain. Both agrin and the laminin network are anchored to the cell surface by interactions with integrins, syndecans and α-dystroglycan. Adapted from [34], Copyright© 2012 Landes Bioscience.

### *1.2.1. Laminin polymerization*

Laminin polymerization is a key process to direct BM assembly and organization, and occurs by a thermally reversible mechanism dependent on the presence of calcium ions [30-32]. This process is better explained by the three-arm interaction model (Fig. 2B) [31, 32], which proposes that the three laminin N-terminal short arms (with exception for laminins comprising α3A-, α4- and γ2-subunits (Fig. 1B)) interact with the globular N-terminal domains of other laminins to form a polygonal network (Fig. 2B) [30-32, 35, 36]. The long arm of the laminin heterotrimer, in turn, is predicted not to be involved in the network formation, being free to interact with cells out of the plan of the polymer. Further studies were conducted, to characterize in more detail the mechanism of polymerization in different laminin isoforms [37-39]. It was demonstrated that laminin assembly is not restricted to the self-polymerization of one specific laminin isoform with the formation of a homopolymer, but can also occur by co-polymerization of laminin heterotrimers from different laminin isoforms [32]. Additionally, different studies suggest that *in vivo*, the process of laminin assembly is favored by laminin interaction with cell surface receptors (*e.g.* integrins, dystroglycan) [36, 40-42]. Nevertheless, there is still some controversy on the exact mechanism underlying the cross-talk between laminin assembly and cell surface receptors. Some works evidenced that laminin polymerization induces clustering of integrins and dystroglycan in the cell membrane, and aggregation of intracellular cytoskeletal components [43, 44]. Other studies, in turn, showed that dystroglycan null embryoid bodies are able to develop a BM [45]. Therefore, studies to better understand the impact of different cell surface receptors on laminin assembly need to be conducted.

Laminin polymerization can be reproduced *in vitro* under specific conditions [30, 46].[30]. More specifically, laminin was showed to be able to spontaneously polymerize in solution either at neutral pH, requiring a minimal protein concentration of approximately 60 nM [30], or can be triggered in acidic conditions independently of its concentration [46].

### *1.2.2. Laminin role in the assembly and stability of basement membranes*

BM assembly and stability depends on the proper interconnection between different ECM components, including laminin and collagen IV, as well as other proteins, such as nidogen (entactin) and HSPGs (*e.g.* agrin and perlecan) (Fig. 2C). Nidogen is a sulfated glycoprotein ubiquitously found in the BM, known to interact strongly [47] with an LE module within the laminin γ1 subunit [48, 49]. In contrast, a weaker nidogen binding has been observed in

laminin γ2 and γ3 subunits [50]. This protein also interacts with other ECM proteins, including perlecan, one of the major HSPGs, thus working as an intermediate for the interaction between this HSPG and laminin. Agrin, a multi-domain HSPG, which has a key role in synapse formation and maintenance at the neuromuscular junction [51], was showed to mediate a high affinity interaction with a sequence of 20 conserved residues within laminin γ1 chain (dissociation constant ($K_D$) ≅ 5 nM) through its N-terminal (NtA) domain [52]. This interaction is required for the integration of agrin into the synaptic basal lamina and other BMs [53]. Perlecan and agrin, through the direct or indirect interaction with laminin, will mediate the interaction of the laminin polymeric network with the cell surface assembled collagen IV, thus contributing to BM assembly and stabilization [34, 54, 55]. The interactions mediating the incorporation of laminin polymeric structures into the supramolecular network of the BM depend on the laminin isoform, namely on the structural domains present on laminin short arms (Fig. 1B). While laminin-111, -211 and -511 form a classical polymeric network, in which LN domain interactions with other ECM components are well described, little is known about the mechanisms behind the integration of laminin isoforms lacking LN domains in BM, such as those comprising α3A and α4 chains (Fig. 1B). In this regard, previous studies have demonstrated that although truncated, the N-terminal region of laminin 332 associates with other ECM components, including laminin 311 [56], collagen VII [57, 58], collagen XVII [59] and fibulin [60]. Despite this, further studies are necessary to better understand if these interactions are sufficient to maintain these laminin isoforms anchored to the BM, or if additional interactions are required.

#### *1.2.3. Cell adhesion-promoting activity*

Different cell surface receptors, including integrins, syndecans and dystroglycan [23] (Fig. 2B-C), interact with the LG domains in the C-terminal end of the laminin α chain. While LG1-3 domains mediate interaction with integrin receptors [23-25], the LG4-5 pair contains binding sites for α-dystroglycan and syndecans [23, 26-28].

Laminin-binding integrins α3β1, α6β1,α7β1 and α6β4 present different specificities depending on the laminin isoform [61], and most specifically on the laminin α chain [62]. For example, while integrin α6β1 has a broad affinity for all laminin isoforms, α3β1 and α6β4 bind almost exclusively to laminins comprising the α3 and α5 chains, while α7β1 prefers isoforms with the laminin α2 and α5 chains. Laminin isoforms composed by α5 are the preferred ligands for laminin-binding integrins, whereas the ones composed by α4 chains constitute the poorest ligands [62]. Integrins binding to LG domains require that both the LG1-LG3 domains and the coiled-coil to be intact. Indeed, some studies showed that modifications of the LG1-LG3 domain or on the coiled-coil structure, abolishes cell

adhesion-promoting activity. Although integrins bind to the LG1-3 domain comprised in the α-chain [3, 6, 63], it was demonstrated that β- and γ-chains also play a role in the mediation of laminin-integrin binding [64, 65]. In addition to the LG1-3 domains, integrin-binding to laminins can also occur at other recognition motifs, namely at the cryptic RGD domain in laminin α1 chain, which only becomes accessible after proteolytic cleavage [66]. α-dystroglycan displays a narrower binding spectrum, compared to integrins, presenting a high affinity only for laminin α1 and α2 chains [3]. Although the LG4-5 domains are the preferred α-dystroglycan binding domains, it was demonstrated that the α2 chain contains additional binding sites in the LG1-3 domains [3, 23, 63]. Syndecans are type I transmembrane HSPG cell receptors that interact with laminin LG4-5 domains that are responsible for the mediation of important cellular events [67]. In addition to α-dystroglycan and syndecans, other non-integrin laminin receptors, which do not interact with LG domains, were also described. These include the 110 kDa [68] and the 67 kDa cell surface receptors [69], which bind with high affinity to the IKVAV sequence within the laminin α1 chain and the YIGSR sequence within the laminin β1 chain, respectively. Overall, all transmembrane receptors described will have a key role in the formation and deposition of laminin matrices and will be involved in the modulation of cell-ECM and cell-cell interactions, as well as on the regulation of different cell functions and fate.

Ultimately, the laminin-associated matrix proteins in concert with cell-surface receptors will be key for the proper assembly and/or deposition of laminin matrices, and will work to fine-tune both matrix formation and its function.

## 2. Laminin in the central nervous system (CNS)

Laminin is differentially expressed within central nervous system (CNS), during development and homeostasis, with an impact on the modulation of cell function and fate. Despite its involvement in many aspects of CNS physiology and neuronal functions, there is still a lack of understanding on the exact role of laminin in the formation, development and function of neuronal networks. In this regard, several studies have been conducted to better characterize the expression and distribution of specific laminin chains or isoforms in different CNS regions, both during embryogenesis and adulthood (Table 1).

**Table 1.** Expression and distribution of laminin subunits in the central nervous system (CNS) during embryogenesis and adulthood. Adapted from [70], Copyright© 2018, with permission from John Wiley and Sons

| | Laminin subunit | Expression/Distribution sites | References |
|---|---|---|---|
| Embryogenesis | α1 | Cerebellum, neuroretina, olfactory bulbs, meninges, cortical plate, floor plate of spinal cord and spinal cord neurons and glial cells | [71-76] |
| | α2 | Meninges, cortical plate, choroid plexus, dorsal root ganglion, ventricular region and spinal cord neurons and glial cells | [71-74, 76-78] |
| | α3 | Neuroectoderm, trigeminal nerve, cerebellum and spinal cord/brain neurons and glial cells | [76, 79] |
| | α4 | Dorsal root ganglion, cortical plate, endothelial cells, spinal cord/brain neurons and glial cells | [11, 72, 74, 76] |
| | α5 | Neural folds, cortical plate, spinal cord/brain neurons and glial cells | [74, 76, 80] |
| | β1 | Floor plate of spinal cord, spinal cord/brain neurons and glial cells | [75, 76] |
| | β2 | Cortical plate and spinal cord/brain neurons | [74, 76] |
| | β3 | Floor plate of spinal cord (?) | [75, 76] |
| | β4 | - | |
| | γ1 | Neural folds, neuroectoderm, basement membrane (BM) and pia, floor plate of spinal cord, spinal cord/brain neurons and glial cells | [75, 76, 80-86] |
| | γ2 | Epithelial cells and spinal cord/brain glial cells | [76, 87] |
| | γ3 | Cerebellar pia and retinal vascular BM | [81, 88] |
| Adulthood | α1 | Blood vessels | [89] |
| | α2 | Astrocytes, pericytes, neurons, oligodendrocytes, microglia, ependymal cell layer, blood vessels and fractones in neurogenic niches | [70, 84, 90-96] |
| | α3 | Microglia | [70] |
| | α4 | Brain microvascular endothelial cells (BMECs), pericytes, oligodendrocytes, microglia ependymal cell layer, blood vessels and fractones in neurogenic niches | [70, 82, 85, 86, 94, 95, 97] |
| | α5 | BMECs, pericytes, hippocampal neurons, oligodendrocytes, microglia, ependymal cell layer, blood vessels and fractones in neurogenic niches | [70, 82, 85, 86, 94, 95, 97-101] |

| | | |
|---|---|---|
| β1 | BMECs, astrocytes, pericytes, neurons oligodendrocytes, ependymal cell layer, blood vessels and fractones in neurogenic niches | [82, 84-86, 89-91, 94, 95, 97-102] |
| β2 | Blood vessels, pericytes and oligodendrocytes | [94, 97] |
| β3 | Oligodendrocytes | [94] |
| β4 | - | - |
| γ1 | BMECs, astrocytes, pericytes, neurons, oligodendrocytes, ependymal cell layer and fractones in neurogenic niches | [82, 84-86, 89-91, 94, 95, 97-104] |
| γ2 | Oligodendrocytes, ependymal cell layer, blood vessels and fractones in neurogenic niches | [94, 95] |
| γ3 | Veins and small-diameter capillaries, ependymal cell layer and fractones in neurogenic niches | [88, 95] |

Evidence from human fetal and mouse embryonic studies, demonstrated that laminin-111 is expressed throughout the CNS during embryogenesis and progressively disappears during development [75, 105, 106]. Further studies, revealed that different laminin subunits (α1, α2, α3, α4, α5, β1, β2, γ1, γ3) are expressed in the fetal human and embryonic mouse ventricular (VZ) and subventricular (SVZ) zone, cortical plate, and cerebellum, but the biological significance of these chains is still not well understood [70, 107]. In addition, laminins comprising the α5 chain was showed to have a functional role in neural tube formation and neural crest cell migration during mouse embryogenesis [108, 109]. Of note, the expression of laminin β3 chain at the embryonic stage, is still subject of great controversy [75, 76].

In the adult CNS, laminin can be found in almost all cell types, with a key role on the modulation of distinct functions [70, 95]. Among the different laminin isoforms, heterotrimers comprising the α5 chain (*e.g.* laminin-511 and -521) have been identified as the major neuronal laminins in adulthood [4-7].

### 3. Laminin in neurogenic niches

NSCs are multipotent stem cells responsible for generating the main cell types in the CNS (neurons and glial cells) during development and adulthood. Therefore, these cells will have a key role on the maintenance, repair and regeneration of the CNS. NSCs reside within specialized structures, the stem cell niches, where cell-cell interactions and local microenvironmental cues, including those from neighboring cells, humoral factors and ECM, are key to regulate stem cell behavior. During development, NSCs are distributed along the VZ of the neural tube, while in adult brain NSCs are restricted to specific neurogenic niches,

which include the subgranular zone (SGZ) of the dentate gyrus in the hippocampus or the SVZ on the lateral ventricules, which is the largest and most studied NSC niche [110].

The neurogenic niche in the SVZ of the adult brain (Fig. 3) is composed by support cells (endothelial cells and astrocytes), immature precursors and a monolayer of ependymal cells lining the lateral ventricle [111]. Moreover, the resident stem cell lineage in the SVZ comprises the relatively quiescent NSCs (type B cells) [112], which can self-renew or generate transit-amplifying cells (type C cells). The latter can, in turn, give rise to migratory neuroblasts (type A cells) and oligodendrocyte precursors [113, 114]. In the niche NSCs are surrounded by fractones, branched structures closely associated to blood vessels rich in several ECM components, including laminin, collagen IV, nidogen and proteoglycans [111]. These fingerlike projections of ECM can sequester neurogenic growth factors, such as fibroblast growth factor 2 from the ventricular cerebrospinal fluid, and, as such, are believed to be key for the modulation of neurogenesis *via* ECM-growth factor interactions [89]. Moreover, fractones are suggested to have a key role on the sequestration and maintenance of NSCs within the niche, mediated by cell-cell interactions. This was supported by studies showing that the *in vivo* blockage of the laminin $\alpha 6\beta 1$ receptor expressed by SVZ NSCs, favors the release of cells from the basal lamina and a subsequent increase in proliferation [115].

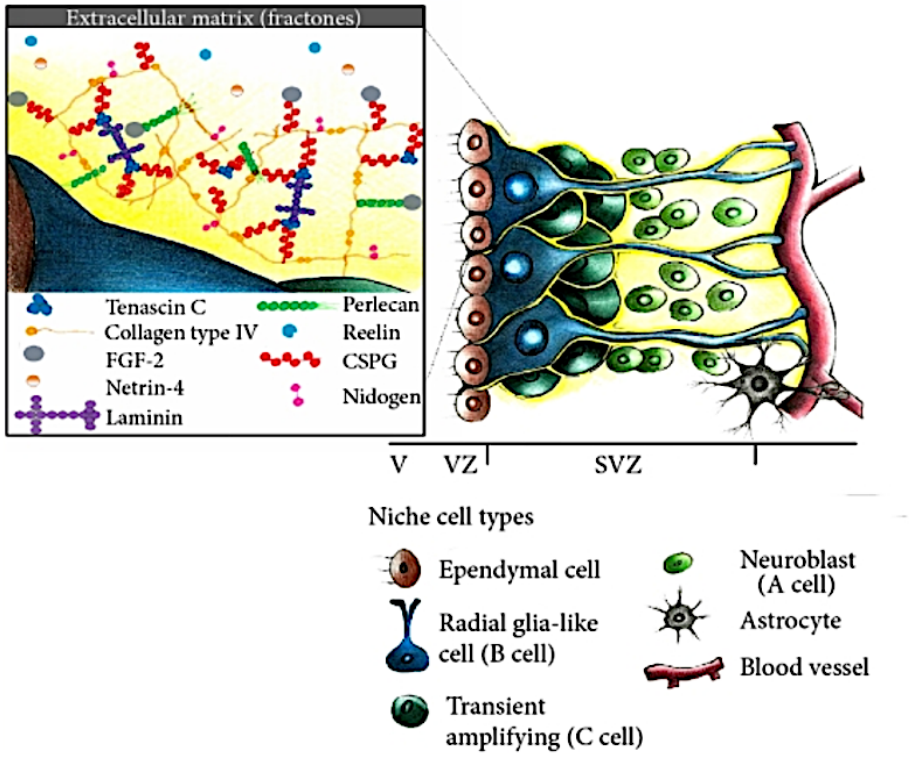


**Figure 3. The adult ventricular and subventricular zone (V-SVZ).** Three types of progenitor cells are found in close proximity to the ependymal cell layer and include a population of quiescent

NSCs/radial glia-like cells (type B cells) that can generate transit-amplifying cells (type C cells), which, in turn, will give rise to neuroblasts (type A cells). Endothelial cells and astrocytes, which function as support cells, as well as immature precursors can also be found within NSC niche. In addition to the cellular components, the SVZ includes several ECM components (yellow) called fractones, which include laminin, collagen IV, nidogen and proteoglycans. These contact with the different cell types composing the niche and are involved on the modulation of different cell functions. Adapted from [110], Copyright© 2016, Creative Commons License.

Laminin is one of the most important and well described ECM proteins within the neurogenic niches [89, 95]. This is evidenced by its key role in the modulation of neuronal progenitors proliferation and survival [116, 117], neurodevelopment [70] (Table 1), hippocampal regeneration [103] and on the regulation of growth factors concentration [89]. The expression of multiple $\alpha$, $\beta$ and $\gamma$ laminin chains have been described in association with the ependymal cells [95], the blood vessels [95], supporting cells (*e.g.* astrocytes) [118], and proliferating transit-amplifying cells (type C cells), under homeostatic conditions, as well as with cells of the NSC lineage in the regenerative niche [95]. More specifically, laminin $\alpha$1 chain can be found on blood vessels but not on fractones of adult rat, mouse or human NSC niche [89]. Laminin-511, in turn, is the major neuronal laminin in adult mice hippocampus BM and was showed to be important for hippocampal regeneration [100]. The differential expression of laminin isoforms, influence their ability to mediate different functions within the NSC niches. For example, laminin isoforms comprising the $\alpha$2 chain where shown to be required for oligodendrocyte maturation and CNS myelination in adult mice [96] under homeostasis conditions, while laminin-411 or -511 and laminin-111 or -211 produced by endothelial cells and astrocytes, respectively, participate in the formation of the blood-brain barrier [85]. Mutations in laminin $\beta$2 (mice) [119], $\gamma$1 (mice) [120] and $\gamma$3 (mice and human) [119, 121] chains, in turn, were showed to disturb processes like cortical histogenesis, as well as the formation of the pial BM. Nevertheless, the mechanism by which differentially expressed laminin isoforms modulate adult neurogenesis in not yet fully understood. In this regard, some studies suggest that rather than differences in ECM expression, changes in the expression of the major laminin receptors - integrins, dystroglycan and syndecans, seem to be responsible for the changes in ECM signaling that contribute to stem cell activation. Under normal conditions, although in adult mice NSCs and precursor cells reside in similar niches being exposed to similar ECM signals, NSCs, as result of the low expression of laminin receptors, have limited interaction with the laminin-rich microenvironment, remaining relatively quiescent [95]. After stimulation and activation of NSCs (*e.g.* in the regenerative niche that is triggered in the aftermath of a lesion), an increase on laminin synthesis, as well as an upregulation on the expression of different

laminin receptors, including $\alpha 6\beta 1$ integrin and syndecan-1 is observed [95], potentiating its interaction with the cellular and extracellular microenvironment.

The interplay between the niche components and NSCs will determine the balance between stemness and differentiation, quiescence and proliferation. In this regard, a number of experimental approaches perturbing the niches either through the genetic or cytotoxic ablation of the precursor cells or using specific culture models to evaluate the effect of specific components of the niches, have been proposed to better understand how changes in the ECM receptor expression regulates NSC behavior (for a more comprehensive review see [122]). However, the effect of the matrix itself remains to be elucidated. Envisaging the development of three-dimensional (3D) matrices able to recapitulate the complex arrangement of cells and ECM in the nervous system, and dissect the different roles exerted by the ECM and its molecular components on NSC behavior, in the last few years, much attention has been devoted towards the development of engineered matrices able to mimic the *in vivo* characteristics of NSC niches, and ultimately develop more efficient neuroregenerative approaches.

## 4. Laminin-inspired hydrogels to recreate the microenvironment of neurogenic niches

As discussed in the previous section, laminin was found to have a key role in the modulation of NSC function and fate within neurogenic niches. More specifically, this ECM protein was showed to be crucial for the modulation of cell adhesion and viability [123] and neuronal outgrowth and migration [124-126]. Works published to date exploring the immobilization of full-length laminin (Table 2) or their peptide analogues (Table 3), into hydrogel matrices, to recreate the NSC niche microenvironment, are summarized in this section. The developed 3D platforms were applied for the *in vitro* study of NSC biology and to assess their interactions with the surrounding microenvironment, as well as to evaluate the potential of the developed matrices to serve as vehicles for NSC transplantation in the context of neurological disorders. In addition to mimicking the ECM composition, replicating the mechanical and structural properties of the native niche is key for the modulation of different stem cell functions, including survival, proliferation and differentiation [127-129]. Indeed, studies using substrates with mechanical properties similar to that of native CNS (low compressive moduli – 0.1 – 1.0 kPa) have shown ability to support NSC function [130-135].

### *4.1. Hydrogels functionalized with full-length laminin*

The incorporation of a full-length protein onto hydrogels, and more specifically of laminin, has been widely explored for the development of biomimetic 3D matrices, to provide the gels with the bioactivity levels of the native protein. Indeed, several studies showed that the

modification of specific matrices with full-length laminin, in addition to render the microenvironment more permissive for NSC growth and differentiation, also contributed for an enhanced *in vivo* nervous regeneration [136-140]. Since the biological features of a protein result from its multiple bioactive domains and its conformation [141-143], the immobilization strategy explored will have a critical impact on the biofunctionality of the engineered hydrogels. Indeed, this is evident in some of the studies reported in Table 2, which point out that the immobilization approach significantly affects laminin function [144-147]. Strategies explored to date, for full-length laminin immobilization have relied either on its transient non-covalent incorporation or physical entrapment, or alternatively, on its non-selective covalent immobilization by taking advantage of functional groups present in multiple sites of the laminin structure, such as amines and thiols (Fig. 4). Despite widely used, these strategies lack the ability to control the conformation and orientation of bioactive molecules upon immobilization. As such, the exposure of key laminin bioactive domains, including those involved in laminin polymerization and on the modulation of NSC function and fate, can be compromised.

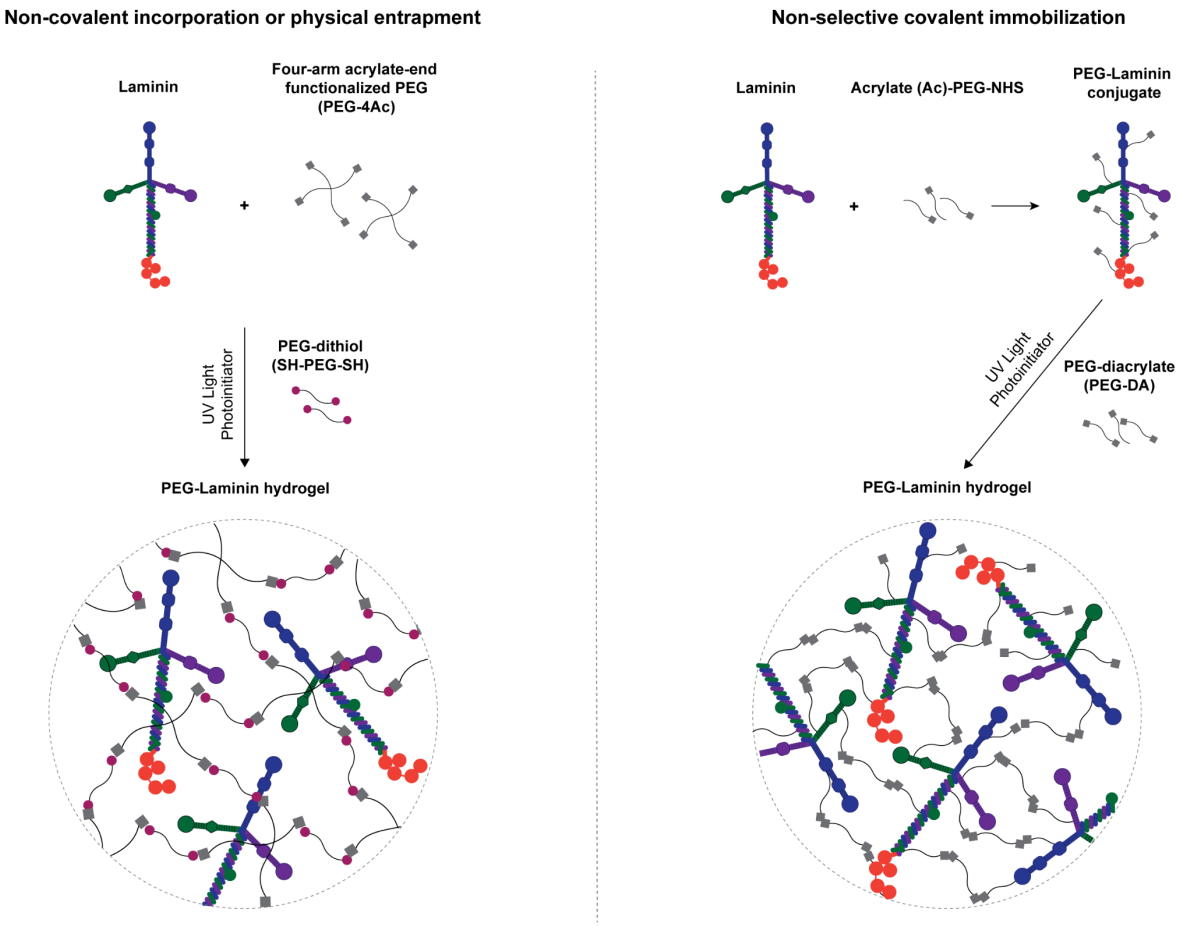


**Figure 4**. **Strategies currently explored for laminin immobilization into 3D cell instructive microenvironments.** Non-covalent incorporation or physical entrapment is used under the assumption the entrapped protein retains the overall properties of laminin matrices *in vivo*. Non-selective covalent immobilization, in turn, takes advantage of functional groups (*e.g.* amines and thiols) present in multiple sites on the laminin structure. Both strategies lack the ability to control the orientation and conformation of laminin upon immobilization, which may compromise the exposure of key laminin bioactive epitopes.

**Table 2.** Hydrogels functionalized with full-length laminin

| 3D Matrix composition | | Laminin immobilization strategy | Cell type | Biological outcome | | References |
|---|---|---|---|---|---|---|
| **Polymeric backbone** | **[Laminin-111]** | | | ***In vitro*** | ***In vivo*** | |
| Oxidized methylcellulose (OXMC) | 1.6 ng/mg OXMC | Schiff base reaction between laminin primary amines and carbonyl groups on OXMC | Primary rat cortical neurons | Supported cell adhesion and viability but not neurite outgrowth | - | [148] |
| Methylcellulose (MC) | 8.2 μg/mL MC | Reaction between laminin primary amines and NHS esters on sulfo-SANPAH ((sulfosuccinimidyl 6-(4'-azido-2'-nitrophenylamino)hexanoate)) and coupling of the photosensitive laminin conjugate to MC by exposure to ultraviolet (UV) light | Mouse neural stem cells (NSC) | Enhanced cell survival and neurite outgrowth; reduced apoptosis and provided an environment that fostered differentiation | Cell transplantation into a murine traumatic brain injury model favored a moderate increase in functional recovery | [144-147] |
| Thiolated HA (HA-S) | 100 μg/mL HA-S | Michael-type addition of laminin free thiol groups to vinyl groups on poly(ethylene glycol) divinyl sulfone (PEGDVS) prior to the crosslinking of HA-S by PEGDVS | Mouse neural stem/progenitor cells (NSPC) | Up-regulated the stromal cell-derived factor-1α (SDF-1α) receptor CXCR4 and provided the appropriate extracellular matrix | Favored the retention and migration of transplanted cells in response to SDF-1α in an intact mouse brain model | [138, 140] |

| | | | | | | |
|---|---|---|---|---|---|---|
| | | | | (ECM) cues to promote cell chemotactic migration in response to SDF-1α | | |
| HA-S + salmon fibrinogen+ salmon thrombin | 100 μg/mL HA-S | Incorporation in the hydrogel precursor solution prior to the cleavage of fibrinogen by thrombin to induce the formation of an interpenetrating polymer network (IPN) hydrogel | Human NSPC | Supported cell proliferation and differentiation. Significantly reduced the cell-mediated degradation seen with fibrin alone. Supported vascularization as evidenced on hNSPCs - human endothelial colony-forming cell-derived endothelial cells (hECFC-ECs) co-culture studies | - | [139] |
| Agarose | 0.120 – 0.162 μg/mL agarose gradient | Reaction between laminin-111 primary amines groups and NHS esters on sulfo-SANPAH and coupling of the laminin-111 photosensitive conjugate to agarose by exposure to UV light | Dorsal root ganglia (DRG) | Neurite extension was significantly higher in the anisotropic scaffolds compared to isotropic scaffolds | - | [136] |

| | | | | | | |
|---|---|---|---|---|---|---|
| Acrylate (Ac)-Poly(ethylene glycol) (PEG) - N-hydroxysuccinimide (NHS) + PEG-diacrylate (DA) | 1 – 100 μg/mL PEG-DA | Reaction between laminin primary amines and NHS groups on Ac-PEG-NHS (4 NHS : 1 laminin) and coupling of the laminin conjugate to PEG-DA by exposure to UV light | DRG | Neurite outgrowth was significantly favored in the presence of increased concentrations of laminin | - | [137] |
| PEG-DA | | Laminin physically entrapped | | | | |
| Collagen I | 1 – 100 μg/mL collagen I | Incorporation in collagen solution prior to the thermally-induced hydrogel gelation | DRG | Increased concentrations of laminin reduced neurite growth without impacting the stiffness of the hydrogels | - | [149] |
| Collagen I + HA | 1.5 mg/mL collagen I + HA | Incorporation in hydrogel precursor solution prior thermally-induced hydrogel gelation | Rat NPC | Increase in oligodendrocyte differentiation | NPCs transplantation within the three-component hydrogel to a rat spinal cord injury (SCI) model promoted an increased functional recovery over 6 weeks | [150] |

| | | | | | | |
|---|---|---|---|---|---|---|
| Dibenzocyclooctyne (DIBO)-PEG | 50 ng/g DIBO-PEG | Reaction between laminin primary amines and NHS groups on azide-PEG-NHS and coupling of the laminin conjugate to DIBO-PEG by copper-free azide-alkyne reaction prior to the addition of the crosslinker (four arm PEG tetraazide) | Rat NSPC | Supported high cell viability and efficiently directed cell differentiation to neurons without the need for additional supplementation | - | [151] |

Studies published to date, exploring full-length laminin immobilization, for the development of 3D matrices mimicking the NSC niche microenvironment, used laminin-111, as this isoform was already showed to successfully promote neuronal outgrowth and differentiation. Nevertheless, and considering the key role of other laminin isoforms (*e.g.* laminin-521) on the *in vitro* modulation of neural cell behavior including neuronal adhesion, viability and network formation [123, 152], future studies evaluating their impact on NSC behavior and function, after incorporation within 3D matrices, should be conducted.

The endogenous process of cell replacement in the adult human CNS is far from being sufficient to repair the damaged caused after an injury. Therefore, and although in this section we highlight the studies exploring hydrogels functionalized with full-length laminin for NSC culture and transplantation, the potential of these hydrogels to allow infiltration of endogenous neural progenitors recruited to the injury site, and ultimately contribute to tissue repair was also evaluated [153]. More specifically, a laminin-functionalized hyaluronic acid (HA)-based hydrogel was showed to efficiently support endogenous cell infiltration and angiogenesis, while inhibited the formation of the glial scar and promoted neurite extension in a rat model of brain lesion.

In addition to their application in the framework of nervous regeneration and tissue engineering, the incorporation of full-length laminin on 3D matrices has also been explored for application in different disease contexts, including skeletal muscle [154, 155], intervertebral disc [156, 157] and vascular regeneration [158, 159].

### *4.2. Hydrogels functionalized with laminin-derived peptides*

Laminin-derived small adhesive sequences have been increasingly explored, in alternative to full-length laminin, to confer bioactivity to 3D matrices. These small sequences have several advantageous features, including their ability to be chemically synthesized in large scale, the higher resistance to denaturation and enzymatic degradation, ability to be incorporated at higher densities for similar amounts of native protein and lower risk of induce immune rejection [160]. Different small peptide sequences derived from laminin, including YIGSR, IKVAV, RGD (cryptic domain in laminin $\alpha$1 chain), RNIAEIIKDI, RKRLQVQSIRT, are known to mediate neuronal adhesion, neurite outgrowth and/or NSC migration, and, as such, have been widely explored for the design of biomimetic 3D matrices for cell culture and transplantation (Table 3).

**Table 3.** Hydrogels functionalized with laminin-derived peptides

| Sequence | Origin | Polymeric backbone | Cell type | Biological outcome | | References |
|---|---|---|---|---|---|---|
| | | | | *In vitro* | *In vivo* | |
| CCRRI**KVAV**WLC (Cyclic IKVAV) | Mouse laminin α1 chain | Poly(ethylene glycol) (PEG) | Human neural stem/progenitor cells (NSPC) | Supported cell adhesion, proliferation, migration and neuronal differentiation | - | [161] |
| IKVAV | Mouse laminin α1 chain | Silk Fibroin | Human neural stem cells (NSC) | Increased cell viability, proliferation, neuronal differentiation and maturation, compared to unmodified hydrogels | - | [162] |
| | | PEG | Mouse neural progenitor cells (NPC) | Long-term cell survival and proliferation | - | [163] |
| | | | PC12 | Supported cell adhesion, viability, outgrowth and neuronal differentiation | - | [164] |
| | | Fibrin | Dorsal root ganglia (DRG) | Increased neurite outgrowth with increased concentration of covalently-bound peptide | - | [165] |

| | | | | | | |
|---|---|---|---|---|---|---|
| | | Peptide amphiphile (PA) | Mouse NPC | Support cell viability, outgrowth and neuronal differentiation | - | [166] |
| | | | Rat NSC | - | Enhanced survival of cells transplanted within RADA16-IKVAV hydrogels and higher tendency towards differentiation along the neuronal lineage | [167] |
| | | | Mouse NPC | IKVAV presentation enhanced the growth of neurites from cells with aligned PA nanofibers. After 2 weeks of culture, the neurons displayed spontaneous electrical activity and ability to establish synaptic connections | IKVAV modification of scaffolds in combination with PA nanofibers alignment promoted an oriented growth of cellular processes on cells transplanted to a rat SCI model | [168] |
| | | Agarose | PC12 | Enhanced neurite outgrowth | - | [169] |

| | | | | | | |
|---|---|---|---|---|---|---|
| YIGSR | Mouse laminin β1 chain | PEG | Mouse NPC | Promoted long-term cell survival and proliferation | - | [163] |
| | | | PC12 | Promoted cell viability and retention of the neuronal phenotype following cell release from the gels | - | [164] |
| | | Fibrin | DRGs | Increased neurite outgrowth with increased concentrations of covalently-bound peptide | - | [165] |
| | | Agarose | DRGs | Enhanced neurite outgrowth | - | [169] |
| RGD | Cryptic domain in laminin α1 chain | Fibrin | DRGs | Increased neurite outgrowth with increasing concentrations of covalently-bound peptide | - | [165, 170] |
| RNIAEIIKDI | Mouse laminin γ1 chain | Fibrin | DRGs | Increased neurite outgrowth with increasing concentrations of | - | [165] |

| | | | | | | |
|---|---|---|---|---|---|---|
| | | | | covalently-bound peptide | | |
| RKRLQVQLSIRT (AG73) | LG4 module of mouse laminin $\alpha$1 chain | Alginate | PC12 | Enhanced cell attachment and neurite outgrowth | - | [171] |
| | | Collagen | | | | [172] |
| | | Agarose | | | | [173] |
| | | Fibrin | Human NSC | Efficiently promoted neurite outgrowth | - | [174] |
| PPFLMLLKGSTR (G3P) | LG3 domain of laminin $\alpha$3 chain | Collagen | Rat NSC | Enhanced cell adhesion and survival | - | [175] |
| LG3 / FNTPSIEKP (LP) | Heterodimer consisting of the LG3 domain of laminin $\alpha$1 chain (LG3) and the C-terminal peptide from laminin $\gamma$1 chain (LP) | Collagen | Rat NSC | Promoted cell viability | - | [176] |

Peptides IKVAV, found in laminin α1 chain [177] and YIGSR, found in laminin β1 chain [69, 178, 179] bind to the 110 kDa [68] and 67 kDa [69] cell surface receptor, respectively, and are both recognized by the β1 integrin receptor subunit, which is highly expressed by neural stem/progenitor cells (NSPCs) [180, 181]. RNIAEIIKDI is a sequence present in mouse laminin γ1 chain [182, 183] found to promote neurite outgrowth of DRGs [165]. The RKRLQVQSIRT sequence, also known as AG73 peptide, is derived from the LG4 module of mouse laminin α1 chain [184] and was showed to interact with syndecan-1 [185, 186] and -4 [187]. This peptide was already successfully used to modify different natural hydrogel matrices, including alginate, agarose, collagen and fibrin, with promising results in terms of the promotion of neurite outgrowth in PC12 cells [171-174, 188] and hNSCs [174]. The RGD domain sequence found in many ECM proteins, including fibronectin and laminin (as a cryptic domain in laminin α1 chain), was shown to interact with α5β1 and αvβ3 integrins [189]. Its incorporation into both natural and synthetic-derived matrices is effective in promoting NSC adhesion and neurite outgrowth [164, 168, 190-192].

Laminin-derived peptide fragments produced by recombinant DNA technology have also been explored for the development of 3D matrices. More specifically, a peptide derived from the LG3 domain of laminin α3 chain - G3P peptide (PPFLMLLKGSTR), which binds with strong affinity to α3β1 integrin [193], was recombinantly modified to include a collagen binding domain. The resultant recombinant peptide was further explored for the functionalization of a collagen-based hydrogel, which evidenced ability to efficiently support NSC adhesion and survival [175]. A different study, explored the incorporation of a recombinant heterodimer combining peptides derived from the LG3 domain of mouse laminin α1 chain and the C-terminal peptide from laminin γ1 chain (LP) [176] on collagen hydrogels. Alternatively, a recombinant laminin fragment - E8 fragment, which is a truncated protein composed of the C-terminal region of the α, β and γ chains, was explored [194]. Unlike the recombinant peptide fragments previously described, this truncated protein retains laminin integrin-binding activity, as evidenced by the ability of laminin-511-derived E8 fragment to strongly promote the adhesion and proliferation of human pluripotent stem cells, when compared to Matrigel and the full-length laminin isoform [195]. Accordingly, and envisaging the development of collagen matrices with laminin-like adhesive activity, the N-terminal of individual chains (α, β and/or γ) in the truncated protein was modified with a collagen-binding domain (CBD), to confer the E8 fragment collagen-binding activity. The developed matrices were shown to support the proliferation of human induced pluripotent stem cells (hiPSCs), both in 2D and 3D, though the morphology of cells grown in each condition was quite different [194].

To better recapitulate the biological activity of laminin chains, in the last few years several studies have been exploring the additive or synergistic effect of the combined incorporation of different laminin cell adhesive peptides (*e.g.* IKVAV, YIGSR, RGD, AG73, RNIAEIIKDI). For example, a study exploring the modification of fibrin hydrogels with a combination, in equimolar ratios, of RGD, IKVAV, YIGSR and RNIAEIIKDI, showed that these peptides have a synergistic effect on neurite outgrowth when used to bridge a 4 mm gap in a rat dorsal root [165]. In a different study, the modification of dextran hydrogels with a mixture of equimolar concentration (1:1) of IKVAV and YIGSR, was showed to better support *in vitro* DRG adhesion and neurite outgrowth, when compared to RGD-modified hydrogels [196]. Despite the promising results obtained to date, the use of the "typical" equimolar concentration of each peptide has not always proven to be efficient, in terms of supporting cell survival and differentiation [197]. Therefore, an important factor one should consider when developing hydrogels incorporating different ECM-derived peptides, is the need to understand the effect of each individual factor, as well as the interacting factor effects for each system. With this in mind, and to make the process less time-consuming, Segura and co-workers proposed the use of multifactorial experiments. Here, candidate adhesion motifs and growth factors were systematically varied *in vitro* to determine the individual and combinatorial effects of each factor on cell activity, enabling the optimization of a system capable of supporting hNPCs (iPS-NPCs) survival, proliferation and differentiation [197, 198]. The optimized hydrogel was further tested *in vivo*, in an animal model of stroke. Results evidenced the ability of the proposed matrix to support the survival of encapsulated hNPCs (iPS-NPCs) after transplantation into the stroke core, as well as to differentially tune transplanted cell fate through the promotion of glial, neuronal or immature/progenitor states [198].

## 5. Engineering laminin-inspired hydrogels: progress and future challenges

As a consequence of the key role of laminin within neurogenic niches, the potential of several laminin-inspired hydrogels, exploring either the full-length laminin or its peptide analogues, in a neural regeneration context, have been explored in different works (Table 2 and 3). Proof-of-principle of the suitability of these hydrogels in terms of ability to create a permissive microenvironment for cell growth and differentiation *in vitro*, as well as the *in vivo* biological performance of several of these matrices when explored for cell delivery, was highlighted in this chapter. The results obtained to date, strongly suggest that these hydrogels may serve as powerful artificial niches to modulate NSC fate and function for regenerative medicine applications.

To pave the way for the translation of laminin-inspired hydrogels to a clinical setting, a number of requisites need to be fulfilled and a few key issues must be taken into

consideration. Different hydrogel factors known to impact stem cell fate, including biocompatibility, controlled biodegradability and non-immunogenicity, should be considered when designing cell-instructive microenvironments. Physical properties (*e.g.* mechanical and structural properties) should also be taken into consideration, as these are known to have an impact on cell behavior and function [127-129]. Therefore, the characterization of the developed hydrogels in terms of physical properties, should be carried out in a number of *in vitro* and *in vivo* set-ups, before considering clinical translation. The selection of the most appropriate system for a specific application, is one of the most important issues to take into consideration, as the selected building blocks should allow the ease modification with bioactive molecules (*e.g.* ECM proteins and/or peptides, growth factors or drugs), while assuring spatial and temporal control over their exposure. As described in the previous sections, a lot of progress has already been achieved in this regard, and specifically on the immobilization of full-length laminin and its peptide analogues. However, a major challenge one faces when developing hydrogels with tethered bioactive factors, such as proteins and peptides, is the selection of the most appropriate immobilization chemistry, as this should assure control over peptide/protein conformation and temporal availability. This was proven to have a significant impact on protein/peptide bioactivity and ultimately on their ability to modulate cellular behavior [141-143, 199]. Therefore, the development of strategies allowing a selective and controlled presentation of bioactive epitopes is highly desirable as these are expected to allow the mirroring of what is observed in the native ECM. Consequently, in recent years immobilization strategies have shift towards site-specific conjugation approaches, such as biorthogonal chemical reactions (click chemistry), enzymatic ligation or affinity binding, using either unnatural amino acids or engineered site-selective amino acid sequences (for a more comprehensive review see [200]). These are expected to provide a higher retention of bioactivity by assuring a better control over biomolecules orientation and conformation.

Despite the effort made in the last few years to improve the potential of laminin-inspired hydrogels, the search for a more accurate platform with application in *in vitro* studies and regenerative medicine is still a long way off.

## References

[1] M. Aumailley, L. Bruckner-Tuderman, W.G. Carter, R. Deutzmann, D. Edgar, P. Ekblom, J. Engel, E. Engvall, E. Hohenester, J.C. Jones, H.K. Kleinman, M.P. Marinkovich, G.R. Martin, U. Mayer, G. Meneguzzi, J.H. Miner, K. Miyazaki, M. Patarroyo, M. Paulsson, V. Quaranta, J.R. Sanes, T. Sasaki, K. Sekiguchi, L.M. Sorokin, J.F. Talts, K. Tryggvason, J. Uitto, I. Virtanen, K. von der Mark, U.M. Wewer, Y. Yamada, P.D. Yurchenco, A simplified laminin nomenclature, Matrix Biol 24(5) (2005) 326-32.

[2] J. Tzu, M.P. Marinkovich, Bridging structure with function: structural, regulatory, and developmental role of laminins, Int J Biochem Cell Biol 40(2) (2008) 199-214.

[3] M. Durbeej, Laminins, Cell Tissue Res 339(1) (2010) 259-68.

[4] J.H. Miner, R.M. Lewis, J.R. Sanes, Molecular cloning of a novel laminin chain, alpha 5, and widespread expression in adult mouse tissues, J Biol Chem 270(48) (1995) 28523-6.

[5] J.H. Miner, P.D. Yurchenco, Laminin functions in tissue morphogenesis, Annu Rev Cell Dev Biol 20 (2004) 255-84.

[6] A. Domogatskaya, S. Rodin, K. Tryggvason, Functional diversity of laminins, Annu Rev Cell Dev Biol 28 (2012) 523-53.

[7] M. Aumailley, The laminin family, Cell Adh Migr 7(1) (2013) 48-55.

[8] K. Ehrig, I. Leivo, W.S. Argraves, E. Ruoslahti, E. Engvall, Merosin, a tissue-specific basement membrane protein, is a laminin-like protein, Proc Natl Acad Sci U S A 87(9) (1990) 3264-8.

[9] B.L. Patton, J.H. Miner, A.Y. Chiu, J.R. Sanes, Distribution and function of laminins in the neuromuscular system of developing, adult, and mutant mice, J Cell Biol 139(6) (1997) 1507-21.

[10] P.D. Yurchenco, Integrating Activities of Laminins that Drive Basement Membrane Assembly and Function, Curr Top Membr 76 (2015) 1-30.

[11] M. Frieser, H. Nockel, F. Pausch, C. Roder, A. Hahn, R. Deutzmann, L.M. Sorokin, Cloning of the mouse laminin alpha 4 cDNA. Expression in a subset of endothelium, Eur J Biochem 246(3) (1997) 727-35.

[12] J. Thyboll, J. Kortesmaa, R. Cao, R. Soininen, L. Wang, A. Iivanainen, L. Sorokin, M. Risling, Y. Cao, K. Tryggvason, Deletion of the laminin alpha4 chain leads to impaired microvessel maturation, Mol Cell Biol 22(4) (2002) 1194-202.

[13] N. Petajaniemi, M. Korhonen, J. Kortesmaa, K. Tryggvason, K. Sekiguchi, H. Fujiwara, L. Sorokin, L.E. Thornell, Z. Wondimu, D. Assefa, M. Patarroyo, I. Virtanen, Localization of laminin alpha4-chain in developing and adult human tissues, J Histochem Cytochem 50(8) (2002) 1113-30.

[14] P. Rousselle, G.P. Lunstrum, D.R. Keene, R.E. Burgeson, Kalinin: an epithelium-specific basement membrane adhesion molecule that is a component of anchoring filaments, J Cell Biol 114(3) (1991) 567-76.
[15] R. Doliana, I. Bellina, F. Bucciotti, M. Mongiat, R. Perris, A. Colombatti, The human alpha3b is a 'full-sized' laminin chain variant with a more widespread tissue expression than the truncated alpha3a, FEBS Lett 417(1) (1997) 65-70.
[16] K.I. Gawlik, J.Y. Li, A. Petersen, M. Durbeej, Laminin alpha1 chain improves laminin alpha2 chain deficient peripheral neuropathy, Hum Mol Genet 15(18) (2006) 2690-700.
[17] P.R. Macdonald, A. Lustig, M.O. Steinmetz, R.A. Kammerer, Laminin chain assembly is regulated by specific coiled-coil interactions, J Struct Biol 170(2) (2010) 398-405.
[18] H.H. Yan, C.Y. Cheng, Laminin alpha 3 forms a complex with beta3 and gamma3 chains that serves as the ligand for alpha 6beta1-integrin at the apical ectoplasmic specialization in adult rat testes, J Biol Chem 281(25) (2006) 17286-303.
[19] K.H. Susek, E. Korpos, J. Huppert, C. Wu, I. Savelyeva, F. Rosenbauer, C. Muller-Tidow, S. Koschmieder, L. Sorokin, Bone marrow laminins influence hematopoietic stem and progenitor cell cycling and homing to the bone marrow, Matrix Biol 67 (2018) 47-62.
[20] K. Beck, I. Hunter, J. Engel, Structure and function of laminin: anatomy of a multidomain glycoprotein, FASEB J 4(2) (1990) 148-60.
[21] D.A. Parry, R.D. Fraser, J.M. Squire, Fifty years of coiled-coils and alpha-helical bundles: a close relationship between sequence and structure, J Struct Biol 163(3) (2008) 258-69.
[22] G. Armony, E. Jacob, T. Moran, Y. Levin, T. Mehlman, Y. Levy, D. Fass, Cross-linking reveals laminin coiled-coil architecture, Proc Natl Acad Sci U S A 113(47) (2016) 13384-13389.
[23] R. Timpl, D. Tisi, J.F. Talts, Z. Andac, T. Sasaki, E. Hohenester, Structure and function of laminin LG modules, Matrix Biol 19(4) (2000) 309-17.
[24] A. Sonnenberg, C.J. Linders, P.W. Modderman, C.H. Damsky, M. Aumailley, R. Timpl, Integrin recognition of different cell-binding fragments of laminin (P1, E3, E8) and evidence that alpha 6 beta 1 but not alpha 6 beta 4 functions as a major receptor for fragment E8, J Cell Biol 110(6) (1990) 2145-55.
[25] M. Aumailley, R. Timpl, A. Sonnenberg, Antibody to integrin alpha 6 subunit specifically inhibits cell-binding to laminin fragment 8, Exp Cell Res 188(1) (1990) 55-60.
[26] J.F. Talts, Z. Andac, W. Gohring, A. Brancaccio, R. Timpl, Binding of the G domains of laminin alpha1 and alpha2 chains and perlecan to heparin, sulfatides, alpha-dystroglycan and several extracellular matrix proteins, EMBO J 18(4) (1999) 863-70.

[27] D. Tisi, J.F. Talts, R. Timpl, E. Hohenester, Structure of the C-terminal laminin G-like domain pair of the laminin alpha2 chain harbouring binding sites for alpha-dystroglycan and heparin, EMBO J 19(7) (2000) 1432-40.

[28] D. Harrison, S.A. Hussain, A.C. Combs, J.M. Ervasti, P.D. Yurchenco, E. Hohenester, Crystal structure and cell surface anchorage sites of laminin alpha1LG4-5, J Biol Chem 282(15) (2007) 11573-81.

[29] J. Ishihara, A. Ishihara, K. Fukunaga, K. Sasaki, M.J.V. White, P.S. Briquez, J.A. Hubbell, Laminin heparin-binding peptides bind to several growth factors and enhance diabetic wound healing, Nat Commun 9(1) (2018) 2163.

[30] P.D. Yurchenco, E.C. Tsilibary, A.S. Charonis, H. Furthmayr, Laminin polymerization in vitro. Evidence for a two-step assembly with domain specificity, J Biol Chem 260(12) (1985) 7636-44.

[31] P.D. Yurchenco, Y.S. Cheng, Self-assembly and calcium-binding sites in laminin. A three-arm interaction model, J Biol Chem 268(23) (1993) 17286-99.

[32] Y.S. Cheng, M.F. Champliaud, R.E. Burgeson, M.P. Marinkovich, P.D. Yurchenco, Self-assembly of laminin isoforms, J Biol Chem 272(50) (1997) 31525-32.

[33] K.J. Hamill, K. Kligys, S.B. Hopkinson, J.C. Jones, Laminin deposition in the extracellular matrix: a complex picture emerges, J Cell Sci 122(Pt 24) (2009) 4409-17.

[34] E. Hohenester, P.D. Yurchenco, Laminins in basement membrane assembly, Cell Adh Migr 7(1) (2013) 56-63.

[35] J.C. Schittny, P.D. Yurchenco, Terminal short arm domains of basement membrane laminin are critical for its self-assembly, J Cell Biol 110(3) (1990) 825-32.

[36] K.K. McKee, D. Harrison, S. Capizzi, P.D. Yurchenco, Role of laminin terminal globular domains in basement membrane assembly, J Biol Chem 282(29) (2007) 21437-47.

[37] S.A. Hussain, F. Carafoli, E. Hohenester, Determinants of laminin polymerization revealed by the structure of the alpha5 chain amino-terminal region, EMBO Rep 12(3) (2011) 276-82.

[38] A. Purvis, E. Hohenester, Laminin network formation studied by reconstitution of ternary nodes in solution, J Biol Chem 287(53) (2012) 44270-7.

[39] F. Carafoli, S.A. Hussain, E. Hohenester, Crystal structures of the network-forming short-arm tips of the laminin beta1 and gamma1 chains, PLoS One 7(7) (2012) e42473.

[40] M.W. Cohen, C. Jacobson, P.D. Yurchenco, G.E. Morris, S. Carbonetto, Laminin-induced clustering of dystroglycan on embryonic muscle cells: comparison with agrin-induced clustering, J Cell Biol 136(5) (1997) 1047-58.

[41] H. Colognato, P.D. Yurchenco, The laminin alpha2 expressed by dystrophic dy(2J) mice is defective in its ability to form polymers, Curr Biol 9(22) (1999) 1327-30.

[42] K.K. McKee, S. Capizzi, P.D. Yurchenco, Scaffold-forming and Adhesive Contributions of Synthetic Laminin-binding Proteins to Basement Membrane Assembly, J Biol Chem 284(13) (2009) 8984-94.
[43] H. Colognato, D.A. Winkelmann, P.D. Yurchenco, Laminin polymerization induces a receptor-cytoskeleton network, J Cell Biol 145(3) (1999) 619-31.
[44] S. Li, P. Liquari, K.K. McKee, D. Harrison, R. Patel, S. Lee, P.D. Yurchenco, Laminin-sulfatide binding initiates basement membrane assembly and enables receptor signaling in Schwann cells and fibroblasts, J Cell Biol 169(1) (2005) 179-89.
[45] S. Li, D. Harrison, S. Carbonetto, R. Fassler, N. Smyth, D. Edgar, P.D. Yurchenco, Matrix assembly, regulation, and survival functions of laminin and its receptors in embryonic stem cell differentiation, J Cell Biol 157(7) (2002) 1279-90.
[46] E. Freire, T. Coelho-Sampaio, Self-assembly of laminin induced by acidic pH, J Biol Chem 275(2) (2000) 817-22.
[47] M. Dziadek, M. Paulsson, R. Timpl, Identification and interaction repertoire of large forms of the basement membrane protein nidogen, EMBO J 4(10) (1985) 2513-8.
[48] M. Paulsson, M. Aumailley, R. Deutzmann, R. Timpl, K. Beck, J. Engel, Laminin-nidogen complex. Extraction with chelating agents and structural characterization, Eur J Biochem 166(1) (1987) 11-9.
[49] T.R. Patel, C. Bernards, M. Meier, K. McEleney, D.J. Winzor, M. Koch, J. Stetefeld, Structural elucidation of full-length nidogen and the laminin-nidogen complex in solution, Matrix Biol 33 (2014) 60-7.
[50] M.S. Ho, K. Bose, S. Mokkapati, R. Nischt, N. Smyth, Nidogens-Extracellular matrix linker molecules, Microsc Res Tech 71(5) (2008) 387-95.
[51] M.A. Ruegg, J.L. Bixby, Agrin orchestrates synaptic differentiation at the vertebrate neuromuscular junction, Trends Neurosci 21(1) (1998) 22-7.
[52] J.B. Mascarenhas, M.A. Ruegg, U. Winzen, W. Halfter, J. Engel, J. Stetefeld, Mapping of the laminin-binding site of the N-terminal agrin domain (NtA), EMBO J 22(3) (2003) 529-36.
[53] G. Bezakova, M.A. Ruegg, New insights into the roles of agrin, Nat Rev Mol Cell Biol 4(4) (2003) 295-308.
[54] V.S. LeBleu, B. Macdonald, R. Kalluri, Structure and function of basement membranes, Exp Biol Med (Maywood) 232(9) (2007) 1121-9.
[55] D.T. Behrens, D. Villone, M. Koch, G. Brunner, L. Sorokin, H. Robenek, L. Bruckner-Tuderman, P. Bruckner, U. Hansen, The epidermal basement membrane is a composite of separate laminin- or collagen IV-containing networks connected by aggregated perlecan, but not by nidogens, J Biol Chem 287(22) (2012) 18700-9.

[56] M.F. Champliaud, G.P. Lunstrum, P. Rousselle, T. Nishiyama, D.R. Keene, R.E. Burgeson, Human amnion contains a novel laminin variant, laminin 7, which like laminin 6, covalently associates with laminin 5 to promote stable epithelial-stromal attachment, J Cell Biol 132(6) (1996) 1189-98.

[57] P. Rousselle, D.R. Keene, F. Ruggiero, M.F. Champliaud, M. Rest, R.E. Burgeson, Laminin 5 binds the NC-1 domain of type VII collagen, J Cell Biol 138(3) (1997) 719-28.

[58] M. Chen, M.P. Marinkovich, J.C. Jones, E.A. O'Toole, Y.Y. Li, D.T. Woodley, NC1 domain of type VII collagen binds to the beta3 chain of laminin 5 via a unique subdomain within the fibronectin-like repeats, J Invest Dermatol 112(2) (1999) 177-83.

[59] K. Tasanen, L. Tunggal, G. Chometon, L. Bruckner-Tuderman, M. Aumailley, Keratinocytes from patients lacking collagen XVII display a migratory phenotype, Am J Pathol 164(6) (2004) 2027-38.

[60] A. Utani, M. Nomizu, Y. Yamada, Fibulin-2 binds to the short arms of laminin-5 and laminin-1 via conserved amino acid sequences, J Biol Chem 272(5) (1997) 2814-20.

[61] M. Yamada, K. Sekiguchi, Molecular Basis of Laminin-Integrin Interactions, Curr Top Membr 76 (2015) 197-229.

[62] R. Nishiuchi, J. Takagi, M. Hayashi, H. Ido, Y. Yagi, N. Sanzen, T. Tsuji, M. Yamada, K. Sekiguchi, Ligand-binding specificities of laminin-binding integrins: a comprehensive survey of laminin-integrin interactions using recombinant alpha3beta1, alpha6beta1, alpha7beta1 and alpha6beta4 integrins, Matrix Biol 25(3) (2006) 189-97.

[63] N. Suzuki, F. Yokoyama, M. Nomizu, Functional sites in the laminin alpha chains, Connect Tissue Res 46(3) (2005) 142-52.

[64] H. Ido, S. Ito, Y. Taniguchi, M. Hayashi, R. Sato-Nishiuchi, N. Sanzen, Y. Hayashi, S. Futaki, K. Sekiguchi, Laminin isoforms containing the gamma3 chain are unable to bind to integrins due to the absence of the glutamic acid residue conserved in the C-terminal regions of the gamma1 and gamma2 chains, J Biol Chem 283(42) (2008) 28149-57.

[65] Y. Taniguchi, H. Ido, N. Sanzen, M. Hayashi, R. Sato-Nishiuchi, S. Futaki, K. Sekiguchi, The C-terminal region of laminin beta chains modulates the integrin binding affinities of laminins, J Biol Chem 284(12) (2009) 7820-31.

[66] M. Aumailley, R. Timpl, W. Risau, Differences in laminin fragment interactions of normal and transformed endothelial cells, Exp Cell Res 196(2) (1991) 177-83.

[67] N. Suzuki, H. Nakatsuka, M. Mochizuki, N. Nishi, Y. Kadoya, A. Utani, S. Oishi, N. Fujii, H.K. Kleinman, M. Nomizu, Biological activities of homologous loop regions in the laminin alpha chain G domains, J Biol Chem 278(46) (2003) 45697-705.

[68] H.K. Kleinman, B.S. Weeks, F.B. Cannon, T.M. Sweeney, G.C. Sephel, B. Clement, M. Zain, M.O. Olson, M. Jucker, B.A. Burrous, Identification of a 110-kDa nonintegrin cell

surface laminin-binding protein which recognizes an A chain neurite-promoting peptide, Arch Biochem Biophys 290(2) (1991) 320-5.
[69] S.P. Massia, S.S. Rao, J.A. Hubbell, Covalently immobilized laminin peptide Tyr-Ile-Gly-Ser-Arg (YIGSR) supports cell spreading and co-localization of the 67-kilodalton laminin receptor with alpha-actinin and vinculin, J Biol Chem 268(11) (1993) 8053-9.
[70] A. Nirwane, Y. Yao, Laminins and their receptors in the CNS, Biol Rev Camb Philos Soc (2018).
[71] R. Vuolteenaho, M. Nissinen, K. Sainio, M. Byers, R. Eddy, H. Hirvonen, T.B. Shows, H. Sariola, E. Engvall, K. Tryggvason, Human laminin M chain (merosin): complete primary structure, chromosomal assignment, and expression of the M and A chain in human fetal tissues, J Cell Biol 124(3) (1994) 381-94.
[72] J.H. Miner, B.L. Patton, S.I. Lentz, D.J. Gilbert, W.D. Snider, N.A. Jenkins, N.G. Copeland, J.R. Sanes, The laminin alpha chains: expression, developmental transitions, and chromosomal locations of alpha1-5, identification of heterotrimeric laminins 8-11, and cloning of a novel alpha3 isoform, J Cell Biol 137(3) (1997) 685-701.
[73] T. Sasaki, R. Giltay, U. Talts, R. Timpl, J.F. Talts, Expression and distribution of laminin alpha1 and alpha2 chains in embryonic and adult mouse tissues: an immunochemical approach, Exp Cell Res 275(2) (2002) 185-99.
[74] J.D. Lathia, B. Patton, D.M. Eckley, T. Magnus, M.R. Mughal, T. Sasaki, M.A. Caldwell, M.S. Rao, M.P. Mattson, C. ffrench-Constant, Patterns of laminins and integrins in the embryonic ventricular zone of the CNS, J Comp Neurol 505(6) (2007) 630-43.
[75] M. Wiksten, R. Liebkind, T. Laatikainen, P. Liesi, Gamma 1 laminin and its biologically active KDI-domain may guide axons in the floor plate of human embryonic spinal cord, J Neurosci Res 71(3) (2003) 338-52.
[76] P. Liesi, G. Fried, R.R. Stewart, Neurons and glial cells of the embryonic human brain and spinal cord express multiple and distinct isoforms of laminin, J Neurosci Res 64(2) (2001) 144-67.
[77] P. Kallunki, K. Sainio, R. Eddy, M. Byers, T. Kallunki, H. Sariola, K. Beck, H. Hirvonen, T.B. Shows, K. Tryggvason, A truncated laminin chain homologous to the B2 chain: structure, spatial expression, and chromosomal assignment, J Cell Biol 119(3) (1992) 679-93.
[78] L.S. Campos, D.P. Leone, J.B. Relvas, C. Brakebusch, R. Fassler, U. Suter, C. ffrench-Constant, Beta1 integrins activate a MAPK signalling pathway in neural stem cells that contributes to their maintenance, Development 131(14) (2004) 3433-44.
[79] M.F. Galliano, D. Aberdam, A. Aguzzi, J.P. Ortonne, G. Meneguzzi, Cloning and complete primary structure of the mouse laminin alpha 3 chain. Distinct expression pattern of the laminin alpha 3A and alpha 3B chain isoforms, J Biol Chem 270(37) (1995) 21820-6.

[80] A.J. Copp, R. Carvalho, A. Wallace, L. Sorokin, T. Sasaki, N.D. Greene, P. Ybot-Gonzalez, Regional differences in the expression of laminin isoforms during mouse neural tube development, Matrix Biol 30(4) (2011) 301-9.
[81] N. Gersdorff, E. Kohfeldt, T. Sasaki, R. Timpl, N. Miosge, Laminin gamma3 chain binds to nidogen and is located in murine basement membranes, J Biol Chem 280(23) (2005) 22146-53.
[82] J. Di Russo, A.L. Luik, L. Yousif, S. Budny, H. Oberleithner, V. Hofschroer, J. Klingauf, E. van Bavel, E.N. Bakker, P. Hellstrand, A. Bhattachariya, S. Albinsson, F. Pincet, R. Hallmann, L.M. Sorokin, Endothelial basement membrane laminin 511 is essential for shear stress response, EMBO J 36(2) (2017) 183-201.
[83] R. Hallmann, N. Horn, M. Selg, O. Wendler, F. Pausch, L.M. Sorokin, Expression and function of laminins in the embryonic and mature vasculature, Physiol Rev 85(3) (2005) 979-1000.
[84] M.J. Hannocks, M.E. Pizzo, J. Huppert, T. Deshpande, N.J. Abbott, R.G. Thorne, L. Sorokin, Molecular characterization of perivascular drainage pathways in the murine brain, J Cereb Blood Flow Metab 38(4) (2018) 669-686.
[85] M. Sixt, B. Engelhardt, F. Pausch, R. Hallmann, O. Wendler, L.M. Sorokin, Endothelial cell laminin isoforms, laminins 8 and 10, play decisive roles in T cell recruitment across the blood-brain barrier in experimental autoimmune encephalomyelitis, J Cell Biol 153(5) (2001) 933-46.
[86] L.F. Yousif, J. Di Russo, L. Sorokin, Laminin isoforms in endothelial and perivascular basement membranes, Cell Adh Migr 7(1) (2013) 101-10.
[87] S. Sugiyama, A. Utani, S. Yamada, C.A. Kozak, Y. Yamada, Cloning and expression of the mouse laminin gamma 2 (B2t) chain, a subunit of epithelial cell laminin, Eur J Biochem 228(1) (1995) 120-8.
[88] Y.N. Li, S. Radner, M.M. French, G. Pinzon-Duarte, G.H. Daly, R.E. Burgeson, M. Koch, W.J. Brunken, The gamma3 chain of laminin is widely but differentially expressed in murine basement membranes: expression and functional studies, Matrix Biol 31(2) (2012) 120-34.
[89] A. Kerever, J. Schnack, D. Vellinga, N. Ichikawa, C. Moon, E. Arikawa-Hirasawa, J.T. Efird, F. Mercier, Novel extracellular matrix structures in the neural stem cell niche capture the neurogenic factor fibroblast growth factor 2 from the extracellular milieu, Stem Cells 25(9) (2007) 2146-57.
[90] M.J. Menezes, F.K. McClenahan, C.V. Leiton, A. Aranmolate, X. Shan, H. Colognato, The extracellular matrix protein laminin alpha2 regulates the maturation and function of the blood-brain barrier, J Neurosci 34(46) (2014) 15260-80.

[91] Y. Yao, Z.L. Chen, E.H. Norris, S. Strickland, Astrocytic laminin regulates pericyte differentiation and maintains blood brain barrier integrity, Nat Commun 5 (2014) 3413.
[92] M. Vanlandewijck, L. He, M.A. Mae, J. Andrae, K. Ando, F. Del Gaudio, K. Nahar, T. Lebouvier, B. Lavina, L. Gouveia, Y. Sun, E. Raschperger, M. Rasanen, Y. Zarb, N. Mochizuki, A. Keller, U. Lendahl, C. Betsholtz, A molecular atlas of cell types and zonation in the brain vasculature, Nature 554(7693) (2018) 475-480.
[93] T. Hagg, C. Portera-Cailliau, M. Jucker, E. Engvall, Laminins of the adult mammalian CNS; laminin-alpha2 (merosin M-) chain immunoreactivity is associated with neuronal processes, Brain Res 764(1-2) (1997) 17-27.
[94] W.K. Kim, D. Kim, J. Cui, H.H. Jang, K.S. Kim, H.J. Lee, S.U. Kim, S.M. Ahn, Secretome analysis of human oligodendrocytes derived from neural stem cells, PLoS One 9(1) (2014) e84292.
[95] I. Kazanis, J.D. Lathia, T.J. Vadakkan, E. Raborn, R. Wan, M.R. Mughal, D.M. Eckley, T. Sasaki, B. Patton, M.P. Mattson, K.K. Hirschi, M.E. Dickinson, C. ffrench-Constant, Quiescence and activation of stem and precursor cell populations in the subependymal zone of the mammalian brain are associated with distinct cellular and extracellular matrix signals, J Neurosci 30(29) (2010) 9771-81.
[96] S.J. Chun, M.N. Rasband, R.L. Sidman, A.A. Habib, T. Vartanian, Integrin-linked kinase is required for laminin-2-induced oligodendrocyte cell spreading and CNS myelination, J Cell Biol 163(2) (2003) 397-408.
[97] A.N. Stratman, K.M. Malotte, R.D. Mahan, M.J. Davis, G.E. Davis, Pericyte recruitment during vasculogenic tube assembly stimulates endothelial basement membrane matrix formation, Blood 114(24) (2009) 5091-101.
[98] Z.L. Chen, J.A. Indyk, S. Strickland, The hippocampal laminin matrix is dynamic and critical for neuronal survival, Mol Biol Cell 14(7) (2003) 2665-76.
[99] Z.L. Chen, S. Strickland, Neuronal death in the hippocampus is promoted by plasmin-catalyzed degradation of laminin, Cell 91(7) (1997) 917-25.
[100] J.A. Indyk, Z.L. Chen, S.E. Tsirka, S. Strickland, Laminin chain expression suggests that laminin-10 is a major isoform in the mouse hippocampus and is degraded by the tissue plasminogen activator/plasmin protease cascade during excitotoxic injury, Neuroscience 116(2) (2003) 359-71.
[101] M.H. Omar, M. Kerrisk Campbell, X. Xiao, Q. Zhong, W.J. Brunken, J.H. Miner, C.A. Greer, A.J. Koleske, CNS Neurons Deposit Laminin alpha5 to Stabilize Synapses, Cell Rep 21(5) (2017) 1281-1292.
[102] Y. Yin, Y. Kikkawa, J.L. Mudd, W.C. Skarnes, J.R. Sanes, J.H. Miner, Expression of laminin chains by central neurons: analysis with gene and protein trapping techniques, Genesis 36(2) (2003) 114-27.

[103] B. Grimpe, S. Dong, C. Doller, K. Temple, A.T. Malouf, J. Silver, The critical role of basement membrane-independent laminin gamma 1 chain during axon regeneration in the CNS, J Neurosci 22(8) (2002) 3144-60.
[104] A.J. Vaananen, P. Rauhala, R.K. Tuominen, P. Liesi, KDI tripeptide of gamma1 laminin protects rat dopaminergic neurons from 6-OHDA induced toxicity, J Neurosci Res 84(3) (2006) 655-65.
[105] P. Liesi, Do neurons in the vertebrate CNS migrate on laminin?, EMBO J 4(5) (1985) 1163-70.
[106] P. Liesi, J. Silver, Is astrocyte laminin involved in axon guidance in the mammalian CNS?, Dev Biol 130(2) (1988) 774-85.
[107] S.A. Fietz, R. Lachmann, H. Brandl, M. Kircher, N. Samusik, R. Schroder, N. Lakshmanaperumal, I. Henry, J. Vogt, A. Riehn, W. Distler, R. Nitsch, W. Enard, S. Paabo, W.B. Huttner, Transcriptomes of germinal zones of human and mouse fetal neocortex suggest a role of extracellular matrix in progenitor self-renewal, Proc Natl Acad Sci U S A 109(29) (2012) 11836-41.
[108] J.H. Miner, J. Cunningham, J.R. Sanes, Roles for laminin in embryogenesis: exencephaly, syndactyly, and placentopathy in mice lacking the laminin alpha5 chain, J Cell Biol 143(6) (1998) 1713-23.
[109] E.G. Coles, L.S. Gammill, J.H. Miner, M. Bronner-Fraser, Abnormalities in neural crest cell migration in laminin alpha5 mutant mice, Dev Biol 289(1) (2006) 218-28.
[110] C. Regalado-Santiago, E. Juarez-Aguilar, J.D. Olivares-Hernandez, E. Tamariz, Mimicking Neural Stem Cell Niche by Biocompatible Substrates, Stem Cells Int 2016 (2016) 1513285.
[111] C.A. Williams, E.B. Lavik, Engineering the CNS stem cell microenvironment, Regen Med 4(6) (2009) 865-77.
[112] C.M. Morshead, B.A. Reynolds, C.G. Craig, M.W. McBurney, W.A. Staines, D. Morassutti, S. Weiss, D. van der Kooy, Neural stem cells in the adult mammalian forebrain: a relatively quiescent subpopulation of subependymal cells, Neuron 13(5) (1994) 1071-82.
[113] F. Doetsch, J.M. Garcia-Verdugo, A. Alvarez-Buylla, Regeneration of a germinal layer in the adult mammalian brain, Proc Natl Acad Sci U S A 96(20) (1999) 11619-24.
[114] A. Alvarez-Buylla, D.A. Lim, For the long run: maintaining germinal niches in the adult brain, Neuron 41(5) (2004) 683-6.
[115] Q. Shen, Y. Wang, E. Kokovay, G. Lin, S.M. Chuang, S.K. Goderie, B. Roysam, S. Temple, Adult SVZ stem cells lie in a vascular niche: a quantitative analysis of niche cell-cell interactions, Cell Stem Cell 3(3) (2008) 289-300.

[116] F. Barnabe-Heider, J.A. Wasylnka, K.J. Fernandes, C. Porsche, M. Sendtner, D.R. Kaplan, F.D. Miller, Evidence that embryonic neurons regulate the onset of cortical gliogenesis via cardiotrophin-1, Neuron 48(2) (2005) 253-65.

[117] P.E. Hall, J.D. Lathia, M.A. Caldwell, C. Ffrench-Constant, Laminin enhances the growth of human neural stem cells in defined culture media, BMC Neurosci 9 (2008) 71.

[118] P. Liesi, D. Dahl, A. Vaheri, Laminin is produced by early rat astrocytes in primary culture, J Cell Biol 96(3) (1983) 920-4.

[119] S. Radner, C. Banos, G. Bachay, Y.N. Li, D.D. Hunter, W.J. Brunken, K.T. Yee, beta2 and gamma3 laminins are critical cortical basement membrane components: ablation of Lamb2 and Lamc3 genes disrupts cortical lamination and produces dysplasia, Dev Neurobiol 73(3) (2013) 209-29.

[120] W. Halfter, S. Dong, Y.P. Yip, M. Willem, U. Mayer, A critical function of the pial basement membrane in cortical histogenesis, J Neurosci 22(14) (2002) 6029-40.

[121] T. Barak, K.Y. Kwan, A. Louvi, V. Demirbilek, S. Saygi, B. Tuysuz, M. Choi, H. Boyaci, K. Doerschner, Y. Zhu, H. Kaymakcalan, S. Yilmaz, M. Bakircioglu, A.O. Caglayan, A.K. Ozturk, K. Yasuno, W.J. Brunken, E. Atalar, C. Yalcinkaya, A. Dincer, R.A. Bronen, S. Mane, T. Ozcelik, R.P. Lifton, N. Sestan, K. Bilguvar, M. Gunel, Recessive LAMC3 mutations cause malformations of occipital cortical development, Nat Genet 43(6) (2011) 590-4.

[122] I. Kazanis, C. ffrench-Constant, Extracellular matrix and the neural stem cell niche, Dev Neurobiol 71(11) (2011) 1006-17.

[123] A. Hyysalo, M. Ristola, M.E. Makinen, S. Hayrynen, M. Nykter, S. Narkilahti, Laminin alpha5 substrates promote survival, network formation and functional development of human pluripotent stem cell-derived neurons in vitro, Stem Cell Res 24 (2017) 118-127.

[124] L. Luckenbill-Edds, Laminin and the mechanism of neuronal outgrowth, Brain Res Brain Res Rev 23(1-2) (1997) 1-27.

[125] S.K. Powell, H.K. Kleinman, Neuronal laminins and their cellular receptors, Int J Biochem Cell Biol 29(3) (1997) 401-14.

[126] S. Plantman, M. Patarroyo, K. Fried, A. Domogatskaya, K. Tryggvason, H. Hammarberg, S. Cullheim, Integrin-laminin interactions controlling neurite outgrowth from adult DRG neurons in vitro, Mol Cell Neurosci 39(1) (2008) 50-62.

[127] E.A. Phelps, N.O. Enemchukwu, V.F. Fiore, J.C. Sy, N. Murthy, T.A. Sulchek, T.H. Barker, A.J. Garcia, Maleimide cross-linked bioactive PEG hydrogel exhibits improved reaction kinetics and cross-linking for cell encapsulation and in situ delivery, Adv Mater 24(1) (2012) 64-70, 2.

[128] N.O. Enemchukwu, R. Cruz-Acuna, T. Bongiorno, C.T. Johnson, J.R. Garcia, T. Sulchek, A.J. Garcia, Synthetic matrices reveal contributions of ECM biophysical and biochemical properties to epithelial morphogenesis, J Cell Biol 212(1) (2016) 113-24.
[129] W.M. Han, S.E. Anderson, M. Mohiuddin, D. Barros, S.A. Nakhai, E. Shin, I.F. Amaral, A.P. Pego, A.J. Garcia, Y.C. Jang, Synthetic matrix enhances transplanted satellite cell engraftment in dystrophic and aged skeletal muscle with comorbid trauma, Sci Adv 4(8) (2018) eaar4008.
[130] L.A. Flanagan, Y.E. Ju, B. Marg, M. Osterfield, P.A. Janmey, Neurite branching on deformable substrates, Neuroreport 13(18) (2002) 2411-5.
[131] A.J. Engler, S. Sen, H.L. Sweeney, D.E. Discher, Matrix elasticity directs stem cell lineage specification, Cell 126(4) (2006) 677-89.
[132] P.C. Georges, W.J. Miller, D.F. Meaney, E.S. Sawyer, P.A. Janmey, Matrices with compliance comparable to that of brain tissue select neuronal over glial growth in mixed cortical cultures, Biophys J 90(8) (2006) 3012-8.
[133] K. Saha, A.J. Keung, E.F. Irwin, Y. Li, L. Little, D.V. Schaffer, K.E. Healy, Substrate modulus directs neural stem cell behavior, Biophys. J. 95(9) (2008) 4426-38.
[134] A. Banerjee, M. Arha, S. Choudhary, R.S. Ashton, S.R. Bhatia, D.V. Schaffer, R.S. Kane, The influence of hydrogel modulus on the proliferation and differentiation of encapsulated neural stem cells, Biomaterials 30(27) (2009) 4695-9.
[135] S.R. Hynes, M.F. Rauch, J.P. Bertram, E.B. Lavik, A library of tunable poly(ethylene glycol)/poly(L-lysine) hydrogels to investigate the material cues that influence neural stem cell differentiation, J Biomed Mater Res A 89(2) (2009) 499-509.
[136] M.C. Dodla, R.V. Bellamkonda, Anisotropic scaffolds facilitate enhanced neurite extension in vitro, J Biomed Mater Res A 78(2) (2006) 213-21.
[137] L. Marquardt, R.K. Willits, Student award winner in the undergraduate's degree category for the Society for Biomaterials 35th Annual Meeting, Orlando, Florida, April 13-16, 2011. Neurite growth in PEG gels: effect of mechanical stiffness and laminin concentration, J Biomed Mater Res A 98(1) (2011) 1-6.
[138] C.P. Addington, J.M. Heffernan, C.S. Millar-Haskell, E.W. Tucker, R.W. Sirianni, S.E. Stabenfeldt, Enhancing neural stem cell response to SDF-1alpha gradients through hyaluronic acid-laminin hydrogels, Biomaterials 72 (2015) 11-9.
[139] J. Arulmoli, H.J. Wright, D.T.T. Phan, U. Sheth, R.A. Que, G.A. Botten, M. Keating, E.L. Botvinick, M.M. Pathak, T.I. Zarembinski, D.S. Yanni, O.V. Razorenova, C.C.W. Hughes, L.A. Flanagan, Combination scaffolds of salmon fibrin, hyaluronic acid, and laminin for human neural stem cell and vascular tissue engineering, Acta Biomater 43 (2016) 122-138.

[140] C.P. Addington, S. Dharmawaj, J.M. Heffernan, R.W. Sirianni, S.E. Stabenfeldt, Hyaluronic acid-laminin hydrogels increase neural stem cell transplant retention and migratory response to SDF-1alpha, Matrix Biol 60-61 (2017) 206-216.
[141] B.G. Keselowsky, D.M. Collard, A.J. Garcia, Surface chemistry modulates fibronectin conformation and directs integrin binding and specificity to control cell adhesion, J Biomed Mater Res A 66(2) (2003) 247-59.
[142] J.C. Rodriguez Hernandez, M. Salmeron Sanchez, J.M. Soria, J.L. Gomez Ribelles, M. Monleon Pradas, Substrate chemistry-dependent conformations of single laminin molecules on polymer surfaces are revealed by the phase signal of atomic force microscopy, Biophys J 93(1) (2007) 202-7.
[143] O.M. Ba, M. Hindie, P. Marmey, O. Gallet, K. Anselme, A. Ponche, A.C. Duncan, Protein covalent immobilization via its scarce thiol versus abundant amine groups: Effect on orientation, cell binding domain exposure and conformational lability, Colloids Surf B Biointerfaces 134 (2015) 73-80.
[144] S.E. Stabenfeldt, G. Munglani, A.J. Garcia, M.C. LaPlaca, Biomimetic microenvironment modulates neural stem cell survival, migration, and differentiation, Tissue Eng Part A 16(12) (2010) 3747-58.
[145] S.E. Stabenfeldt, M.C. LaPlaca, Variations in rigidity and ligand density influence neuronal response in methylcellulose-laminin hydrogels, Acta Biomater 7(12) (2011) 4102-8.
[146] D.K. Cullen, S.E. Stabenfeldt, C.M. Simon, C.C. Tate, M.C. LaPlaca, In vitro neural injury model for optimization of tissue-engineered constructs, J Neurosci Res 85(16) (2007) 3642-51.
[147] S.E. Stabenfeldt, H.I. Irons, D.K. Cullen, C.C. Tate, M.C. LaPlaca, A multilevel analysis of a methylcellulose-laminin scaffold to improve neural stem cell survival in a traumatically injured neural environment, Cell Transplantation, Cognizant Communication Corp, 2007, p. 346.
[148] S.E. Stabenfeldt, A.J. Garcia, M.C. LaPlaca, Thermoreversible laminin-functionalized hydrogel for neural tissue engineering, J Biomed Mater Res A 77(4) (2006) 718-25.
[149] K.E. Swindle-Reilly, J.B. Papke, H.P. Kutosky, A. Throm, J.A. Hammer, A.B. Harkins, R.K. Willits, The impact of laminin on 3D neurite extension in collagen gels, J Neural Eng 9(4) (2012) 046007.
[150] S.A. Geissler, A.L. Sabin, R.R. Besser, O.M. Gooden, B.D. Shirk, Q.M. Nguyen, Z.Z. Khaing, C.E. Schmidt, Biomimetic hydrogels direct spinal progenitor cell differentiation and promote functional recovery after spinal cord injury, J Neural Eng 15(2) (2018) 025004.

[151] H. Li, J. Zheng, H. Wang, M.L. Becker, N.D. Leipzig, Neural stem cell encapsulation and differentiation in strain promoted crosslinked polyethylene glycol-based hydrogels, J Biomater Appl 32(9) (2018) 1222-1230.
[152] A. Bergeron, H. Sherman, P. Pardo, H. Gitschier, H. Nandivada, D. Saxena, Corning® rLaminin-521 (Human) for Expansion and Differentiation of Human Neural Stem Cells, Corning Incorporated | Application Note (2015).
[153] S. Hou, Q. Xu, W. Tian, F. Cui, Q. Cai, J. Ma, I.S. Lee, The repair of brain lesion by implantation of hyaluronic acid hydrogels modified with laminin, J Neurosci Methods 148(1) (2005) 60-70.
[154] M. Marcinczyk, H. Elmashhady, M. Talovic, A. Dunn, F. Bugis, K. Garg, Laminin-111 enriched fibrin hydrogels for skeletal muscle regeneration, Biomaterials 141 (2017) 233-242.
[155] N. Ziemkiewicz, M. Talovic, J. Madsen, L. Hill, R. Scheidt, A. Patel, G. Haas, M. Marcinczyk, S.P. Zustiak, K. Garg, Laminin-111 functionalized polyethylene glycol hydrogels support myogenic activity in vitro, Biomed Mater 13(6) (2018) 065007.
[156] A.T. Francisco, R.J. Mancino, R.D. Bowles, J.M. Brunger, D.M. Tainter, Y.T. Chen, W.J. Richardson, F. Guilak, L.A. Setton, Injectable laminin-functionalized hydrogel for nucleus pulposus regeneration, Biomaterials 34(30) (2013) 7381-8.
[157] A.T. Francisco, P.Y. Hwang, C.G. Jeong, L. Jing, J. Chen, L.A. Setton, Photocrosslinkable laminin-functionalized polyethylene glycol hydrogel for intervertebral disc regeneration, Acta Biomater 10(3) (2014) 1102-11.
[158] S.K. Williams, L.B. Kleinert, V. Patula-Steinbrenner, Accelerated neovascularization and endothelialization of vascular grafts promoted by covalently bound laminin type 1, J Biomed Mater Res A 99(1) (2011) 67-73.
[159] K. Stamati, J.V. Priestley, V. Mudera, U. Cheema, Laminin promotes vascular network formation in 3D in vitro collagen scaffolds by regulating VEGF uptake, Exp Cell Res 327(1) (2014) 68-77.
[160] J.H. Collier, T. Segura, Evolving the use of peptides as components of biomaterials, Biomaterials 32(18) (2011) 4198-204.
[161] X. Li, X. Liu, B. Josey, C.J. Chou, Y. Tan, N. Zhang, X. Wen, Short laminin peptide for improved neural stem cell growth, Stem Cells Transl Med 3(5) (2014) 662-70.
[162] W. Sun, T. Incitti, C. Migliaresi, A. Quattrone, S. Casarosa, A. Motta, Viability and neuronal differentiation of neural stem cells encapsulated in silk fibroin hydrogel functionalized with an IKVAV peptide, J Tissue Eng Regen Med 11(5) (2017) 1532-1541.
[163] T. Zhao, D.L. Sellers, Y. Cheng, P.J. Horner, S.H. Pun, Tunable, Injectable Hydrogels Based on Peptide-Cross-Linked, Cyclized Polymer Nanoparticles for Neural Progenitor Cell Delivery, Biomacromolecules 18(9) (2017) 2723-2731.

[164] S.P. Zustiak, S. Pubill, A. Ribeiro, J.B. Leach, Hydrolytically degradable poly(ethylene glycol) hydrogel scaffolds as a cell delivery vehicle: characterization of PC12 cell response, Biotechnol Prog 29(5) (2013) 1255-64.
[165] J.C. Schense, J. Bloch, P. Aebischer, J.A. Hubbell, Enzymatic incorporation of bioactive peptides into fibrin matrices enhances neurite extension, Nat Biotechnol 18(4) (2000) 415-9.
[166] G.A. Silva, C. Czeisler, K.L. Niece, E. Beniash, D.A. Harrington, J.A. Kessler, S.I. Stupp, Selective differentiation of neural progenitor cells by high-epitope density nanofibers, Science 303(5662) (2004) 1352-5.
[167] T.Y. Cheng, M.H. Chen, W.H. Chang, M.Y. Huang, T.W. Wang, Neural stem cells encapsulated in a functionalized self-assembling peptide hydrogel for brain tissue engineering, Biomaterials 34(8) (2013) 2005-16.
[168] E.J. Berns, S. Sur, L. Pan, J.E. Goldberger, S. Suresh, S. Zhang, J.A. Kessler, S.I. Stupp, Aligned neurite outgrowth and directed cell migration in self-assembled monodomain gels, Biomaterials 35(1) (2014) 185-95.
[169] R. Bellamkonda, J.P. Ranieri, P. Aebischer, Laminin oligopeptide derivatized agarose gels allow three-dimensional neurite extension in vitro, J Neurosci Res 41(4) (1995) 501-9.
[170] J.C. Schense, J.A. Hubbell, Cross-linking exogenous bifunctional peptides into fibrin gels with factor XIIIa, Bioconjug Chem 10(1) (1999) 75-81.
[171] Y. Yamada, K. Hozumi, F. Katagiri, Y. Kikkawa, M. Nomizu, Biological activity of laminin peptide-conjugated alginate and chitosan matrices, Biopolymers 94(6) (2010) 711-20.
[172] Y. Yamada, F. Katagiri, K. Hozumi, Y. Kikkawa, M. Nomizu, Cell behavior on protein matrices containing laminin alpha1 peptide AG73, Biomaterials 32(19) (2011) 4327-35.
[173] Y. Yamada, K. Hozumi, A. Aso, A. Hotta, K. Toma, F. Katagiri, Y. Kikkawa, M. Nomizu, Laminin active peptide/agarose matrices as multifunctional biomaterials for tissue engineering, Biomaterials 33(16) (2012) 4118-25.
[174] A.R. Bento, Improving neurite outgrowth in 3D hydrogel matrices by mimicking cell receptor-ECM interactions occurring in neurogenic niches: an engineering approach to develop more efficient neural stem cell hydrogel carriers, Faculdade de Engenharia, Universidade do Porto, 2018.
[175] M. Hiraoka, K. Kato, T. Nakaji-Hirabayashi, H. Iwata, Enhanced survival of neural cells embedded in hydrogels composed of collagen and laminin-derived cell adhesive peptide, Bioconjug Chem 20(5) (2009) 976-83.
[176] T. Nakaji-Hirabayashi, K. Kato, H. Iwata, Improvement of neural stem cell survival in collagen hydrogels by incorporating laminin-derived cell adhesive polypeptides, Bioconjug Chem 23(2) (2012) 212-21.

[177] K. Tashiro, G.C. Sephel, B. Weeks, M. Sasaki, G.R. Martin, H.K. Kleinman, Y. Yamada, A synthetic peptide containing the IKVAV sequence from the A chain of laminin mediates cell attachment, migration, and neurite outgrowth, J Biol Chem 264(27) (1989) 16174-82.

[178] J. Graf, Y. Iwamoto, M. Sasaki, G.R. Martin, H.K. Kleinman, F.A. Robey, Y. Yamada, Identification of an amino acid sequence in laminin mediating cell attachment, chemotaxis, and receptor binding, Cell 48(6) (1987) 989-96.

[179] H.K. Kleinman, J. Graf, Y. Iwamoto, M. Sasaki, C.S. Schasteen, Y. Yamada, G.R. Martin, F.A. Robey, Identification of a second active site in laminin for promotion of cell adhesion and migration and inhibition of in vivo melanoma lung colonization, Arch Biochem Biophys 272(1) (1989) 39-45.

[180] N. Desban, J.C. Lissitzky, P. Rousselle, J.L. Duband, alpha1beta1-integrin engagement to distinct laminin-1 domains orchestrates spreading, migration and survival of neural crest cells through independent signaling pathways, J Cell Sci 119(Pt 15) (2006) 3206-18.

[181] L. Pan, H.A. North, V. Sahni, S.J. Jeong, T.L. McGuire, E.J. Berns, S.I. Stupp, J.A. Kessler, beta1-Integrin and integrin linked kinase regulate astrocytic differentiation of neural stem cells, PLoS One 9(8) (2014) e104335.

[182] P. Liesi, A. Narvanen, J. Soos, H. Sariola, G. Snounou, Identification of a neurite outgrowth-promoting domain of laminin using synthetic peptides, FEBS Lett 244(1) (1989) 141-8.

[183] S. Murtomaki, J. Risteli, L. Risteli, U.M. Koivisto, S. Johansson, P. Liesi, Laminin and its neurite outgrowth-promoting domain in the brain in Alzheimer's disease and Down's syndrome patients, J Neurosci Res 32(2) (1992) 261-73.

[184] M. Nomizu, W.H. Kim, K. Yamamura, A. Utani, S.Y. Song, A. Otaka, P.P. Roller, H.K. Kleinman, Y. Yamada, Identification of cell binding sites in the laminin alpha 1 chain carboxyl-terminal globular domain by systematic screening of synthetic peptides, J Biol Chem 270(35) (1995) 20583-90.

[185] M.P. Hoffman, M. Nomizu, E. Roque, S. Lee, D.W. Jung, Y. Yamada, H.K. Kleinman, Laminin-1 and laminin-2 G-domain synthetic peptides bind syndecan-1 and are involved in acinar formation of a human submandibular gland cell line, J Biol Chem 273(44) (1998) 28633-41.

[186] L.N. Gama-de-Souza, E. Cyreno-Oliveira, V.M. Freitas, E.S. Melo, V.F. Vilas-Boas, A.S. Moriscot, R.G. Jaeger, Adhesion and protease activity in cell lines from human salivary gland tumors are regulated by the laminin-derived peptide AG73, syndecan-1 and beta1 integrin, Matrix Biol 27(5) (2008) 402-19.

[187] N. Suzuki, N. Ichikawa, S. Kasai, M. Yamada, N. Nishi, H. Morioka, H. Yamashita, Y. Kitagawa, A. Utani, M.P. Hoffman, M. Nomizu, Syndecan binding sites in the laminin alpha1 chain G domain, Biochemistry 42(43) (2003) 12625-33.
[188] M. Mochizuki, Y. Kadoya, Y. Wakabayashi, K. Kato, I. Okazaki, M. Yamada, T. Sato, N. Sakairi, N. Nishi, M. Nomizu, Laminin-1 peptide-conjugated chitosan membranes as a novel approach for cell engineering, FASEB J 17(8) (2003) 875-7.
[189] M.D. Pierschbacher, E. Ruoslahti, Cell attachment activity of fibronectin can be duplicated by small synthetic fragments of the molecule, Nature 309(5963) (1984) 30-3.
[190] U. Freudenberg, A. Hermann, P.B. Welzel, K. Stirl, S.C. Schwarz, M. Grimmer, A. Zieris, W. Panyanuwat, S. Zschoche, D. Meinhold, A. Storch, C. Werner, A star-PEG-heparin hydrogel platform to aid cell replacement therapies for neurodegenerative diseases, Biomaterials 30(28) (2009) 5049-60.
[191] K.S. Straley, S.C. Heilshorn, Independent tuning of multiple biomaterial properties using protein engineering, Soft Matter 5(1) (2009) 114-124.
[192] Y. Luo, M.S. Shoichet, A photolabile hydrogel for guided three-dimensional cell growth and migration, Nat Mater 3(4) (2004) 249-53.
[193] J.M. Kim, W.H. Park, B.M. Min, The PPFLMLLKGSTR motif in globular domain 3 of the human laminin-5 alpha3 chain is crucial for integrin alpha3beta1 binding and cell adhesion, Exp Cell Res 304(1) (2005) 317-27.
[194] R. Sato-Nishiuchi, S. Li, F. Ebisu, K. Sekiguchi, Recombinant laminin fragments endowed with collagen-binding activity: A tool for conferring laminin-like cell-adhesive activity to collagen matrices, Matrix Biol 65 (2018) 75-90.
[195] T. Miyazaki, S. Futaki, H. Suemori, Y. Taniguchi, M. Yamada, M. Kawasaki, M. Hayashi, H. Kumagai, N. Nakatsuji, K. Sekiguchi, E. Kawase, Laminin E8 fragments support efficient adhesion and expansion of dissociated human pluripotent stem cells, Nat Commun 3 (2012) 1236.
[196] S.G. Levesque, M.S. Shoichet, Synthesis of cell-adhesive dextran hydrogels and macroporous scaffolds, Biomaterials 27(30) (2006) 5277-85.
[197] J. Lam, S.T. Carmichael, W.E. Lowry, T. Segura, Hydrogel design of experiments methodology to optimize hydrogel for iPSC-NPC culture, Adv Healthc Mater 4(4) (2015) 534-9.
[198] P. Moshayedi, L.R. Nih, I.L. Llorente, A.R. Berg, J. Cinkornpumin, W.E. Lowry, T. Segura, S.T. Carmichael, Systematic optimization of an engineered hydrogel allows for selective control of human neural stem cell survival and differentiation after transplantation in the stroke brain, Biomaterials 105 (2016) 145-155.

[199] D. Barros, P. Parreira, J. Furtado, F. Ferreira-da-Silva, E. Conde-Sousa, A.J. Garcia, M.C.L. Martins, I.F. Amaral, A.P. Pego, An affinity-based approach to engineer laminin-presenting cell instructive microenvironments, Biomaterials 192 (2019) 601-611.
[200] S.A. Fisher, A.E.G. Baker, M.S. Shoichet, Designing Peptide and Protein Modified Hydrogels: Selecting the Optimal Conjugation Strategy, J Am Chem Soc 139(22) (2017) 7416-7427.

# CHAPTER IV

Biomimetic Synthetic Self-Assembled Hydrogels for Cell Transplantation

# Biomimetic Synthetic Self-Assembled Hydrogels for Cell Transplantation

Daniela Barros [1,2], Isabel Freitas Amaral [1,2,3] and Ana Paula Pêgo [1,2,3,4]

[1] INEB – Instituto de Engenharia Biomédica, Universidade do Porto, Porto, Portugal

[2] i3S - Instituto de Investigação e Inovação em Saúde, Universidade do Porto, Porto, Portugal

[3] FEUP – Faculdade de Engenharia, Universidade do Porto, Porto, Portugal

[4] ICBAS – Instituto de Ciências Biomédicas Abel Salazar, Universidade do Porto, Porto, Portugal

---

**Published in Current Topics in Medicinal Chemistry, Volume 15, Issue 13, 2015**

DOI 10.2174/1568026615666150330111057

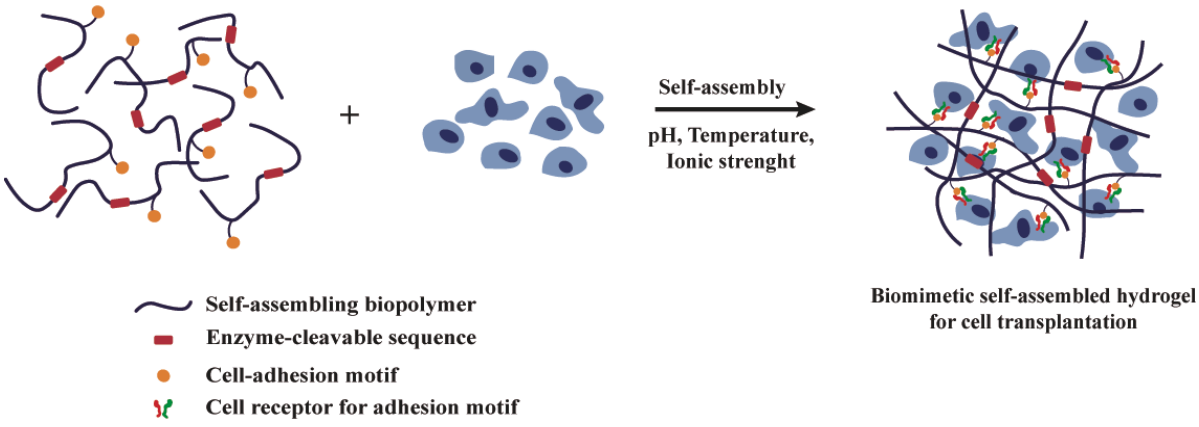

**Abstract**

The development of three-dimensional matrices capable of recapitulating the main features of native extracellular matrix and contribute for the establishment of a favorable microenvironment for cell behavior and fate is expected to circumvent some of the main limitations of cell-based therapies. In this context, self-assembly has emerged as a promising strategy to engineer cell-compatible hydrogels. A wide number of synthetically-derived biopolymers, such as proteins, peptides and DNA/RNA, with intrinsic ability to self-assemble into well-defined nanofibrous structures, are being explored. The resulting hydrogels, in addition to closely resembling the architecture of native cellular microenvironments, present a versatile and dynamic behavior that allows them to be designed to undergo sol-to-gel transition in response to exogenous stimulus. This review presents an overview on the state-of-the-art of the different strategies being explored for the development of injectable synthetic self-assembled hydrogels for cell transplantation and/or recruitment of endogenous cells, with an emphasis on their biological performance, both *in vitro* and *in vivo*. Systems based on peptides are the most widely explored and have already generated promising results in pre-clinical *in vivo* studies involving different repair/regenerative scenarios, including cartilage, bone, nerve and heart. On the other hand, systems based on DNA and hybrid hydrogels are now emerging for application in the biomedical field with high potential. Finally, the main challenges hampering the translation of these systems to the clinic and the issues that need to be addressed for these to progress from bench-to-bedside are discussed.

**Cell transplantation in the context of regenerative medicine**

As our understanding of cell biology and ability to control cell behavior, both in *vitro* and *in vivo*, improves, cell-based therapies are growing in interest within the field of regenerative medicine [1]. Their effectiveness relies on the ability of transplanted cells to mediate a therapeutic effect that potentiates the repair/regeneration processes [2]. Nevertheless, before the effective translation of these therapies into the clinic, a number of issues still have to be solved, such as low cell survival, lack of control of cell fate and poor cell engraftment following transplantation [3, 4].

Within biological systems, cells reside in the extracellular matrix (ECM), a complex and highly dynamic microenvironment that provides structural, mechanical, and biochemical support to cells, ultimately determining their behavior, function and fate. In this sense, and to improve the efficacy of cell transplantation therapies, biomaterial-based matrices mimicking the ECM are being designed to be used as vehicles for cell delivery. The goal is to create a permissive niche for the transplanted cells, promoting cell survival, proliferation, differentiation, and integration within the host tissue. One of the major challenges one faces when designing a cell-compatible matrix is the recapitulation of the instructive cellular niches of natural tissues and the control of the bidirectional interaction between cells and the surrounding microenvironment.

The design of such matrices must take into account a number of biological and physical criteria, as follows:

**(i)** *Biocompatibility*. The developed matrix should be able of perform its function without causing any toxic or undesirable effects.

**(ii)** *Mechanical properties*. The matrix mechanical properties should closely match those of the target tissue, since these will impact cell behavior and, consequently, determine the therapeutic efficacy of the transplanted cells.

**(iii)** *Permeability*. The matrix should allow the continuous exchange of gases, ions, nutrients and metabolites with the surrounding microenvironment, which is vital for the survival and proliferation of transplanted/encapsulated cells.

**(iv)** *Degradation.* Envisaging an application in the context of tissue repair/regeneration a degradable matrix is preferred in the majority of cases. It is paramount that the rate and mechanism of matrix degradation are adjusted to the process of tissue remodeling.

In the last few years, the incorporation of biochemical and biophysical ECM cues – cell adhesion, cell-triggered proteolytic degradation, mechanical stimulation and ECM/growth factor binding - into matrices of both synthetic and natural origin was explored to better mimic the native cellular microenvironment, with different degrees of development and success (consult references [5-7] for a comprehensive review on engineered matrices as ECM mimics).

**Hydrogels as attractive vehicles for cell transplantation**

Hydrogels are reticulated structures comprising cross-linked hydrophilic polymers with high water content (over 90% of water) [8]. A number of unique features make hydrogels highly promising matrices for cell transplantation and even for endogenous cell recruitment in the context of tissue repair/regeneration. These include a highly hydrated nature, good permeability and elasticity, resembling the nature of soft tissue microenvironments [5]. These properties will favor cell-cell and cell-matrix interactions, ultimately influencing cell behavior and fate. Moreover, the structural and mechanical properties of hydrogels can be easily tuned to mimic the tissue-specific ECM microenvironment, by varying the polymer molecular weight and/or its concentration, or by adjusting the cross-linking degree of the network [1]. This is crucial for the development of cell-compatible hydrogels, as cells also respond to biophysical properties of the microenvironment not specifically related to its molecular composition, but to the overall structural and mechanical characteristics of the matrix.

Cells are particularly sensitive to mechanical stimuli, and small changes in matrix stiffness or rigidity can alter cell behavior in many aspects, such as morphology, migration, proliferation, differentiation and, in the case of stem cells, lineage specification and commitment [9, 10]. For instance, mesenchymal stem cells (MSCs) cultured on variably compliant poly(acrylamide) gels were found to undergo neurogenic differentiation on gels with elastic moduli ($E$) mimicking brain tissue ($< 1$ kPa), while on gels mimicking skeletal muscle ($E = 11$ kPa) and collagenous bone ($E = 34$ kPa) these cells differentiated along the myogenic and osteogenic lineages, respectively [10]. The mechanism by which cells convert mechanical signals into biochemical responses is termed mechanotransduction, a dynamic process orchestrated by the ECM, mechanosensitive molecules and cellular components (*e.g*. integrins, focal adhesions, stretch-activated ion channels, cadherins, cytoskeleton filaments, nuclei) [11]. Particularly important for matrix elasticity sensing are focal adhesions, multiprotein complexes formed upon integrin binding to ECM adhesion ligands, which link the ECM to the intracellular cytoskeleton. Focal adhesions act as mechanosensitive receptors, through which alterations in the conformation of ECM molecules caused by mechanical stimuli (*e.g.* tension/loading) are transmitted to

cytoskeleton proteins, leading to cytoskeletal (re)organization, contraction, and activation of mechanotransduction signaling pathways affecting cell morphology, migration, and gene expression profile.

Hydrogels, rather than implanted, can be designed to be injected and create a three-dimensional (3D) network *in situ*. This is highly advantageous when envisaging clinical translation as it (i) allows the homogenous encapsulation of cells and bioactive molecules; (ii) enables the use of minimally invasive procedures for implantation; and (iii) ensures the conformational filling of the injured site, which usually has an irregular shape, leaving no gaps between the matrix and the degenerated/damaged tissue. *In situ* forming hydrogels will thus favor a more close contact and, consequently, a more efficient integration of the matrix within the host tissue. Injectable hydrogels could be further designed to have thixotropic properties (becoming less viscous when subjected to an applied stress). This is achieved through the control of different variables (*e.g.* temperature, pH and ionic strength) that influence directly the *in situ* gelling process (for a more extensive review on strategies explored to design *in situ* forming hydrogels see [12, 13]). When the cross-linking occurs in the presence of cells, either mediated by (bio)chemical (*e.g.* enzymatically, Michael-type addition or photopolymerization) or physical (*e.g*. ionic interactions or self-assembly) processes [13], care must be taken so that the impact on cell viability is limited and minute.

These properties have made hydrogels very attractive in the design of either acellular systems, specifically designed to allow the infiltration of endogenous cells, or cellular grafts to promote tissue remodeling and regeneration [14].

Naturally-derived polymers (*e.g.* collagen, fibrin or alginate) have been widely explored in the design of hydrogels due to their inherent biocompatibility and ability to mimic several features of native ECM. Nevertheless, their use is very often hindered by batch-to-batch variability, risk of immunogenicity and limited range of mechanical properties [15, 16]. Therefore, recent strategies have focused on the use of hydrogels derived from either purely synthetic polymers (*e.g*. poly(ethylene glycol) (PEG) and poly(vinyl alcohol)) or synthetically-derived biopolymers (*e.g*. proteins, peptides and DNA/RNA). Their synthetic nature, as well as their well-defined and versatile structure allows them to be engineered, through the incorporation of bioactive sequences (*e.g.* cell adhesive and protease sensitive), originating bioactive and bioresponsive hydrogels [16, 17]. In this context, synthetically-derived biopolymers are being more extensively explored, due to the several advantageous features of these materials, when compared with purely synthetic polymers. In contrast with the simpler and stochastic structure of purely synthetic polymers, synthetically-derived biopolymers can be engineered to attain a complex and reproducible structure. Moreover, by being synthesized using solid-phase synthesis or recombinant

technology (eventually combined with genetic engineering) [18], they present a monodisperse distribution of the molecular weights. Finally, their inherent ability to be cleaved by enzymes allows a more tight control over the kinetics of hydrogel degradation and, as a result, over the remodeling process.

**Self-assembled hydrogels**

An important feature to take into account when engineering matrices to serve as ECM mimics is the architecture of native ECM. Attaining 3D networks structurally mimicking the nanofibrous structure of the ECM is highly desirable. This is expected to favor the creation of an instructive microenvironment for cell anchorage and cell migration, ultimately leading to the implant, colonization and integration within the host tissue. In this sense, "top-down" approaches, such as electrospinning and phase separation, have been explored in the design of scaffolds for such purposes. However, with these techniques one has a limited control over the scaffold structure at the nanoscale level, as well as over the reproducibility of the process. In the last few years, molecular self-assembly has emerged as the most promising and attractive strategy in this context [19-21]. This is a natural and spontaneous "bottom-up" approach driving the association and organization of single molecules into supramolecular structures. Self-assembly results from the establishment of multiple non-covalent intermolecular interactions (*e.g.* hydrogen bonding, electrostatic interactions, Van der Waals forces and aromatic π-stacking) [22, 23]. A wide number of biopolymers existing in nature (*e.g*. proteins, peptides, polysaccharides and DNA/RNA) present intrinsic ability to self-assemble into highly-ordered structural elements. As a result, their building blocks are being explored to develop synthetic self-assembled networks [18], leading to hydrogels with a nanofibrillar structure, closely resembling the architecture of native ECM. Moreover, the weak and transient nature of established interactions allows the design of hydrogels that undergo a sol-to-gel transition in response to exogenous stimulus (*e.g*. pH, temperature and ionic strength), which provides matrices with a "smart" and dynamic behavior [19, 24]. In the following sections, we present the state-of-the-art of synthetic self-assembled hydrogels, focusing on their application as matrices for cell transplantation in the context of regenerative medicine.

**Engineered protein-based hydrogels**

A number of naturally-occurring proteins (*e.g.* elastin, collagen and silk) have remarkable structural and biological properties that prompted their use in the design of self-assembled hydrogels [25]. In particular, the ones derived from constituents of the mammalian ECM proteins, like collagen, fibronectin or laminin, additionally present biological active peptide domains recognized by cell adhesion receptors and cell-secreted proteolytic enzymes.

These features have made protein-based hydrogels highly advantageous in the context of cell therapies [26]. However, the use of proteins derived from natural sources is very often hampered by low scalability, reproducibility, stability and price. In this sense, in the last few years, engineered proteins have arisen as a promising alternative for the design of self-assembled hydrogels. The synthetic nature of these proteins allows the combination in one structure of key attributes of native ECM, including cell adhesion, growth factor and ECM binding domains, as well as sequences that confer to the final protein elasticity and proteolytic degradation. But while maintaining the main attractive biological features of naturally derived proteins, precise control over the primary amino acid sequence and molecular weight can be achieved, allowing the fine-tuning of the gelation process and of the hydrogel structural and mechanical properties.

As the number of engineered proteins that can be used for the development of self-assembled hydrogels [26, 27] is too large to be effectively covered by this review, only the engineered protein-based hydrogels that have shown the most promising results, both *in vitro* and *in vivo,* were addressed. These include hydrogels based on elastin- and silk-like polypeptides, as well as hydrogels based on *de novo* engineered proteins, such as leucine zipper coiled-coil-based polypeptides and amphiphilic block co-polypeptides.

***Elastin-like polypeptides***

Elastin is an ECM structural protein, essentially composed of β-sheet structures, that mediates important biological functions, such as cell-cell and ECM-cell interactions, providing tissues with unique physical characteristics in terms of tensile strength and elasticity [25]. A broad number of synthetic polypeptides have been designed inspired by this natural protein, among which elastin-like polypeptides (ELPs). These are genetically engineered sequences containing the pentapeptide repeat - $(VPGXG)_n$ - in which X can be any amino acid except proline [28]. ELPs are thermally-responsive and thus can undergo a reversible inverse phase transition in response to temperature changes (Fig. 1A) [25, 29]. At temperatures below a specific transition temperature ($T_t$), ELP molecules exist in a disordered and bulky conformation, while above the $T_t$ they self-associate through the establishment of hydrophobic interactions, forming an insoluble and highly viscous coacervate (Fig. 1A). The $T_t$ of an ELP is highly dependent on its composition, molecular weight and concentration, and thus can be easily tuned by changing any of these parameters [30, 31]. The thermal responsiveness of ELPs provides a natural trigger for self-assemble that can be exploited for the development of injectable defect-filling hydrogels [32, 33] (for a more extensive review on ELPs stimulus responsive behavior see [34, 35]). These molecules have been shown to be biocompatible, biodegradable and non-immunogenic, which makes them highly attractive for tissue engineering purposes [26].

The self-assembly of ELP-based hydrogels can also be achieved by chemical cross-linking (Fig. 1A) [36]. For this purpose, ELPs are engineered to include lysine residues, enabling primary amine reactive cross-linking [37]. The mechanical properties of the formed hydrogels, as well as the rate of the gelation process, can be easily tuned by varying the number of lysine residues and the pH of the cross-linking reaction [38]. Chemical cross-linking was found not to affect cell viability, as shown by studies using mouse fibroblasts [37, 39].

ELP-based hydrogels can be engineered to incorporate specific bioactive sequences, such as cell adhesive and/or proteolytic sensitive domains, to impart them with bioactivity. As an example, a chemically cross-linked biomimetic matrix comprising ELP structural domains modified with the RGD cell adhesion motif and a sequence sensitive to urokinase plasminogen activator (uPA) was designed for purposes of neural regeneration [40]. Apart from being able to support PC-12 neuronal-like cell line adhesion, proliferation and differentiation, the resulting hydrogel showed highly tunable degradation rates, depending on the degree of exposure to uPA [40]. Also, a chemically cross-linked ELP hydrogel designed with an RGD cell-adhesion motif have shown to be able of promote neurite outgrowth of encapsulated dorsal root ganglia (DRG) cells [41].

To improve the mechanical and biological properties of ELPs, a different class of genetically engineered materials - silk-elastin-like polypeptides (SELPs), was developed. These are composed by repeating units of silk (GAGAGS) and elastin (GVGXP) peptide sequences [25, 42-44]. Silk-like blocks provide chemical and thermal stability, due to their ability to form hydrogen-bonded β-sheets, while elastin-like blocks introduce flexibility and aqueous solubility to SELPs, by reducing their degree of crystallization [25]. The sequence and length of silk- and elastin-like blocks, as well as their ratio strongly influence the extent of the gelation process, as well as the biological and physicochemical properties of the developed hydrogels [42, 45].

***Leucine zipper coiled-coil-based polypeptides***

Engineered protein-based hydrogels assembled through the leucine zipper coiled-coil domains have been widely explored in the context of tissue engineering. Leucine-zipper coiled-coil domain is an α-helical structural motif with a heptad repeat sequence $(abcdefg)_n$, comprising hydrophobic (*a* and *d*), charged (*e* and *g*) and polar (*b*, *c* and *f*) residues that form an amphiphilic α-helical structure, through the establishment of hydrophobic and ionic interactions (Fig. 1B). The design rules guiding the formation of a coiled-coil structure were extensively reviewed by Mason and Arndt [46]. The formed structure reversibly self-assembles into coiled-coils, whose physical association will favor the formation of an

engineered hydrogel network [47]. Based on the advantageous features of this self-assembly module, a number of genetically engineered triblock copolymers were synthesized. These are composed by a random coil water-soluble segment (Ala-Gly-rich sequence), flanked by two short leucine zipper end motifs (each containing six heptad repeats) that drive the formation of the network through a reversible gelation process triggered by changes in pH and temperature (Fig. 1B) [47-49]. The formed physically cross-linked hydrogels (Fig. 1B) display shear-thinning properties and rapid recovery after injection, allowing encapsulated cells to survive [49]. Moreover, the degradation rate of the developed hydrogels can be easily controlled by engineering the amino acid composition of the leucine zipper coiled-coil [50]. Due to their modular structure these hydrogels can be endowed with bioactivity through the incorporation, within the central domain of the triblock polypeptide, of cell-adhesion ligands and proteolytic-sensitive sequences. Indeed, when modified with the RGD-cell adhesion ligand, the developed matrices have shown to be able to support human foreskin fibroblasts and human umbilical vein endothelial cells (HUVECs) attachment, spreading and proliferation, as well as focal adhesion formation [51-53].

***Amphiphilic block co-polypeptides***

A different approach that is being increasingly used in the development of protein-based self-assembled hydrogels explores amphiphilic block co-polypeptides composed by a repeating sequence of charged amino acids (Lysine (K) or Glutamate (E)), usually ranging from 80 to 380 residues in length, and another of hydrophobic residues (Leucine (L) or Valine (V)), comprising 10 to 40 residues in length (Fig. 1C) [54]. Such block co-polypeptides usually present sequences like $K_xL_y$, $K_xV_y$ or $E_xL_y$. Self-assembling occurs by a process not found in nature and that is dependent on physical interactions between hydrophobic α-helical domains (Fig. 1C) [54]. These domains associate into “twisted fibrillar tapes with helices packed perpendicular to the fibril axes” [54]. This arrangement contributes to the formation of a hydrogel with increased stability at high temperatures and with ability to rapidly recover after stress, as a result of the weak and reversible nature of the interactions mediating the self-assembly process [54, 55].

A number of self-assembled hydrogels based on di- [55, 56], tri- [57] and pentablock [58] copolymers, differing in the length and/or composition of the hydrophobic domain, have been proposed. The length of the hydrophobic domain significantly impacts the stability of the formed hydrogels, with shorter segments resulting in weaker hydrogels.

Due to the similarity between the stiffness of some of these amphiphilic block co-polypeptides and the brain tissue (~200 Pa), their influence on cellular behavior has been further assessed in this system [56].

***Mixing-induced two-component hydrogel***

The concept of protein-protein interaction between specific association domains was explored by Heilshorn´s group for the design of mixing-induced two-component hydrogels [59, 60]. The first component of such system comprises proline-rich peptides (PPxY) linked by hydrophilic spacers (Fig. 1D). The second is composed by engineered repeats of WW domain linked together by hydrophilic spacers containing the cell adhesion motif RGDS (Fig. 1D). The inclusion of such domain imparts flexibility and biofunctionality to component 2. Upon mixing, under physiological conditions, the two components are physically cross-linked leading to the formation of a self-assembled hydrogel. The strength of the resultant material can be tuned by changing the number of repeats per component and by adjusting the strength of protein-protein interactions mediating the self-assemble process [60].

As in this system, self-assembly occurs without the need of an external trigger like temperature, pH and ionic strength, physiological conditions are kept unaltered during the cross-linking process, which is highly advantageous when envisaging the use of such systems for cell transplantation [59]. Indeed, mixing-induced two-component hydrogels have shown to be able to support the growth and differentiation of PC12 neuronal-like cells, HUVECs, and primary murine neural stem cells (NSCs) [59], constituting highly promising injectable materials for cell transplantation. Moreover, these hydrogels present shear-thinning properties, resulting from the weak nature of the established interactions [59].

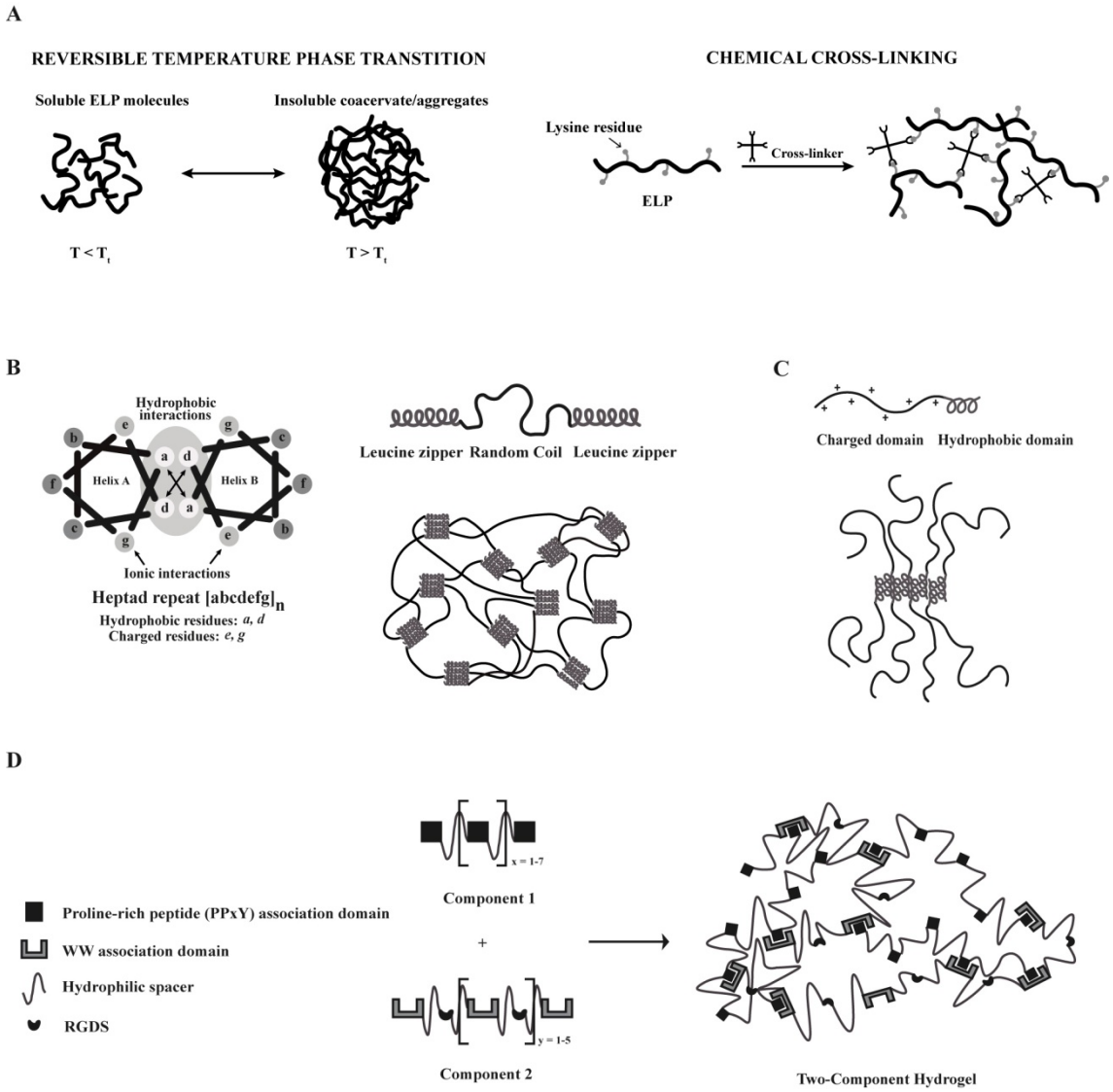


**Figure 1. Engineered protein-based self-assembled hydrogels**. **A)** Self-assembly of elastin-like polypeptide (ELP)-based hydrogels. Temperature triggered self-assembly occurs at temperatures above the Tt, leading to the formation of an insoluble and highly viscous coacervate. Adapted from [61]. Chemical cross-linking self-assembly is mediated by the reaction between the lysine-containing ELPs and the amine reactive cross-linker. Adapted from [62]. **B)** Self-assembly of leucine zipper coiled-coil domains. Representation of the heptad repeat sequence $(abcdefg)_n$, as well as the interactions guiding the formation of leucine zipper coiled-coil domains. The physical association of the formed structures will favor the development of an engineered hydrogel network. Adapted from [47]. **C)** Self-assembled hydrogels based on amphiphilic block co-polypeptides composed by alternating charged and hydrophobic amino acids ($K_xL_y$). Self-assembly is mediated by the hydrophobic interactions between α-helical domains. Adapted from [56]. **D)** Schematic representation of mixing-induced two-component hydrogel. WW domains form a physically cross-linked network with proline-rich peptide (PPxY) domains, under physiological conditions, being that

the strength of this interaction varies according to the specific WW domain used. WW domains are linked by hydrophilic spacers containing the RGDS cell-adhesion motif. Adapted from [59].

### Peptide-based synthetic hydrogels

Recently, hydrogels formed based on peptide self-assembly constitute one of the most actively investigated class of biomaterials in the context of tissue engineering. Peptide-based molecules, unlike other biopolymers (*e.g*. proteins and DNA/RNA), can be obtained with high purity, reproducibility and good yields, crucial features when envisaging a clinical application. Depending on the nature of the molecular building blocks (natural and non-natural amino acids), peptide sequences with acidic, basic, polar, non-polar or aromatic features can be developed [18, 63]. These features can influence, *per se,* different biological functions, including cell adhesion, proliferation and differentiation [18], thus circumventing the need of using more complex proteins. Nevertheless, the bioactivity and biofunctionality of the resulting systems can be further improved through the incorporation of specific cell adhesion domains (*e.g.* fibronectin- or collagen-derived RGDS [64-66], laminin-derived IKVAV [67], bone-marrow homing peptides (BMHP) -1 and -2 [66] and the osteogenic growth peptide ALK [68]), or proteolytic-sensitive sequences (*e.g.* matrix metalloproteinase (MMP)-2 [69] and -13 [70] specific cleavage sites)).

The mechanisms behind the self-assembly processes mediating the formation of peptide-based hydrogels was thoroughly reviewed by Zhang and co-workers [71, 72]. These hydrogels are usually engineered to self-assemble according to the design rules derived from natural proteins, by adopting basic secondary structural motifs, such as β-sheets, β-hairpins or α-helices. However, a number of new approaches based on electrostatic, amphiphilic or aromatic interactions are being widely explored for the development of new self-assembled hydrogels.

In the following sections, we present the state-of-the-art of the two main categories of peptide-based self-assembled hydrogels.

#### *Self-assembling peptides*

Self-assembling peptides based on naturally-derived amino acids have been proposed as promising structural elements for the development of novel hydrogels for tissue engineering applications [71]. Inspired by the yeast protein zuotin [73], Zhang's group synthesized a number of ionic self-complementary peptides, including EAK16 [74, 75], RADA16 [76, 77], FEK16 [78] and KLD-12 [79]. These are composed by alternating charged hydrophilic and hydrophobic natural amino acids and have an intrinsic ability to self-assemble into highly ordered β-sheet nanofibrous scaffolds (Fig. 2A). The self-assembly process can be further accelerated by changes in pH or in salt solution concentration [74-76]. Ultimately, the non-

covalent nature of the established interactions, in combination with the dependence on external stimulus (*e.g.* pH, temperature and ionic strength), allows the self-assembly process to be reversible and, as a result, the development of "smart" hydrogels [77]. The stimulus-responsiveness of the developed hydrogels allows a more tight control over the self-assembling process, which can be of interest for obtaining an *in situ* forming gel for cells and/or biomolecules delivery. These ionic self-complementary peptides have been successfully applied in a number of tissue engineering applications, namely as 3D matrices for *in vitro* cell culture [76, 79-82] and as vehicles for cell transplantation [80] and/or endogenous cell recruitment [83]. Peptides based on RADA16 self-assembling motif are the most frequently employed due to the ease with which it is synthesized and modified for specific applications. RADA16-based hydrogels are able of effectively support the differentiation of adult rat liver progenitor cells into functional hepatocyte-like spheroid clusters [81], PC-12 neuronal-like cell viability, neurite outgrowth and synapse formation [80], and hippocampal neuronal cell culture [82].

To afford peptide-based self-assembled hydrogels with additional biological activity, a number of specific bioactive sequences were incorporated. For instance, RADA16-based hydrogels incorporating cell adhesion motifs from collagen VI (RGDS), as well as BMHP- 1 and -2, have been developed and their *in vitro* biological performance evaluated using mouse adult NSCs [66]. As compared with non-functionalized matrices, the bioactive hydrogels showed improved ability to support NSC survival, proliferation and differentiation. [66]. Similar hydrogels comprising bioactive sequences known to enhance osteoblast behavior, such as the osteogenic growth peptide ALK, osteopontin cell-adhesion motif (DGR) and 2-unit RGD motifs (PGR), were also designed, and shown to support mouse pre-osteoblastic MC3T3-E1 cells adhesion, proliferation and migration, as well as osteogenic differentiation [68].

β-sheet self-assembly was also explored in the development of triblock peptides, comprising an amphiphilic triblock peptide motif (Fig. 2B). The central B block comprises alternating hydrophilic (glutamine) and hydrophobic (leucine) residues ($(QL)_{n=1-6}$ repeat), whose interactions lead to the formation of peptide dimmers [84]. These in turn, form β-sheet hydrogen bonds with each other, which keep them aligned perpendicularly to the peptide backbone axis, allowing the formation of highly-ordered nanofibrous matrices (Fig. 2B). On the other hand, the A block is composed by two to four positively charged lysine residues which, due to electrostatic repulsions, will affect the conditions required for peptide self-assembly at physiological conditions. Therefore, a balance of repulsive and attractive forces must be attained to control the self-assembly of triblock peptides into well-defined nanostructures and the properties of the resultant hydrogels [84]. The modular nature of

amphiphilic triblock peptides can be harnessed to favor a more tunable control over hydrogel mechanical properties. For instance, the careful selection of the amino acid residues composing A and B blocks significantly influences the gelation conditions, the length and diameter of the formed nanofibers, and the viscoelastic properties of the resultant hydrogel [85]. To improve the bioactivity of developed hydrogels, an MMP-2 specific cleavage site and an RGD cell adhesion motif were incorporated in the central B block and in the A block, respectively [69]. The combination of these two bioactive motifs resulted in increased viability, spreading and migration of MSCs from human exfoliated deciduous teeth within the hydrogel when compared with the non-functionalized ones.

An alternative design based on β-sheet motifs was developed, in which an amphiphilic β-hairpin secondary structure was used as self-assembling motif [8, 86]. Here, peptide sequences fold in response to different external stimulus, including pH [87], temperature [88] and ionic strength [89]. The formed hydrogels present a controllable shear-thin recovery kinetic, due to the weak and transient nature of the interactions mediating the self-assemble process [90]. This allows the encapsulation and subsequent delivery of cells to the injured sites, by minimally invasive procedures. β-hairpin-based hydrogels were shown to be cytocompatible, being able to mediate the adhesion, migration and proliferation of NIH3T3 murine fibroblasts (seeded on their surface), even in the absence of serum proteins or cell-adhesive motifs [91]. Through the incorporation of sequences sensitive to MMP-13, the degradation of such hydrogels can be efficiently controlled [70].

***Self-assembling peptide amphiphiles***

Peptide amphiphiles (PAs) are composed by a peptide sequence with a covalently linked chemical tail (*e.g.* short hydrophobic sequences or aromatic moieties) with intrinsic ability to self-assemble. These molecules can combine, thus, the structural features of amphiphilic molecules with the chemical functionality/bioactivity of small peptide sequences [92-94]. In the last decade, pioneering work of Stupp and co-workers resulted in the proposal of a broad range of PAs comprising a hydrophilic sequence covalently linked to an alkyl chain [94]. These molecules are typically composed by four distinct domains (Fig. 2C): (1) short *hydrophobic tail* responsible to drive the self-assembly process; (2) *β-sheet peptide domain,* which, through the formation of hydrogen bonds, promotes the cohesion of the formed nanofibers; (3) *charged residues* to confer water solubility; and (4) *bioactive domain* to mediate a specific biological response. Their self-assembly into long and stable nanofibers (Fig. 2C) is driven by the hydrophobic tail and occurs under specific pH, temperature or ionic strength conditions [95]. The resulting structures further undergo a sol-to-gel transition under physiological conditions in the presence of multivalent ions, which allows injection and *in situ* gel formation [64]. As result of the self-assembly process, the peptide sequence

will be orientated towards the aqueous environment. This, in combination with the versatility and modular nature of PAs, allows the easy incorporation of bioactive sequences at the extremity of the peptide domain (Fig. 2C) and the development of bioactive hydrogels. As an example, PAs functionalized with the IKVAV epitope from laminin, revealed higher ability to promote NSC adhesion, migration and differentiation into a neuronal phenotype, as well as neurite outgrowth, when compared to laminin-coated surfaces [67]. These promising outcomes were associated to the high density of IKVAV epitopes present on the nanofibers surface [67]. Therefore, both the epitope density and their presentation on the nanofiber surface were found to contribute to such a pronounced biological response. Also in the context of nerve regeneration, a hydrogel based on a PA engineered with a heparin sulfate mimetic and an IKVAV epitope was developed [96]. The two bioactive moieties have demonstrated a cooperative effect in the promotion of PC12 neuronal-like cells neurite outgrowth, even when in presence of inhibitory components, such as chondrotin sulfate proteoglycans [96]. For application in bone regenerative therapies, a hydrogel was engineered with BMP-receptor binding peptides, termed osteopromotive domains [97]. The developed hydrogels showed ability to promote cell survival and osteoblastic differentiation of human bone marrow stromal cells (BMSCs) [97].

Aromatic PAs comprising short (*e.g.* di- or tri-) peptide sequences capped, at the N-terminal, with a synthetic aromatic moiety have been also explored for the development of self-assembled hydrogels. These PAs have the intrinsic ability to self-assemble and drive the formation of highly-ordered amphiphilic hydrogels, by a combination of hydrophobic and π-π interactions [98]. A number of PAs comprising the fluoren-9-ylmethyloxycarbonyl (Fmoc) aromatic stacking ligand were developed [99-101]. The simplicity of the aromatic moieties (only 2-3 amino acids in length) allows the easy modification of the peptide sequence and a more tunable control over the structure and mechanical properties of the resultant hydrogels [99-101]. The structure of the self-assembled PAs, resembles in several aspects the native ECM, namely in their hydrated nature, nanofibrous architecture and rigidity (G'~10 kPa) [100-102]. To endow these hydrogels with bioactivity, a modular design strategy combining an Fmoc-RGD peptide with the Fmoc-diphenylalanine (Fmoc-FF) sequence was explored [65]. The developed hydrogels showed ability to support the adhesion, migration and proliferation of human adult dermal fibroblasts, in an integrin-dependent manner. By changing the ratio in which the two components are mixed, a more tunable control over hydrogel mechanical and biological properties may be achieved. Alternatively, some authors explored the use of naphthalene (Nap), rather than the Fmoc moiety, as aromatic capping group to synthesize the Nap-FFGEY peptide. The tyrosine residue (Y) present in the resultant aromatic PA could be easily phosphorylated by the

action of a kinase, leading to the formation of a molecule with increased hydrophilicity, not capable of self-assemble and form a hydrogel. Interestingly, when injected in a mouse model it was observed that the phosphorylated PA was converted to a gel by the action of naturally occurring phosphatase enzymes [103, 104]. Therefore, injectable hydrogels based on these PAs can be developed by taking advantage of this enzymatic switch.

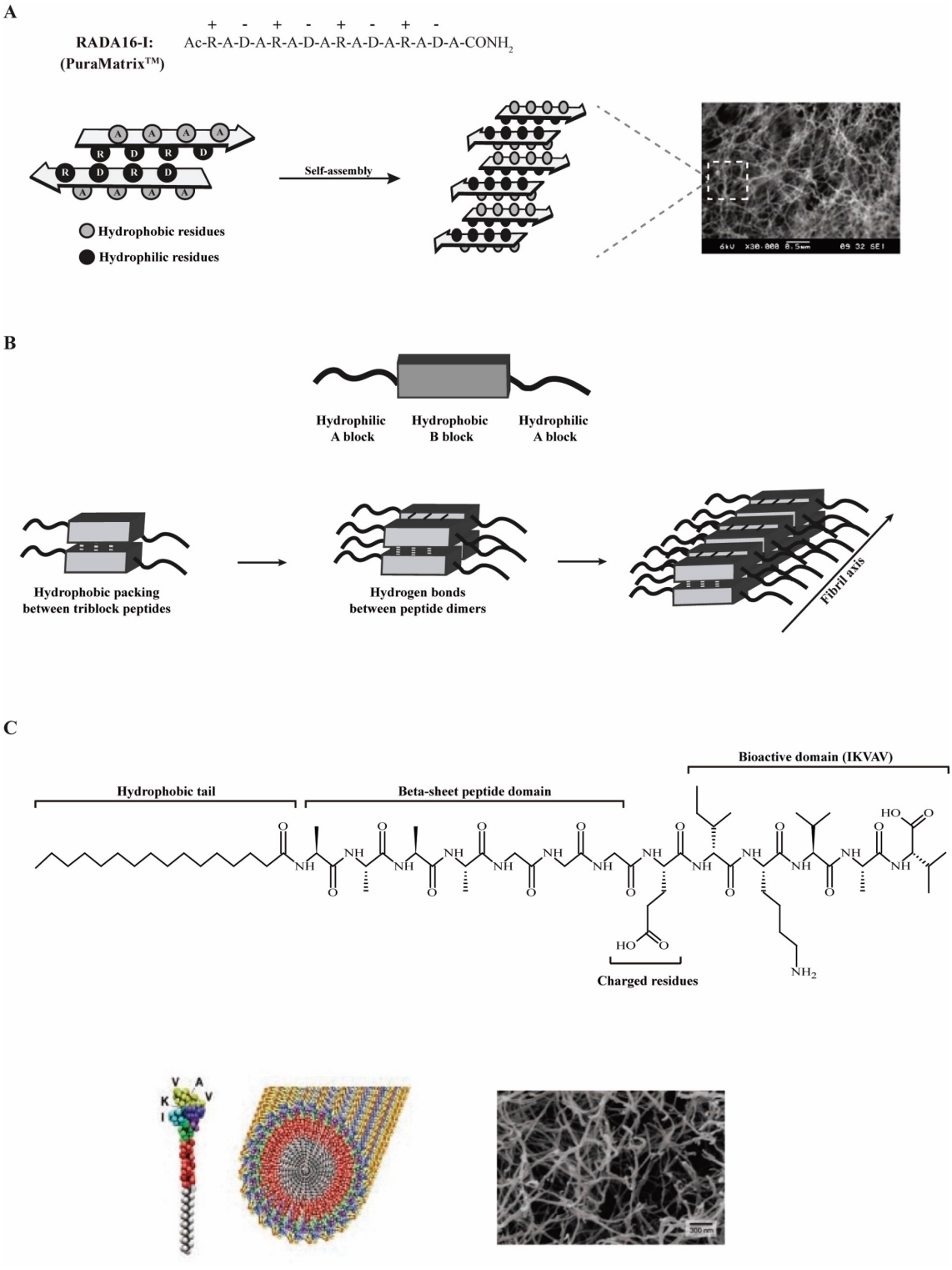


**Figure 2. Peptide-based self-assembled hydrogels**. **A)** β-sheet forming ionic self-complementary peptide – RADA16 (PuraMatrix™). Self-assembly into highly porous β-sheet nanofibrous scaffolds occurs through the formation of hydrophobic and ionic interactions. Adapted from [105]. Electron microscopy image of RADA-16-based nanofibrous scaffold. Reproduced from [106], with permission from Elsevier. **B)** Amphiphilic triblock peptides. The hydrophobic central block (B) mediates the self-

assembly process through the establishment of hydrophobic interactions between triblock peptides (resulting in peptide dimers), as well as hydrogen bonds among peptide dimers along the fiber axis. The hydrophilic A block is composed by charged lysine residues that will affect the conditions required for peptide self-assembly at physiologic conditions. Adapted from [84]. **C)** Chemical structure of a self-assembling peptide amphiphile (PA) comprising four key structural domains. Molecular representation of an IKVAV-PA molecule and it's self-assembly into long and stable nanofibers. Reproduced from [67], with permission from American Association for the Advancement of Science.

### DNA-based hydrogels

Despite the high costs associated at present with DNA synthesis, this molecule has several advantageous features that make it highly attractive for the development of self-assembled hydrogels [107]. These include its hydrophilic nature, inherent biocompatibility and ability to form stable and flexible secondary structures through specific Watson-Crick base-pairing (Fig. 3A) [107]. Moreover, DNA can be easily tailored either by varying the number and type of nucleic bases or through the incorporation of bioactive motifs, while retaining the ability to self-assemble into highly-ordered nanostructures [18, 107, 108]. Ultimately, one of the most important and unique properties of these molecules is the wide range of molecular biology tools available for their synthesis and modification [109]. In fact, no other molecule simultaneously meets all the aforementioned properties, making DNA a highly attractive and versatile material for the development of self-assembled hydrogels. The unique features, as well as the inherent ability of DNA to self-assemble allow it to be used as structural component of nanoscale materials, thus behaving *per se* as a biopolymer.

To design complex and stable nanoscale structures based on DNA, Lu and co-workers, taking advantage of the Watson-Crick base-pair rules aforementioned (Fig. 3A), engineered branched DNA molecules with complementary sticky-ends. The self-assembly and the formation of a cross-linked hydrogel network occurs under physiological conditions and in the presence of a DNA ligase (Fig. 3B) [110]. Therefore, the developed matrices can be used to encapsulate live mammalian cells, without any deleterious effect on their viability [110]. To promote a more tunable control over the self-assembly process and over the structure of the resultant hydrogel, the adjustment of the concentration and type of branched DNA monomers [110], as well as the development of stimuli-responsive (*e.g.* pH [111], temperature [112] or enzymatic activity [112]) hydrogels, can be exploited. Indeed, a number of DNA-based hydrogels with responsive properties that self-assemble rapidly without the need of any chemical cross-linker were developed [111, 112]. The properties and applications of such hydrogels were comprehensively reviewed by Tan and co-workers [108]. More recently, DNA hydrogels formed by self-assembly of linear DNA molecules

comprising sticky ends have been developed (Fig. 3C) [113]. These hydrogels are thermoresponsive, allowing a more tight control over the self-assembling process, which can be of interest to obtain an *in situ* forming gel for cell and biomolecule delivery. To the best of our knowledge, the effect of such hydrogels on cell behavior has not been assessed yet.

Despite the recent advances on the use of DNA as structural component for the development of self-assembled hydrogels, the weak nature of the designed matrices [114], as well as their poor stability against extra- and intra-cellular degradation, mainly mediated by nucleases [115], still constitutes some of the main obstacles to the application of DNA-based hydrogels in the biomedical field. Therefore, in the last few years a number of chemical modifications to native DNA have been explored in an attempt to favor the formation of more stable and resistant hydrogels [115]. Also, to develop mechanically robust hydrogels, DNA are being explored as cross-linking agent, rather than biopolymer, to mediate the assembly of synthetic polymers, forming DNA-hybrid hydrogels [114, 116], which will be addressed in the following section.

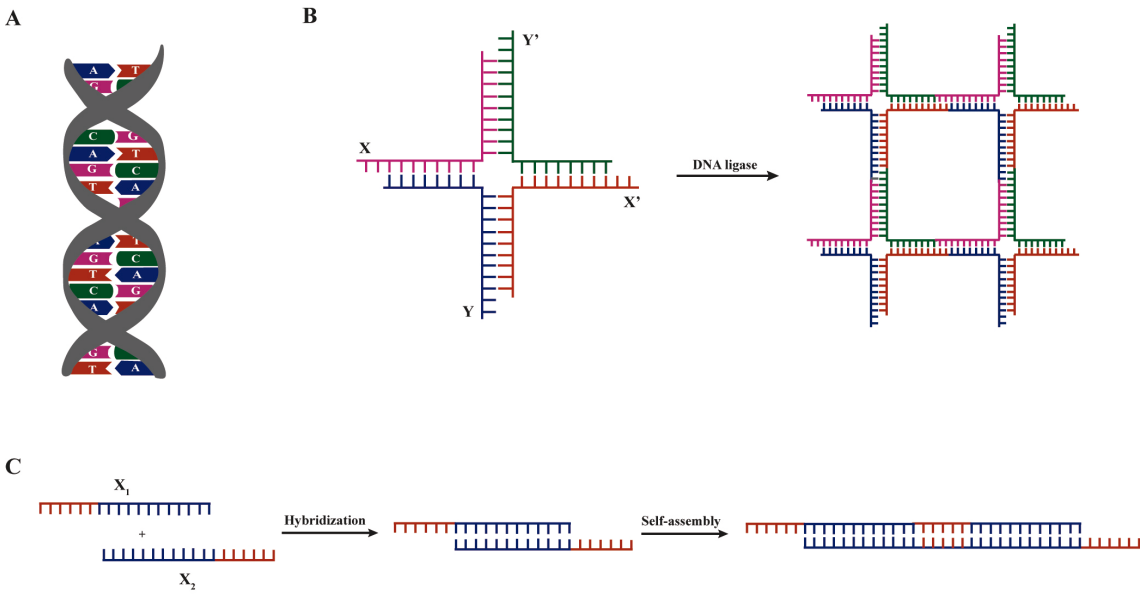


**Figure 3. DNA-based self-assembled hydrogels**. **A)** Two complementary single strands hybridize, based on Watson-Crick base pairing rules - adenine (A) with thymine (T) and guanine (G) with cytosine (C) – forming a double-stranded DNA molecule. **B)** Sticky-end self-assembly of branched DNA molecules mediated by DNA ligase. Adapted from [109]. **C)** Single-stranded DNA molecules hybridize into a monomeric double-stranded DNA building block, who's self-assembly occurs through the interaction between complementary sticky-ends. Adapted from [113].

### Hybrid hydrogels

Hybrid hydrogels combine the advantageous properties of biological (macro)molecules with the tunable and reproducible structural and mechanical features of synthetic polymers [117, 118]. The combination of these two distinct classes of molecules, either through covalent or non-covalent interactions, can result in hydrogels with a higher level of structural organization and improved properties, when compared with their individual components. The biological components are usually molecules adopting basic conformational secondary structures (β-sheets or α-helices), such as peptides, proteins, or DNA/RNA. Their use allows the tunable control over the structural organization and properties of developed hydrogels [117, 118]. The synthetic segments contribute, normally, for the improvement of the mechanical performance of the network. Despite the wide variety of synthetic polymers that can be used in the design of hybrid hydrogels, PEG and poly(N-(2-hydroxypropyl)methacrylamide) (pHPMA) are the ones usually selected, due to their hydrophilicity, biocompatibility and non-immunogenicity. Moreover, the incorporation of these polymers can contribute to increase the stability of the final network in time by delaying its (enzymatic) degradation, which may be highly advantageous when envisaging a clinical translation.

The concept of using biopolymers to guide the self-assembly of synthetic polymeric matrices has been increasingly explored. Indeed, a number of hybrid block copolymers containing biologically-inspired proteins/peptides adopting β-sheet or coiled-coil structures, have been engineered for the development of self-assembled hybrid hydrogels (for a more extensive review see [118]). Despite their conjugation with a synthetic polymer, these coiled-coil and β-sheet forming biopolymers retain their ability to self-assemble and thus can be used to induce the formation of a highly-ordered nanofibrous network. One of the first and well-known examples of hybrid hydrogels formed based on this concept, explores a hybrid diblock copolymer comprising β-sheet forming peptide sequences, derived from the natural occurring β-amyloid protein, conjugated with a PEG polymer [119, 120]. Since then, a number of other β-sheet-forming proteins/peptides have been explored for the design of self-assembled hybrid hydrogels. As an example, block copolymers comprising ELPs ($(VPGVG)_4$ and $(VPAVG)_4$) conjugated with a PEG backbone were used. Here, the self-assembly is driven by a reversible temperature transition, culminating in the formation of an insoluble and supramolecular thermoresponsive coacervate [121, 122]. Further, hybrid hydrogels in which the synthetic polymer self-assembly is guided by the chemical cross-linking of elastin domains modified with lysine residues were also developed [123, 124]. The resulting hydrogels present elastomeric and shear-thinning properties, allowing these to be injected and form a matrix *in situ* [123, 124]. Moreover, these hydrogels enable

a tunable control over the density of elastin cell adhesion domains, as well as of matrix stiffness, which is highly desirable to modulate cell behavior and when studying cell-matrix interactions. Indeed, ELP-PEG hybrid hydrogels have shown to be able of support fibroblasts growth, migration and proliferation [123, 124]. β-sheet forming peptides were also explored as component of hybrid graft copolymers. A pHPMA polymer grafted with complementary β-sheet peptides were developed and endowed with bioactivity through the coupling of RGD cell-adhesion domains to each complementary hybrid graft copolymer (Fig. 4A). These hydrogels have shown ability to support MC3T3-E1 cell viability and proliferation.

The self-assembly properties of coiled-coil forming peptides were also explored to create hybrid hydrogels. Diblock copolymers of PEG and coiled-coil forming peptides that self-assemble into a two-stranded α-helical coiled-coil conformation in aqueous solution, illustrate such strategy [125, 126]. It has been shown that the conjugation of coiled-coil domains with a synthetic polymer favors their thermal stability, resulting from the formation of a PEG hydrophilic shell around the coiled-coil structure [125, 126]. Further, genetically engineered coiled-coil forming peptides (CC1 and CC2), non-covalently grafted to a pHPMA synthetic backbone have been explored for the development of hybrid graft copolymers [127]. Here, the physical cross-linking and the consequent hybrid hydrogel formation were favored by a temperature-induced conformational change of coiled-coil peptides [127]. The temperature-responsiveness of these hydrogels allows the development of “smart” materials and a more tunable control over the material properties. Another design involving the pHPMA hydrophilic polymer and peptide grafts forming homodimers and higher aggregates were also described [128, 129]. In this case, a minimum of four heptad repeats was found to be needed to induce self-assembly and the formation of homodimers [128, 129]. The number and concentration of the copolymer, as well as temperature proved to have a crucial role on the control of the gelation process [129]. Still, this design is very often limited by the possibility of dimer formation between grafted peptides attached to the same macromolecule. To avoid this and to guarantee the formation of a well-ordered 3D structure, a modified approach was proposed. In this new design, a pHPMA synthetic backbone was grafted with a pair of oppositely charged coiled-coil forming peptides (CCE and CCK) (Fig. 4B) [130, 131]. The oppositely charged peptide grafts self-assemble into antiparallel heterodimeric motifs and induce the formation of a physically cross-linked hydrogel [130, 131]. Here, a reversible self-assembly occurs when the graft copolymers, CCE-P and CCK-P, are mixed equimolarly at neutral pH.

A different approach for the design of hybrid hydrogels consists in using star-shaped macromolecules, such as 4-arm PEG, in combination with biological molecules, responsible

for mediating the self-assembly process. As an example, four-arm star-shaped PEG polymers functionalized with either thymine or adenine nucleotides were used to create injectable hydrogels, assembled by base pairing between the two complementary nucleotides (Fig. 4C) [56, 116]. These hydrogels were explored for soft tissue engineering applications, namely for the encapsulation of adipose-derived stem cells. The gelation time (and therefore cell entrapment time) was shown to be dependent on the type of nucleotides used, and the developed hydrogels found to support cell viability and growth [116].

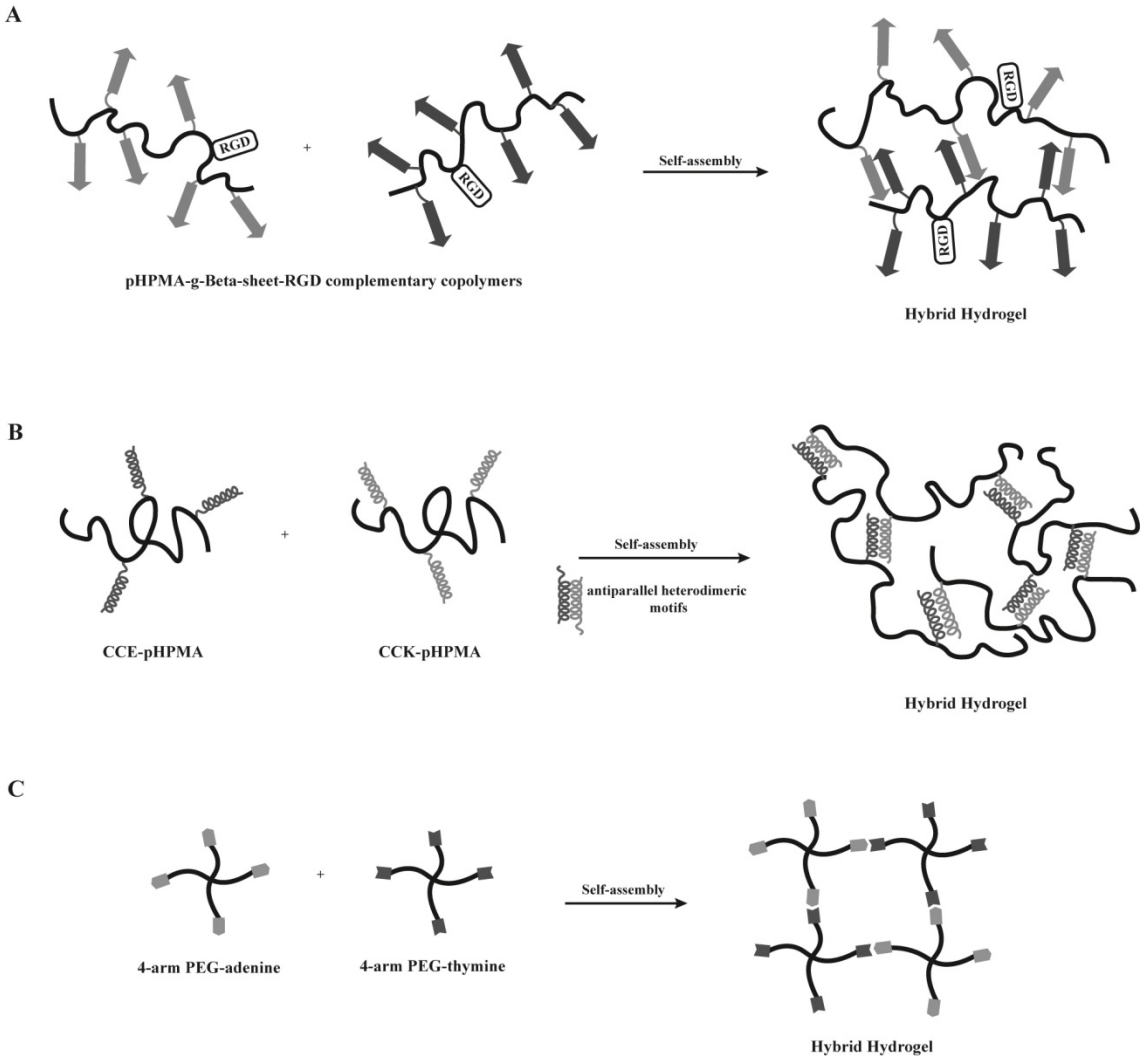


**Figure 4. Hybrid hydrogels**. **A)** Hybrid hydrogels based on pHPMA-g-β-sheet-RGD complementary copolymers. The self-assembly of these copolymers is driven by the formation of hydrogen bonds among grafted β-sheet peptides. Adapted from [132]. **B)** Hybrid hydrogels comprising pHPMA hydrophilic polymer grafted with a pair of oppositely charged coiled-coil forming peptides (CCE and CCK). The self-assembly into highly-ordered hydrogels is mediated by antiparallel heterodimeric coiled-coil association. Adapted from [130]. **C)** Self-assembly of four-arm PEG copolymers by base pairing between the two complementary nucleotides (adenine and thymine). Adapted from [116].

### *In vivo* biological performance of synthetic self-assembled hydrogels

The self-assembled hydrogels discussed so far in this review were designed envisaging their application as 3D scaffolds for cell transplantation. Proof-of principle of the suitability of these hydrogels in terms of ability to create a permissive microenvironment for cell growth and differentiation, *in vitro*, has been highlighted. However, several of these systems have already been evaluated *in vivo*. In this section, an overview of the *in vivo* biological performance of several of these hydrogels, when explored for cell delivery, is presented in Table **1**, namely that of the most recent and promising bioactive self-assembled hydrogels designed for cell transplantation and/or endogenous cell recruitment, in the context of cartilage, bone, nerve and cardiac regeneration.

**Table 1.** Main outcomes of *in vivo* biological performance of self-assembled hydrogels as 3D scaffolds for cell transplantation and/or endogenous cell recruitment.

| Application | Hydrogel | Cells | *In vivo* model | Main outcomes | Ref. |
|---|---|---|---|---|---|
| **Cartilage rengeneration** | Chemical cross-linked ELPs | - | Goat model of osteochondral defect | Crosslinked ELPs were rapidly degraded (within 3 months), allowing cell infiltration and endogenous matrix deposition | [133] |
| | SELP | - | Rabbit model of osteochondral defect | Allowed the infiltration and integration of endogenous stem cells, favoring matrix remodeling (evidenced by the production of type I collagen and proteoglycans) | [134] |
| | KLD-12 | MSCs | Rat model of knee osteoarthritis | Hydrogel remained for 6 weeks after the injection. Promoted chondroprotection (contributed to prevent/reduce chondrocyte apoptosis and inflammation) | [135] |

| | | | | | |
|---|---|---|---|---|---|
| | Poly(L-lactide-co-ε-caprolactone) scaffolds + mixture of KLD-12 and KLD-12-collagen mimetic peptide (CMP7) | BMSCs | Subcutaneous implantation at mice dorsa | Stimulated chondrogenic differentiation of BMSCs and deposition of chondral ECM (*e.g.* glycosaminoglycans) | [136] |
| **Bone regeneration** | Demineralized bone matrix modified with RADA16 | MSCs | Mouse model of femoral defect | Favored the adhesion, proliferation and differentiation of transplanted MSCs, creating a permissive microenvironment for bone regeneration (high yield of osteogenic cells (MSCs) and growth factors, namely bone morphogenetic protein-6, platelet-derived growth factor-BB, vascular endothelial growth factor (VEGF) and fibroblast growth factor) | [137] |
| | | | Goat model of femoral defect | Bone regeneration/ remodeling was efficiently completed at 16-weeks post injury | [138] |
| | RGDS + Phosphoserine -PA | - | Rat model of femoral defect | Increased bone formation was observed 4 weeks after injury | [139] |
| | Ti-6Al-4V macroporous structure filled with RGDS + phosphoserine-PA | MC3T3-E1 | Rat model of femoral defect | No significant cytotoxic effect to cells was observed. Promoted *de novo* bone formation in and around the implant and of angiogenesis, within 4 weeks | [140] |
| **Nerve regeneration** | $K_{180}L_{20}$ Amphiphilic diblock co-polypeptide | - | Mouse forebrain | No detectable toxicity or adverse tissue response. | [56] |

| | | | | | |
|---|---|---|---|---|---|
| | | | | Degraded and cleared over 8 weeks. Allowed gradual infiltration of endogenous endothelial and glial cells | |
| | Heparin-RGD-4-arm PEG | NSCs | Rat brain parenchyma | Promoted NSCs migration and neuronal differentiation, as well as axo-dendritic outgrowth. Good histocompatibility | [141] |
| | $K_2(QL)_6K_2(QL)_6$ Ionic self-complementary peptide | Neural progenitor cells (NPCs) | Rat model of spinal cord injury (SCI) | Supported survival and differentiation of transplanted NPCs, as well as their integration into the host tissue. Neuroprotective effect (reduction of inflammation and astrogliosis and preservation of motor neurons). Reduced of cystic cavity volume. Promoted of forelimb functional recovery | [142, 143] |
| | RADA16 | Schawnn cells (SCs) and NPCs | Rat model of SCI | Supported survival, migration and differentiation of transplanted SCs and NPCs. Promoted axonal growth, angiogenesis, as well as robust migration of endogenous cells. | [144] |
| | RADA16 | - | Hamster model of an optic tract lesion | Created a permissive environment for axonal regeneration and reconnection to target tissues. | [145] |

| | | | | | |
|---|---|---|---|---|---|
| | | | | Functional return of vision | |
| | IKVAV-RADA16 | NSCs | Rat model of brain injury | Improved survival, proliferation, migration and neuronal differentiation of NSCs. Promoted brain tissue regeneration after 6-weeks post-transplantation | [146] |
| | IKVAV-PA | - | Mouse model of SCI | Hindered glial scar formation. Promoted regeneration of motor and sensory axons. Improved functional recovery | [147, 148] |
| | YIGSR-PA | - | Rabbit corneal stromal pocket model | Induced keratocyte migration, stromal regeneration, and collagen I synthesis | [149] |
| | PLGA tube filled with aligned RGDS-PA | SCs | Rat model of sciatic nerve defect | Promoted the alignment, proliferation and migration of transplanted SCs, as well as axon alignment. Significant recovery of motor and sensory function | [150] |
| **Cardiac regeneration** | Mixing-induced two-component hydrogels – 8-arm PEG | Human induced pluripotent stem cell-derived endothelial cells (hiPSC-ECs)) | Mouse model of hindlimb ischemia | Supported hiPSC-EC survival and proliferation. Reduced necrosis and inflammation with improved muscle tissue regeneration | [151] |
| | RADA16 | Stem cells antigen-1 (Sca-1) positive | Mouse model of myocardial infarction | Supported the differentiation of Sca-1 positive cardiac progenitors into | [152] |

| | | | | | |
|---|---|---|---|---|---|
| | | cardiac progenitors | | cardiomyocytes and vascular smooth muscle cells.<br>Inhibited apoptosis, promoted angiogenesis and myocardial regeneration.<br>Restoration of cardiac function | |
| | Poly(caprolactone methacryloyloxyethyl ester) (PCLMA) matrix filled with RADA16 | Subcutaneous adipose tissue-derived progenitor cells (Sub-ATDPCs) | Mouse model of myocardial infarction | Creation of a permissive microenvironment for sub-ATDPC survival, proliferation and differentiation along the cardiac lineage.<br>Promoted angiogenesis | [153] |
| | RADA16 + -Substance P -RADA16 | - | Mice model of hind limb ischemia | Hydrogels remained until 28 days in the injected sites.<br>Promoted the recruitment of endogenous MSCs.<br>Prevented cardiac fibrosis and induced angiogenesis | [154] |
| | VEGF-mimetic peptide-PA | - | Mouse model of hind-limb ischemia | Significant functional recovery linked to the pro-angiogenic behavior of VEGF-mimetic peptide | [155] |

**Translation of synthetic self-assembled hydrogels into the clinic: progress and future challenges**

As discussed in the previous section, the potential of several synthetic self-assembled hydrogels for use in cell transplantation and/or endogenous cell recruitment has been already demonstrated in a number of pre-clinical *in vivo* studies involving different repair/regenerative scenarios (Table 1). Although the promising results have fueled the interest of the research community and manufacturers into the use of these materials, just now these begin to enter clinical testing. To the best of our knowledge, only one product based on self-assembled hydrogels is presently on the market - NuCore™ Injectable Nucleus developed by Spine Wave (Shelton, CT) [156]. This system consists of a recombinant protein copolymer comprising blocks derived from silk and elastin structural proteins and it was already evaluated in a pilot clinical trial to assess product safety for potential application in the repair and regeneration of invertebral disc [157]. The trial did not involve the transplantation of cells. No complications or adverse effects to the patient have been reported. Moreover, the system seems to slow the degenerative process over time. Despite the promising results obtained in this pilot study, further investigation on product safety and efficacy need to be performed prior its clinical use.

While trying to bring synthetic self-assembled hydrogels from bench-to-bedside, a number of requisites need to be fulfilled and few key issues must be taken into consideration. A wide number of self-assembled systems (proteins, peptides, DNA, synthetic polymers or hybrid structures) have been proposed for the design of cell-compatible hydrogels. Therefore, one of the most important issues to be addressed upon the development of these products and that most possibly significantly contributes to delay their translation, is the selection of the most suitable system for each particular application. The chosen building blocks should be biocompatible, biodegradable and able to mimic the cellular microenvironment of the surrounding tissues, as discussed in previous sections. The characterization of the proposed systems in terms of degradation rate and degradation by-products, as well as of biofunctionality (including inflammatory response) should be carried out in a number of *in vitro* and *in vivo* set-ups, before considering clinical translation. Scalability is also an important issue to take into account, since some building blocks, such as proteins and DNA, are difficult to obtain in large scale and in good yields, what has put a strain in costs. Nevertheless, the efforts made in the last few years towards the efficient chemical synthesis of such systems will possibly contribute to enhance their feasibility for biomedical applications. Also, production-related issues, such as purification and sterilization will be paramount to define if these will reach the market.

A challenge while developing injectable *in situ* forming hydrogels is to gain control over the 3D architecture of the hydrogel fibrillar network. The building blocks of synthetic self-assembled hydrogels typically assemble into randomly oriented networks, and the nanofibrillar structures formed in several peptide hydrogels are also randomly oriented. To better mimic the natural anisotropic structure and functional features of the ECM, control over fibrillar orientation both at the nano- and the micro-scale should be achieved. This is particularly important in hydrogels envisaged for application in highly organized tissues (*e.g.* nerve and bone), in which the structural and mechanical properties of the ECM fulfill important biomechanical properties and regulate cell behavior. For instance, longitudinally-oriented aligned structures have been shown to induce directional axonal re-growth and alignment of transplanted cells, by providing contact guidance, which can be of most importance in therapies for the treatment of spinal cord and peripheral nerve injuries [158]. Attempts to develop *in situ* forming hydrogels of aligned self-assembled PA nanofibers were made. This was achieved by exposing isotropic PA solutions to elevated temperatures, under which plaque-like structures are formed, which break apart into aligned bundles of multiple PA nanofibers upon cooling [159]. Upon pipetting the resultant liquid crystalline solution into $CaCl_2$-containing physiological buffer, string-like gels containing aligned nanofibers are formed. When modified with IKVAV or RGDS epitopes, aligned PA hydrogels containing neurons or neural progenitor cells (added to the $CaCl_2$ solution prior hydrogel formation), were able to guide neurite extension from neurons along the direction of the nanofibers *in vitro*, and to promote the growth of oriented processes from transplanted neural progenitor cells within the spinal cord, *in vivo* [160]. Control over the architecture of *in situ* forming hydrogels is therefore worthy to explore, and likely to be most rewarding.

The complexity and highly dynamic nature of biological systems constitutes another major challenge in the design and application of cell-compatible hydrogels. Hydrogels should be engineered not only to serve as vehicles for cell and/or biomolecule delivery, but also to guide cell behavior and fate. Therefore, hydrogels able to change their biological and/or physical properties along the different stages of cell engraftment and tissue regeneration are much awaited. In this context, the exploration of molecular self-assembly constitutes a highly promising strategy, once by being mediated by multiple weak and transitory interactions the supramolecular hydrogel structure can be easily reconfigured.

Another advantage of these synthetic hydrogels is that they can be combined with a number of bioactive molecules, including ECM proteins, growth factors or drugs that can additionally or synergistically modulate cell behavior and fate. Unsolved is the spatial and temporal control over the availability of these cues. These would allow the mirroring of those

observed in the native ECM in the context of repair/regenerative processes in which gradients of biochemical and physical cues are key players of the process.

In conclusion, the development of biomimetic synthetic self-assembled hydrogels is rapidly progressing, supported in part by technology advances in the field of recombinant proteins, solid-phase synthesis and polymer chemistry. In particular, with hybrid hydrogels one can combine the advantageous properties of biological (macro)molecules with the tunable and reproducible structural and mechanical features of synthetic polymers, conferring superior properties to the resulting systems. However, when envisaging the use of such hydrogels for cellular therapies, mimicking the complexity and functionality of the natural ECM without compromising important features for application in a clinical setting, like injectability, still remains a major challenge.

**Acknowledgments**

The authors would like to acknowledge the FEDER funds through the *Programa Operacional Factores de Competitividade* – COMPETE and the Portuguese funds through FCT – *Fundação para a Ciência e a Tecnologia* (HMSP-ICT/0020/2010, PTDC/SAU-BMA/118869/2010 and PEst/SAU/LA0002/2013) that supported this work. D Barros is supported by FCT (SFRH/BI/52379/2013) and I.F. Amaral by QREN through program ON.2, in the framework of "Project on Biomedical Engineering for Regenerative Therapies and Cancer" (NORTE-07-0124-FEDER-000005).

## References

[1] M. Guvendiren, J.A. Burdick, Engineering synthetic hydrogel microenvironments to instruct stem cells, Curr. Opin. Biotechnol. 24(5) (2013) 841-6.

[2] C. Wang, R.R. Varshney, D.A. Wang, Therapeutic cell delivery and fate control in hydrogels and hydrogel hybrids, Adv. Drug Deliv. Rev. 62(7-8) (2010) 699-710.

[3] O. Lindvall, Z. Kokaia, Stem cells for the treatment of neurological disorders, Nature 441(7097) (2006) 1094-6.

[4] M.P. Lutolf, P.M. Gilbert, H.M. Blau, Designing materials to direct stem-cell fate, Nature 462(7272) (2009) 433-41.

[5] M.W. Tibbitt, K.S. Anseth, Hydrogels as Extracellular Matrix Mimics for 3D Cell Culture, Biotechnol. Bioeng. 103(4) (2009) 655-663.

[6] H. Geckil, F. Xu, X. Zhang, S. Moon, U. Demirci, Engineering hydrogels as extracellular matrix mimics, Nanomedicine 5(3) (2010) 469-84.

[7] K.B. Fonseca, P.L. Granja, C.C. Barrias, Engineering proteolytically-degradable artificial extracellular matrices, Prog. Polym. Sci. 39(12) (2014) 2010-2029.

[8] P.M. Kharkar, K.L. Kiick, A.M. Kloxin, Designing degradable hydrogels for orthogonal control of cell microenvironments, Chem. Soc. Rev. 42(17) (2013) 7335-72.

[9] C.M. Lo, H.B. Wang, M. Dembo, Y.L. Wang, Cell movement is guided by the rigidity of the substrate, Biophys. J. 79(1) (2000) 144-52.

[10] A.J. Engler, S. Sen, H.L. Sweeney, D.E. Discher, Matrix elasticity directs stem cell lineage specification, Cell 126(4) (2006) 677-89.

[11] D.E. Ingber, Cellular mechanotransduction: putting all the pieces together again, FASEB J. 20(7) (2006) 811-27.

[12] R. Jin, In-situ Forming Biomimetic Hydrogels for Tissue Regeneration, in: C. Lin (Ed.), Biomedicine, InTech2012.

[13] J.-A. Yang, J. Yeom, B.W. Hwang, A.S. Hoffman, S.K. Hahn, In situ-forming injectable hydrogels for regenerative medicine, Prog. Polym. Sci. 39(12) (2014) 1973-1986.

[14] F. Wang, Z.Q. Li, M. Khan, K. Tamama, P. Kuppusamy, W.R. Wagner, C.K. Sen, J.J. Guan, Injectable, rapid gelling and highly flexible hydrogel composites as growth factor and cell carriers, Acta Biomater. 6(6) (2010) 1978-1991.

[15] G.A. Saracino, D. Cigognini, D. Silva, A. Caprini, F. Gelain, Nanomaterials design and tests for neural tissue engineering, Chem. Soc. Rev. 42(1) (2013) 225-62.

[16] J. Zhu, R.E. Marchant, Design properties of hydrogel tissue-engineering scaffolds, Expert Rev. Med. Devices 8(5) (2011) 607-26.

[17] E.S. Place, J.H. George, C.K. Williams, M.M. Stevens, Synthetic polymer scaffolds for tissue engineering, Chem. Soc. Rev. 38(4) (2009) 1139-51.

[18] N. Stephanopoulos, J.H. Ortony, S.I. Stupp, Self-Assembly for the Synthesis of Functional Biomaterials, Acta Mater. 61(3) (2013) 912-930.
[19] T. Lu, Y. Li, T. Chen, Techniques for fabrication and construction of three-dimensional scaffolds for tissue engineering, Int. J. Nanomedicine 8 (2013) 337-50.
[20] H. Cao, T. Liu, S.Y. Chew, The application of nanofibrous scaffolds in neural tissue engineering, Adv. Drug Deliv. Rev. 61(12) (2009) 1055-64.
[21] M. Nune, P. Kumaraswamy, U.M. Krishnan, S. Sethuraman, Self-assembling peptide nanofibrous scaffolds for tissue engineering: novel approaches and strategies for effective functional regeneration, Curr. Protein Pept. Sci. 14(1) (2013) 70-84.
[22] G.M. Whitesides, B. Grzybowski, Self-assembly at all scales, Science 295(5564) (2002) 2418-2421.
[23] S.G. Zhang, Fabrication of novel biomaterials through molecular self-assembly, Nature Biotechnol. 21(10) (2003) 1171-1178.
[24] R.J. Mart, R.D. Osborne, M.M. Stevens, R.V. Ulijn, Peptide-based stimuli-responsive biomaterials, Soft Matter 2(10) (2006) 822-835.
[25] R. Silva, B. Fabry, A.R. Boccaccini, Fibrous protein-based hydrogels for cell encapsulation, Biomaterials 35(25) (2014) 6727-38.
[26] A.M. Jonker, D.W.P.M. Lowik, J.C.M. van Hest, Peptide- and Protein-Based Hydrogels, Chem. Mater. 24(5) (2012) 759-773.
[27] S. Banta, I.R. Wheeldon, M. Blenner, Protein engineering in the development of functional hydrogels, Annu. Rev. Biomed. Eng. 12 (2010) 167-86.
[28] T. Kowalczyk, K. Hnatuszko-Konka, A. Gerszberg, A.K. Kononowicz, Elastin-like polypeptides as a promising family of genetically-engineered protein based polymers, World J. Microb. Biot. 30(8) (2014) 2141-2152.
[29] W.F. Daamen, J.H. Veerkamp, J.C.M. van Hest, T.H. van Kuppevelt, Elastin as a biomaterial for tissue engineering, Biomaterials 28(30) (2007) 4378-4398.
[30] D.W. Urry, Physical chemistry of biological free energy transduction as demonstrated by elastic protein-based polymers, J. Phys. Chem. B 101(51) (1997) 11007-11028.
[31] D.E. Meyer, A. Chilkoti, Quantification of the effects of chain length and concentration on the thermal behavior of elastin-like polypeptides, Biomacromolecules 5(3) (2004) 846-51.
[32] H. Betre, S.R. Ong, F. Guilak, A. Chilkoti, B. Fermor, L.A. Setton, Chondrocytic differentiation of human adipose-derived adult stem cells in elastin-like polypeptide, Biomaterials 27(1) (2006) 91-9.
[33] H. Betre, L.A. Setton, D.E. Meyer, A. Chilkoti, Characterization of a genetically engineered elastin-like polypeptide for cartilaginous tissue repair, Biomacromolecules 3(5) (2002) 910-6.

[34] S.R. MacEwan, A. Chilkoti, Elastin-like polypeptides: biomedical applications of tunable biopolymers, Biopolymers 94(1) (2010) 60-77.
[35] A. Chilkoti, T. Christensen, J.A. MacKay, Stimulus responsive elastin biopolymers: Applications in medicine and biotechnology, Curr. Opin. Chem. Biol. 10(6) (2006) 652-7.
[36] J. Lee, C.W. Macosko, D.W. Urry, Elastomeric polypentapeptides cross-linked into matrixes and fibers, Biomacromolecules 2(1) (2001) 170-179.
[37] D.W. Lim, D.L. Nettles, L.A. Setton, A. Chilkoti, Rapid cross-linking of elastin-like polypeptides with (hydroxymethyl)phosphines in aqueous solution, Biomacromolecules 8(5) (2007) 1463-70.
[38] K. Trabbic-Carlson, L.A. Setton, A. Chilkoti, Swelling and mechanical behaviors of chemically cross-linked hydrogels of elastin-like polypeptides, Biomacromolecules 4(3) (2003) 572-80.
[39] D.W. Lim, D.L. Nettles, L.A. Setton, A. Chilkoti, In situ cross-linking of elastin-like polypeptide block copolymers for tissue repair, Biomacromolecules 9(1) (2008) 222-30.
[40] K.S. Straley, S.C. Heilshorn, Independent tuning of multiple biomaterial properties using protein engineering, Soft Matter 5(1) (2009) 114-124.
[41] K.J. Lampe, A.L. Antaris, S.C. Heilshorn, Design of three-dimensional engineered protein hydrogels for tailored control of neurite growth, Acta Biomater. 9(3) (2013) 5590-9.
[42] Z. Megeed, J. Cappello, H. Ghandehari, Genetically engineered silk-elastinlike protein polymers for controlled drug delivery, Adv. Drug Deliv. Rev. 54(8) (2002) 1075-91.
[43] A. Nagarsekar, J. Crissman, M. Crissman, F. Ferrari, J. Cappello, H. Ghandehari, Genetic synthesis and characterization of pH- and temperature-sensitive silk-elastinlike protein block copolymers, J. Biomed. Mater. Res. 62(2) (2002) 195-203.
[44] A. Nagarsekar, J. Crissman, M. Crissman, F. Ferrari, J. Cappello, H. Ghandehari, Genetic engineering of stimuli-sensitive silkelastin-like protein block copolymers, Biomacromolecules 4(3) (2003) 602-607.
[45] X.X. Xia, Q. Xu, X. Hu, G. Qin, D.L. Kaplan, Tunable self-assembly of genetically engineered silk--elastin-like protein polymers, Biomacromolecules 12(11) (2011) 3844-50.
[46] J.M. Mason, K.M. Arndt, Coiled coil domains: stability, specificity, and biological implications, Chembiochem : a European journal of chemical biology 5(2) (2004) 170-6.
[47] W.A. Petka, J.L. Harden, K.P. McGrath, D. Wirtz, D.A. Tirrell, Reversible hydrogels from self-assembling artificial proteins, Science 281(5375) (1998) 389-92.
[48] C. Xu, V. Breedveld, J. Kopecek, Reversible hydrogels from self-assembling genetically engineered protein block copolymers, Biomacromolecules 6(3) (2005) 1739-49.
[49] B.D. Olsen, J.A. Kornfield, D.A. Tirrell, Yielding Behavior in Injectable Hydrogels from Telechelic Proteins, Macromolecules 43(21) (2010) 9094-9099.

[50] W. Shen, K.C. Zhang, J.A. Kornfield, D.A. Tirrell, Tuning the erosion rate of artificial protein hydrogels through control of network topology, Nature Mater. 5(2) (2006) 153-158.
[51] L. Mi, S. Fischer, B. Chung, S. Sundelacruz, J.L. Harden, Self-assembling protein hydrogels with modular integrin binding domains, Biomacromolecules 7(1) (2006) 38-47.
[52] S.E. Fischer, X. Liu, H.Q. Mao, J.L. Harden, Controlling cell adhesion to surfaces via associating bioactive triblock proteins, Biomaterials 28(22) (2007) 3325-37.
[53] S.E. Fischer, L. Mi, H.Q. Mao, J.L. Harden, Biofunctional coatings via targeted covalent cross-linking of associating triblock proteins, Biomacromolecules 10(9) (2009) 2408-17.
[54] T.J. Deming, Polypeptide hydrogels via a unique assembly mechanism, Soft Matter 1(1) (2005) 28-35.
[55] A.P. Nowak, V. Breedveld, L. Pakstis, B. Ozbas, D.J. Pine, D. Pochan, T.J. Deming, Rapidly recovering hydrogel scaffolds from self-assembling diblock copolypeptide amphiphiles, Nature 417(6887) (2002) 424-8.
[56] C.Y. Yang, B. Song, Y. Ao, A.P. Nowak, R.B. Abelowitz, R.A. Korsak, L.A. Havton, T.J. Deming, M.V. Sofroniew, Biocompatibility of amphiphilic diblock copolypeptide hydrogels in the central nervous system, Biomaterials 30(15) (2009) 2881-98.
[57] A.P. Nowak, J. Sato, V. Breedveld, T.J. Deming, Hydrogel formation in amphiphilic triblock copolypeptides, Supramol. Chem. 18(5) (2006) 423-427.
[58] Z.B. Li, T.J. Deming, Tunable hydrogel morphology via self-assembly of amphiphilic pentablock copolypeptides, Soft Matter 6(11) (2010) 2546-2551.
[59] C.T. Wong Po Foo, J.S. Lee, W. Mulyasasmita, A. Parisi-Amon, S.C. Heilshorn, Two-component protein-engineered physical hydrogels for cell encapsulation, P Natl Acad Sci USA 106(52) (2009) 22067-72.
[60] W. Mulyasasmita, J.S. Lee, S.C. Heilshorn, Molecular-level engineering of protein physical hydrogels for predictive sol-gel phase behavior, Biomacromolecules 12(10) (2011) 3406-11.
[61] S. Wong, M.S. Shim, Y.J. Kwon, Synthetically designed peptide-based biomaterials with stimuli-responsive and membrane-active properties for biomedical applications, J. Mater. Chem. B 2(6) (2014) 595-615.
[62] L. Cai, C.B. Dinh, S.C. Heilshorn, One-pot Synthesis of Elastin-like Polypeptide Hydrogels with Grafted VEGF-Mimetic Peptides, Biomater. Sci. 2(5) (2014) 757-765.
[63] R. Fairman, K.S. Akerfeldt, Peptides as novel smart materials, Curr. Opin. Struc. Biol. 15(4) (2005) 453-463.
[64] E. Beniash, J.D. Hartgerink, H. Storrie, J.C. Stendahl, S.I. Stupp, Self-assembling peptide amphiphile nanofiber matrices for cell entrapment, Acta Biomater. 1(4) (2005) 387-97.

[65] M. Zhou, A.M. Smith, A.K. Das, N.W. Hodson, R.F. Collins, R.V. Ulijn, J.E. Gough, Self-assembled peptide-based hydrogels as scaffolds for anchorage-dependent cells, Biomaterials 30(13) (2009) 2523-2530.

[66] C. Cunha, S. Panseri, O. Villa, D. Silva, F. Gelain, 3D culture of adult mouse neural stem cells within functionalized self-assembling peptide scaffolds, Int. J. Nanomedicine 6 (2011) 943-55.

[67] G.A. Silva, C. Czeisler, K.L. Niece, E. Beniash, D.A. Harrington, J.A. Kessler, S.I. Stupp, Selective differentiation of neural progenitor cells by high-epitope density nanofibers, Science 303(5662) (2004) 1352-5.

[68] A. Horii, X. Wang, F. Gelain, S. Zhang, Biological designer self-assembling peptide nanofiber scaffolds significantly enhance osteoblast proliferation, differentiation and 3-D migration, PloS one 2(2) (2007) e190.

[69] K.M. Galler, L. Aulisa, K.R. Regan, R.N. D'Souza, J.D. Hartgerink, Self-assembling multidomain peptide hydrogels: designed susceptibility to enzymatic cleavage allows enhanced cell migration and spreading, J. Am. Chem. Soc. 132(9) (2010) 3217-23.

[70] M.C. Giano, D.J. Pochan, J.P. Schneider, Controlled biodegradation of self-assembling beta-hairpin peptide hydrogels by proteolysis with matrix metalloproteinase-13, Biomaterials 32(27) (2011) 6471-7.

[71] S.G. Zhang, Emerging biological materials through molecular self-assembly, Biotechnol. Adv. 20(5-6) (2002) 321-339.

[72] S.G. Zhang, D.M. Marini, W. Hwang, S. Santoso, Design of nanostructured biological materials through self-assembly of peptides and proteins, Curr. Opin. Chem. Biol. 6(6) (2002) 865-871.

[73] S. Zhang, C. Lockshin, A. Herbert, E. Winter, A. Rich, Zuotin, a putative Z-DNA binding protein in Saccharomyces cerevisiae, EMBO J. 11(10) (1992) 3787-96.

[74] S. Zhang, T. Holmes, C. Lockshin, A. Rich, Spontaneous assembly of a self-complementary oligopeptide to form a stable macroscopic membrane, P Natl Acad Sci USA 90(8) (1993) 3334-8.

[75] S. Zhang, C. Lockshin, R. Cook, A. Rich, Unusually stable beta-sheet formation in an ionic self-complementary oligopeptide, Biopolymers 34(5) (1994) 663-72.

[76] S. Zhang, T.C. Holmes, C.M. DiPersio, R.O. Hynes, X. Su, A. Rich, Self-complementary oligopeptide matrices support mammalian cell attachment, Biomaterials 16(18) (1995) 1385-93.

[77] H. Yokoi, T. Kinoshita, S. Zhang, Dynamic reassembly of peptide RADA16 nanofiber scaffold, P Natl Acad Sci USA 102(24) (2005) 8414-9.

[78] J.H. Collier, B.H. Hu, J.W. Ruberti, J. Zhang, P. Shum, D.H. Thompson, P.B. Messersmith, Thermally and photochemically triggered self-assembly of peptide hydrogels, J. Am. Chem. Soc. 123(38) (2001) 9463-4.

[79] J. Kisiday, M. Jin, B. Kurz, H. Hung, C. Semino, S. Zhang, A.J. Grodzinsky, Self-assembling peptide hydrogel fosters chondrocyte extracellular matrix production and cell division: implications for cartilage tissue repair, P Natl Acad Sci USA 99(15) (2002) 9996-10001.

[80] T.C. Holmes, S. de Lacalle, X. Su, G. Liu, A. Rich, S. Zhang, Extensive neurite outgrowth and active synapse formation on self-assembling peptide scaffolds, P Natl Acad Sci USA 97(12) (2000) 6728-33.

[81] C.E. Semino, J.R. Merok, G.G. Crane, G. Panagiotakos, S. Zhang, Functional differentiation of hepatocyte-like spheroid structures from putative liver progenitor cells in three-dimensional peptide scaffolds, Differentiation; research in biological diversity 71(4-5) (2003) 262-70.

[82] C.E. Semino, J. Kasahara, Y. Hayashi, S. Zhang, Entrapment of migrating hippocampal neural cells in three-dimensional peptide nanofiber scaffold, Tissue Eng. 10(3-4) (2004) 643-55.

[83] D.A. Narmoneva, R. Vukmirovic, M.E. Davis, R.D. Kamm, R.T. Lee, Endothelial cells promote cardiac myocyte survival and spatial reorganization: implications for cardiac regeneration, Circulation 110(8) (2004) 962-8.

[84] H. Dong, S.E. Paramonov, L. Aulisa, E.L. Bakota, J.D. Hartgerink, Self-assembly of multidomain peptides: balancing molecular frustration controls conformation and nanostructure, J. Am. Chem. Soc. 129(41) (2007) 12468-72.

[85] L. Aulisa, H. Dong, J.D. Hartgerink, Self-assembly of multidomain peptides: sequence variation allows control over cross-linking and viscoelasticity, Biomacromolecules 10(9) (2009) 2694-8.

[86] D. Pantoja-Uceda, C.M. Santiveri, M.A. Jimenez, De novo design of monomeric beta-hairpin and beta-sheet peptides, Methods Mol. Biol. 340 (2006) 27-51.

[87] J.P. Schneider, D.J. Pochan, B. Ozbas, K. Rajagopal, L. Pakstis, J. Kretsinger, Responsive hydrogels from the intramolecular folding and self-assembly of a designed peptide, J. Am. Chem. Soc. 124(50) (2002) 15030-7.

[88] D.J. Pochan, J.P. Schneider, J. Kretsinger, B. Ozbas, K. Rajagopal, L. Haines, Thermally reversible hydrogels via intramolecular folding and consequent self-assembly of a de novo designed peptide, J. Am. Chem. Soc. 125(39) (2003) 11802-3.

[89] B. Ozbas, J. Kretsinger, K. Rajagopal, J.P. Schneider, D.J. Pochan, Salt-triggered peptide folding and consequent self-assembly into hydrogels with tunable modulus, Macromolecules 37(19) (2004) 7331-7337.

[90] L. Haines-Butterick, K. Rajagopal, M. Branco, D. Salick, R. Rughani, M. Pilarz, M.S. Lamm, D.J. Pochan, J.P. Schneider, Controlling hydrogelation kinetics by peptide design for three-dimensional encapsulation and injectable delivery of cells, P Natl Acad Sci USA 104(19) (2007) 7791-7796.

[91] J.K. Kretsinger, L.A. Haines, B. Ozbas, D.J. Pochan, J.P. Schneider, Cytocompatibility of self-assembled beta-hairpin peptide hydrogel surfaces, Biomaterials 26(25) (2005) 5177-86.

[92] D.W. Lowik, J.C. van Hest, Peptide based amphiphiles, Chem. Soc. Rev. 33(4) (2004) 234-45.

[93] S. Cavalli, F. Albericio, A. Kros, Amphiphilic peptides and their cross-disciplinary role as building blocks for nanoscience, Chem. Soc. Rev. 39(1) (2010) 241-263.

[94] H. Cui, M.J. Webber, S.I. Stupp, Self-assembly of peptide amphiphiles: from molecules to nanostructures to biomaterials, Biopolymers 94(1) (2010) 1-18.

[95] J.D. Hartgerink, E. Beniash, S.I. Stupp, Peptide-amphiphile nanofibers: a versatile scaffold for the preparation of self-assembling materials, P Natl Acad Sci USA 99(8) (2002) 5133-8.

[96] B. Mammadov, R. Mammadov, M.O. Guler, A.B. Tekinay, Cooperative effect of heparan sulfate and laminin mimetic peptide nanofibers on the promotion of neurite outgrowth, Acta Biomater. 8(6) (2012) 2077-86.

[97] J.Y. Lee, J.E. Choo, Y.S. Choi, J.S. Suh, S.J. Lee, C.P. Chung, Y.J. Park, Osteoblastic differentiation of human bone marrow stromal cells in self-assembled BMP-2 receptor-binding peptide-amphiphiles, Biomaterials 30(21) (2009) 3532-41.

[98] S. Fleming, S. Debnath, P.W. Frederix, T. Tuttle, R.V. Ulijn, Aromatic peptide amphiphiles: significance of the Fmoc moiety, Chem. Commun. (Camb.) 49(90) (2013) 10587-9.

[99] Y. Zhang, H. Gu, Z. Yang, B. Xu, Supramolecular hydrogels respond to ligand-receptor interaction, J. Am. Chem. Soc. 125(45) (2003) 13680-1.

[100] V. Jayawarna, M. Ali, T.A. Jowitt, A.E. Miller, A. Saiani, J.E. Gough, R.V. Ulijn, Nanostructured hydrogels for three-dimensional cell culture through self-assembly of fluorenylmethoxycarbonyl-dipeptides, Adv. Mater. 18(5) (2006) 611-+.

[101] A. Mahler, M. Reches, M. Rechter, S. Cohen, E. Gazit, Rigid, self-assembled hydrogel composed of a modified aromatic dipeptide, Adv. Mater. 18(11) (2006) 1365-+.

[102] V. Jayawarna, A. Smith, J.E. Gough, R.V. Ulijn, Three-dimensional cell culture of chondrocytes on modified di-phenylalanine scaffolds, Biochem. Soc. Trans. 35(Pt 3) (2007) 535-7.

[103] Z.M. Yang, H.W. Gu, D.G. Fu, P. Gao, J.K. Lam, B. Xu, Enzymatic formation of supramolecular hydrogels, Adv. Mater. 16(16) (2004) 1440-+.

[104] Z.M. Yang, G.L. Liang, L. Wang, B. Xu, Using a kinase/phosphatase switch to regulate a supramolecular hydrogel and forming the supramoleclar hydrogel in vivo, J. Am. Chem. Soc. 128(9) (2006) 3038-3043.

[105] H. Tsutsumi, H. Mihara, Soft materials based on designed self-assembling peptides: from design to application, Mol. Biosyst. 9(4) (2013) 609-17.

[106] Y. Loo, S. Zhang, C.A. Hauser, From short peptides to nanofibers to macromolecular assemblies in biomedicine, Biotechnol. Adv. 30(3) (2012) 593-603.

[107] Z.G. Wang, B. Ding, DNA-based self-assembly for functional nanomaterials, Adv. Mater. 25(28) (2013) 3905-14.

[108] X.L. Xiong, C.C. Wu, C.S. Zhou, G.Z. Zhu, Z. Chen, W.H. Tan, Responsive DNA-Based Hydrogels and Their Applications, Macromol. Rapid Commun. 34(16) (2013) 1271-1283.

[109] D. Yang, M.J. Campolongo, T.N. Nhi Tran, R.C. Ruiz, J.S. Kahn, D. Luo, Novel DNA materials and their applications, Wiley Interdiscip. Rev. Nanomed. Nanobiotechnol. 2(6) (2010) 648-69.

[110] S.H. Um, J.B. Lee, N. Park, S.Y. Kwon, C.C. Umbach, D. Luo, Enzyme-catalysed assembly of DNA hydrogel, Nature Mater. 5(10) (2006) 797-801.

[111] E. Cheng, Y. Xing, P. Chen, Y. Yang, Y. Sun, D. Zhou, L. Xu, Q. Fan, D. Liu, A pH-triggered, fast-responding DNA hydrogel, Angew. Chem. Int. Ed. Engl. 48(41) (2009) 7660-3.

[112] Y. Xing, E. Cheng, Y. Yang, P. Chen, T. Zhang, Y. Sun, Z. Yang, D. Liu, Self-assembled DNA hydrogels with designable thermal and enzymatic responsiveness, Adv. Mater. 23(9) (2011) 1117-21.

[113] T. Noll, H. Schonherr, D. Wesner, M. Schopferer, T. Paululat, G. Noll, Construction of three-dimensional DNA hydrogels from linear building blocks, Angew. Chem. Int. Ed. Engl. 53(32) (2014) 8328-32.

[114] G. Sicilia, C. Grainger-Boultby, N. Francini, J.P. Nagunsson, A.O. Saeed, F. Fernández-Trillo, S.G. Spain, C. Alexander, Programmable polymer-DNA hydrogels with dual input and multiscale responses, Biomater. Sci. 2 (2014) 203-211.

[115] P.M. Moreno, A.P. Pego, Therapeutic antisense oligonucleotides against cancer: hurdling to the clinic, Front. Chem. 2 (2014) 87.

[116] H. Tan, C. Xiao, J. Sun, D. Xiong, X. Hu, Biological self-assembly of injectable hydrogel as cell scaffold via specific nucleobase pairing, Chem. Commun. (Camb.) 48(83) (2012) 10289-91.

[117] A. Carlsen, S. Lecommandoux, Self-assembly of polypeptide-based block copolymer amphiphiles, Curr. Opin. Colloid Interface Sci. 14(5) (2009) 329-339.

[118] G.W.M. Vandermeulen, H.A. Klok, Peptide/protein hybrid materials: Enhanced control of structure and improved performance through conjugation of biological and synthetic polymers, Macromol. Biosci. 4(4) (2004) 383-398.
[119] T.S. Burkoth, T.L.S. Benzinger, D.N.M. Jones, K. Hallenga, S.C. Meredith, D.G. Lynn, C-terminal PEG blocks the irreversible step in beta-amyloid(10-35) fibrillogenesis, J. Am. Chem. Soc. 120(30) (1998) 7655-7656.
[120] T.S. Burkoth, T.L.S. Benzinger, V. Urban, D.G. Lynn, S.C. Meredith, P. Thiyagarajan, Self-assembly of A beta((10-35))-PEG block copolymer fibrils, J. Am. Chem. Soc. 121(32) (1999) 7429-7430.
[121] M. Pechar, J. Brus, L. Kostka, C. Konak, M. Urbanova, M. Slouf, Thermoresponsive self-assembly of short elastin-like polypentapeptides and their poly(ethylene glycol) derivatives, Macromol. Biosci. 7(1) (2007) 56-69.
[122] L. Ayres, M.R.J. Vos, P.J.H.M. Adams, I.O. Shklyarevskiy, J.C.M. van Hest, Elastin-based side-chain polymers synthesized by ATRP, Macromolecules 36(16) (2003) 5967-5973.
[123] S.E. Grieshaber, A.J. Farran, S. Lin-Gibson, K.L. Kiick, X. Jia, Synthesis and Characterization of Elastin-Mimetic Hybrid Polymers with Multiblock, Alternating Molecular Architecture and Elastomeric Properties, Macromolecules 42(7) (2009) 2532-2541.
[124] H. Wang, L. Cai, A. Paul, A. Enejder, S.C. Heilshorn, Hybrid elastin-like polypeptide-polyethylene glycol (ELP-PEG) hydrogels with improved transparency and independent control of matrix mechanics and cell ligand density, Biomacromolecules 15(9) (2014) 3421-8.
[125] M. Pechar, P. Kopeckova, L. Joss, J. Kopecek, Associative diblock copolymers of poly(ethylene glycol) and coiled-coil peptides, Macromol. Biosci. 2(5) (2002) 199-206.
[126] G.W.M. Vandermeulen, C. Tziatzios, H.A. Klok, Reversible self-organization of poly(ethylene glycol)-based hybrid block copolymers mediated by a De Novo four-stranded alpha-helical coiled coil motif, Macromolecules 36(11) (2003) 4107-4114.
[127] C. Wang, R.J. Stewart, J. Kopecek, Hybrid hydrogels assembled from synthetic polymers and coiled-coil protein domains, Nature 397(6718) (1999) 417-420.
[128] J. Yang, C. Xu, P. Kopeckova, J. Kopecek, Hybrid hydrogels self-assembled from HPMA copolymers containing peptide grafts, Macromol. Biosci. 6(3) (2006) 201-9.
[129] K. Wu, J.Y. Yang, C. Konak, P. Kopeckova, J. Kopecek, Novel synthesis of HPMA copolymers containing peptide grafts and their self-assembly into hybrid hydrogels, Macromol. Chem. Phys. 209(5) (2008) 467-475.
[130] J. Yang, C. Xu, C. Wang, J. Kopecek, Refolding hydrogels self-assembled from N-(2-hydroxypropyl)methacrylamide graft copolymers by antiparallel coiled-coil formation, Biomacromolecules 7(4) (2006) 1187-95.

[131] J. Yang, K. Wu, C. Konak, J. Kopecek, Dynamic light scattering study of self-assembly of HPMA hybrid graft copolymers, Biomacromolecules 9(2) (2008) 510-7.
[132] L.C. Wu, J.Y. Yang, J. Kopecek, Hybrid hydrogels self-assembled from graft copolymers containing complementary beta-sheets as hydroxyapatite nucleation scaffolds, Biomaterials 32(23) (2011) 5341-5353.
[133] D.L. Nettles, K. Kitaoka, N.A. Hanson, C.M. Flahiff, B.A. Mata, E.W. Hsu, A. Chilkoti, L.A. Setton, In situ crosslinking elastin-like polypeptide gels for application to articular cartilage repair in a goat osteochondral defect model, Tissue Eng. Part A 14(7) (2008) 1133-40.
[134] D.L. Nettles, T.P. Vail, C.M. Flahiff, J. Walkenhorst, A.J. Carter, L.A. Setton, Injectable silk-elastin for articular cartilage defect repair, Trans. of the ORS Washington, DC 30 (2005) 1366 paper.
[135] J.E. Kim, S.M. Lee, S.H. Kim, P. Tatman, A.O. Gee, D.H. Kim, K.E. Lee, Y. Jung, S.J. Kim, Effect of self-assembled peptide-mesenchymal stem cell complex on the progression of osteoarthritis in a rat model, Int. J. Nanomedicine 9 Suppl 1 (2014) 141-57.
[136] J.E. Kim, S.H. Kim, Y. Jung, In situ chondrogenic differentiation of bone marrow stromal cells in bioactive self-assembled peptide gels, J. Biosci. Bioeng. (2014).
[137] T. Hou, Z. Li, F. Luo, Z. Xie, X. Wu, J. Xing, S. Dong, J. Xu, A composite demineralized bone matrix--self assembling peptide scaffold for enhancing cell and growth factor activity in bone marrow, Biomaterials 35(22) (2014) 5689-99.
[138] Z. Li, T. Hou, F. Luo, Z. Chang, X. Wu, J. Xing, M. Deng, J. Xu, Bone marrow enriched graft, modified by self-assembly peptide, repairs critically-sized femur defects in goats, Int. Orthop. 38(11) (2014) 2391-8.
[139] A. Mata, Y. Geng, K.J. Henrikson, C. Aparicio, S.R. Stock, R.L. Satcher, S.I. Stupp, Bone regeneration mediated by biomimetic mineralization of a nanofiber matrix, Biomaterials 31(23) (2010) 6004-12.
[140] T.D. Sargeant, M.O. Guler, S.M. Oppenheimer, A. Mata, R.L. Satcher, D.C. Dunand, S.I. Stupp, Hybrid bone implants: Self-assembly of peptide amphiphile nanofibers within porous titanium, Biomaterials 29(2) (2008) 161-171.
[141] U. Freudenberg, A. Hermann, P.B. Welzel, K. Stirl, S.C. Schwarz, M. Grimmer, A. Zieris, W. Panyanuwat, S. Zschoche, D. Meinhold, A. Storch, C. Werner, A star-PEG-heparin hydrogel platform to aid cell replacement therapies for neurodegenerative diseases, Biomaterials 30(28) (2009) 5049-60.
[142] Y. Liu, H. Ye, K. Satkunendrarajah, G.S. Yao, Y. Bayon, M.G. Fehlings, A self-assembling peptide reduces glial scarring, attenuates post-traumatic inflammation and promotes neurological recovery following spinal cord injury, Acta Biomater. 9(9) (2013) 8075-88.

[143] M. Iwasaki, J.T. Wilcox, Y. Nishimura, K. Zweckberger, H. Suzuki, J. Wang, Y. Liu, S.K. Karadimas, M.G. Fehlings, Synergistic effects of self-assembling peptide and neural stem/progenitor cells to promote tissue repair and forelimb functional recovery in cervical spinal cord injury, Biomaterials 35(9) (2014) 2617-29.

[144] J. Guo, H. Su, Y. Zeng, Y.X. Liang, W.M. Wong, R.G. Ellis-Behnke, K.F. So, W. Wu, Reknitting the injured spinal cord by self-assembling peptide nanofiber scaffold, Nanomedicine 3(4) (2007) 311-21.

[145] R.G. Ellis-Behnke, Y.X. Liang, S.W. You, D.K. Tay, S. Zhang, K.F. So, G.E. Schneider, Nano neuro knitting: peptide nanofiber scaffold for brain repair and axon regeneration with functional return of vision, P Natl Acad Sci USA 103(13) (2006) 5054-9.

[146] T.Y. Cheng, M.H. Chen, W.H. Chang, M.Y. Huang, T.W. Wang, Neural stem cells encapsulated in a functionalized self-assembling peptide hydrogel for brain tissue engineering, Biomaterials 34(8) (2013) 2005-16.

[147] V.M. Tysseling-Mattiace, V. Sahni, K.L. Niece, D. Birch, C. Czeisler, M.G. Fehlings, S.I. Stupp, J.A. Kessler, Self-assembling nanofibers inhibit glial scar formation and promote axon elongation after spinal cord injury, J. Neurosci. 28(14) (2008) 3814-23.

[148] V.M. Tysseling, V. Sahni, E.T. Pashuck, D. Birch, A. Hebert, C. Czeisler, S.I. Stupp, J.A. Kessler, Self-assembling peptide amphiphile promotes plasticity of serotonergic fibers following spinal cord injury, J. Neurosci. Res. 88(14) (2010) 3161-70.

[149] G. Uzunalli, Z. Soran, T.S. Erkal, Y.S. Dagdas, E. Dinc, A.M. Hondur, K. Bilgihan, B. Aydin, M.O. Guler, A.B. Tekinay, Bioactive self-assembled peptide nanofibers for corneal stroma regeneration, Acta Biomater. 10(3) (2014) 1156-66.

[150] A. Li, A. Hokugo, A. Yalom, E.J. Berns, N. Stephanopoulos, M.T. McClendon, L.A. Segovia, I. Spigelman, S.I. Stupp, R. Jarrahy, A bioengineered peripheral nerve construct using aligned peptide amphiphile nanofibers, Biomaterials 35(31) (2014) 8780-90.

[151] W. Mulyasasmita, L. Cai, R.E. Dewi, A. Jha, S.D. Ullmann, R.H. Luong, N.F. Huang, S.C. Heilshorn, Avidity-controlled hydrogels for injectable co-delivery of induced pluripotent stem cell-derived endothelial cells and growth factors, J. Control. Release 191 (2014) 71-81.

[152] M. Tokunaga, M.L. Liu, T. Nagai, K. Iwanaga, K. Matsuura, T. Takahashi, M. Kanda, N. Kondo, P. Wang, A.T. Naito, I. Komuro, Implantation of cardiac progenitor cells using self-assembling peptide improves cardiac function after myocardial infarction, J. Mol. Cell Cardiol. 49(6) (2010) 972-983.

[153] C. Soler-Botija, J.R. Bago, A. Llucia-Valldeperas, A. Valles-Lluch, C. Castells-Sala, C. Martinez-Ramos, T. Fernandez-Muinos, J.C. Chachques, M.M. Pradas, C.E. Semino, A. Bayes-Genis, Engineered 3D bioimplants using elastomeric scaffold, self-assembling

peptide hydrogel, and adipose tissue-derived progenitor cells for cardiac regeneration, Am. J. Transl. Res. 6(3) (2014) 291-301.

[154] J.H. Kim, Y. Jung, B.S. Kim, S.H. Kim, Stem cell recruitment and angiogenesis of neuropeptide substance P coupled with self-assembling peptide nanofiber in a mouse hind limb ischemia model, Biomaterials 34(6) (2013) 1657-68.

[155] M.J. Webber, J. Tongers, C.J. Newcomb, K.T. Marquardt, J. Bauersachs, D.W. Losordo, S.I. Stupp, Supramolecular nanostructures that mimic VEGF as a strategy for ischemic tissue repair, P Natl Acad Sci USA 108(33) (2011) 13438-43.

[156] L.M. Boyd, A.J. Carter, Injectable biomaterials and vertebral endplate treatment for repair and regeneration of the intervertebral disc, Eur. Spine J. 15 Suppl 3 (2006) S414-21.

[157] U. Berlemann, O. Schwarzenbach, An injectable nucleus replacement as an adjunct to microdiscectomy: 2 year follow-up in a pilot clinical study, Eur. Spine J. 18(11) (2009) 1706-12.

[158] D. Ceballos, X. Navarro, N. Dubey, G. Wendelschafer-Crabb, W.R. Kennedy, R.T. Tranquillo, Magnetically aligned collagen gel filling a collagen nerve guide improves peripheral nerve regeneration, Exp. Neurol. 158(2) (1999) 290-300.

[159] S. Zhang, M.A. Greenfield, A. Mata, L.C. Palmer, R. Bitton, J.R. Mantei, C. Aparicio, M.O. de la Cruz, S.I. Stupp, A self-assembly pathway to aligned monodomain gels, Nature Mater. 9(7) (2010) 594-601.

[160] E.J. Berns, S. Sur, L. Pan, J.E. Goldberger, S. Suresh, S. Zhang, J.A. Kessler, S.I. Stupp, Aligned neurite outgrowth and directed cell migration in self-assembled monodomain gels, Biomaterials 35(1) (2014) 185-95.

# PART 2

# CHAPTER V

An Affinity-Based Approach to Engineer Laminin-Presenting Cell Instructive Microenvironments

# An Affinity-Based Approach to Engineer Laminin-Presenting Cell Instructive Microenvironments

Daniela Barros [1,2,3], Paula Parreira [1,2], Joana Furtado [1,4#], Frederico Ferreira-da-Silva [1,4], Eduardo Conde-Sousa [1,2], Andrés J. García [5,6], M. Cristina L. Martins [1,2,3], Isabel Freitas Amaral [1,2,7,*], Ana Paula Pêgo [1,2,3,7,*]

[1] i3S - Instituto de Investigação e Inovação em Saúde, Universidade do Porto (UPorto), Portugal

[2] INEB - Instituto de Engenharia Biomédica, UPorto, Portugal

[3] ICBAS - Instituto de Ciências Biomédicas Abel Salazar, UPorto, Portugal

[4] IBMC - Instituto de Biologia Molecular e Celular, UPorto, Portugal

[5] Parker H. Petit Institute for Bioengineering and Biosciences, Georgia Institute of Technology, Atlanta, Georgia, USA

[6] George W. Woodruff School of Mechanical Engineering, Georgia Institute of Technology, Atlanta, Georgia, USA

[7] FEUP - Faculdade de Engenharia, UPorto, Portugal.

---

**Published in Biomaterials, Volume 192, 2019**

DOI 10.1016/j.biomaterials.2018.10.039

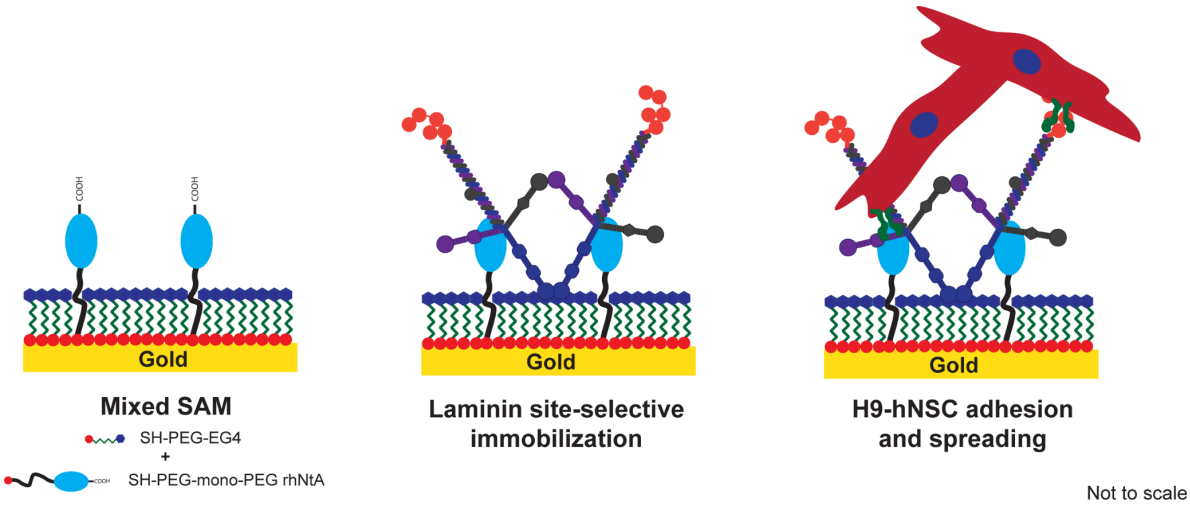

**Abstract**

Laminin immobilization into diverse biological and synthetic matrices has been explored to replicate the microenvironment of stem cell niches and gain insight into the role of extracellular matrix (ECM) on stem cell behavior. However, the site-specific immobilization of this heterotrimeric glycoprotein and, consequently, control over its orientation and bioactivity has been a challenge that has limited many of the explored strategies to date. In this work, we establish an affinity-based approach that takes advantage of the native high affinity interaction between laminin and the human N-terminal agrin (hNtA) domain. This interaction is expected to promote the site-selective immobilization of laminin to a specific substrate, while preserving the exposure of its key bioactive epitopes. Recombinant hNtA (rhNtA) domain was produced with high purity (>90%) and successfully conjugated at its N-terminal with a thiol-terminated poly(ethylene glycol) (PEG) without affecting its affinity to laminin. Self-assembled monolayers (SAMs) of mono-PEGylated rhNtA on gold (mPEG rhNtA-SAMs) were then prepared to evaluate the effectiveness of this strategy. The site-specific immobilization of laminin onto mPEG rhNtA-SAMs was shown to better preserve protein bioactivity in comparison to laminin immobilized on SAMs of thiol-PEG-succinimidyl glutaramide (SH-PEG-SGA), used for the non-selective covalent immobilization of laminin, as evidenced by its enhanced ability to efficiently self-polymerize and mediate cell adhesion and spreading of human neural stem cells. These results highlight the potential of this novel strategy to be used as an alternative to the conventional immobilization approaches in a wide range of applications, including engineered coatings for neuroelectrodes and two-dimensional (2D) substrates for cell culture, as well as biofunctionalization of three-dimensional (3D) matrices.

## 1. Introduction

In the framework of regenerative medicine and tissue engineering, much attention has been devoted towards the development of engineered matrices incorporating bioadhesive cues present in stem cell niches, to recapitulate the dynamic nature and biological complexity of these microenvironments, as well as gain more insight into the function of specific extracellular matrix (ECM) components on stem cell behavior. The ECM is an essential component of the stem cell niche, as it modulates important biological functions including proliferation, self-renewal and differentiation of stem cells. Among major ECM constituents, laminins play crucial and essential roles in many aspects of tissue physiology and function [1-5]. These heterotrimeric glycoproteins comprise several bioactive domains involved in the modulation of different biological functions. The latter include the interaction with other ECM proteins (*e.g*. nidogen, netrin 4 and collagen VII) mediated by the laminin short arms (N-terminus), which contributes to the assembly and stability of basement membranes. These domains are also responsible for the laminin ability to polymerize [6-8], even in the absence of other basement membrane components, forming the molecular network that will be in contact with the cellular surface. In addition to its structural role, laminin comprises multiple bioactive domains that interact with cell surface receptors (*e.g*. integrins, dystroglycans, and syndecans), modulating different cell functions including cell adhesion, proliferation, migration and differentiation, as well as ECM deposition [9-11].

Laminin has been incorporated into both two-dimensional (2D) [12] and three-dimensional (3D) [13-20] cell-instructive microenvironments for applications in regenerative therapies or to get insights into the role of laminin on the modulation of cell behavior. Strategies explored for laminin immobilization have relied either on its non-specific adsorption or entrapment or, alternatively, on its non-specific covalent immobilization to different substrates through the use of functional groups present in multiple sites of the laminin structure such as amines [13-17] and thiols [18, 20]. One of the main caveats presented by these strategies is the inability to control orientation and conformation of laminin upon immobilization, which were proven to be crucial for the modulation of cellular behavior [21-23]. As such, the exposure of key laminin bioactive epitopes can be compromised. In an attempt to assure the control over the tethering of laminin, in recent years protein immobilization strategies have shifted toward site-specific conjugation, with special focus on biorthogonal chemical reactions (click chemistry), enzymatic ligation and affinity binding, using either unnatural amino acids or engineered site-selective amino acid sequences [24-26]. These strategies are expected to provide a higher retention of bioactivity, by favoring the access to the active sites of immobilized proteins. To the best of our knowledge, to date, only one study reported the site-selective immobilization of laminin [27]. To control the presentation of full-length ECM

proteins without altering their bioactivity, Lee and co-workers explored click chemistry to anchor collagen, fibronectin and laminin onto polyacrylamide gels by their N-terminus [27]. Nevertheless, despite guaranteeing the site-selective immobilization of the proteins, as result of the use of laminin N-terminus, this approach compromises one of laminin's hallmark features, which is its ability to polymerize. Affinity-binding has been increasingly explored for the site-specific and reversible conjugation of proteins and peptides, because of its versatility and ability to generate dynamic biomimetic systems. However, the successful implementation of this strategy is strongly dependent on the appropriate selection of the binding pairs. Binding systems using high affinity interactions, such as streptavidin and biotin, although often used, require the protein of interest to be either recombinantly or chemically modified [28, 29]. In contrast, the use of natural binding partners constitutes an attractive alternative, as strong non-covalent interactions can be achieved without the need for protein modification [30, 31].

In this study, we examined an alternative strategy that explores the well described native high affinity interaction (dissociation constant ($K_D$) = 5 nM) between laminin and the N-terminal agrin (NtA) domain [32, 33]. The agrin-binding site in laminin is localized in the central region of its coiled-coil domain and maps to a sequence of 20 conserved residues within the $\gamma$1 chain [33, 34]. Interestingly, this interaction requires a coiled-coil conformation of the agrin-binding site [34]. To assess the ability of this affinity-based approach to immobilize laminin with retention of bioactivity, recombinant human NtA (rhNtA) domain was successfully produced and further conjugated at its N-terminus with a thiol-terminated poly(ethylene glycol) (PEG) to enable the preparation of self-assembled monolayers (SAMs) of NtA on gold. To the best of our knowledge, this is the first report on the production and characterization of the human variant of NtA domain. In order to study the specific interactions between the immobilized laminin and cells, SAMs were herein used as proof-of-concept platforms, since they can be easily produced and specifically tailored to provide a chemically well-defined molecular monolayer [35]. The binding ligand was characterized and its ability to mediate laminin immobilization through a high affinity interaction was shown by solid-binding assay, surface plasmon resonance (SPR) and quartz crystal microbalance with dissipation monitoring (QCM-D). The bioactivity of mono-PEGylated rhNtA-immobilized laminin was subsequently investigated by evaluating its ability to self-polymerize and modulate the behavior of human neural stem cells (hNSCs). hNSCs were herein used due to the well described role of laminin on the modulation of neural cell behavior [36]. This strategy represents a promising and versatile approach for the site-selective immobilization of laminin, while preserving its bioactivity, and can be potentially useful for the development of cell instructive microenvironments for tissue engineering and regenerative medicine.

## 2. Materials and Methods

### 2.1. Recombinant human N-terminal agrin (rhNtA) domain expression and purification

The NtA domain, comprising residues Thr 30 – Pro 157 of the human agrin protein (Uniprot reference O00468), was expressed in *Escherichia coli* (*E. coli*) strain BL21(DE3) using the pCoofy2 expression vector [37] (gift from Sabine Suppmann – Addgene plasmid # 43981). pCoofy2 is a derivative of pETM22 vector that contains a thioredoxin-poly-$His_6$ (6x Histidine residues) (Trx-$His_6$) N-terminal tag followed by an HRV 3C recognition site located downstream of the N-terminal tag [37]. Details on cloning of human NtA gene and expression vector are presented in Supplementary Materials and Methods. The fusion protein (Trx-$His_6$-hNtA) was expressed by induction of log-phase cultures with 0.2 mM of isopropyl β-D-1-thiogalactopyranoside (IPTG; Sigma-Aldrich) at 20 ºC for 5 h and purified by immobilized metal affinity chromatography using an HisTrap column (GE Healthcare), according to manufacturer's instructions. A concentration gradient of 0 to 500 mM of imidazole was applied to elute the fusion protein. The N-terminal Trx-$His_6$ tag was then cleaved during dialysis using HRV 3C protease (kindly provided by Biochemical and Biophysical Technologies (B2Tech) Platform of i3S) in a protease:target protein ratio (unit/μg) of 1:10. Untagged recombinant human NtA (rhNtA) contains additional Gly and Pro residues at its N-terminus (Fig. S1). rhNtA was dialyzed against 10 mM phosphate buffered saline (PBS) pH 7.4, concentrated in a 10 kDa molecular weight cut-off (MWCO) ultrafiltration membrane (GE Healthcare) and stored at -80 ºC until further use. Final domain concentration was estimated by measuring the absorbance at 280 nm. The purity of the rhNtA domain was assessed by sodium dodecyl sulfate–polyacrylamide gel electrophoresis (SDS-PAGE) analysis and Western blotting using the anti-agrin antibody - rabbit polyclonal agrin antibody (1:5000; Abcam, ab85174). The rhNtA molecular weight was determined by mass spectrometry, as described in section 2.7.

### 2.2. Solid-phase binding assay

Binding of rhNtA to immobilized laminin was assessed performing an enzyme-linked binding assay (ELISA). 96-well microtiter ELISA plates (BD Falcon) were coated with poly(D-lysine) (PDL; 20 μg/mL; Sigma-Aldrich) and then incubated with laminin-111 from mouse Engelbreth-Holm-Swarm sarcoma (msLn-111;10 μg/mL; Sigma-Aldrich) in 50 mM sodium bicarbonate buffer pH 9.6 (overnight, 4 ºC). After blocking with 2.5% (w/v) bovine serum albumin (BSA; Biowest; 1.5 h, room temperature (RT)), wells were incubated with 2-fold serial dilutions of rhNtA (0.1 – 100 nM; 2 h, 37 ºC). Plates were then washed with PBS/0.05% (v/v) Tween® 20 and incubated with rabbit polyclonal agrin antibody (1:5000; 2

h, RT). A goat anti-rabbit IgG (H+L) coupled to horseradish peroxidase (HRP) (1:2000; Life Technologies, A16023) was used as secondary antibody, and color was developed using 3,3',5,5' tetramethyl benzidine (TMB) as substrate (Biolegend; 30 min, RT). The reaction was stopped with 2 M $H_2SO_4$ and the absorbance measured at 450 nm (BioTek® Synergy™ Mx). The dissociation constant ($K_D$) value of rhNtA to msLn-111 was estimated by non-linear regression analysis using GraphPad Prism 6 software (San Diego).

### 2.3. Surface plasmon resonance (SPR)

Real-time interactions between rhNtA and immobilized laminin were detected by SPR at 25 ºC using a BIACORE X100 (GE Healthcare). Laminin was immobilized on a CM5 sensor chip (GE Healthcare) using amine-coupling chemistry. Briefly, the flow cells surface was activated with a 1:1 mixture of 0.1 M N-hydroxysuccinimide (NHS; Sigma-Aldrich) and 0.4 M 3-(N,N-dimethylamino) propyl-N-ethylcarbodiimide (EDC; Sigma-Aldrich) at a flow rate of 10 μL/min. msLn-111 or recombinant human laminin-521 (rhLn-521; Biolamina) (50 μg/mL in 10 mM sodium acetate pH 3.5) were immobilized at a density of 4000 resonance units. The reactive groups in excess were then deactivated with 1 M ethanolamine-HCl pH 8.5 (Sigma-Aldrich). For binding measurements, 5-fold serial dilutions of rhNtA (500 – 0.8 nM) were prepared in 10 mM 4-(2-hydroxyethyl)-1-piperazineethanesulfonic acid (HEPES; pH 7.4, containing 150 mM sodium chloride (NaCl; VWR), 3 mM Ethylenediamine tetra-acetic acid (Sigma-Aldrich) and 0.005% (v/v) surfactant P20 (GE Healthcare)) and flowed at 30 μL/min onto the flow cells. Proteins were allowed to associate and dissociate for 120 and 1600 s, respectively. Experimental results were fitted with Langmuir 1:1 binding kinetics within Biacore X100 Evaluation software version 2.0.1 (GE Healthcare).

### 2.4. Culture of H9 – Derived Human Neural Stem Cells

Human neural stem cells (hNSCs) derived from the National Institutes of Health (NIH) approved H9 (WA09) human embryonic stem cells were purchased from Life Technologies (N7800-200). Cells were expanded according to the manufacturer's protocol in poly(ornithine)/msLn-111-coated tissue culture-treated plates in serum-free StemPro® NSC SFM growth medium (Life Technologies).

### 2.5. Cell adhesion centrifugation assay

To evaluate the ability of rhNtA-immobilized msLn-111 to promote the adhesion of hNSCs, a centrifugation cell adhesion assay was performed [38]. Here, controllable and reproducible detachment forces were applied to adherent cells, providing relative measurements of adhesion strength [38]. 96-well tissue culture plates (Corning) were coated with increased concentrations of rhNtA (0 – 40 μg/mL) overnight at 4 ºC and blocked

with 1% (w/v) BSA for 1 h at RT to prevent non-specific adhesion to the substrate. msLn-111 was then added at a fixed concentration (10 μg/mL), the plate incubated for 2 h at 37 ºC and hNSC adhesion assessed as described in Supplementary Materials and Methods. Wells incubated with 1% (w/v) BSA or 20 μg/mL poly(ornithine) / 10 μg/mL msLn-111 were used as negative and positive control, respectively. To assess the effect of the domain *per se* on cell adhesion, wells incubated with 10 μg/mL rhNtA were used.

### 2.6. N-terminal PEGylation of rhNtA

A 5 mg/mL rhNtA solution in 0.1 M sodium phosphate ($NaH_2PO_4$) pH 6.5 was added to thiol-PEG-succinimidyl glutaramide (SH-PEG-SGA; 3.5 kDa; purity > 90%, Jenkem USA) at a protein:PEG molar ratio of 1:2. The reaction was allowed to proceed for 4 h at 4 ºC and then quenched with 2 M hydroxylamine pH 7.4. The solution was diluted to a final protein concentration of 0.5 mg/mL with 1 mM HCl and the pH adjusted to 3.5 with 1 M HCl. The reaction mixture was then diluted (100×) with 20 mM sodium acetate pH 4.0 and loaded onto a HiTrap SP HP cation exchange column (GE Healthcare). A gradient of 0 to 1 M NaCl in 20 mM sodium acetate pH 4.0 was used to elute the different PEGylated fractions. The peak corresponding to the mono-N-terminal conjugate was dialyzed against 10 mM PBS pH 7.4, concentrated in a 10 kDa MWCO ultrafiltration membrane (GE Healthcare) and stored at -80 ºC until further use. Protein concentration was estimated by measuring the absorbance at 280 nm and the conjugate was characterized by SDS-PAGE and MALDI-TOF mass spectrometry (MALDI-TOF MS).

### 2.7. Protein and PEGylated conjugate characterization by mass spectrometry

The native or mono-PEGylated rhNtA, as well as unmodified SH-PEG-SGA, were analyzed by MALDI-TOF MS. Briefly, samples were diluted 1:4 (v/v) in MALDI matrix (sinapinic acid 10 mg/mL, 50% acetonitrile, 0.1% trifluoroacetic acid, all purchased from Sigma-Aldrich), spotted onto a target plate and analyzed in linear positive mode. Mass spectra were internally calibrated with thioredoxin (m/z 11674) and apomyoglobin (m/z 16952). To characterize the site of PEG conjugation to rhNtA, peptide mapping of native and mono-PEGylated rhNtA was performed using a previously published procedure [39], which is briefly described in Supplementary Materials and Methods.

### 2.8. Self-assembled monolayers (SAMs) preparation

Mixed SAMs of mono-PEGylated rhNtA (mPEG rhNtA-SAM) or SH-PEG-SGA (SGA-SAM) were prepared on gold-coated substrates (0.5 × 0.5 $cm^2$), obtained from Instituto de Engenharia de Sistemas e Computadores – Microsistemas e Nanotecnologias, Portugal (INESC-MN). Prior to use, gold surfaces were cleaned as described elsewhere [40]. Gold

substrates were then incubated in ethanolic solutions (99.9%; Merck-Millipore) of either mono-PEGylated rhNtA (2.5, 5.0 or 10.0 μM), for laminin affinity binding; or SH-PEG-SGA (5.0 μM), for non-selective covalent immobilization of laminin. After 4 h at RT and under inert conditions (glove chamber saturated with dry nitrogen), SAMs were rinsed with absolute ethanol to remove any physically adsorbed molecules. For proper monolayer packing mPEG rhNtA- and SGA- SAMs were subsequently incubated with a 100.0 μM absolute ethanolic solution of (11-mercaptoundecyl) tetraethylene glycol (EG4, SensoPath Technologies) for 16 h at RT and under the inert conditions mentioned above. Afterwards, SAMs were thoroughly rinsed with absolute ethanol (99.9%; Merck-Millipore). EG4-SAMs, used as control surfaces, were prepared by immersing cleaned gold substrates in a 100.0 μM ethanolic solution of EG4 for 16 h at RT and under inert conditions.

### 2.9. Quartz crystal microbalance with dissipation monitoring (QCM-D)

Gold-coated QCM-D sensors (Biolin Scientific) were cleaned as previously described [41]. Clean sensors were further modified following the procedure reported in 2.8. A QCM-D system (Q-Sense E4 instrument, Biolin Scientific) was used to monitor in real time the frequency (Δf) and dissipation (ΔD) shifts related to laminin adsorption as described in Supplementary Materials and Methods. Data was modeled using the Voigt model [41] in the QTools® V3 software. Results are presented as mass per surface area (ng/cm$^2$).

### 2.10. Laminin self-polymerization

mPEG rhNtA-SAMs were equilibrated in 10 mM HEPES pH 7.4, to favor the affinity interaction with laminin, while SGA-SAMs were equilibrated in 100 mM sodium bicarbonate pH 8.5, to favor the non-selective covalent interaction with laminin amine groups, and then incubated with msLn-111 (20 μg/mL; 2 h, RT). The substrates were then thoroughly washed, to remove any unbound laminin. To assess the ability of laminin to self-polymerize, a msLn-111 solution (50 μg/mL) in 20 mM Tris-HCl pH 7.0, containing 1 mM $CaCl_2$, was used. The laminin concentration used was below the critical protein concentration necessary to trigger laminin polymerization in neutral pH solution [6]. Mixed SAMs with affinity- (mPEG rhNtA-SAMs) or covalent-bound (SGA-SAMs) msLn-111 were incubated with the laminin solution for 24 h at 37 ºC [42]. Finally, samples were processed for laminin immunostaining, as described in Supplementary Materials and Methods, and observed under confocal laser scanning microscopy (CLSM) (TCS SP5 II; Leica Mycrosystems), using a Plan-Apochromat 63×/1.4NA oil objective. A z-section of 15 μm was acquired and subsequently projected into a 2D image. Processing and quantitative analysis of the acquired images were performed in ImageJ/Fiji and MATLAB® software, respectively, as described in detail in the Supplementary Materials and Methods.

### 2.11. Cell adhesion and morphology

To determine the impact of the immobilization approach on the cell adhesion-promoting activity of laminin, mPEG rhNtA- or SGA-SAMs were equilibrated in 10 mM HEPES pH 7.4 and then incubated for 2 h at RT with rhLn-521 (20 μg/mL). After being washed with 10 mM HEPES pH 7.4 to remove unbound laminin, hNSCs (50,000 viable cells/cm$^2$) were added to the substrates and incubated at 37 ºC with 5% $CO_2$ for 24 h. Samples were processed for F-actin/DNA staining, as described in Supplementary Materials and Methods, and imaged with the IN Cell Analyzer 2000 imaging system (GE Healthcare) using a Nikon 20×/0.45 NA Plan Fluor objective. A z-section of 45 μm was acquired per field of view (FOV) and then projected into a 2D image. Images spanning a total area of 4.6 mm$^2$ were analyzed using CellProfiler image analysis software [43]. Briefly, nuclei were segmented through an Otsu thresholding method from the 4',6-diamidino-2-phenylindole (DAPI) channel while cells cytoplasm was segmented from the actin channel through a propagation from the previously identified nucleus, using a minimum cross entropy threshold. Measurements were obtained for total number of adhered cells, average cell spreading area (μm$^2$) and average occupied area (μm$^2$) *per* field of view (FOV). Representative images for each condition were also obtained by CLSM using a Plan-Apochromat 63×/1.4NA oil objective. A z-section of 12 μm was acquired and subsequently projected into a 2D image.

### 2.12. Statistical Analysis

Individual experiments with biological replicates were performed at least in duplicate and statistical analysis was performed using GraphPad Prism 6 software (San Diego). Statistically significant differences between two conditions were detected using a non-parametric Mann Whitney U-test. Comparisons between three or more groups were performed with one-way ANOVA analysis, followed by the Bonferroni correction for pairwise comparisons or the Dunnett's two-tailed test for comparisons with the control condition. For all analyses, differences were considered significant at $p < 0.05$.

## 3. Results and Discussion

### 3.1. Recombinant human N-terminal agrin (rhNtA) domain was successfully produced

In contrast with most of reports published to date in which the NtA used was derived from chicken agrin [32, 33], we produced the human variant of this domain because of its higher clinical relevance. This is of particular interest when envisaging the use of this domain in platforms for human-disease modelling, cell culture/delivery or engineered coatings for neuroelectrodes.

The produced fusion protein Trx-$His_6$-hNtA, revealed high affinity binding to msLn-111 with an equilibrium dissociation constant ($K_D$) of 6.49 ± 0.58 nM, as determined by solid-phase binding assay (Fig. S2), similar to that reported for chicken NtA - msLn-111 interaction ($K_D$ = 5 nM) [32, 33]. Cleavage of the N-terminal tag was subsequently conducted to enable conjugation of a thiol-terminated PEG moiety to the domain N-terminal, for further immobilization of rhNtA to the selected substrate. This immobilization approach was chosen to assure the exposure of the high-affinity laminin binding site of rhNtA, located on the C-terminal [32, 44]. Untagged rhNtA domain was produced with a high purity (> 90%) and with the expected MW 14.5 kDa, as evidenced by Coomassie blue staining (Fig. 1A) and Western blot analysis (Fig. 1B). Molecular weight was further confirmed by MALDI-TOF MS (MW 14.8 kDa) (Fig. 1C).

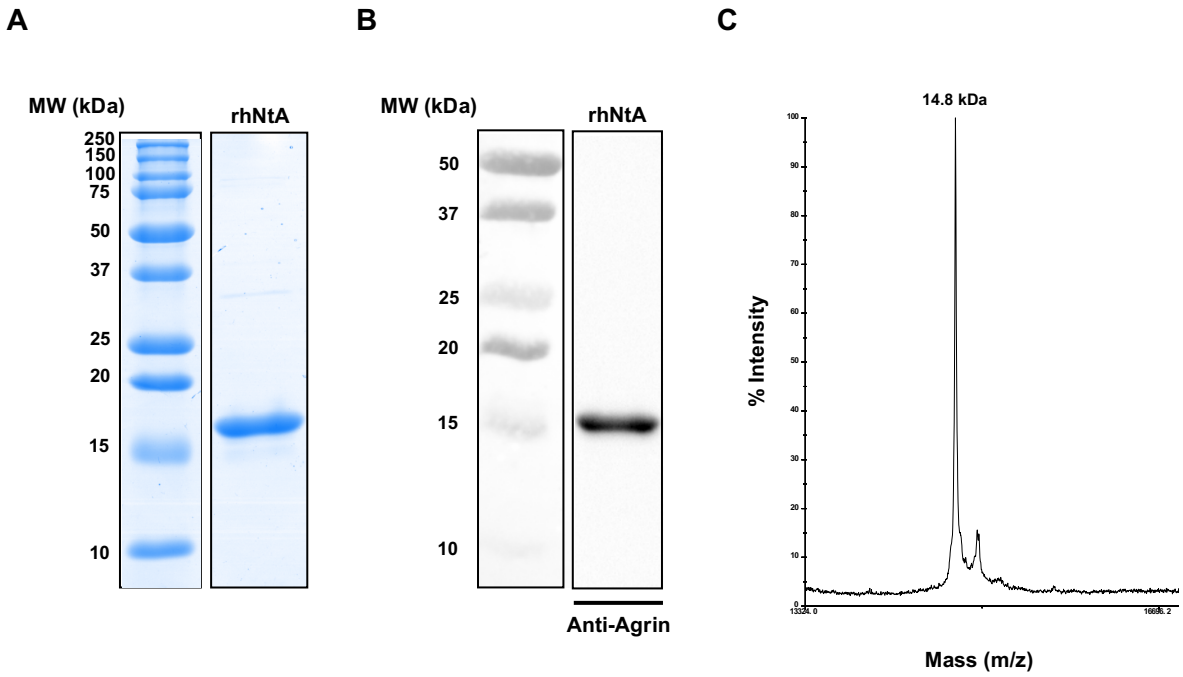


**Figure 1. Recombinant human NtA (rhNtA) domain characterization. A)** Coomassie Blue stained 15% SDS-PAGE gel and **B)** Western-blot analysis of 10 μg of purified rhNtA. MW, Molecular Weight marker. **C)** MALDI-TOF MS spectra of purified rhNtA.

rhNtA was shown to mediate a high affinity interaction with msLn-111 ($K_D$ = 5.85 ± 0.43 nM), as evidenced by solid-phase binding assay (Fig. 2). To monitor in real time the interaction between rhNtA and immobilized msLn-111 or rhLn-521, SPR was conducted (Table 1). Native rhNtA was found to interact with high affinity with both msLn-111 and rhLn-521 ($K_D$ = 0.98 ± 0.02 and 0.54 ± 0.14 nM, respectively; Table 1), showing that binding

affinity towards laminin was retained independently of the laminin isoform. Results from both techniques indicate that the laminin binding site of the produced rhNtA domain preserved its bioactivity, namely the ability to interact with high affinity with laminin.

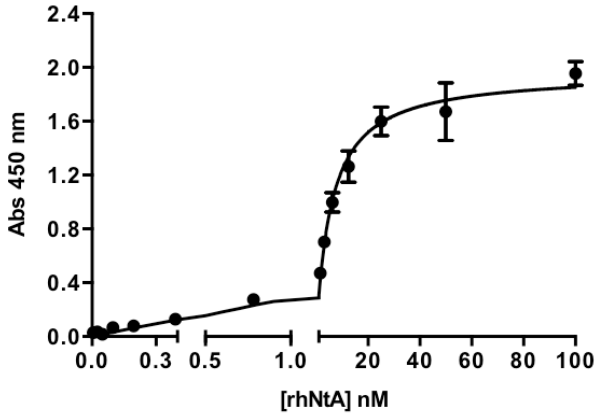


**Figure 2**. **rhNtA Bioactivity**. Solid-phase assay of rhNtA binding to immobilized msLn-111 (10 µg/mL). The results are shown as fitted curve of the mean ± standard deviation (SD) of three replicate samples from one experiment representative of three independent assays. Non-linear regression analysis revealed a $K_D$ value of rhNtA to msLn-111 of 5.85 ± 0.43 nM ($r^2$ = 0.99).

**Table 1.** Kinetic parameters ($k_a$, association rate constant; $k_d$, dissociation rate constant) and affinity constant ($K_D$, dissociation constant) of rhNtA to immobilized msLn-111 or rhLn-521, estimated by SPR. Data represent mean ± SD of three independent experiments.

| | $k_a$ (x$10^5$) $M^{-1}.s^{-1}$ | $k_d$ (x$10^{-4}$) $s^{-1}$ | $K_D$ (nM) |
|---|---|---|---|
| **msLn-111** | 5.25 ± 1.83 | 5.12 ± 1.71 | 0.98 ± 0.02 |
| **rhLn-521** | 4.86 ± 1.55 | 2.52 ± 0.43 | 0.54 ± 0.14 |

### 3.2. rhNtA-immobilized laminin is able to mediate cell adhesion of human neural stem cells

Laminin mediates integrin- and non-integrin-dependent adhesion of neural stem cell (NSCs) [45-47], being commonly used as a surface coating for NSC culture. As the site-specific immobilization of laminin should preserve exposure of its multiple bioactive domains interacting with cell adhesion receptors and, therefore, its cell adhesion-promoting activity, we assessed the ability of rhNtA-immobilized msLn-111 to mediate cell adhesion of hNSCs. These cells were seeded on cell culture wells coated with rhNtA-immobilized msLn-111 and

cell adhesion quantified, as a function of rhNtA concentration, using a centrifugation adhesion assay [38] (Fig. 3). The application of a constant centrifugal force revealed an increase in cell adhesion with the increase of the rhNtA concentration from 0.1 to 10 μg/mL (Fig. 3), at which the levels of cell adhesion observed on rhNtA-immobilized msLn-111 reached values similar to those on the msLn-111 positive control (Fig. 3). This suggests that under these conditions, the amount of affinity-immobilized msLn-111 attained a plateau, which is in agreement with the isotherm of rhNtA adsorption (Fig. S3) that shows a saturation plateau at domain concentrations ≥ 2.5 μg /mL. The cell adhesion levels observed in the absence of rhNtA (0 μg/mL rhNtA) are most likely due to the competitive displacement of adsorbed BSA by laminin, an effect also known as the Vroman effect [48]. Cell adhesion to wells incubated only with rhNtA (10 μg/mL) was, as expected, comparable to that observed on the negative control (BSA; Fig. 3), due to the absence in the rhNtA of bioactive cell adhesion domains. These results demonstrate that, when immobilized through rhNtA, laminin retains its ability to mediate cell adhesion, suggesting the correct exposure of laminin's main bioactive sites interacting with cell surface receptors.

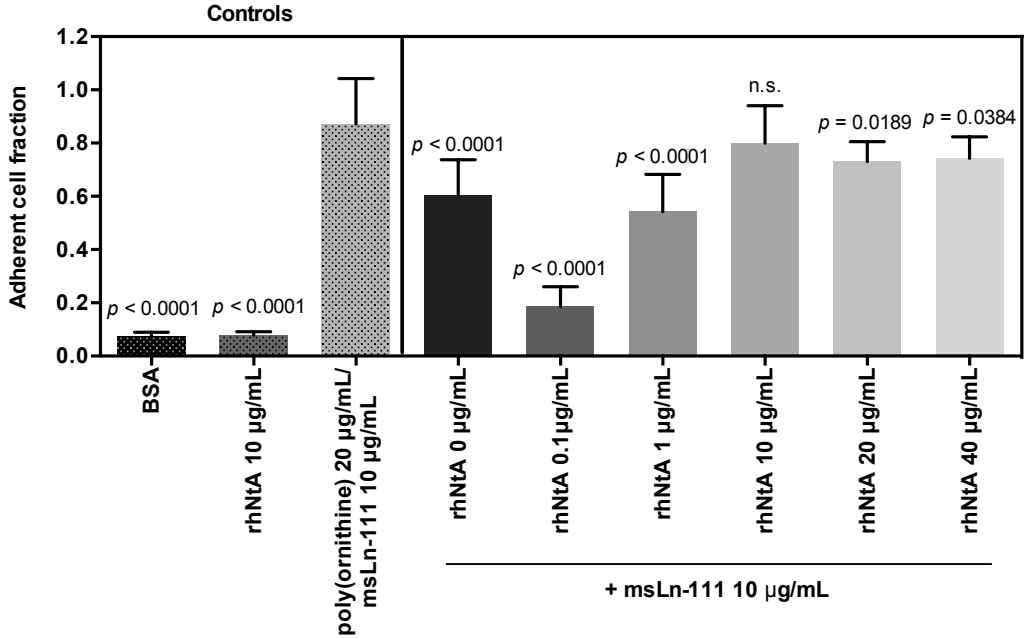


**Figure 3.** hNSC adhesion to rhNtA-immobilized msLn-111 (10 μg/mL) as a function of rhNtA concentration (0.1 – 40 μg/mL), evaluated performing a cell adhesion centrifugation assay. The number of adherent cells on wells coated with BSA (1% (w/v), negative control), rhNtA (10 μg/mL) and 20 μg/mL poly(ornithine)/ 10 μg/mL msLn-111 (positive control), is also shown. Data represent mean ± SD of 10 to 18 replicates from two independent experiments; one-way ANOVA followed by Dunnett's test (*vs.* poly(ornithine)/msLn-111).

### 3.3. rhNtA is selectively PEGylated at the N-terminus

The rhNtA sequence comprises seven primary amines, including the α-amine of Gly1 and the ε-amine of six Lys residues (Fig. S1), which can theoretically react with the SGA group in SH-PEG-SGA. The site-specific addition of the PEG moiety at the N-terminal domain (α-amine) of rhNtA can be controlled by adjusting the pH at which the PEGylation reaction occurs and by adjusting the protein:PEG molar ratio. The conjugation reaction was performed at pH 6.5 and using a protein:PEG molar ratio of 1:2. The slightly acidic pH directs the PEGylation reaction to the α-amino group at the N-terminal of rhNtA, by taking advantage of the differences in pKa values of the α-amino group (pKa 7.8) [49, 50] *versus* that of the ε-amino groups (pKa 10.1) [49, 50] on the side chains of Lys residues. These conditions favor the protonation of the ε-amino groups of Lys, while assuring the availability of the α-amino group at the N-terminal as nucleophile. The cation-exchange chromatogram of the conjugation mixture (Fig. 4A) showed three different fractions, which correspond, as evidenced by molecular weight estimation from SDS-PAGE analysis (Fig. 4B), to rhNtA PEG conjugates containing either a double (MW ≅ 36.5 kDa; di-PEGylated rhNtA, peak 1) or single (MW ≅ 28.8 kDa; mono-PEGylated rhNtA, peak 2) PEG molecule and native rhNtA (MW ≅ 14.5 kDa, peak 3). The efficiency of the PEGylation reaction was determined based on the SDS-PAGE analysis (Fig. 4B). A PEGylation yield of 47% was obtained, from which 94% corresponds to mono-PEGylated rhNtA and the remaining 6% to di-PEGylated rhNtA. Since the large hydrodynamic volume of PEGylated proteins retards their mobility on SDS-PAGE gels, resulting in higher molecular weight estimates [49], PEGylation reaction products were further analyzed by MALDI-TOF MS for an absolute estimation of their molecular weight. The MALDI-TOF MS spectra of native and PEGylated rhNtA (Fig. 4C) indicate a molecular weight centered at 18.4 and 22.1 kDa for mono- and di-PEGylated rhNtA, respectively (the MW of native rhNtA was found to be 14.8 kDa, confirming the previously determined value (Figure 1C)).

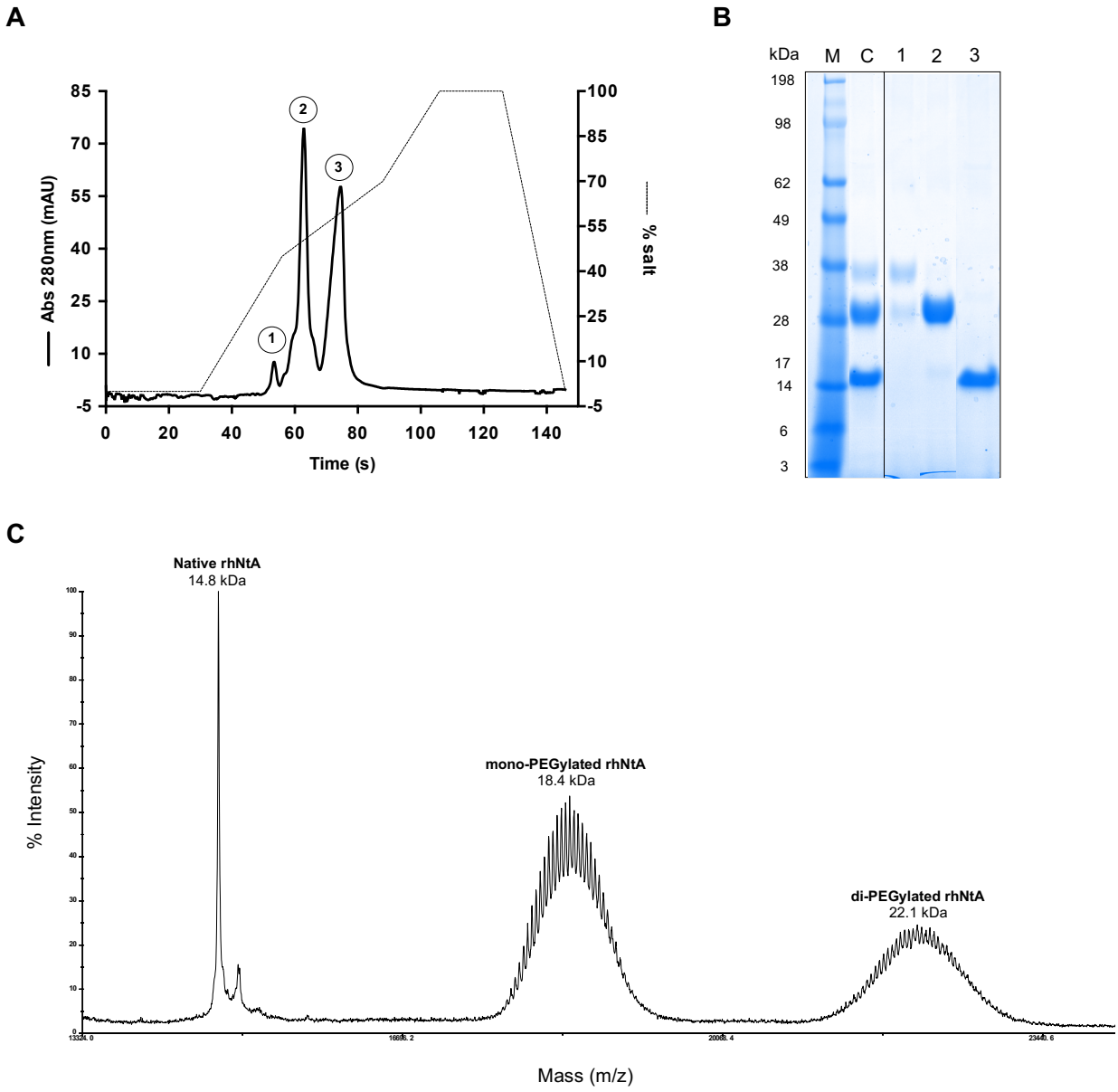


**Figure 4. Characterization of N-terminal PEGylated rhNtA. A)** Cation-exchange chromatogram of the conjugation mixture. The chromatogram was obtained by monitoring the eluent at 280 nm and using a HiTrap SP HP column (GE Healthcare); 1, di-PEGylated rhNtA; 2, mono-PEGylated rhNtA; 3, Native rhNtA. **B)** Coomassie Blue stained 4-12% Bis-Tris gel of native and PEGylated rhNtA after purification. M, MW marker; C, Conjugation mixture before cation-exchange chromatography; 1, di-PEGylated rhNtA band at around 36.5 kDa; 2, mono-PEGylated rhNtA band at around 28.8 kDa; 3, native rhNtA at around 14.9 kDa. **C)** MALDI-TOF MS spectra of native and PEGylated rhNtA. The presented molecular weight corresponds to the value obtained for the high intensity peak – Native rhNtA 14.8 kDa; mono-PEGylated rhNtA 18.4 kDa; di-PEGylated rhNtA 22.1 kDa.

The position of the conjugated PEG moiety on the purified mono-PEGylated rhNtA conjugate was further determined by peptide mapping, comparing the fingerprint of native- and PEGylated rhNtA. The majority of the theoretical fragments, as well as the rhNtA N-terminus were experimentally detected in both samples (Table S2). Also, their molecular masses, which were experimentally determined by MALDI-TOF MS, are very similar to the predicted values obtained in *web.expasy.org/peptide_mass* (Table S2). Two peaks corresponding to the N-terminus of rhNtA domain were identified in both native and mono-PEGylated rhNtA – GPTCPER (F1) [1-7] m/z 816.3677 (Table S2, Fig. S4A) and GPTCPERALER (F2) [1-11] m/z 1285.6278 (Table S2, Fig. S4B). In the conjugated sample, a significant decrease in the signal-to-noise ratio was observed for F1, while the peak correspondent to F2 was not detected. These evidences demonstrate that the $\alpha$-amine of Gly1 was selectively modified with the PEG moiety.

### 3.4. N-terminal PEGylated rhNtA binds with high affinity to laminin

SPR analysis was conducted to evaluate the impact of N-terminal PEGylation on rhNtA laminin binding ability. N-terminal PEGylation led to a decrease of the binding affinity for both msLn-111 ($K_D$ = 3.36 $\pm$ 0.11 nM) and rhLn-521 ($K_D$ = 1.58 $\pm$ 0.41 nM) (Table 2), estimated as a 3.4- and 2.9- fold decrease, respectively, compared to native rhNtA (Table 1). This suggests that PEG conjugation to rhNtA slowed down the rate of domain association ($k_a$) towards immobilized laminin, while the dissociation rate ($k_d$) was not affected (Table 2). Interestingly, the affinity of both native (Table 1) and mono-PEGylated rhNtA (Table 2) for rhLn-521 was found to be slightly higher than that determined for msLn-111. Moreover, the complex formed with this laminin isoform appears to be more stable, as evidenced by higher $k_d$ values (Table 1 and 2). Previous studies suggest that the affinity between NtA and laminin is regulated by laminin chain composition, and that although the agrin binding site is located within the $\gamma$1 chain, $\alpha$ and $\beta$ laminin chains may also contribute to the binding, even though to a lesser extent, [32, 33, 51]. Therefore, the differences observed in the binding affinity of native and mono-PEGylated rhNtA to msLn-111 and rhLn-521 can be related to the chain composition of the laminin isoforms tested.

**Table 2.** Kinetic parameters ($k_a$ and $k_d$) and affinity constant ($K_D$) of mono-PEGylated rhNtA to immobilized msLn-111 or rhLn-521, estimated by SPR. Data represent mean ± SD of three independent experiments.

| | $k_a$ (x$10^5$) $M^{-1}.s^{-1}$ | $k_d$ (x$10^{-4}$) $s^{-1}$ | $K_D$ (nM) |
|---|---|---|---|
| **msLn-111** | 1.38 ± 0.05 | 4.64 ± 0.31 | 3.36 ± 0.11 |
| **rhLn-521** | 1.66 ± 0.63 | 2.47 ± 0.40 | 1.58 ± 0.41 |

### 3.5. N-terminal PEGylated rhNtA can be used for the site-selective immobilization of laminin with retention of bioactivity

The potential of mono-PEGylated rhNtA to promote the site-selective immobilization of laminin onto substrates was explored using mixed SAMs of mono-PEGylated rhNtA and (11-mercaptoundecyl) tetraethylene glycol (EG4) (mPEG rhNtA-SAMs) as a model surface. EG4 was used to prevent nonspecific protein immobilization and thus guarantee signal specificity and maximum bioactivity of the immobilized biomolecules, while also enhancing the correct monolayer packing [52]. Mixed SAMs of SH-PEG-SGA and EG4 (SGA-SAMs) were also prepared to promote the non-selective covalent immobilization of laminin through the reaction with protein amine groups present in multiple locations within the laminin structure.

To avoid steric effects and have a finer control over the binding ligand surface density, which ultimately would determine the amount of affinity-bound laminin, an initial screening was conducted to determine the most suitable mono-PEGylated rhNtA domain concentration. QCM-D analysis was conducted with different mono-PEGylated rhNtA concentrations (2.5, 5.0 and 10.0 μM) while keeping that of EG4 constant (100.0 μM), to evaluate laminin immobilization (Fig. S5). Results show a more effective laminin immobilization when an intermediate concentration of mono-PEGylated rhNtA (5.0 μM) was used (638 ± 29 ng/cm$^2$, compared to the 146 ± 115 and 445 ± 57 ng/cm$^2$, obtained for 2.5 and 10.0 μM mono-PEGylated rhNtA, respectively) (Fig. S5). Based on these results, mixed SAMs were prepared using an intermediate concentration (5.0 μM) of either mono-PEGylated rhNtA or SH-PEG-SGA.

Infrared reflection absorption spectroscopy (IRRAS) analysis was performed to characterize the prepared mixed mPEG rhNtA- and SGA-SAMs, using Au surfaces as background. EG4-SAMs and adsorbed native rhNtA to Au surfaces were used as controls. The presence of rhNtA domain was confirmed by the detection of the two protein characteristic absorption

bands correspondent to amide I (1690 ± 45 $cm^{-1}$), which is mainly associated with C=O stretching vibration and is directly related to the backbone conformation, and amide II (1540 ± 60 $cm^{-1}$), which results from the N-H and C-N vibration that were observed on both native rhNtA and mPEG rhNtA spectra (Fig. S6). An adsorption band correspondent to amide I (1690 ± 45 $cm^{-1}$) is also observed in the PEG-SGA spectra and is attributed to the C=O stretching vibration resultant from the presence of the SGA group.

### 3.5.1. Site-selective immobilized laminin retains its ability to self-polymerize

Laminin polymerization is a key process to direct basement membrane assembly and organization and occurs by a thermally reversible process dependent on the presence of calcium ions [6-8]. Previous studies exploring this hallmark feature of laminin demonstrated that this ECM protein is able to spontaneously self-polymerize in solution at neutral pH, requiring a minimal protein concentration of approximately 60 nM [6]. The three-arm interaction model has been proposed by Cheng and co-workers (Fig. 5A) to explain the mechanism of laminin polymerization. This model proposes that the three laminin N-terminal short arms are able to interact with the globular N-terminal domains of other laminins to form a polygonal network, contributing to the basement membrane architecture [6-8, 53]. The long arm of the laminin heterotrimer, in turn, is predicted not to be involved in the network formation, being free to interact with cells out of the plan of the polymer. Based on this evidence, we evaluated the ability of laminin to self-polymerize when immobilized onto mPEG rhNtA-SAMs (Fig. 5B, left panel) or SGA-SAMs (Fig. 5B, right panel). Differences between the two conditions were assessed by image processing and quantitative analysis, using ImageJ/Fiji and MATLAB® software, respectively. Four different variables were measured, including number of aggregates (Fig. 5C), aggregate average size (Fig. 5D), perimeter (Fig. 5E) and maximum Feret's diameter (Fig. 5F). More information about the specific meaning of each measured variable can be found in https://imagej.nih.gov/ij/docs/menus/analyze.html. The relationship among the number of aggregates, aggregate average size, and perimeter provides information on laminin's ability to form larger organized polygonal-shape structures versus several small unstructured aggregates, whereas the maximum Feret's diameter provides a good indicator of network organization. An organized polygonal network consisting mainly of lamellar aggregates was consistently observed when laminin was selectively immobilized onto mPEG rhNtA-SAMs (Fig. 5B, left panel). Data from image quantitative analysis (Fig. 5C-F) support this observation, as a higher tendency for the formation of larger polygonal-based (Fig. 5C-E) and organized (Fig. 5F) structures is evident as result of laminin polymerization. Moreover, the formed homogeneous matrix presents a fractal-like organization (Fig. 5B, left panel) and resembles the pattern of the networks reported in literature [42, 54, 55]. On the other hand,

the non-selective covalent immobilization of laminin onto SGA-SAMs, led to the formation of a matrix consisting mainly of several smaller aggregates (Fig. 5C-E), which are extended over several focal plans with no observable formation of polygon-based structures (Fig. 5B, right panel). The inability to form a more organized structure is evidenced by the lower values of maximum Feret's diameter (Fig. 5F). The 3D structures of the different formed laminin matrices can be better appreciated in the animation movies presented as Movie S1 – S2 in Supporting Information. The combination of the three independent variables (aggregate average size, perimeter and maximum Feret's diameter) and its analysis using the Fisher's combined probability test [56], also revealed statistically significant differences ($p < 0.0001$) on laminin self-polymerization between mPEG rhNtA- and SGA-SAMs. Overall, the results obtained showed that depending on the binding ligand (mono-PEGylated rhNtA *vs.* SH-PEG-SGA), structural distinct matrices can be formed. Moreover, we demonstrate that only when we promote the site-selective immobilization of laminin (mPEG rhNtA-SAMs), one retains its natural/intrinsic ability to self-polymerize.

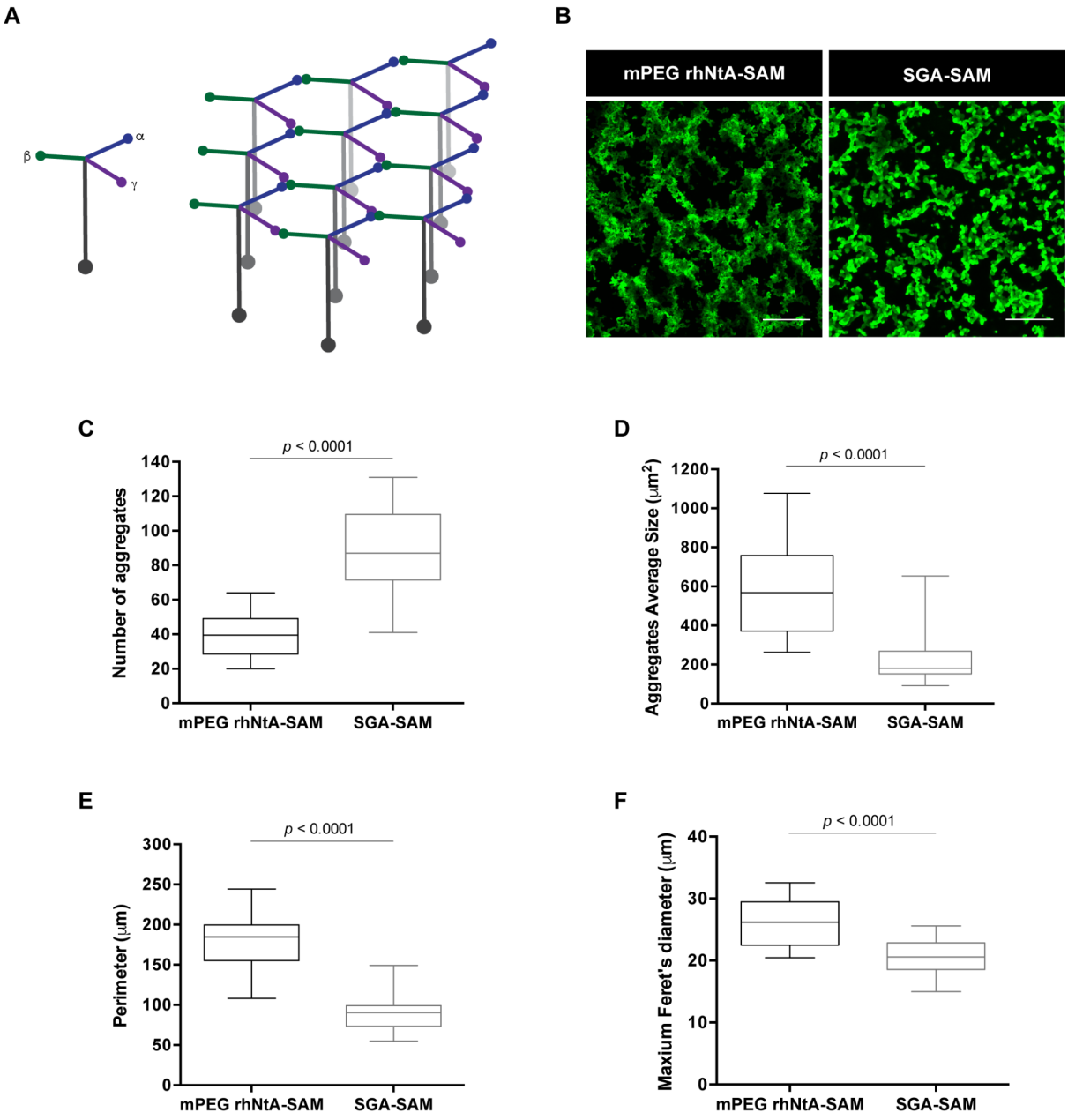


**Figure 5. Assessment of the ability of site-selective immobilized laminin to self-polymerize**. **A)** Schematic representation of laminin self-polymerization (not to scale). Adapted from [57]. N-terminal domains of α, β and γ chains interact to form a polygonal network. The long arm is not involved in the network formation. **B)** mPEG rhNtA-SAM (left panel) or SGA-SAM (right panel) were incubated with msLn-111 (50 μg/mL) for 24 h, under neutral conditions (pH 7.0), and samples processed for immunofluorescence staining of laminin. Scale Bar = 50 μm. **C)** Number of aggregates; **D)** Aggregate average size (μm$^2$); **E)** Perimeter (μm); and **F)** Maximum Feret's diameter (μm) determined by image processing and quantitative analysis using ImageJ/Fiji and MATLAB® software, respectively. Data represent median and interquartile range (IQR) of 13-16 replicate samples from three independent assays; non-parametric Mann-Whitney U-test.

### 3.5.2. Site-selective immobilized rhLn-521 support hNSC adhesion and spreading

rhLn-521 has a key role in the modulation of neural cell behavior, including neuronal adhesion, viability and network formation [36, 58]. Indeed, several studies have shown the potential of this laminin isoform to be used as a robust substratum for the culture and renewal of human embryonic [59] and pluripotent [36] stem cells. With this in mind, to assess laminin ability to mediate hNSC adhesion and spreading upon its binding to mPEG rhNtA-SAMs, rhLn-521was used. QCM-D analysis was first conducted to follow the kinetics of rhLn-521 immobilization onto SAMs (Fig. 6 A-B). Then, to characterize whether the proposed strategy favored the exposure of rhLn-521 cell-adhesive domains, hNSC adhesion and spreading was assessed (Fig. 6 C-E).

QCM-D monitoring of rhLn-521 immobilization onto mPEG rhNtA-SAMs indicated a protein immobilization (638 $\pm$ 29 ng/cm$^2$, Fig. 6B), with mass per surface area values close to the theoretical value calculated for laminin immobilization under these conditions (952 ng/cm$^2$). This suggests that the immobilized mono-PEGylated rhNtA retained a 3D conformation that allowed the selective interaction with laminin. Moreover, mPEG rhNtA SAMs led to an immobilization degree statistically similar to that observed for uncoated Au surfaces (1130 $\pm$ 348 ng/cm$^2$), in which laminin may randomly adsorb over the entire surface. SGA-SAMs, in contrast, presented lower amounts of immobilized rhLn-521 (342 $\pm$ 44 ng/cm$^2$) (Figure 6B), when compared to mPEG rhNtA-SAMs. As SH-PEG-SGA moieties can randomly interact with different amine groups within a single laminin molecule, these results suggest that the conformation of covalently-bound laminin and its spatial arrangement at the surface were distinct from that of affinity-bound laminin, leaving less area for the immobilization of other laminin molecules. As expected, the amount of adsorbed rhLn-521 on EG4-SAMs, was very low (20 $\pm$ 1 ng/cm$^2$) (Fig. 6B).

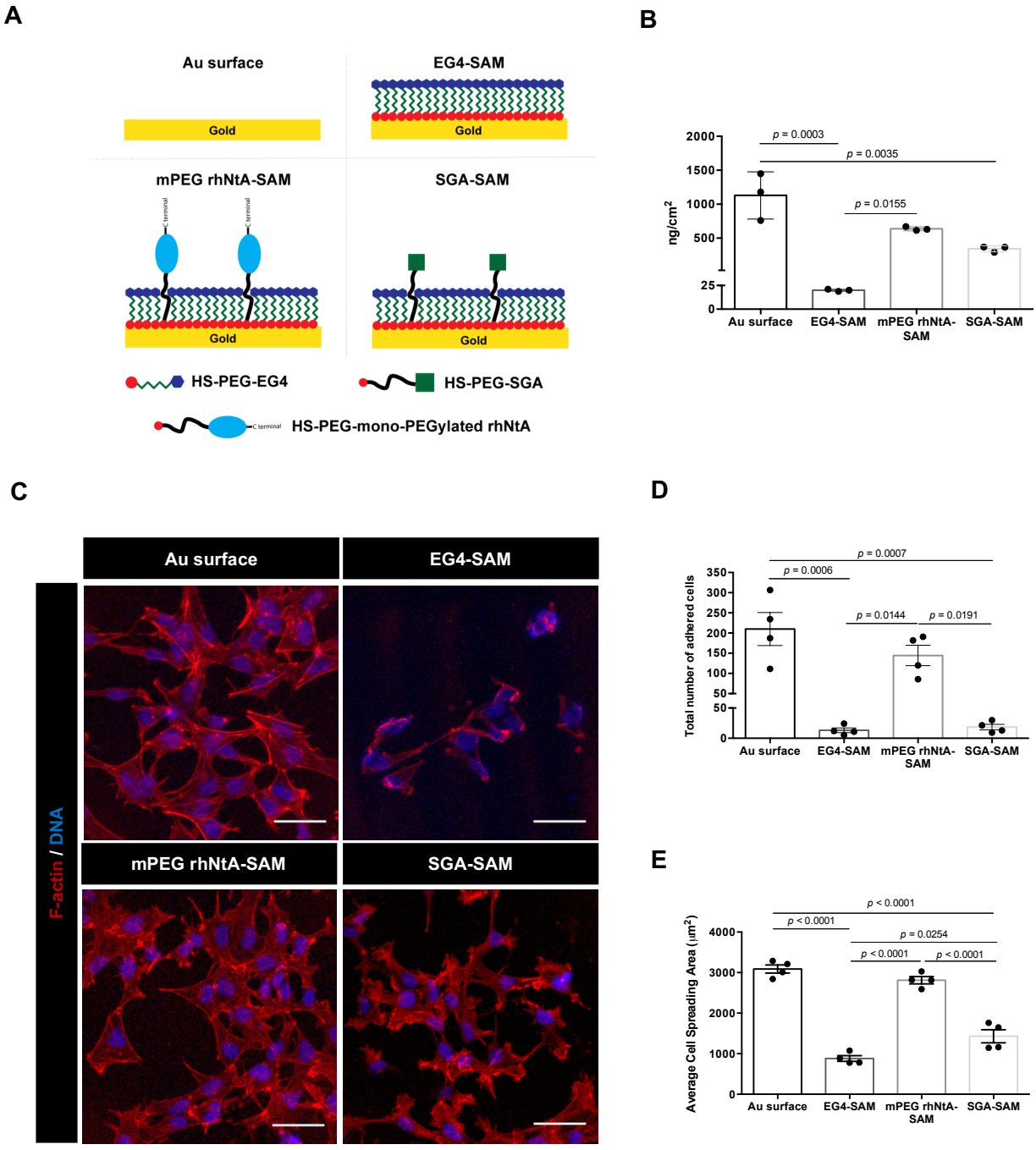


**Figure 6. Immobilization of rhLn-521 onto SAMs and its effect on hNSC adhesion and spreading. A)** Schematic representation of the prepared surfaces (not to scale) – Au surface (control surface), EG4-SAM (non-fouling surface), mPEG rhNtA-SAM (for site-selective immobilization of laminin) and SGA-SAM (for non-specific covalent immobilization of laminin). **B)** QCM-D analysis of rhLn-521 immobilization (ng/cm$^2$) on SAMs. Data represent mean ± SD of three independent experiments; one-way ANOVA followed by Bonferroni's test. **C)** Representative 2D projections of CLSM 3D stack images of adhered hNSCs, after 24 h of culture. Scale Bar = 50 μm; **D)** Total number of adherent cells; and **E)** Average cell spreading area (μm$^2$) determined by quantitative analysis of images acquired with an IN Cell Analyzer 2000 imaging system. Data represent mean ± standard

error of the mean (SEM) of four replicate samples from an experiment representative of three independent assays; one-way ANOVA followed by Bonferroni's test.

Site-selective immobilization of laminin onto mPEG rhNtA-SAMs led to hNSC adhesion comparable to that observed on rhLn-521-coated Au surfaces, used here as a control surface for hNSC adhesion (Fig. 6D and S8). After 24 h of culture, cells were well-spread (Fig. 6E and S9), exhibiting a morphology (Fig. 6C) comparable to that observed for cells seeded on rhLn-521-coated Au surfaces (Fig. 6C). Moreover, cells adhered to mPEG rhNtA-SAMs exhibit an average spreading area of 2812 $\pm$ 89 $\mu m^2$ (Fig. 6E), comparable to that observed for cells cultured on rhLn-521-coated Au surfaces (3089 $\pm$ 101 $\mu m^2$; Figure 6E). TCPS surfaces, which are conventional used in adhesion studies, were used herein as additional control surfaces. The morphology of cells seeded on rhLn-521- site-selective immobilized on SAMs or -coated on Au surfaces is comparable to that observed on rhLn-521-modified TCPS surfaces (Fig. S7). In addition, the average cell spreading area in these conditions is similar to that observed in TCPS surfaces (3496 $\pm$ 483 $\mu m^2$). The non-selective immobilization of laminin onto SGA-SAMs, in turn, resulted in a significantly lower cell adhesion ($p$ = 0.0191; Fig. 6D and S8) and average spreading area (1430 $\pm$ 161 $\mu m^2$; $p$ < 0.0001; Fig. 6E and S9) when compared to mPEG rhNtA-SAMs. Moreover, cells with both spread (Fig. 6C) and round (Fig. S7) morphology were observed. These results suggest that the non-selective nature of the immobilization process partially compromises the exposure of laminin cell binding domains, despite the considerable amount of rhLn-521 bound to SGA-SAMs (342.3 $\pm$ 43.6 ng/cm$^2$) (Fig. 6B). As expected, on EG4-SAMs, the few adherent cells (Fig. 6D and S8) presented mainly a round morphology (Fig. 6C and S7), as evidenced by the low average cell spreading area (881 $\pm$ 70 $\mu m^2$, Fig. 6E). Overall, these results clearly demonstrate that site-specific immobilization of laminin through the use of mono-PEGylated rhNtA better preserved laminin bioactivity in terms of ability to self-polymerize and to mediate hNSC adhesion and spreading, when compared to non-selective covalent immobilization approaches.

## 4. Conclusion

The present work demonstrates the potential of mono-PEGylated rhNtA as an effective natural affinity binding ligand for site-selective immobilization of laminin, allowing the preservation of laminin ability to self-polymerize and mediate cell adhesion and spreading. This affinity binding strategy overcomes several drawbacks associated with the currently available strategies for laminin immobilization. Moreover, this approach is highly versatile, as result of the ability of NtA to bind the different laminin isoforms that comprise the $\gamma$1 chain,

which represent more than 50% of the isoforms identified to date [60], with variations in affinity imposed by $\alpha$ and $\beta$ chains. Therefore, this strategy enables the immobilization of different laminin isoforms, which can be of interest for particular cell types and for application in specific disease contexts. Overall, the proposed strategy is highly attractive for a broad range of applications, including 2D coatings for cell culture, functionalization of 3D matrices for cell and/or drug delivery, engineered coatings for neuroelectrodes, among others.

## Acknowledgments

The mass spectrometry technique was performed at the Proteomics i3S Scientific Platform (Roteiro/0028/2013; LISBOA-01-0145-FEDER-022125) with the assistance of Hugo Osório. IRRAS analysis was performed at the Biointerfaces and Nanotechnology Scientific Platform, with the assistance of Ricardo Vidal. In Cell Analyzer experiments were performed at the Biosciences Screening i3S Scientific Platform, member of the PPBI (PPBI-POCI-01-0145-FEDER-022122) with the assistance of André Maia. Confocal microscopy was conducted at the Bioimaging i3S Scientific Platform, member of the PPBI (PPBI-POCI-01-0145-FEDER-022122), with the assistance of Maria Lázaro. This work was funded by projects NORTE-01-0145-FEDER-000008 and NORTE-01-0145-FEDER-000012, supported by Norte Portugal Regional Operational Programme (NORTE 2020), under the PORTUGAL 2020 Partnership Agreement, through the European Regional Development Fund (ERDF) and FEDER - Fundo Europeu de Desenvolvimento Regional funds through the COMPETE 2020 - Operacional Programme for Competitiveness and Internationalisation (POCI), Portugal 2020; by Portuguese funds through FCT/MCTES in the framework of the project "Institute for Research and Innovation in Health Sciences" (POCI-01-0145-FEDER-007274), and by Santa Casa da Misericordia de Lisboa through project COMBINE (Prémio Neurociências Melo e Castro 1068-2015).

D.B. was supported by FCT PhD Programs (PD/BD/105953/2014) and Programa Operacional Potencial Humano (POCH), in the scope of the BiotechHealth Program (Doctoral Program on Cellular and Molecular Biotechnology Applied to Health Sciences), Programa FLAD Healthcare 2020 and the project PARES (Prémio Albino Aroso). Eduardo Conde-Sousa was supported by a post-doctoral grant of the project PPBI-POCI-01-0145-FEDER-022122, in the scope of FCT National Roadmap of Research Infrastructures.

# SUPPLEMENTARY DATA

## Supplementary Materials and Methods

*Selection and cloning of human N-terminal agrin domain (hNtA) gene and pCoofy expression vector*

The human N-terminal agrin (hNtA) domain gene was synthesized by GenScript (Piscataway, NJ, USA) – Clone ID: B25738, from the protein sequence with the Uniprot reference O00468 (Thr 30 – Pro 157). A gene of 395bp length was produced in pUC57 cloning vector and the conditions for expression in *Escherichia coli (E. coli)* optimized. A high-throughput expression screening was conducted to select, among the several pCoofy expression vectors available [37], the most suitable for the expression of the soluble protein. pCoofy2 expression vector – 6080 bp (gift from Sabine Suppmann – Addgene plasmid # 43981) was the one selected. Both hNtA gene and pCoofy2 expression vector were polymerase chain reaction (PCR) linearized using specific-designed primers and LP1 forward and LP2 reverse primers, respectively (Table S1). Following PCR amplification, the hNtA gene was sub-cloned into the pCoofy2 expression vector using a sequence and ligation independent cloning (SLIC) reaction, as described in [37]. The efficiency of DNA insert incorporation into the expression vector was confirmed by colony PCR and DNA sequencing (Macrogen).

*Western blot analysis*

Ten micrograms of rhNtA was resolved in a 15% SDS-PAGE gel and transferred onto a nitrocellulose membrane (0.45 μm, GE Healthcare). Unspecific binding was prevented by incubating the membrane with blocking solution (5% (w/v) BSA in Tris-buffered saline – 0.1% Tween® 20 (TBS-T) for 2h at RT. The membrane was then incubated with the primary antibody - rabbit polyclonal agrin antibody (1:1000; Abcam, ab85174), overnight at 4 ºC. After washing with PBS/0.05% (v/v) Tween® 20, the membrane was incubated with the goat anti-rabbit IgG (H+L) coupled to horseradish peroxidase (HRP) secondary antibody (1:2000; Life Technologies, A16023) for 1h at RT. The membrane was finally washed three times with PBS/0.05% (v/v) Tween® 20 and the blots developed with HRP-reactive chemiluminescence reagents (GE Healthcare).

*rhNtA adsorption isotherm*

96-well microtiter ELISA plates (BD Falcon) were coated with 2-fold serial dilution of rhNtA (0 – 40 μg/mL; overnight, 4 ºC) and blocked with 1% (w/v) BSA to prevent non-specific adhesion to substrate. The wells were then incubated with the primary antibody - rabbit polyclonal agrin antibody (1:5000; 2h, RT). Goat anti-rabbit IgG (H+L) coupled to HRP

secondary antibody (1:2000) was incubated for 1,5 h at RT. The color was developed using 3, 3', 5, 5' tetramethyl benzidine (TMB) substrate (Biolegend), incubated for 30 min at RT. The reaction was stopped using 2 M $H_2SO_4$ and the absorbance measured at 450 nm (BioTek® Synergy™ Mx).

*Cell adhesion centrifugation assay*

hNSCs were fluorescently-labelled with 2 μM of Calcein AM (Molecular Probes, 10 min, 37ºC), suspended in StemPro® NSC SFM medium (Life Technologies) and transferred to rhNtA-immobilized msLn-111-adsorbed surfaces at $3\times10^5$ viable cells/cm$^2$. Cells were allowed to adhere for 5 h and before subjecting the cells to centrifugation, initial fluorescence intensity was measured using a microwell plate reader (BioTek® Synergy™ Mx). After overfilling the wells with 10 mM PBS pH 7.4, until a positive meniscus was observed, the plates were sealed with transparent tape, inverted, and spun at 50 RCF for 5 min. Following cell detachment, the medium was changed, and the wells filled with fresh medium for measurement of final fluorescence. For each well, the adherent cell fraction was determined as the ratio of post-spin (final) to pre-spin (initial) fluorescence readings ($\lambda_{ex}$ = 485 nm; $\lambda_{em}$ = 535 nm).

*Peptide mapping*

All the reagents used to perform the peptide mapping and protein identification were purchased from Sigma-Aldrich unless otherwise stated.

Protein bands correspondent to native or mono-PEGylated rhNtA were cut from the gel, washed with ultrapure water and de-stained with 50% (v/v) acetonitrile (ACN) in 50 mM ammonium bicarbonate. The samples were then reduced with 50 mM dithiothreitol (20 min, 56 ºC) and alkylated with 55 mM iodoacetamide, (20 min, RT in the dark). Next, protein *in gel* enzymatic digestion was performed by the addition of 20 ng of trypsin for 3 h at 37 ºC in the presence of 0.01% surfactant (ProteaseMAX™, Promega). Resulting peptides were extracted from gel plugs with 2.5% trifluoroacetic acid (TFA; 15 min at 1400 rpm), dried under vacuum and resuspended in 0.1% TFA.

Protein identification was performed by a MALDI-TOF/TOF mass spectrometer (4800 Plus, SCIEX). Protein digests were purified by reversed-phase C18 chromatography (ZipTips®, Millipore) following the manufacturer's instructions and eluted in the MALDI sample plate using the MALDI matrix *alpha-Cyano-4-hydroxycinnamic acid* (CHCA) elution solution at 8 mg/mL in 50% ACN, 0.1% TFA, 6 mM ammonium phosphate. Peptide mass spectra were acquired in positive MS reflector mode in the mass range of *m/z* 700-5000 and internally calibrated with trypsin autolysis peaks. Individual peptides from both native and mono-PEGylated rhNtA were identified by peptide mass fingerprint (PMF) approach using MS-

Bridge software version 5.16.1 (ProteinProspector, University of California, San Francisco, CA) and the protein sequence data (Figure S1). The protein search settings were: cysteine carbamidomethylation (constant modification), methionine oxidation (variable modification), up to two missed trypsin cleavages, minimum and maximum digest fragment mass of 500 and 4000 Da, respectively, and a minimum digest fragment length of five amino acids. To estimate the location of the PEG moiety in the conjugate, experimental ion peaks obtained in the peptide map of purified mono-PEGylated rhNtA conjugate were compared to the peptide content of native rhNtA. In addition, an indirect estimation of PEG moiety position in the rhNtA sequence was performed by comparing the mass difference between the conjugated and unmodified PEG molecule.

*Quartz crystal microbalance with dissipation monitoring (QCM-D)*

For QCM-D real-time monitoring of laminin immobilization, sensors were pre-incubated with 10 mM HEPES pH 7.4 for 15 min at a constant flow rate of 0.1 μL/min followed by an additional 15 min incubation, under static conditions, to establish the baseline. Then, 300 μL/sensor of rhLn-521 (20 μg/mL) in 10 mM HEPES pH 7.4 was injected at a constant flow rate of 0.1 μL/min, followed by 1 h incubation in static conditions. After, the system was flushed with 10 mM HEPES pH 7.4 during 30 min at a constant flow rate of 0.1 μL/min. All the experiments were conducted at 25 ºC. The total amount of immobilized laminin was calculated with application of the Voigt model [41], which takes into account the viscoelastic contributions of the hydrated layer. The fluid density and viscosity of rhLn-521 solution were established at 1000 kg/m$^3$ and 0.001 kg/m·s, respectively and data from the 5$^{th}$ harmonic was used in the analysis.

*Infrared reflection absorption spectroscopy (IRRAS)*

IRRAS spectra were obtained using a Perkin Elmer FTIR spectrophotometer, model 2000, coupled with a VeeMax II Accessory (PIKE) and a liquid-nitrogen-cooled MTC detector. To avoid water vapor adsorption, instrument was purged with dry nitrogen for 5 min before and during each sample analysis. Au substrates were here used as a background. Incident light was p-polarized and spectra were collected using the 80º grazing angle reflection mode. The analysis of each sample was performed through the acquisition of 100 scans with 4 cm$^{-1}$ resolution.

*Laminin self-polymerization – Immunocytochemistry and Image processing and analysis*

mPEG rhNtA- or SGA-SAMs incubated with msLn-111 were fixed with 3.7% (w/v) paraformaldehyde (PFA) for 20 min at RT and washed 3× with 10 mM PBS pH 7.4. Samples were then incubated with blocking buffer (5% (w/v) BSA in PBS for 30 min at RT), followed

by incubation with the primary antibody – rabbit polyclonal laminin antibody (1:30; Sigma-Aldrich, L9393), overnight at 4 ºC. Samples were washed 3× with 10 mM PBS pH 7.4 and incubated with Alexa Fluor® 488 conjugated anti-rabbit secondary antibody (1:300; Life Technologies, A11034), for 1 h at RT. Samples were observed under confocal laser scanning microscopy (CLSM, Leica TCS SP5II) using a Plan-Apochromat 63×/1.4NA oil objective and acquired z-sections of 15 μm were processed using the ImageJ/Fiji software [61, 62]. Briefly, the rolling ball algorithm was first applied to maximum intensity projection 2D images, to fix uneven background and followed by the application of a Gaussian blur with $\sigma$ = 1 to reduce noise. Aggregates were segmented through an Otsu thresholding method and a closing morphological filter was then used to unify structures distanced by less than 1 μm. Lastly, all the structures with an area below 10 $\mu m^2$ were removed/rejected. For each resulting image, measurements were obtained for number of aggregates, aggregate average size ($\mu m^2$), perimeter (μm) and maximum Feret's diameter (μm). To evaluate differences on the data resultant from both conditions, statistical analysis of the different variables was conducted on MATLAB® software (R2018a) using the non-parametric Mann-Whitney U-test. Moreover, differences resultant from the combination of the different variables measured were determined by application of the Fisher's combined probability test [56] and an overall *p*-value determined. This test is applied under the assumption that variables must be independent from each other. As the number of aggregates is not independent from the other variables, for the Fisher's combined probability test, only average size, perimeter and maximum Feret's diameter of aggregates were considered.

*Cell adhesion and morphology – F-actin/DNA staining*

hNSC adhesion and morphology was assessed, after 24 h of culture, in samples processed for F-actin/DNA staining. Cells were fixed with 2% (w/v) PFA for 20 min at RT, permeabilized with 0.5% (v/v) Triton X-100 (Sigma-Aldrich) for 10 min at RT and stained with Alexa Fluor® 647 phalloidin (1:50; Biolegend, 424205) for 20 min at RT. The nuclei were counterstained with 0.1 μg/mL of Hoechst 33342 (Life Technologies, H1399) for 20 min at RT. Samples were imaged with the IN Cell Analyzer 2000 imaging system (GE Healthcare) using a Nikon 20×/0.45 NA Plan Fluor objective and CLSM (TCS SP5 II; Leica Mycrosystems) using a Plan-Apochromat 63×/1.4NA oil objective.

*Cell adhesion – DNA fluorescence*

Cell adhesion was also estimated from Hoechst 33342 average fluorescence intensity of samples processed for F-actin/DNA staining. Briefly, samples were transferred to the wells of black 24-well plates (ibidi) and the fluorescence of each surface measured ($\lambda_{ex}$ = 350 nm;

$\lambda_{em}$ = 461 nm) using a microwell plate reader (BioTek® Synergy™ Mx). The measurement was performed using the area scan mode with the optics position set to the bottom. The fluorescence intensity (FI) of unseeded SAMs, processed in parallel, was subtracted and the average FI determined.

## Supplementary Figures and Tables

GPTCPERALERREEEANVVLTGTVEEILNVDPVQHTYSCKVRVWRYLKGKDLVARESLL
DGGNKVVISGFGDPLICDNQVSTGDTRIFFVNPAPPYLWPAHKNELMLNSSLMRITLRNL
EEVEFCVEDKP

**Figure S1.** Amino acid sequence of recombinant human N-terminal agrin (rhNtA) domain after purification and N-terminal tag cleavage.

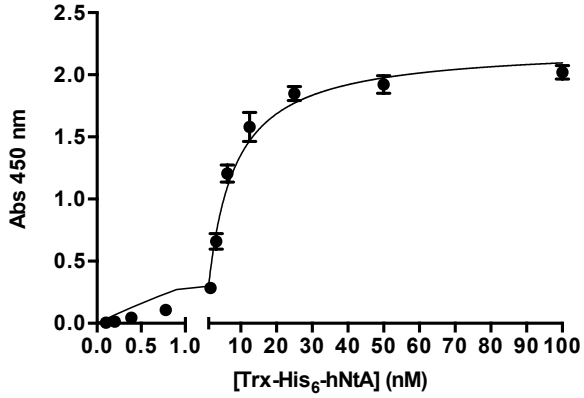


**Figure S2.** Solid-phase assay of Trx-$His_6$-hNtA binding to immobilized msLn-111 (10 µg/mL). The results are shown as fitted curve of the mean ± standard deviation (SD) of three replicate samples from one experiment representative of three independent assays. Non-linear regression analysis revealed a $K_D$ value of Trx-$His_6$-hNtA to msLn-111 of 6.49 ± 0.58 nM ($r^2$ = 0.98).

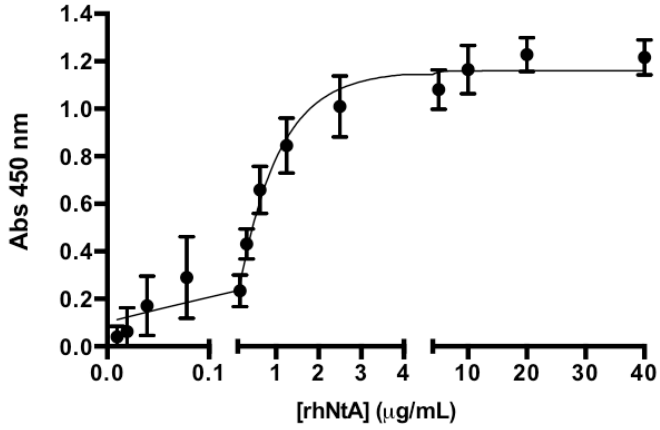


**Figure S3.** Isotherm of rhNtA adsorption determined using a direct ELISA assay. The results are shown as fitted curves of the mean ± SD of twelve replicate samples analyzed from two independent experiments ($r^2$ = 0.94).

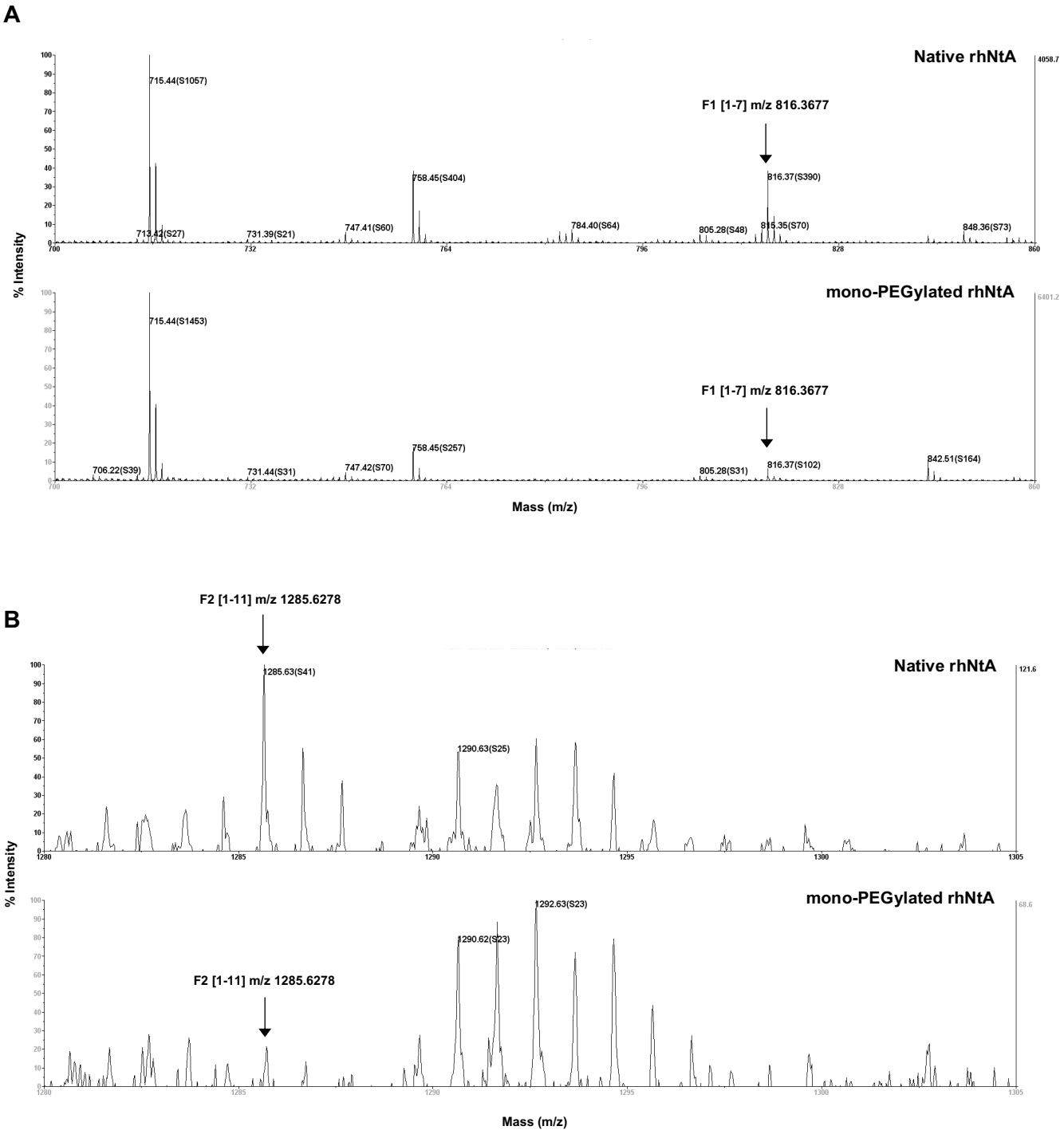


**Figure S4.** Position of conjugated PEG moiety on the purified mono-PEGylated rhNtA determined by peptide mapping. Positive mode MALDI-TOF/TOF identification of the fragments obtained upon digestion of native and mono-PEGylated rhNtA with trypsin. Two peaks correspondent to the N-terminus were identified on both native and mono-PEGylated rhNtA (arrows) – (**A**) F1 - GPTCPER [1-7] m/z 816.3677 and (**B**) F2 - GPTCPERALER [1-11] m/z 1285.6278.

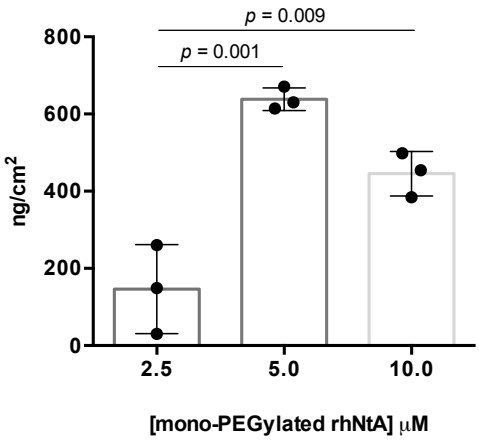


**Figure S5.** Immobilization of rhLn-521 (ng/cm$^2$) onto mPEG rhNtA-SAMs, as a function of the mono-PEGylated rhNtA concentration. SAMs were prepared using a fixed concentration of EG4 (100.0 μM) and increasing concentrations of mono-PEGylated rhNtA (2.5, 5.0 and 10.0 μM). rhLn-521 immobilization was monitored in real time by QCM-D analysis and data modeled with application of the Voigt model. Results represent mean ± SD of three independent experiments; one-way ANOVA followed by Bonferroni's test.

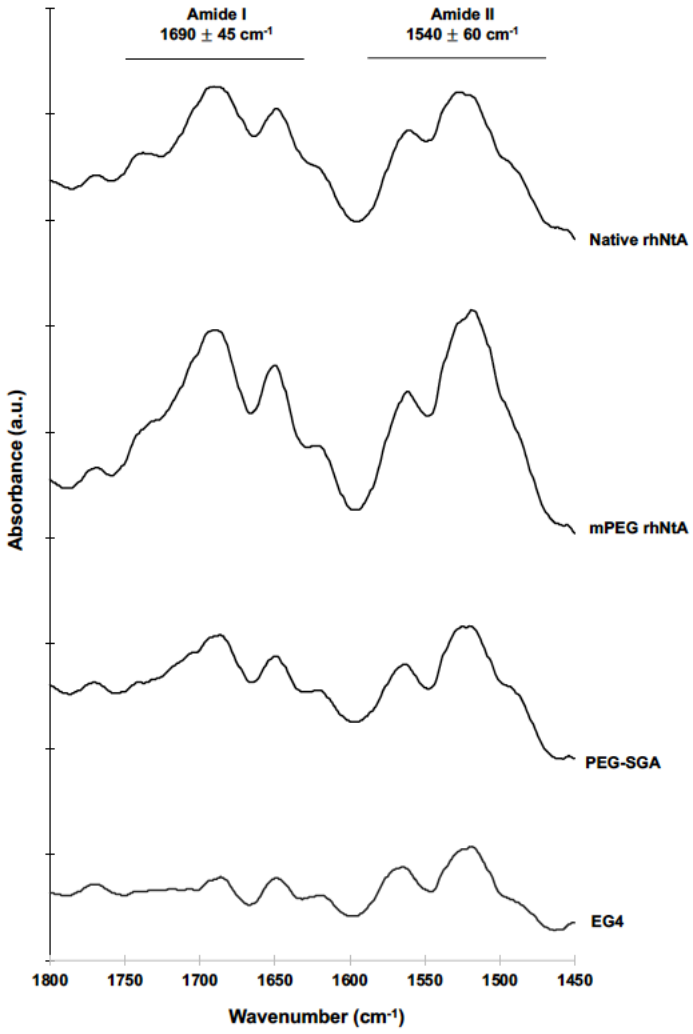


**Figure S6.** IRRAS spectra of mPEG rhNtA- and SGA- SAMs. EG4-SAMs and native rhNtA-adsorbed to Au surfaces were used as controls. A baseline correction and smoothing were applied to all the spectra. Two protein characteristic bands were identified – amide I (1690 ± 45 $cm^{-1}$) and II (1540 ± 60 $cm^{-1}$).

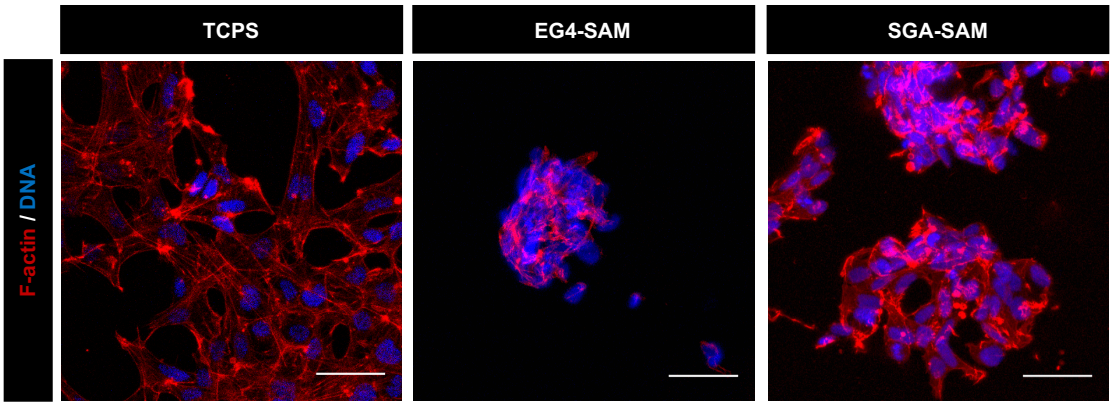


**Figure S7.** Representative 2D projections of CLSM 3D stack images of hNSCs adhered to TCPS and EG4- and SGA-SAMs. Images were acquired after 24h of culture. Scale Bar = 50 μm.

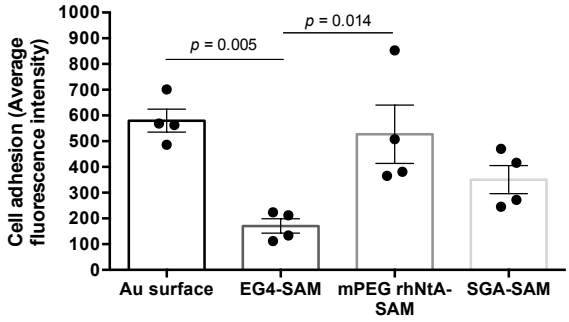


**Figure S8.** hNSC adhesion to SAMs determined measuring the average fluorescence intensity of Hoechst 33342 in samples processed for F-actin/DNA staining. Data represent mean ± SEM of four replicate samples from one experiment representative of three independent assays; one-way ANOVA followed by Bonferroni's test.

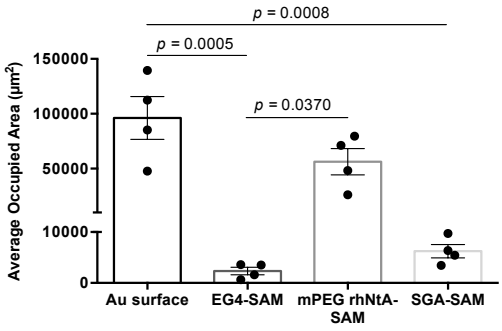


**Figure S9.** hNSCs average occupied area ($\mu m^2$) determined by quantitative analysis of images acquired in IN Cell Analyzer 2000 imaging system. Data represent mean ± SEM of four replicate samples of an experiment representative of three independent assays; one-way ANOVA followed by Bonferroni's test.

**Table S1**. Oligonucleotide sequences used for PCR linearization of hNtA gene and pCoofy2 expression vector

| Primer | Sequence 5' – 3' |
|---|---|
| **3C - LP1 forward vector primer** [a] | 5' AAGTTCTGTTCCAGGGGCCC 3' |
| **ccdB - LP2 reverse vector primer** [a] | 5' CCCCAGAACATCAGGTTAATGGCG 3' |
| **hNtA forward primer (3C)** [b] | 5' AAGTTCTGTTCCAGGGGCCCGGCACCTGTCCGGAACGCGC 3' |
| **hNtA reverse primer (ccdB)** [b] | 5'CCCCAGAACATCAGGTTAATGGCGTTACGGTTTATCTTCAACGCA AAATTC 3' |

[a] Primers for vector amplification were obtained from [37].
[b] Primers used for hNtA gene amplification were specifically designed to have gene specific sequences plus 15 to 25 bp extensions complementary to LP1 and LP2 vector primers.

**Table S2.** Fragments obtained upon digestion of native- and mono-PEGylated rhNtA with trypsin. The N-terminus sequence of rhNtA fragment is depicted in bold

| Sample | Fragments | Sequence | Molecular Mass (Da) | |
|---|---|---|---|---|
| | | | Calculated[a] | Experimental[b] |
| rhNtA | **1-7** | **GPTCPER** | **816.3668** | **816.3677** |
| mono-PEG rhNtA | | | | **816.3736** |
| rhNtA | **1-11** | **GPTCPERALER** | **1285.6317** | **1285.6278** |
| mono-PEG rhNtA | | | | ***c*** |
| rhNtA | 8-40 | ALERREEEANVVLTGTVEEILNVDPVQHTYSCK | 3741.8752 | 3798.9145 |
| mono-PEG rhNtA | | | | 3798.9299 |
| rhNtA | 12-40 | REEEANVVLTGTVEEILNVDPVQHTYSCK | 3329.6317 | 3329.6360 |
| mono-PEG rhNtA | | | | 3329.6489 |
| rhNtA | 13-40 | EEEANVVLTGTVEEILNVDPVQHTYSCK | 3173.5306 | 3173.5747 |
| mono-PEG rhNtA | | | | 3173.5818 |
| rhNtA | 41-45 | VRVWR | 715.4362 | 715.4423 |
| mono-PEG rhNtA | | | | 715.4426 |
| rhNtA | 46-55 | YLKGKDLVAR | 1162.6930 | *c* |
| mono-PEG rhNtA | | | | 1162.6930 |
| rhNtA | 49-55 | GKDLVAR | 758.4519 | 758.4529 |
| mono-PEG rhNtA | | | | 758.4524 |
| rhNtA | 56-64 | ESLLDGGNK | 932.4745 | *c* |
| mono-PEG rhNtA | | | | 932.4745 |
| rhNtA | 56-86 | ESLLDGGNKVVISGFGDPLICDNQVSTGDTR | 3263.5848 | 3263.5940 |
| mono-PEG rhNtA | | | | 3263.6089 |
| rhNtA | 65-86 | VVISGFGDPLICDNQVSTGDTR | 2350.1343 | 2350.1294 |
| mono-PEG rhNtA | | | | 2350.1355 |
| rhNtA | 87-102 | IFFVNPAPPYLWPAHK | 1897.0159 | 1897.0105 |
| mono-PEG rhNtA | | | | 1897.0167 |
| rhNtA | 87-113 | IFFVNPAPPILWPAHKNELMLNSSLMR | 3217.6325 | 3217.6418 |
| mono-PEG rhNtA | | | | 3217.6716 |
| rhNtA | 103-113 | NELMLNSSLMR | 1339.6344 | 1339.6328 |

| | | | | |
|---|---|---|---|---|
| mono-PEG rhNtA | | | | 1339.6374 |
| rhNtA | 114-130 | ITLRNLEEVEFCVEDKP | 2091.0426 | 2091.0317 |
| mono-PEG rhNtA | | | | 2091.0422 |
| rhNtA | 118-130 | NLEEVEFCVEDKP | 1607.7257 | 1607.7244 |
| mono-PEG rhNtA | | | | 1607.7286 |

[a] Theoretical molecular mass of the fragments calculated in *web.expasy.org/peptide_mass*. [b] Experimental molecular masses determined by MALDI-TOF MS. [c] Fragment not found.

**Movie S1.** Projection of the 3D structures formed after laminin self-polymerization, under neutral conditions, on mPEG rhNtA-SAMs. The projection was generated from a series of confocal optical slices (the same shown in Fig. 5B *left panel*) using ImageJ software (AVI).

**Movie S2.** Projection of the 3D structures formed after laminin self-polymerization, under neutral conditions, on SGA-SAMs. The projection was generated from a series of confocal optical slices (the same shown in Fig. 5B *right panel*) using ImageJ software (AVI).

## References

[1] J.H. Miner, B.L. Patton, S.I. Lentz, D.J. Gilbert, W.D. Snider, N.A. Jenkins, N.G. Copeland, J.R. Sanes, The laminin alpha chains: expression, developmental transitions, and chromosomal locations of alpha1-5, identification of heterotrimeric laminins 8-11, and cloning of a novel alpha3 isoform, J Cell Biol 137(3) (1997) 685-701.

[2] M. Falk, M. Ferletta, E. Forsberg, P. Ekblom, Restricted distribution of laminin alpha1 chain in normal adult mouse tissues, Matrix Biol 18(6) (1999) 557-68.

[3] H. Colognato, P.D. Yurchenco, Form and function: the laminin family of heterotrimers, Dev Dyn 218(2) (2000) 213-34.

[4] T. Sasaki, R. Giltay, U. Talts, R. Timpl, J.F. Talts, Expression and distribution of laminin alpha1 and alpha2 chains in embryonic and adult mouse tissues: an immunochemical approach, Exp Cell Res 275(2) (2002) 185-99.

[5] J. Tzu, M.P. Marinkovich, Bridging structure with function: structural, regulatory, and developmental role of laminins, Int J Biochem Cell Biol 40(2) (2008) 199-214.

[6] P.D. Yurchenco, E.C. Tsilibary, A.S. Charonis, H. Furthmayr, Laminin polymerization in vitro. Evidence for a two-step assembly with domain specificity, J Biol Chem 260(12) (1985) 7636-44.

[7] P.D. Yurchenco, Y.S. Cheng, Self-assembly and calcium-binding sites in laminin. A three-arm interaction model, J Biol Chem 268(23) (1993) 17286-99.

[8] Y.S. Cheng, M.F. Champliaud, R.E. Burgeson, M.P. Marinkovich, P.D. Yurchenco, Self-assembly of laminin isoforms, J Biol Chem 272(50) (1997) 31525-32.

[9] J.D. Lathia, B. Patton, D.M. Eckley, T. Magnus, M.R. Mughal, T. Sasaki, M.A. Caldwell, M.S. Rao, M.P. Mattson, C. ffrench-Constant, Patterns of laminins and integrins in the embryonic ventricular zone of the CNS, J Comp Neurol 505(6) (2007) 630-43.

[10] K.J. Hamill, K. Kligys, S.B. Hopkinson, J.C. Jones, Laminin deposition in the extracellular matrix: a complex picture emerges, J Cell Sci 122(Pt 24) (2009) 4409-17.

[11] M. Aumailley, The laminin family, Cell Adh Migr 7(1) (2013) 48-55.

[12] A.C. Taylor, C.H. Gonzalez, B.S. Miller, R.J. Edgington, P. Ferretti, R.B. Jackman, Surface functionalisation of nanodiamonds for human neural stem cell adhesion and proliferation, Sci Rep 7(1) (2017) 7307.

[13] S.E. Stabenfeldt, A.J. Garcia, M.C. LaPlaca, Thermoreversible laminin-functionalized hydrogel for neural tissue engineering, J Biomed Mater Res A 77(4) (2006) 718-25.

[14] S.E. Stabenfeldt, G. Munglani, A.J. Garcia, M.C. LaPlaca, Biomimetic microenvironment modulates neural stem cell survival, migration, and differentiation, Tissue Eng Part A 16(12) (2010) 3747-58.

[15] S.E. Stabenfeldt, M.C. LaPlaca, Variations in rigidity and ligand density influence neuronal response in methylcellulose-laminin hydrogels, Acta Biomater 7(12) (2011) 4102-8.

[16] A.T. Francisco, R.J. Mancino, R.D. Bowles, J.M. Brunger, D.M. Tainter, Y.T. Chen, W.J. Richardson, F. Guilak, L.A. Setton, Injectable laminin-functionalized hydrogel for nucleus pulposus regeneration, Biomaterials 34(30) (2013) 7381-8.

[17] A.T. Francisco, P.Y. Hwang, C.G. Jeong, L. Jing, J. Chen, L.A. Setton, Photocrosslinkable laminin-functionalized polyethylene glycol hydrogel for intervertebral disc regeneration, Acta Biomater 10(3) (2014) 1102-11.

[18] C.P. Addington, J.M. Heffernan, C.S. Millar-Haskell, E.W. Tucker, R.W. Sirianni, S.E. Stabenfeldt, Enhancing neural stem cell response to SDF-1alpha gradients through hyaluronic acid-laminin hydrogels, Biomaterials 72 (2015) 11-9.

[19] J. Arulmoli, H.J. Wright, D.T.T. Phan, U. Sheth, R.A. Que, G.A. Botten, M. Keating, E.L. Botvinick, M.M. Pathak, T.I. Zarembinski, D.S. Yanni, O.V. Razorenova, C.C.W. Hughes, L.A. Flanagan, Combination scaffolds of salmon fibrin, hyaluronic acid, and laminin for human neural stem cell and vascular tissue engineering, Acta Biomater 43 (2016) 122-138.

[20] C.P. Addington, S. Dharmawaj, J.M. Heffernan, R.W. Sirianni, S.E. Stabenfeldt, Hyaluronic acid-laminin hydrogels increase neural stem cell transplant retention and migratory response to SDF-1alpha, Matrix Biol 60-61 (2017) 206-216.

[21] B.G. Keselowsky, D.M. Collard, A.J. Garcia, Surface chemistry modulates fibronectin conformation and directs integrin binding and specificity to control cell adhesion, J Biomed Mater Res A 66(2) (2003) 247-59.

[22] J.C. Rodriguez Hernandez, M. Salmeron Sanchez, J.M. Soria, J.L. Gomez Ribelles, M. Monleon Pradas, Substrate chemistry-dependent conformations of single laminin molecules on polymer surfaces are revealed by the phase signal of atomic force microscopy, Biophys J 93(1) (2007) 202-7.

[23] O.M. Ba, M. Hindie, P. Marmey, O. Gallet, K. Anselme, A. Ponche, A.C. Duncan, Protein covalent immobilization via its scarce thiol versus abundant amine groups: Effect on orientation, cell binding domain exposure and conformational lability, Colloids Surf B Biointerfaces 134 (2015) 73-80.

[24] C.D. Spicer, B.G. Davis, Selective chemical protein modification, Nat Commun 5 (2014) 4740.

[25] O. Boutureira, G.J. Bernardes, Advances in chemical protein modification, Chem Rev 115(5) (2015) 2174-95.

[26] S.A. Fisher, A.E.G. Baker, M.S. Shoichet, Designing Peptide and Protein Modified Hydrogels: Selecting the Optimal Conjugation Strategy, J Am Chem Soc 139(22) (2017) 7416-7427.

[27] J.P. Lee, E. Kassianidou, J.I. MacDonald, M.B. Francis, S. Kumar, N-terminal specific conjugation of extracellular matrix proteins to 2-pyridinecarboxaldehyde functionalized polyacrylamide hydrogels, Biomaterials 102 (2016) 268-76.

[28] C.C. Lin, K.S. Anseth, Controlling Affinity Binding with Peptide-Functionalized Poly(ethylene glycol) Hydrogels, Adv Funct Mater 19(14) (2009) 2325.

[29] J. Parker, N. Mitrousis, M.S. Shoichet, Hydrogel for Simultaneous Tunable Growth Factor Delivery and Enhanced Viability of Encapsulated Cells in Vitro, Biomacromolecules 17(2) (2016) 476-84.

[30] S.E. Sakiyama-Elbert, J.A. Hubbell, Controlled release of nerve growth factor from a heparin-containing fibrin-based cell ingrowth matrix, J Control Release 69(1) (2000) 149-58.

[31] S.E. Sakiyama-Elbert, J.A. Hubbell, Development of fibrin derivatives for controlled release of heparin-binding growth factors, J Control Release 65(3) (2000) 389-402.

[32] J.B. Mascarenhas, M.A. Ruegg, U. Winzen, W. Halfter, J. Engel, J. Stetefeld, Mapping of the laminin-binding site of the N-terminal agrin domain (NtA), EMBO J 22(3) (2003) 529-36.

[33] A.J. Denzer, T. Schulthess, C. Fauser, B. Schumacher, R.A. Kammerer, J. Engel, M.A. Ruegg, Electron microscopic structure of agrin and mapping of its binding site in laminin-1, EMBO J 17(2) (1998) 335-43.

[34] R.A. Kammerer, T. Schulthess, R. Landwehr, B. Schumacher, A. Lustig, P.D. Yurchenco, M.A. Ruegg, J. Engel, A.J. Denzer, Interaction of agrin with laminin requires a coiled-coil conformation of the agrin-binding site within the laminin gamma1 chain, EMBO J 18(23) (1999) 6762-70.

[35] G.A. Hudalla, W.L. Murphy, Chemically well-defined self-assembled monolayers for cell culture: toward mimicking the natural ECM, Soft Matter 7(20) (2011) 9561-9571.

[36] A. Hyysalo, M. Ristola, M.E. Makinen, S. Hayrynen, M. Nykter, S. Narkilahti, Laminin alpha5 substrates promote survival, network formation and functional development of human pluripotent stem cell-derived neurons in vitro, Stem Cell Res 24 (2017) 118-127.

[37] J. Scholz, H. Besir, C. Strasser, S. Suppmann, A new method to customize protein expression vectors for fast, efficient and background free parallel cloning, BMC Biotechnol 13 (2013) 12.

[38] C.D. Reyes, A.J. Garcia, A centrifugation cell adhesion assay for high-throughput screening of biomaterial surfaces, J Biomed Mater Res A 67(1) (2003) 328-33.

[39] C. Gomes, A. Almeida, J.A. Ferreira, L. Silva, H. Santos-Sousa, J. Pinto-de-Sousa, L.L. Santos, F. Amado, T. Schwientek, S.B. Levery, U. Mandel, H. Clausen, L. David, C.A. Reis, H. Osorio, Glycoproteomic analysis of serum from patients with gastric precancerous lesions, J Proteome Res 12(3) (2013) 1454-66.

[40] P. Parreira, A. Magalhaes, I.C. Goncalves, J. Gomes, R. Vidal, C.A. Reis, D.E. Leckband, M.C. Martins, Effect of surface chemistry on bacterial adhesion, viability, and morphology, J Biomed Mater Res A 99(3) (2011) 344-53.

[41] F. Costa, D.M. Sousa, P. Parreira, M. Lamghari, P. Gomes, M.C.L. Martins, N-acetylcysteine-functionalized coating avoids bacterial adhesion and biofilm formation, Sci Rep 7(1) (2017) 17374.

[42] E. Freire, F.C. Gomes, R. Linden, V.M. Neto, T. Coelho-Sampaio, Structure of laminin substrate modulates cellular signaling for neuritogenesis, J Cell Sci 115(Pt 24) (2002) 4867-76.

[43] A.E. Carpenter, T.R. Jones, M.R. Lamprecht, C. Clarke, I.H. Kang, O. Friman, D.A. Guertin, J.H. Chang, R.A. Lindquist, J. Moffat, P. Golland, D.M. Sabatini, CellProfiler: image analysis software for identifying and quantifying cell phenotypes, Genome Biol 7(10) (2006) R100.

[44] J. Stetefeld, M. Jenny, T. Schulthess, R. Landwehr, B. Schumacher, S. Frank, M.A. Ruegg, J. Engel, R.A. Kammerer, The laminin-binding domain of agrin is structurally related to N-TIMP-1, Nat Struct Biol 8(8) (2001) 705-9.

[45] M.C. Tate, A.J. Garcia, B.G. Keselowsky, M.A. Schumm, D.R. Archer, M.C. LaPlaca, Specific beta1 integrins mediate adhesion, migration, and differentiation of neural progenitors derived from the embryonic striatum, Mol Cell Neurosci 27(1) (2004) 22-31.

[46] L.A. Flanagan, L.M. Rebaza, S. Derzic, P.H. Schwartz, E.S. Monuki, Regulation of human neural precursor cells by laminin and integrins, J Neurosci Res 83(5) (2006) 845-56.

[47] J. Silva, A.R. Bento, D. Barros, T.L. Laundos, S.R. Sousa, P. Quelhas, M.M. Sousa, A.P. Pego, I.F. Amaral, Fibrin functionalization with synthetic adhesive ligands interacting with alpha6beta1 integrin receptor enhance neurite outgrowth of embryonic stem cell-derived neural stem/progenitors, Acta Biomater 59 (2017) 243-256.

[48] S.L. Hirsh, D.R. McKenzie, N.J. Nosworthy, J.A. Denman, O.U. Sezerman, M.M. Bilek, The Vroman effect: competitive protein exchange with dynamic multilayer protein aggregates, Colloids Surf B Biointerfaces 103 (2013) 395-404.

[49] O. Kinstler, G. Molineux, M. Treuheit, D. Ladd, C. Gegg, Mono-N-terminal poly(ethylene glycol)-protein conjugates, Adv Drug Deliv Rev 54(4) (2002) 477-85.

[50] J. Wang, T. Hu, Y. Liu, G. Zhang, G. Ma, Z. Su, Kinetic and stoichiometric analysis of the modification process for N-terminal PEGylation of staphylokinase, Anal Biochem 412(1) (2011) 114-6.

[51] A.J. Denzer, R. Brandenberger, M. Gesemann, M. Chiquet, M.A. Ruegg, Agrin binds to the nerve-muscle basal lamina via laminin, J Cell Biol 137(3) (1997) 671-83.

[52] P. Parreira, A. Magalhaes, C.A. Reis, T. Boren, D. Leckband, M.C. Martins, Bioengineered surfaces promote specific protein-glycan mediated binding of the gastric pathogen Helicobacter pylori, Acta Biomater 9(11) (2013) 8885-93.

[53] K.K. McKee, D. Harrison, S. Capizzi, P.D. Yurchenco, Role of laminin terminal globular domains in basement membrane assembly, J Biol Chem 282(29) (2007) 21437-47.

[54] H. Colognato, D.A. Winkelmann, P.D. Yurchenco, Laminin polymerization induces a receptor-cytoskeleton network, J Cell Biol 145(3) (1999) 619-31.

[55] C. Hochman-Mendez, M. Cantini, D. Moratal, M. Salmeron-Sanchez, T. Coelho-Sampaio, A fractal nature for polymerized laminin, PLoS One 9(10) (2014) e109388.

[56] R.R. Sokal, F.J. Rohlf, Biometry: The Principles and Practices of Statistics in Biological Research, W.H. Freeman and Company, 1994.

[57] E. Hohenester, P.D. Yurchenco, Laminins in basement membrane assembly, Cell Adh Migr 7(1) (2013) 56-63.

[58] A. Bergeron, H. Sherman, P. Pardo, H. Gitschier, H. Nandivada, D. Saxena, Corning® rLaminin-521 (Human) for Expansion and Differentiation of Human Neural Stem Cells, Corning Incorporated | Application Note (2015).

[59] S. Rodin, L. Antonsson, C. Niaudet, O.E. Simonson, E. Salmela, E.M. Hansson, A. Domogatskaya, Z. Xiao, P. Damdimopoulou, M. Sheikhi, J. Inzunza, A.S. Nilsson, D. Baker, R. Kuiper, Y. Sun, E. Blennow, M. Nordenskjold, K.H. Grinnemo, J. Kere, C. Betsholtz, O. Hovatta, K. Tryggvason, Clonal culturing of human embryonic stem cells on laminin-521/E-cadherin matrix in defined and xeno-free environment, Nat Commun 5 (2014) 3195.

[60] M. Aumailley, L. Bruckner-Tuderman, W.G. Carter, R. Deutzmann, D. Edgar, P. Ekblom, J. Engel, E. Engvall, E. Hohenester, J.C. Jones, H.K. Kleinman, M.P. Marinkovich, G.R. Martin, U. Mayer, G. Meneguzzi, J.H. Miner, K. Miyazaki, M. Patarroyo, M. Paulsson, V. Quaranta, J.R. Sanes, T. Sasaki, K. Sekiguchi, L.M. Sorokin, J.F. Talts, K. Tryggvason, J. Uitto, I. Virtanen, K. von der Mark, U.M. Wewer, Y. Yamada, P.D. Yurchenco, A simplified laminin nomenclature, Matrix Biol 24(5) (2005) 326-32.

[61] J. Schindelin, I. Arganda-Carreras, E. Frise, V. Kaynig, M. Longair, T. Pietzsch, S. Preibisch, C. Rueden, S. Saalfeld, B. Schmid, J.Y. Tinevez, D.J. White, V. Hartenstein, K. Eliceiri, P. Tomancak, A. Cardona, Fiji: an open-source platform for biological-image analysis, Nat Methods 9(7) (2012) 676-82.

[62] C.T. Rueden, J. Schindelin, M.C. Hiner, B.E. DeZonia, A.E. Walter, E.T. Arena, K.W. Eliceiri, ImageJ2: ImageJ for the next generation of scientific image data, BMC Bioinformatics 18(1) (2017) 529.

# CHAPTER VI

Engineering Hydrogels with Affinity-Bound Laminin as 3D Neural Stem Cell Culture Systems

# Engineering Hydrogels with Affinity-Bound Laminin as 3D Neural Stem Cell Culture Systems

Daniela Barros [1,2,3], Eduardo Conde-Sousa [1,2], Woojin M. Han [4,5], Andrés J. García [4,5], Isabel F. Amaral [1,2,6], Ana P. Pêgo [1,2,3,6]

[1] i3S - Instituto de Investigação e Inovação em Saúde, Universidade do Porto (UPorto), Portugal

[2] INEB - Instituto de Engenharia Biomédica, UPorto, Portugal

[3] ICBAS - Instituto de Ciências Biomédicas Abel Salazar, UPorto, Portugal

[4] Parker H. Petit Institute for Bioengineering and Biosciences, Georgia Institute of Technology, Atlanta, Georgia, USA

[5] George W. Woodruff School of Mechanical Engineering, Georgia Institute of Technology, Atlanta, Georgia, USA

[6] FEUP - Faculdade de Engenharia, UPorto, Portugal.

---

**Under Review**

**Abstract**

Laminin incorporation into biological or synthetic hydrogels has been explored to recapitulate the dynamic nature and biological complexity of neural stem cell (NSC) niches. However, the strategies currently explored for laminin immobilization within three-dimensional (3D) matrices do not address a critical aspect influencing cell-matrix interactions, which is the control over laminin conformation and orientation upon immobilization. This is a key feature for the preservation of the protein bioactivity. In this work, we explored an affinity-based approach to mediate the site-selective immobilization of laminin into a degradable synthetic hydrogel. Specifically, a four-arm maleimide terminated poly(ethylene glycol) (PEG-4MAL) macromer was functionalized with a mono-PEGylated recombinant human N-terminal agrin (NtA) domain, to promote high affinity binding of laminin. Different NtA concentrations (10, 50 and 100 μM) were used to investigate the impact of NtA density on laminin incorporation, hydrogel biophysical properties, and biological outcome. Laminin was efficiently incorporated for all the conditions tested (laminin incorporation > 95%), and the developed hydrogels revealed mechanical properties (average storage modulus (G') ranging from 187 to 256 Pa) within the values preferred for NSC proliferation and neurite branching and extension. Affinity-bound laminin PEG-4MAL hydrogels better preserve laminin bioactivity, compared to unmodified hydrogels and hydrogels containing physically entrapped laminin, being this effect dependent on NtA concentration. This was evidenced by the 10 μM NtA-functionalized PEG-4MAL gels incorporating laminin that support enhanced human NSC proliferation and neuronal network formation, compared to the latter. Overall, this work highlights the potential of the proposed engineered matrices to be used as defined 3D platforms for the establishment of artificial NSC niches and as extracellular matrix-mimetic microenvironments to support human NSC transplantation.

## 1. Introduction

Neural stem cells (NSCs) hold great potential for application in regenerative medicine and tissue engineering, specifically for the treatment of central nervous system (CNS) disorders (*e.g.* traumatic brain and spinal cord injury and neurodegenerative diseases, such as Parkinson's and Alzheimer's disease) [1-3]. NSCs reside within a dynamic and complex microenvironment, the NSC niche*,* where cell-cell interactions and local microenvironmental cues, including those from neighboring cells, humoral factors and extracellular matrix (ECM), regulate stem cell behavior [4-6]. However, the intrinsic regulatory mechanisms allowing NSCs to integrate this complex array of signals remain poorly understood, as the traditional culture systems are unable to recapitulate several important features of these microenvironments [7]. Therefore, the development of new platforms providing a better understanding of the role of different niche components on the modulation of NSC fate is highly desirable. This will be highly advantageous to better understand and overcome some of the main drawbacks limiting the efficacy of current stem cell-based therapies. These limitations include low cell survival, lack of control of cell fate, and poor cell engraftment within the host tissue after transplantation [8]. Different three-dimensional (3D) cell culture systems, including spheroids, porous scaffolds and hydrogels [9, 10], have been explored. These platforms replicate some of the physical and chemical elements of the native stem cell niche and provide valuable insights into cell physiology and interactions with the surrounding microenvironment. Among the different platforms explored, hydrogels constitute the most widespread option, as they are well-defined and tunable matrices that share many key physical properties with native ECM [7], including high-water content, and permeability and elasticity resembling those of soft tissue microenvironments [11, 12]. Indeed, different studies already explored both natural and synthetic polymer-based hydrogels mimicking critical aspects of NSC niches [13-16]. However, their use as permissive microenvironments for cell culture and transplantation is still a challenge. One of the main caveats is related with the inability to control cell spatial organization within the developed matrices, as this is highly dependent not only on the dynamic modulation of cell-cell interactions but also cell-matrix interactions [4-7]. In this sense, in the last few years the use of hybrid hydrogels, which combine the bioactivity and the dynamic responsiveness of natural proteins, with the tunable and reproducible structural and mechanical features provided by synthetic polymers, have been the focus of significant research [12].

Laminin has a key role in the modulation of NSC behavior, including cell adhesion and viability [17], and neuronal outgrowth and migration [18-20]. Furthermore, laminin has other paramount roles in CNS homeostasis, such as synapse function and stability [21, 22]. This makes this heterotrimeric glycoprotein highly attractive for the design of NSC niche

microenvironments. Indeed, some works already explored laminin immobilization onto different biological and synthetic materials [23]. However, the non-selective nature of the immobilization strategies explored to date (*i.e.* physical entrapment or non-selective covalent immobilization) prevents the control over laminin orientation and conformation upon immobilization. This may compromise the exposure of crucial laminin bioactive epitopes and consequently, limit its ability to modulate cellular behavior, making these matrices ill-suited to get insight for controlled studies of cell-laminin interactions. Therefore, laminin immobilization strategies that assure both conformation and bioactivity are highly desirable. To fulfill these requirements, we previously proposed an affinity-based approach for laminin immobilization [24, 25], which takes advantage of the native high-affinity interaction (dissociation constant ($K_D$) = 5 nM) between laminin and the human N-terminal agrin (hNtA) domain [26, 27]. Using self-assembled monolayers, we showed that the site-selective immobilization of laminin better preserves its bioactivity, when compared to non-selective covalent immobilization approaches. This immobilization method translated in an enhanced ability of laminin to polymerize and mediate human NSC (hNSC) adhesion and spreading [24]. Consequently, hNtA was herein explored for attaining the site-selective immobilization of laminin within a degradable synthetic hydrogel. A four-arm maleimide terminated poly(ethylene glycol) (PEG-4MAL) macromer was used as the hydrogel base material (Fig. 1), due to excellent cytocompatibility and *in vivo* tolerance [28-30], and well characterized biochemical and biophysical properties [30-32]. PEG-4MAL macromer was functionalized with a thiol-containing mono-PEGylated rhNtA (NtA) domain, for the site-selective immobilization of laminin on hydrogels (Fig. 1). To allow the hNSC 3D culture that would span the time frame of hNSC proliferation and neuronal differentiation, a mix of protease degradable (cysteine-flanked matrix metalloproteinase 2 (MMP2)-sensitive peptide) [33] and non-degradable (PEG-dithiol) cross-linkers was used to mediate, under physiological conditions, the formation of a degradable hydrogel network (Fig. 1).

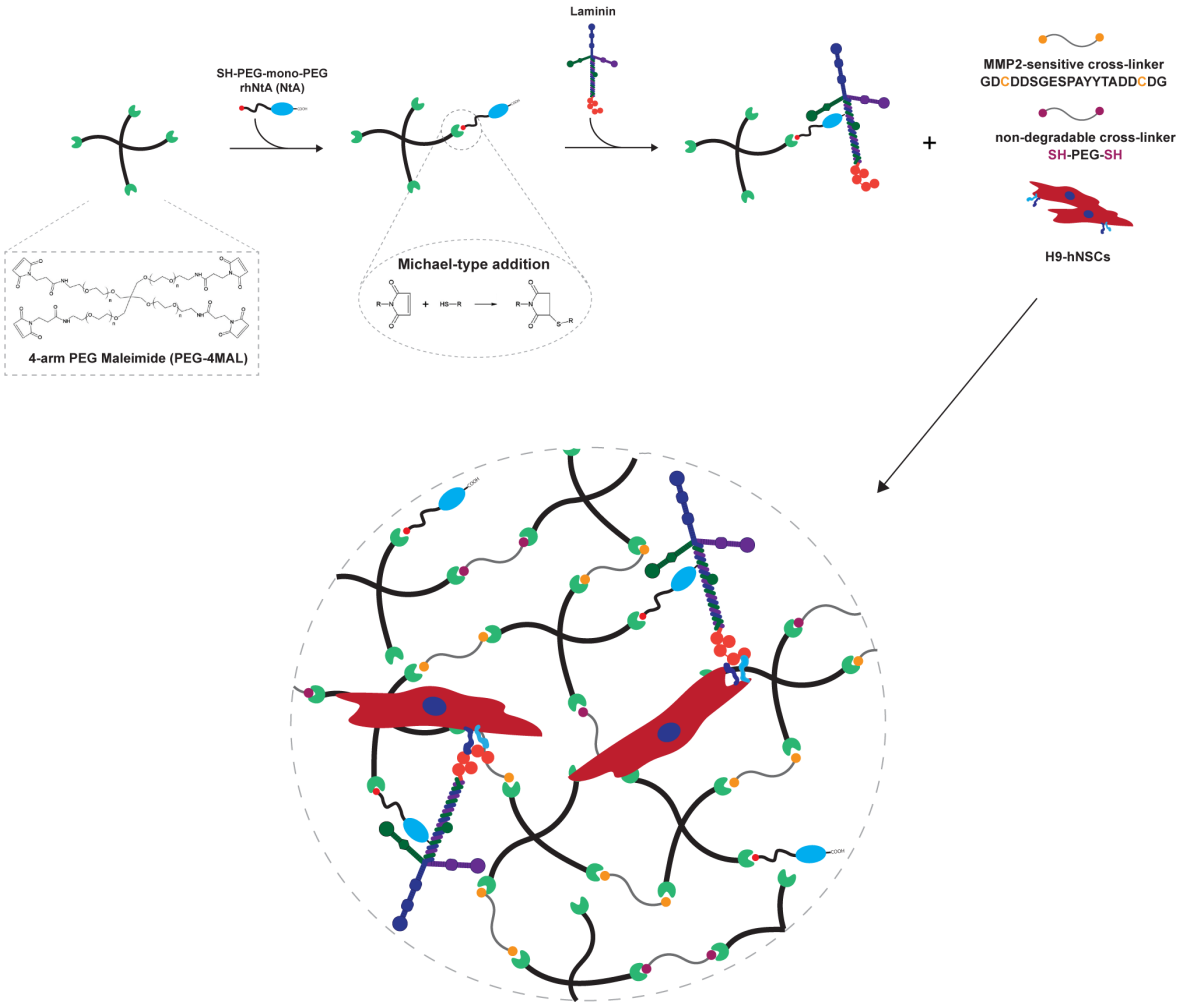


**Figure 1. Schematic representation of the preparation of cell-laden affinity-bound laminin PEG-4MAL hydrogels (not to scale).** PEG-4MAL macromer is firstly functionalized with a thiol-containing mono-PEGylated rhNtA (NtA) domain, which will then mediate the binding of laminin with high affinity. Functionalized PEG-4MAL is then reacted with a mixture of protease degradable (MMP2-sensitive peptide) and non-degradable (PEG-dithiol) cross-linkers to allow the formation, under physiological conditions, of a hydrogel network in the presence of cells.

The 3D synthetic matrices proposed in this work allow the controlled immobilization of laminin while preserving the exposure of key bioactive domains involved in NSC proliferation and outgrowth, which is promoted in the proposed hydrogels. Ultimately, these results highlight the potential of the engineered hydrogels to be used as artificial niches to support hNSC culture, and hopefully, transplantation.

## 2. Materials and Methods

### 2.1. Hydrogel components

A four-arm maleimide terminated poly(ethylene glycol) (PEG-4MAL; 40 kDa, > 95% purity, > 90% substitution, Jenkem USA) was chosen as the hydrogel base material. A macromer solution was prepared in 10 mM 4-(2-hydroxyethyl)piperazine-1-ethanesulfonic acid (HEPES) in phosphate buffered saline (PBS, pH 7.4) at a final polymer concentration of 10.0% (w/v). Mono-PEGylated recombinant human N-terminal agrin (NtA) domain was produced as previously described [24]. Laminin-111 from mouse Engelbreth-Holm-Swarm sarcoma (msLn-111) was obtained from Sigma-Aldrich. A cysteine-flanked matrix metalloproteinase-2 (MMP2)-sensitive peptide (Acetyl (Ac)-GD*C*DD**SGESPAY↓YTA**DD*C*DG-Amide ($NH_2$); 2.1 kDa, > 85% purity, GenScript) and a PEG-dithiol (3.5 kDa, ≥ 95% purity, Jenkem USA) were used as the degradable and non-degradable cross-linkers, respectively.

### 2.2. Mono-PEGylated rhNtA tethering efficiency

To determine the tethering efficiency of NtA to PEG-4MAL, free/unreacted thiols in the reaction mixture were quantified using the Measure-iT thiol assay kit (Invitrogen) according to the manufacturer's instructions. Briefly, PEG-4MAL was functionalized with the NtA domain (input NtA concentration: 10, 50 or 100 μM) for 15 min in 10 mM HEPES in PBS (pH 7.4). The samples were then mixed with thiol-quantitation reagent in a black 96-well plate and the fluorescence measured ($\lambda_{ex}$ = 494 nm; $\lambda_{em}$ = 517 nm) using a microwell plate reader (BioTek® Synergy™ Mx). A calibration curve of glutathione (0 – 55 μM) was used to calculate the concentration of free thiols.

### 2.3. Preparation of affinity-bound laminin PEG-4MAL hydrogels

A schematic representation of affinity-bound laminin PEG-4MAL hydrogel preparation is presented in Fig. 1. Briefly, PEG-4MAL was first functionalized with the NtA domain (input NtA concentration in the gel:10, 50, or 100 μM) for 15 min in 10 mM HEPES in PBS (pH 7.4). msLn-111 (input laminin concentration in the gel: 100 μg/mL) was then added to the mixture and allowed to bind to NtA for 30 min. Functionalized PEG-4MAL precursors were then cross-linked into a hydrogel by addition of a mix of a MMP2-sensitive peptide and a PEG-dithiol prepared in 10 mM HEPES in PBS (pH 6.5), at different % molar ratios (100:0; 80:20; 50:50; 20:80; 0:100). The cross-linkers were added at a 1:1 molar ratio of cysteine residues on the cross-linkers to remaining maleimide groups on NtA-functionalized PEG-4MAL. Hydrogels were polymerized at 37 ºC, 5% $CO_2$ for 15 min. Unmodified PEG-4MAL gels and PEG-4MAL gels containing entrapped msLn-111 (100 μg/mL) were also prepared and used as controls.

### 2.4. Laminin incorporation within PEG-4MAL hydrogels

Laminin incorporation within PEG-4MAL hydrogels was quantified by an enzyme-linked immunosorbent assay (ELISA). The hydrogels were prepared as previously described and incubated at 37 ºC in 125 μL of PBS (pH 7.4). At day 1 and 7, the supernatant was collected, stored at -80 ºC and then analyzed using a mouse laminin ELISA kit (Abcam, ab119572) according to the manufacturer's instructions. Absorbance values were measured at 450 nm using a microwell plate reader (BioTek® Synergy™ Mx).

### 2.5. Rheological properties and mesh size estimation of affinity-bound laminin PEG-4MAL hydrogels

The rheological properties of PEG-4MAL hydrogels were characterized using a strain-controlled Kinexus Pro Rheometer (Malvern Instruments Ltd, Malvern, UK) and an 8 mm diameter parallel-plate geometry. Hydrogels for each condition (∅ 8 mm) were prepared as previously described, and allowed to hydrate in PBS (pH 7.4) at 37 ºC for 24 h. The samples were then tested in a humidified environment at physiological temperature (37 ºC) and with application of 30% compression (oscillatory measurement gap). Amplitude strain sweeps (0.1 – 100% at 0.1 Hz) were initially performed for each condition to define the linear viscoelastic region (LVR). Frequency sweeps (0.01 – 10 Hz at 1% strain) were then performed and the storage (G'), loss (G'') and complex (G*) modulus, as well as the phase angle (δ, º) were determined within the LVR, by averaging all data points acquired from a 0.01 – 1 Hz interval. The relative mesh size (nm) value was estimated using the following equation [34]:

$$\xi = \left(\frac{G'A}{RT}\right)^{-\frac{1}{3}}$$

where G' = storage modulus in Pa, A = Avogadro's constant ($6.022140857 \times 10^{23}$ $mol^{-1}$), R = gas constant (8.314 $m^3.Pa.mol^{-1}.K^{-1}$), T = temperature (37 ºC = 310.15 K).

### 2.6. Culture of human neural stem cells

Human neural stem cells (hNSCs) derived from the NIH approved H9 (WA09) human embryonic stem cell line were purchased from Life Technologies (N7800-200). Cells were expanded according to the manufacturer's protocol on poly(ornithine)/msLn-111-coated tissue coated polystyrene (TCPS) plates (Corning) in expansion medium - StemPro® NSC serum-free medium (SFM; Life Technologies) supplemented with basic fibroblast growth factor (bFGF, 20 ng/mL; Life Technologies) and epidermal growth factor (EGF, 20 ng/mL; Life Technologies).

### 2.7. Culture of hNSCs within affinity-bound laminin PEG-4MAL hydrogels

hNSCs were dissociated into single cells using StemPro accutase cell dissociation reagent (Life Technologies) and further suspended in the solution containing laminin-functionalized PEG-4MAL precursors (4 x $10^6$ viable cells/mL). Cell-laden hydrogels were formed by mixing the PEG-4MAL precursor solution containing cells with the MMP2-sensitive peptide and PEG-dithiol cross-linkers, dissolved in 10 mM HEPES in PBS (pH 6.5), at different molar ratios (%), and subsequently incubating the polymerizing gels at 37 ºC, 5% $CO_2$ for 15 minutes. hNSCs were initially cultured in expansion medium and, at day 2 of culture, the medium was switched to the StemPro NSC SFM media-Neurobasal/B27 (Life Technologies) (1:1) mix, without growth factors. At day 8, half of the medium was replaced by the StemPro NSC SFM-Neurobasal/B27 (1:3) mix supplemented with 10 ng/mL of brain-derived neurotrophic factor (BDNF; Peprotech) and 500 μM of $N^6$, 2'-O-Dibutyryladenosine 3', 5'-cyclic monophosphate sodium salt (dibutyril cAMP; Sigma). Half of the medium was changed every other day, up to 14 days. hNSCs cultured within unmodified and PEG-4MAL gels containing entrapped msLn-111 (100 μg/mL) were herein used as controls.

### 2.8. Cell viability

The distribution of viable and dead cells within PEG-4MAL hydrogels was assessed at day 7 of cell culture using a live/dead assay. Cell-hydrogel matrices were rinsed with warm PBS pH 7.4 and incubated with 4 μM calcein AM (Life Technologies) and 6 μM propidium iodide (PI; Life Technologies) at 37 ºC for 30 min, for detection of viable and dead cells, respectively. After incubation, the samples were rinsed twice with PBS pH 7.4, transferred to the culture medium, and immediately observed under confocal laser scanning microscopy (CLSM, Leica TCS SP5). Quantitative analysis of live and dead cells was also conducted using immunocytometry (See Supplementary Materials and Methods).

### 2.9. DNA quantification

The growth of hNSCs cultured within PEG-4MAL hydrogels was estimated from total cell number after 7 days of cell culture, determined using the CyQUANT® cell proliferation assay kit (Life Technologies) according to the manufacturer's instructions. Briefly, cells were extracted from the hydrogels, through sequential incubation with 1.25 mg/mL of collagenase type II (Gibco; 1 h at 37 ºC) and StemPro accutase cell dissociation reagent (Life Technologies; 20 min at 37 ºC) under stirring (70 rpm). Cells were mechanically dissociated by pipetting, diluted in Glasgow Minimum Essential Medium (GMEM; Life Technologies) supplemented with 10% (v/v) inactivated fetal bovine serum (FBS), centrifuged and the cell pellet stored at -80 ºC. The cell pellet was then thawed at room temperature (RT) and incubated with CyQUANT® GR dye/cell lysis buffer. Fluorescence ($\lambda_{ex}$ = 480 nm; $\lambda_{em}$ = 520

nm) was measured, after mixing with CyQUANT GR dye, in a microwell plate reader (BioTek® Synergy™ Mx). The total number of cells for each condition was estimated from a standard curve generated with a known amount of hNSCs over a range of 50 to 250,000 cells. Cell samples used to generate the standard curve were measured in triplicate. For each condition, hydrogels without cells, cultured in parallel and processed similarly to those with cells, were used as blanks and their background fluorescence values subtracted.

### 2.10. hNSC neurite outgrowth

The effect of laminin site-selective immobilization on neurite outgrowth was assessed after 14 days of culture, under neuronal differentiation conditions. Samples were processed as whole-mounts for βIII-tubulin/DNA staining as described in Supplementary Materials and Methods, and z-sections covering a thickness of 200 μm or 80 μm were acquired with the CLSM using an HC Plan APO CS 10× / 0.40 NA or HC Plan APO CS 20× / 0.70 NA objective, respectively. Neurite outgrowth was assessed in the projected two-dimensional (2D) images using a developed ImageJ script. Briefly, nuclei were segmented through an Otsu thresholding method, while neurites were segmented through subtraction of the previously identified nucleus, using a Huang thresholding method. Measurements were obtained for total neurite length (μm) and total number of neurites per image.

### 2.11. Statistical Analysis

Statistical analysis was performed using GraphPad Prism 6 software (San Diego). Sample distribution was initially tested for normality using the Kolmogorov-Smirnov test. Comparisons between three or more groups were performed with one-way ANOVA analysis, followed by the Bonferroni correction for pairwise comparisons or the Dunnett's two-tailed test for comparisons with control conditions. For all analysis, differences were considered significant at $p < 0.05$.

## 3. Results and Discussion

### 3.1. PEG-4MAL hydrogels provide independent control of different biochemical and biophysical properties

A hydrogel platform based on a PEG-4MAL macromer (Fig. 1) was selected as the base material for this work, as we have seen it exhibits excellent *in vitro* and *in vivo* biocompatibility with different cell types, including muscle stem cells [30] and pancreatic islets [28]. Moreover, the modular nature of PEG-4MAL hydrogels allows independent control over different biochemical and biophysical properties such as type and density of cell-adhesive ligands, mechanical and structural properties, and protease-dependent degradation [30-32]. Therefore, the use of these matrices is especially advantageous to

assess the effect of a particular biochemical or biophysical cue on the modulation of cell behavior. In addition, the biophysical properties of these hydrogels were extensively characterized in several studies from the García group [30-32]. The described properties allowed us to initially define the molecular weight (40 kDa) and the final polymer density (10% (w/v) of the PEG-4MAL macromer, that would result in hydrogels with mechanical properties within the range of values preferred for NSC proliferation (100 – 1000 Pa) and neurite branching and extension (200 – 400 Pa) [35-40].

### *3.1.1. Control over affinity-bound laminin PEG-4MAL hydrogel degradability is required for hNSC long-term culture*

Hydrogel degradability, a critical factor for matrix remodeling, was shown to be essential for *in vitro* cell survival and proliferation within synthetic niches [16, 30, 32] and, therefore, is a key feature to take into consideration when designing cell instructive microenvironments. In this context, the incorporation of protease-sensitive peptide cross-linkers has been widely explored to better control material degradation [33]. Among the different protease-degradable peptides characterized to date, a fast-degrading sequence shown to be relatively specific for MMP2 [33] was used, as this metalloproteinase is expressed at high levels by NSCs [41, 42].

The fast gelation kinetics of the thiol-maleimide reaction (Michael-type addition; Fig. 1) may lead to the formation of heterogeneous hydrogels, which in turn can translate into variable cell biological outcomes [43]. Consequently, to increase the pKa of the thiol group and thereby reduce the availability of the reactive thiolate [43], the di-thiol-containing MMP2-sensitive cross-linker peptide used in this work, was designed to include negatively charged amino acids flanking the thiol-bearing cysteine residue (D*C*DD). This strategy allowed the thorough mixing of the hydrogel precursor solutions prior to use.

The fast-degrading nature of the selected MMP2 sequence, combined with the high levels of MMP2 production by NSCs, led us to hypothesize that fully degradable hydrogels might not be able to support the 3D culture of hNSCs, up to 14 days. To test this hypothesis, affinity-bound laminin hydrogels cross-linked by addition of a MMP2-sensitive peptide (degradable) and a PEG-dithiol (non-degradable) at different % molar ratios (100:0; 80:20; 50:50; 20:80; 0:100) were evaluated and the combination allowing the hNSC 3D culture that would span the time frame of hNSC proliferation and neuronal differentiation established. hNSCs showed a significantly higher number of viable cells, with cellular extensions at day 14 of cell culture, in gels formulated with a combination of degradable and non-degradable cross-linkers, specifically for the 80% MMP2-sensitive peptide to 20% PEG-dithiol cross-linker molar ratio, when compared to fully degradable hydrogels ($p = 0.018$ *vs.* 100:0 cross-

linker molar ratio (%); Fig. S1, in Supplementary Data). As such, all subsequent studies were performed using this degradable and non-degradable cross-linkers molar ratio (%).

### *3.1.2. Mono-PEGylated rhNtA (NtA) mediates efficient site-selective laminin incorporation*

Maleimide groups in PEG-4MAL macromer efficiently react with thiol-containing peptides through Michael-type addition [31]. This enables a fine-tuning over ligand incorporation and cross-linking efficiency, ultimately leading to the formation of structurally defined matrices. To favor the site-selective immobilization of laminin, PEG-4MAL was first reacted with a thiol-containing NtA domain (Fig. 1). This domain was tethered onto the PEG-4MAL macromer with high yields, for all the concentrations tested (10, 50 and 100 μM), evidencing a precise control over NtA density (Fig. 2A). The effect of different NtA concentrations on laminin incorporation within hydrogels was then assessed. Efficient laminin incorporation was observed for all the NtA concentrations tested, as evidenced by ELISA results (incorporation efficiency > 95%, determined after 1 and 7 days of incubation in PBS; Fig. 2B). We hypothesize that the lack of significant differences between laminin entrapped *vs.* immobilized can be explained by limitations on protein diffusion imposed by the reduced hydrogel mesh size (20 – 30 nm), which will hinder the diffusion of laminin due to its high hydrodynamic diameter (≅ 42 nm) [44, 45].

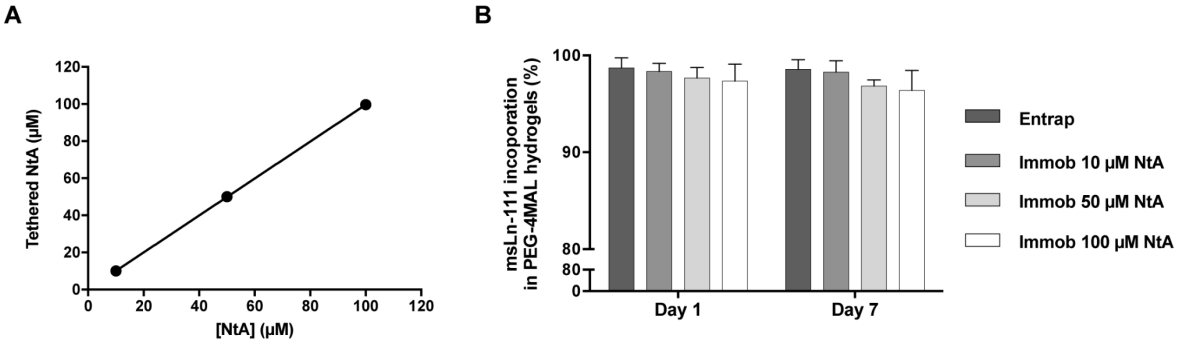


**Figure 2. Effect of NtA concentration on laminin incorporation A)** Density of NtA tethered to PEG-4MAL hydrogel as a function of input NtA concentration. Linear regression: y = 0.9954 x + 0.1115; $R^2$ = 0.9999. Data represent mean ± standard deviation (SD) of three hydrogels prepared independently. **B)** Laminin incorporation by physical entrapment (Entrap) or by immobilization using an affinity binding ligand (Immob) into PEG hydrogels, determined by ELISA, after 1 and 7 days of incubation in PBS. Data represent mean ± SD of three hydrogels prepared independently. No significant differences were detected (two-way ANOVA).

As free thiol groups in laminin could also react with maleimide groups from PEG-4MAL and thus contribute to the laminin immobilization into PEG-4MAL hydrogels, the availability of

free/unreacted thiols in laminin stock solution (pH 7.4) was assessed. Free thiols were not detected (< 2.75 μM, the lower detection limit of the assay), indicating that the molar ratio of free thiols in laminin was less than 0.22%, and assuring minimal contribution of laminin free thiol groups to laminin incorporation into PEG-4MAL hydrogel.

### *3.1.3. The approach used for laminin incorporation impacts hydrogel mechanical and structural properties*

Hydrogel mechanical and structural (equilibrium swelling and mesh size) properties have a key role on the modulation of different cellular functions (*e.g.* survival, proliferation, and differentiation) [30-32], as well as in the stability of the hydrogel *in vivo* [35-40, 46]. The fine control of these properties is, therefore, crucial to direct neural stem cell fate [35, 38-40].

The effect of the binding ligand (NtA) density and laminin incorporation on hydrogel mechanical properties and structure (mesh size) was assessed through rheological studies. All the prepared hydrogels presented Storage modulus (G') > Loss modulus (G'') (Table 1), showing that PEG-4MAL has transitioned from a viscous liquid to a gelled state. Moreover, the hydrogels presented a "solid-like" behavior after 24h at 37 ºC, as evidenced by the values of phase angle (δ) below 10º (Table 1), meaning that the viscoelastic properties of the hydrogels were stable for the conditions tested.

**Table 1.** Storage modulus (G'), Loss modulus (G'') and Phase angle (δ,º) of hydrogels determined by rheological analysis. Data represent mean ± Standard error of the mean (SEM); n = 6.

| Hydrogel | | Input NtA concentration (μM) | Storage Modulus (G', Pa) | Loss Modulus (G'', Pa) | Phase Angle (δ, º) |
|---|---|---|---|---|---|
| | **Unm** | - | 259.1 ± 13.8 | 10.6 ± 1.7 | 2.3 ± 0.2 |
| **msLn-111** | **Entrap** | - | 314.0 ± 16.3 | 9.3 ± 0.3 | 2.1 ± 0.1 |
| | **Immob** | 10 | 256.0 ± 14.2 | 10.0 ± 0.0 | 2.3 ± 0.1 |
| | | 50 | 213.9 ± 16.4 | 10.3 ± 1.7 | 2.8 ± 0.4 |
| | | 100 | 187.0 ± 29.5 | 10.3 ± 0.7 | 3.7 ± 0.7 |

The covalent immobilization of increasing concentrations of NtA (from 10 to 100 μM) led to a trend for reduced in the storage modulus (G') (Table 1) and to the formation of a slightly looser polymer network, as evidenced by the tendency for larger mesh size values (Fig. 3B). The tethering of NtA reduces the number of maleimide-terminated PEG chains available for cross-linking, thus reducing the number of cross-linking points. This is in an excellent agreement with the trend for a lower stiffness observed with increasing

concentrations of NtA (Fig. 3A). These results suggest that the approach used for laminin incorporation (physical entrapment *vs.* affinity immobilization) impacts the hydrogel mechanical and structural properties. Results presented are consistent with previous studies, exploring PEG-diacrylate hydrogels, in which it was shown that the covalent immobilization of laminin through a PEG chain significantly reduces the hydrogel stiffness, as opposed to the physical entrapment of the protein [47].

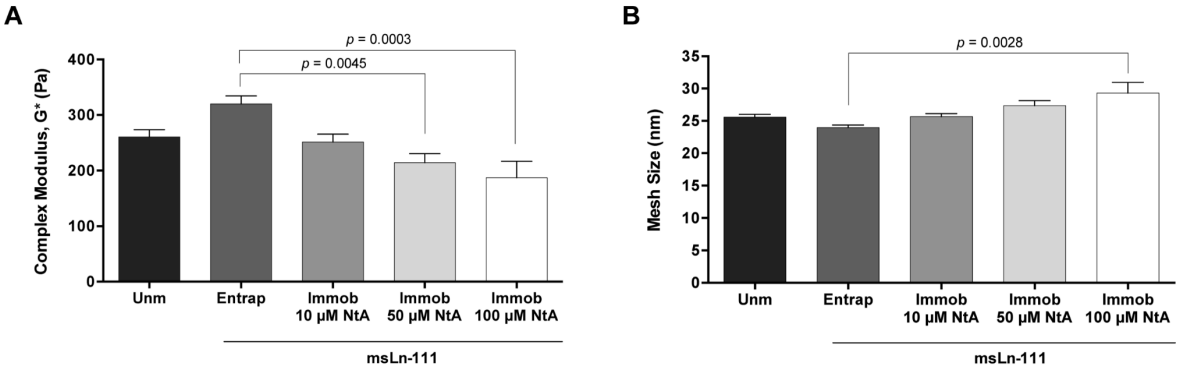


**Figure 3. Influence of laminin incorporation approach (physical entrapment *vs.* affinity immobilization) on PEG-4MAL hydrogel mechanical and structural properties. A)** Complex modulus (G*) of hydrogels determined by rheological analysis; and **B)** Estimation of hydrogels mesh size, based on the measured storage modulus (G'). Data represent mean ± SEM; n = 6; one-way ANOVA followed by Bonferroni's test.

## 3.2. Affinity-bound laminin PEG-4MAL hydrogels support hNSC culture and biological function

The potential of PEG-4MAL hydrogels incorporating affinity-bound laminin to support hNSC biological function, namely viability, proliferation, and outgrowth, was subsequently investigated. Laminin incorporation within PEG-4MAL hydrogels using 10 and 50 μM NtA, favored the formation of stiffer hydrogels (Fig. 3A), able to better support hNSC culture for longer periods (up to 14 days). As result, these hydrogels were used to perform the qualitative and quantitative analysis of cell behavior. PEG-4MAL hydrogels unmodified or containing physically entrapped laminin were also prepared and used as controls.

### *3.2.1. Laminin-modified hydrogels support hNSC survival and proliferation*

To get insight into the effect of controlled immobilization of laminin on hNSC survival and proliferation, cells were cultured for 7 days within degradable PEG-4MAL hydrogels with either entrapped or immobilized laminin. Confocal microscopy showed the presence of live cells widely distributed throughout all hydrogels, often growing as cellular spheroids (Fig. 4A). The quantitative analysis of live/dead cells, assessed by flow cytometry, showed values

of average cell viability greater than 75% for all the conditions tested, evidencing the good cytocompatibility of the proposed matrices (Fig. 4B) [48].

In contrast to the physical entrapment of laminin, site-selective immobilization of laminin using 10 μM and 50 μM NtA supported higher hNSC growth compared to unmodified hydrogels, with significantly higher cell numbers being observed in 10 μM NtA - laminin immobilized hydrogels ($p$ = 0.0180) (Fig. 4C). An increase in the cell number of 1.5-, 1.9-, 4.2- and 3.1-fold (*vs.* initial cell density - 4 × $10^4$ cells/hydrogel) was observed for unmodified, laminin entrapped, 10 μM and 50 μM NtA - laminin immobilized hydrogels, respectively (Fig. 4C). Since laminin incorporation in PEG-4MAL hydrogels was similar regardless of being physically entrapped or affinity-bounded (Fig. 2B), these results suggest that the site-selective immobilization of laminin through the use of 10 μM of NtA, better preserved the exposure of laminin domains interacting with cell adhesion receptors, as compared to laminin physically entrapped.

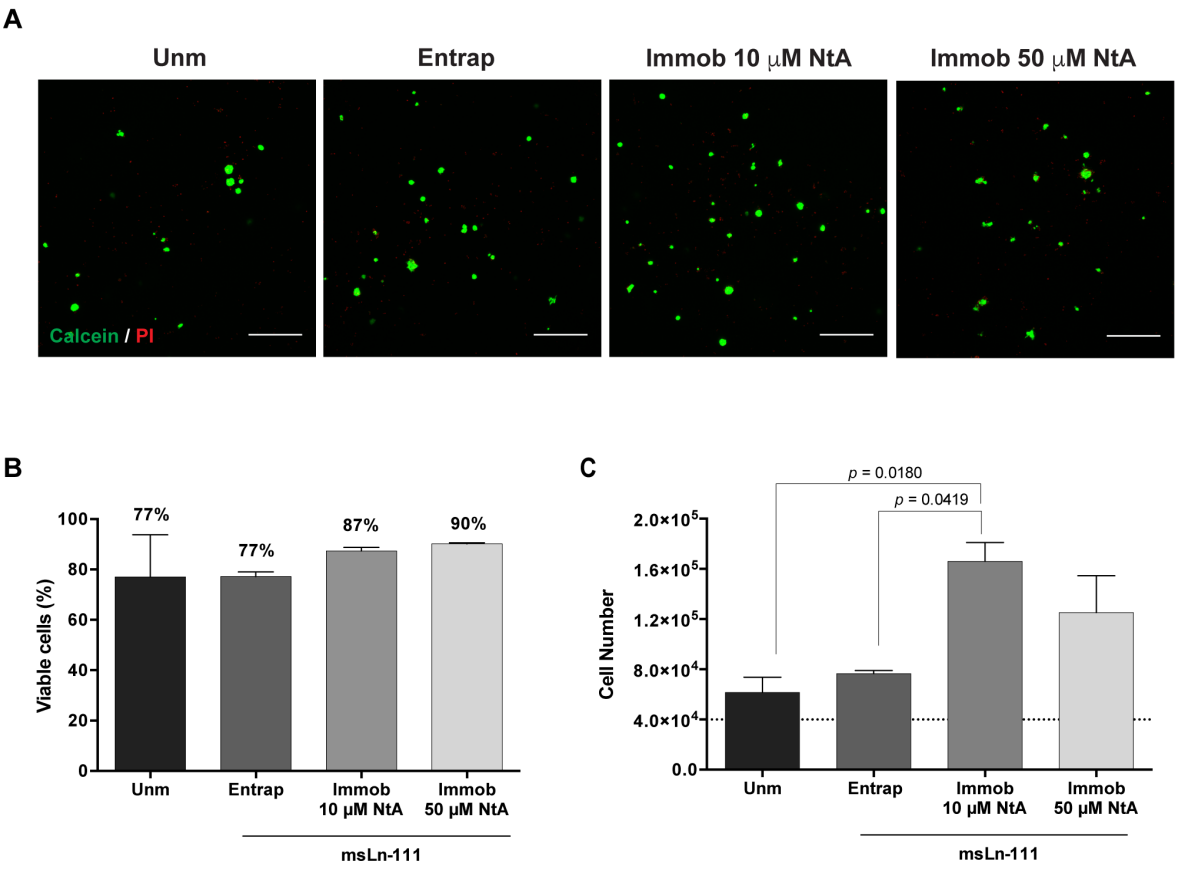


**Figure 4. Ability of affinity-bound laminin to support hNSC viability and proliferation**. **A)** Representative 2D projections of CLSM 3D stack images of cell-laden hydrogels covering a thickness of 300 μm, showing the distribution of live (in green) and dead (in red) cells at day 7 of cell culture. Scale bar = 300 μm. **B)** Quantitative analysis of live cells at day 7, as determined by flow cytometry. Data represent mean ± SD of three independent experiments. No significant differences

were detected (one-way ANOVA followed by Bonferroni's test). **C)** Quantitative analysis of total cell number at day 7, as determined by CyQuant® Cell Proliferation kit. The dotted line represents the initial cell density/hydrogel ($4 \times 10^4$ cells/hydrogel). Data represent mean $\pm$ SEM of three independent experiments performed in triplicate; one-way ANOVA followed by Bonferroni's test.

### *3.2.2. Controlled laminin immobilization promotes neurite outgrowth*

Laminin presents several bioactive domains with neurite outgrowth promoting ability, and, as a result, plays a key role in mediating NSC migration, differentiation and neurite extension both *in vitro* and *in vivo* [18, 20]. The effect of laminin site-selective immobilization on hNSC neurite outgrowth was assessed after 14 days of culture under differentiation conditions (Fig. 5). A population of differentiated neurons, expressing βIII-tubulin, with the evident formation of a denser neuronal network, was observed within 10 μM NtA affinity-immobilized laminin PEG-4MAL hydrogels (Fig. 5A). Differences between the conditions tested were assessed by image processing and quantitative analysis, using ImageJ/Fiji. Total neurite length (μm) and total number of neurites were quantified (Fig. 5B-D). The controlled immobilization of laminin using 10 μM NtA supported a more pronounced neuronal network formation, compared with any of the other conditions tested, as evidenced by the higher values of total neurite length ($p = 0.0035$ *vs.* Unm; $p = 0.0152$ *vs.* Entrap; Fig. 5B) and total number of neurites ($p = 0.0007$ *vs.* Unm; $p = 0.0079$ *vs.* Entrap; Fig. 5C). The use of 50 μM NtA, despite leading to similar amounts of laminin incorporation (Fig. 2B), resulted in significantly lower values of total neurite length ($p = 0.0056$; Fig. 5C) and total number of neurites ($p = 0.0073$; Fig. 5D) compared to 10 μM NtA affinity-bound laminin. The reduction in neurite outgrowth (Fig. 5C-D) and the reduction in cell number (Fig.4C) observed for cells cultured within hydrogels with 50 μM NtA - immobilized laminin may be related with the inability of the protein to bind the NtA domain, as result of steric effects. The results obtained contrast to previous studies in which no significant differences on neurite outgrowth were observed when laminin was covalently immobilized using a non-selective approach, *vs*. physically entrapped laminin [47]. This gives a good indication that the strategy proposed in this study, indeed, potentiate laminin bioactivity.

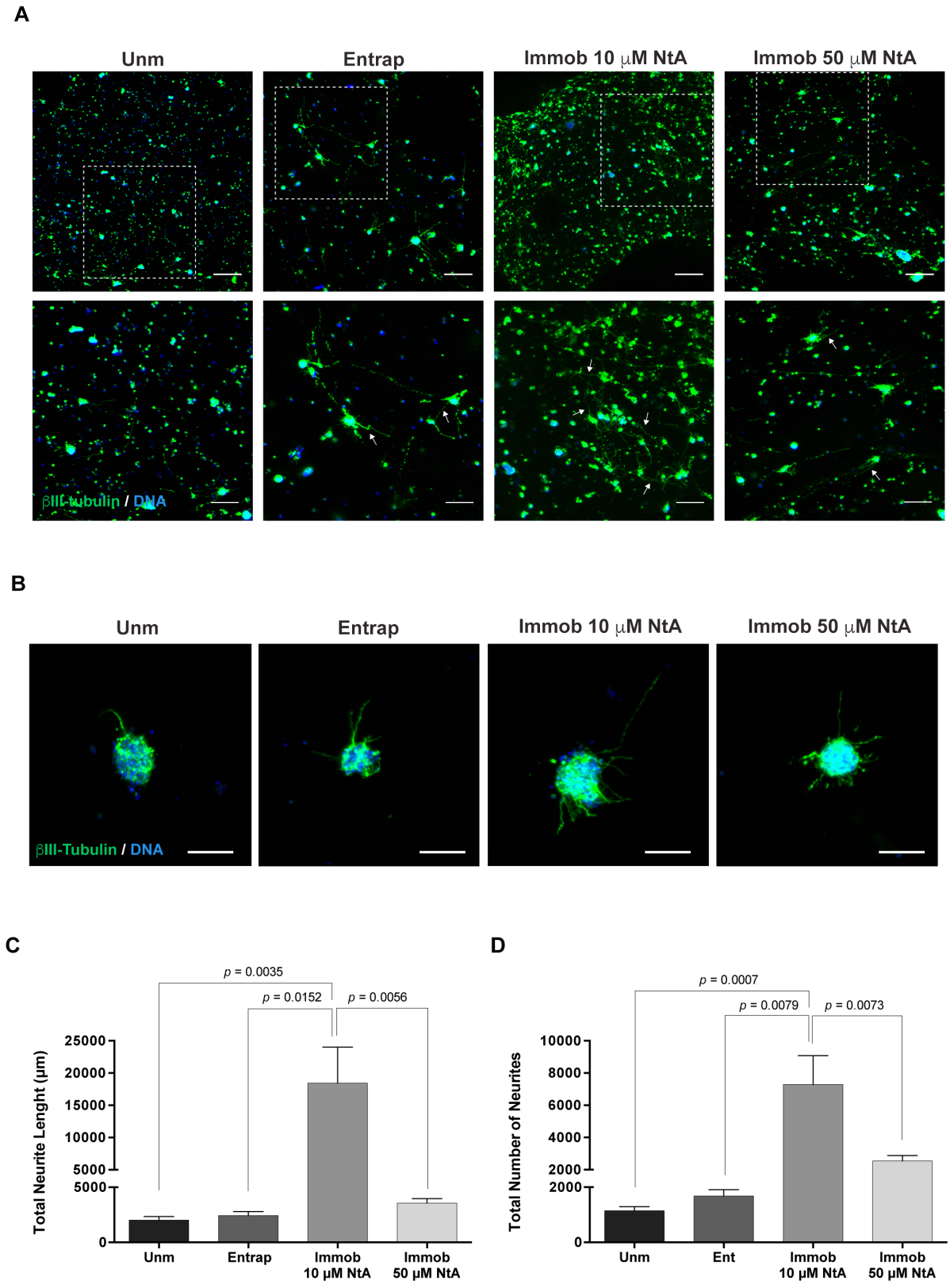


**Figure 5**. **Affinity-bound laminin PEG-4MAL hydrogels and its effect on hNSC neurite outgrowth. A)** hNSCs cultured within unmodified (Unm), laminin physically entrapped (Entrap) and

NtA affinity-bound laminin (Immob) PEG-4MAL hydrogels after 14 days of culture, under differentiation conditions. Images show 2D projections of CLSM 3D stack images of cells processed for immunofluorescence labeling of βIII-tubulin/DNA covering a thickness of 200 μm (top images) and 100 μm (bottom images). Lower panels show magnified views of selected regions highlighted by dashed squares in the upper panel. Arrows depict neurites expressing βIII-tubulin protruding from neurospheres. Scale Bar = 200 μm (top images); 100 μm (bottom images). **B)** Representative 2D projections of CLSM 3D stack images of hNSC outgrowth, covering a thickness of 80 μm, after 14 days of culture under differentiation conditions. Scale Bar = 80 μm. **B)** Total Neurite Length; and **C)** Total Number of Neurites determined by quantitative analysis of images acquired in CLSM. Data represent mean ± SD of 12-15 images analyzed per condition; one-way ANOVA followed by Bonferroni's test.

Overall, these results clearly demonstrate that the site-selective immobilization of laminin through the use of 10 μM NtA better preserved protein bioactivity in terms of ability to promote hNSC proliferation and outgrowth, when compared to laminin physically entrapped.

## 4. Conclusion

The present work demonstrates the potential of a PEG-4MAL hydrogel modified with affinity-bound laminin as a dynamic 3D platform enabling NSC proliferation and differentiation. The proposed strategy allows the oriented and controlled immobilization of laminin, with preservation of protein bioactivity, thus overcoming some of the main drawbacks associated with the currently available strategies (*i.e.* physically entrapment and non-selective covalent immobilization). Moreover, the immobilization approach used in this work is highly versatile, as result of the ability of NtA to bind with high affinity to different laminin isoforms comprising the γ1 chain, which represents more than 50% of the isoforms identified to date. Therefore, the reported 3D matrices can be used for the site-selective immobilization of different laminin isoforms and used for the study of cell-laminin interactions occurring in different stem cell niches and disease contexts. These hydrogels can be also of interest to provide a controlled niche with instructive cues to improve survival, engraftment and long-term function of transplanted stem cells; for the creation of tissue-engineered constructs; and for the development of cell expansion and biomanufacturing systems.

**Acknowledgments**

Confocal microscopy was conducted at the Bioimaging i3S Scientific Platform, member of the PPBI (PPBI-POCI-01-0145-FEDER-022122), with the assistance of Maria Lázaro. This work was funded by projects NORTE-01-0145-FEDER-000008 and NORTE-01-0145-FEDER-000012, supported by Norte Portugal Regional Operational Programme (NORTE 2020), under the PORTUGAL 2020 Partnership Agreement, through the European Regional Development Fund (ERDF) and FEDER - Fundo Europeu de Desenvolvimento Regional funds through the COMPETE 2020 - Operacional Programme for Competitiveness and Internationalisation (POCI), Portugal 2020; by Portuguese funds through FCT/MCTES in the framework of the project "Institute for Research and Innovation in Health Sciences" (POCI-01-0145-FEDER-007274), and by Santa Casa da Misericordia de Lisboa through project COMBINE (Prémio Neurociências Melo e Castro 1068-2015).
DB was supported by FCT PhD Programs (PD/BD/105953/2014) and Programa Operacional Potencial Humano (POCH), in the scope of the BiotechHealth Program (Doctoral Program on Cellular and Molecular Biotechnology Applied to Health Sciences), Programa FLAD Healthcare 2020 and the project PARES (Prémio Albino Aroso). Eduardo Conde-Sousa was supported by a post-doctoral grant of the project PPBI-POCI-01-0145-FEDER-022122, in the scope of FCT National Roadmap of Research Infrastructures. AJG acknowledges support from the National Institutes of Health (R01 AR062368).

# SUPPLEMENTARY DATA

## Supplementary Materials and Methods

*Screening Degradable (*SGESPAY↓YTA*) : Non-degradable (PEG-dithiol) cross-linker molar ratio (%)*

After 14 days in culture, the viability of human neural stem cells (hNSCs) within hydrogels cross-linked with different molar ratios (%) of cysteine-flanked matrix metalloproteinase-2 (MMP2)-sensitive peptide (SGESPAY↓YTA) and PEG-dithiol was assessed using a Live/Dead assay, performed according the protocol described in section 2.8. Average occupied area ($\mu m^2$) by live ($Calcein^+$) cells was assessed in the projected two-dimensional (2D) images through the application of an Otsu thresholding method and determination of the total area occupied by cells in each image.

*Cell viability - Immunocytometry*

Quantitative analysis of cell viability was conducted by immunocytometry performed in six-pooled hydrogels, after hydrogel dissociation. Briefly, the hydrogels were sequentially incubated with 1.25 mg/mL of collagenase type II (Gibco; 1h at 37 ºC) and StemPro accutase cell dissociation reagent (Life Technologies; 20 min at 37 ºC) under stirring (70 rpm). Cells were mechanically dissociated by pipetting, diluted in Glasgow Minimal Essential Medium (GMEM; Life Technologies) supplemented with 10% (v/v) inactivated fetal bovine serum (FBS) and centrifuged. For live/dead staining, cells were then transferred to a round-bottomed 96-well plate and stained with calcein AM (67 nM, 20 min at 37 ºC) and propidium iodide (PI; 6 μM, 10 min at 37 ºC). Cells were finally washed trice and suspended in FACS buffer (PBS pH 7.4 supplemented with 2% (v/v) FBS) for flow cytometry analysis on BD FACSCanto™ II (BD Biosciences). Unlabeled cells were used to set the fluorescence gates and cells stained with calcein AM and PI only were used to establish the compensation settings. For each flow cytometry analysis, 10,000 events were acquired inside the respective gate.

*Neurite outgrowth - Immunohistochemistry*

The ability of hNSCs to extend neurites was assessed after 14 days of cell culture, under differentiation conditions, in samples processed for βIII-tubulin/DNA staining. Cell-laden hydrogels were fixed in 3.7% (w/v) paraformaldehyde (PFA) solution diluted 1:1 in culture media (30 min; 37 ºC) and permeabilized with 0.2% (v/v) Triton X-100 in PBS (45 min; room temperature (RT)). Samples were then incubated with blocking buffer (5% (v/v) bovine serum albumin (BSA) in PBS) for 1 h at RT, followed by incubation with the primary antibody – mouse anti-βIII-tubulin (1:500; Biolegend, 801201), overnight at 4 ºC. To detect primary

antibodies, samples were incubated with Alexa Fluor® 488 conjugated anti-mouse secondary antibody (1:1000; Life Technologies, A21202) overnight (ON) at 4 ºC. The nuclei were counterstained with 0.1 μg/mL Hoechst 33342 (Life Technologies, H1399) for 20 min at RT. Samples were observed under confocal laser scanning microscopy (CLSM; TCS SP5II; Leica Microsystems).

## Supplementary Figures

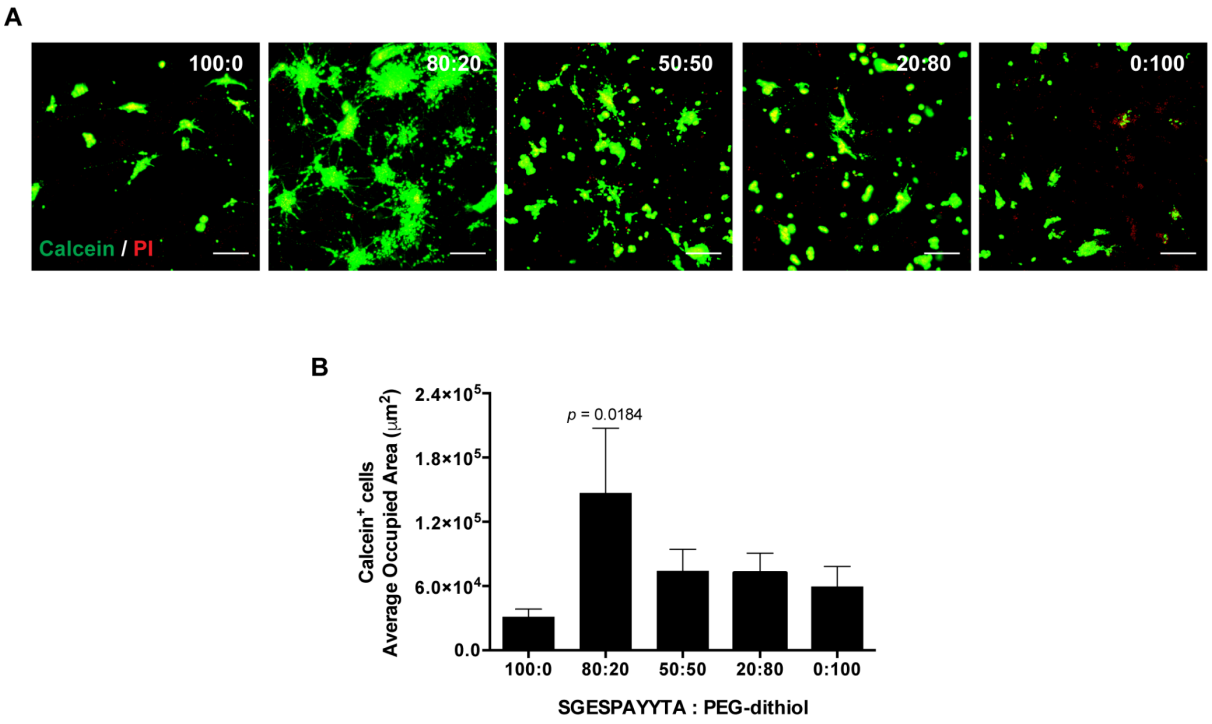


**Figure S1. Optimization of MMP2-sensitive peptide (SGESPAY↓YTA): PEG-dithiol molar ratio (%) in affinity-bound laminin PEG-4MAL hydrogels (50 μM NtA; 20 μg/mL rhLn-521 (Biolamina)). A)** Representative 2D projections of CLSM three-dimensional (3D) stack images of cell-laden affinity-bound laminin PEG-4MAL hydrogels at day 14 of cell culture covering a thickness of 200 μm, showing the distribution of live (green) and/or dead (red) cells. Scale Bar = 200 μm. **B)** Calcein$^+$ cells average occupied area ($\mu m^2$) after 14 days of culture, as determined by quantitative image analysis of 2D projections of CLSM 3D stack images of cell-laden hydrogels incubated with calcein AM (viable cells) and PI (dead cells). Data represent mean ± standard error of the mean (SEM) of 6-9 images from two independent experiments; one-way ANOVA followed by Dunnett's test (*vs.* 100:0)

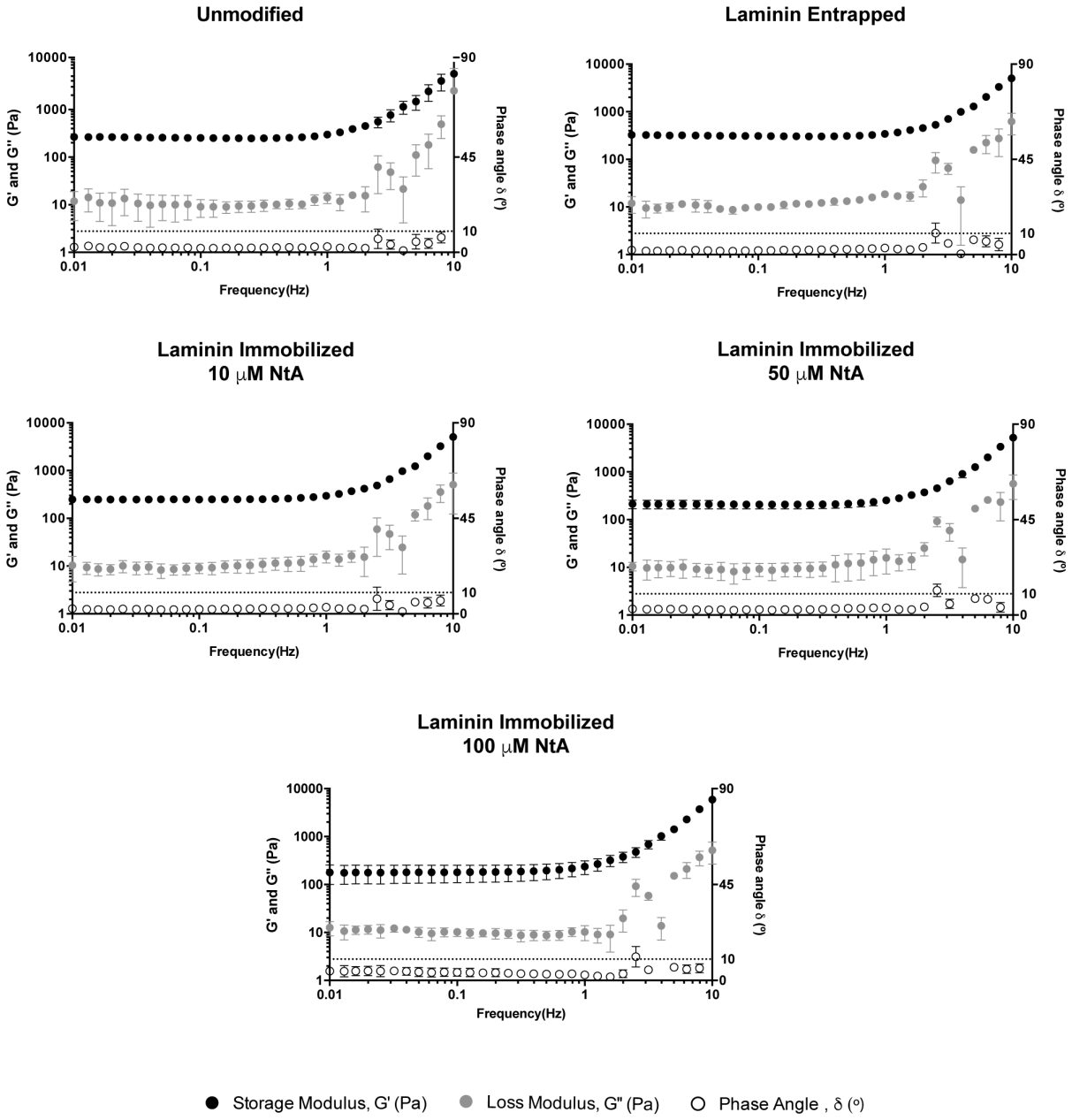


**Figure S2.** Frequency sweep analysis of unmodified, physically entrapped laminin and affinity-bound laminin (10, 50 and 100 μM NtA) hydrogels after stabilization in PBS (pH 7.4) for 24 h. The analysis was performed within a frequency range of 0.01 – 10 Hz, at a constant strain of 1% and 37 ºC. Data represent mean ± standard deviation (SD); n = 6.

## References

[1] S. Pluchino, L. Zanotti, M. Deleidi, G. Martino, Neural stem cells and their use as therapeutic tool in neurological disorders, Brain Res Brain Res Rev 48(2) (2005) 211-9.

[2] C. Cossetti, C. Alfaro-Cervello, M. Donega, G. Tyzack, S. Pluchino, New perspectives of tissue remodelling with neural stem and progenitor cell-based therapies, Cell Tissue Res 349(1) (2012) 321-9.

[3] F.H. Gage, S. Temple, Neural stem cells: generating and regenerating the brain, Neuron 80(3) (2013) 588-601.

[4] F. Gattazzo, A. Urciuolo, P. Bonaldo, Extracellular matrix: a dynamic microenvironment for stem cell niche, Biochim Biophys Acta 1840(8) (2014) 2506-19.

[5] S.W. Lane, D.A. Williams, F.M. Watt, Modulating the stem cell niche for tissue regeneration, Nat Biotechnol 32(8) (2014) 795-803.

[6] A. Vishwakarma, J. Rouwkema, P.A. Jones, J.M. Karp, The Need to Study, Mimic and Target Stem Cell Niches, in: A. Vishwakarma, J.M. Karp (Eds.), Biology and Engineering of Stem Cell Niches, Elsevier2017.

[7] J.L. Wilson, T.C. McDevitt, Biofunctional Hydrogels for Three-Dimensional Stem Cell Culture, in: A. Vishwakarma, J.M. Karp (Eds.), Biology and Engineering of Stem Cell Niches, Elsevier2017.

[8] M.H. Amer, F. Rose, K.M. Shakesheff, M. Modo, L.J. White, Translational considerations in injectable cell-based therapeutics for neurological applications: concepts, progress and challenges, NPJ Regen Med 2 (2017) 23.

[9] F. Ruedinger, A. Lavrentieva, C. Blume, I. Pepelanova, T. Scheper, Hydrogels for 3D mammalian cell culture: a starting guide for laboratory practice, Appl Microbiol Biotechnol 99(2) (2015) 623-36.

[10] Technology Platforms for 3D Cell Culture: A User's Guide, John Wiley & Sons Ltd.2017.

[11] M.W. Tibbitt, K.S. Anseth, Hydrogels as Extracellular Matrix Mimics for 3D Cell Culture, Biotechnol. Bioeng. 103(4) (2009) 655-663.

[12] D. Barros, I.F. Amaral, A.P. Pego, Biomimetic synthetic self-assembled hydrogels for cell transplantation, Curr Top Med Chem 15(13) (2015) 1209-26.

[13] K.J. Lampe, S.C. Heilshorn, Building stem cell niches from the molecule up through engineered peptide materials, Neurosci Lett 519(2) (2012) 138-46.

[14] J. Lam, S.T. Carmichael, W.E. Lowry, T. Segura, Hydrogel design of experiments methodology to optimize hydrogel for iPSC-NPC culture, Adv Healthc Mater 4(4) (2015) 534-9.

[15] C. Regalado-Santiago, E. Juarez-Aguilar, J.D. Olivares-Hernandez, E. Tamariz, Mimicking Neural Stem Cell Niche by Biocompatible Substrates, Stem Cells Int 2016 (2016) 1513285.

[16] C.M. Madl, B.L. LeSavage, R.E. Dewi, C.B. Dinh, R.S. Stowers, M. Khariton, K.J. Lampe, D. Nguyen, O. Chaudhuri, A. Enejder, S.C. Heilshorn, Maintenance of neural progenitor cell stemness in 3D hydrogels requires matrix remodelling, Nat Mater 16(12) (2017) 1233-1242.

[17] A. Hyysalo, M. Ristola, M.E. Makinen, S. Hayrynen, M. Nykter, S. Narkilahti, Laminin alpha5 substrates promote survival, network formation and functional development of human pluripotent stem cell-derived neurons in vitro, Stem Cell Res 24 (2017) 118-127.

[18] L. Luckenbill-Edds, Laminin and the mechanism of neuronal outgrowth, Brain Res Brain Res Rev 23(1-2) (1997) 1-27.

[19] S.K. Powell, H.K. Kleinman, Neuronal laminins and their cellular receptors, Int J Biochem Cell Biol 29(3) (1997) 401-14.

[20] S. Plantman, M. Patarroyo, K. Fried, A. Domogatskaya, K. Tryggvason, H. Hammarberg, S. Cullheim, Integrin-laminin interactions controlling neurite outgrowth from adult DRG neurons in vitro, Mol Cell Neurosci 39(1) (2008) 50-62.

[21] R.S. Rogers, H. Nishimune, The role of laminins in the organization and function of neuromuscular junctions, Matrix Biol 57-58 (2017) 86-105.

[22] H. Nishimune, G. Valdez, G. Jarad, C.L. Moulson, U. Muller, J.H. Miner, J.R. Sanes, Laminins promote postsynaptic maturation by an autocrine mechanism at the neuromuscular junction, J Cell Biol 182(6) (2008) 1201-15.

[23] M. Talovic, M. Marcinczyk, N. Ziemkiewicz, K. Garg, Laminin Enriched Scaffolds for Tissue Engineering Applications, Advances in Tissue Engineering and Regenerative Medicine 2(3) (2017).

[24] D. Barros, P. Parreira, J. Furtado, F. Ferreira-da-Silva, E. Conde-Sousa, A.J. Garcia, M.C.L. Martins, I.F. Amaral, A.P. Pego, An affinity-based approach to engineer laminin-presenting cell instructive microenvironments, Biomaterials 192 (2019) 601-611.

[25] D. Barros, I.F. Amaral, A.P. Pêgo, Laminin immobilization, methods and uses thereof, Provisional Patent Application, 2018.

[26] J.B. Mascarenhas, M.A. Ruegg, U. Winzen, W. Halfter, J. Engel, J. Stetefeld, Mapping of the laminin-binding site of the N-terminal agrin domain (NtA), EMBO J 22(3) (2003) 529-36.

[27] A.J. Denzer, T. Schulthess, C. Fauser, B. Schumacher, R.A. Kammerer, J. Engel, M.A. Ruegg, Electron microscopic structure of agrin and mapping of its binding site in laminin-1, EMBO J 17(2) (1998) 335-43.

[28] J.D. Weaver, D.M. Headen, J. Aquart, C.T. Johnson, L.D. Shea, H. Shirwan, A.J. Garcia, Vasculogenic hydrogel enhances islet survival, engraftment, and function in leading extrahepatic sites, Sci Adv 3(6) (2017) e1700184.

[29] R. Cruz-Acuna, M. Quiros, A.E. Farkas, P.H. Dedhia, S. Huang, D. Siuda, V. Garcia-Hernandez, A.J. Miller, J.R. Spence, A. Nusrat, A.J. Garcia, Synthetic hydrogels for human intestinal organoid generation and colonic wound repair, Nat Cell Biol 19(11) (2017) 1326-1335.

[30] W.M. Han, S.E. Anderson, M. Mohiuddin, D. Barros, S.A. Nakhai, E. Shin, I.F. Amaral, A.P. Pego, A.J. Garcia, Y.C. Jang, Synthetic matrix enhances transplanted satellite cell engraftment in dystrophic and aged skeletal muscle with comorbid trauma, Sci Adv 4(8) (2018) eaar4008.

[31] E.A. Phelps, N.O. Enemchukwu, V.F. Fiore, J.C. Sy, N. Murthy, T.A. Sulchek, T.H. Barker, A.J. Garcia, Maleimide cross-linked bioactive PEG hydrogel exhibits improved reaction kinetics and cross-linking for cell encapsulation and in situ delivery, Adv Mater 24(1) (2012) 64-70, 2.

[32] N.O. Enemchukwu, R. Cruz-Acuna, T. Bongiorno, C.T. Johnson, J.R. Garcia, T. Sulchek, A.J. Garcia, Synthetic matrices reveal contributions of ECM biophysical and biochemical properties to epithelial morphogenesis, J Cell Biol 212(1) (2016) 113-24.

[33] J. Patterson, J.A. Hubbell, Enhanced proteolytic degradation of molecularly engineered PEG hydrogels in response to MMP-1 and MMP-2, Biomaterials 31(30) (2010) 7836-45.

[34] M. Rubinstein, R.H. Colby, Polymer physics, Oxford University Press, 2003.

[35] L.A. Flanagan, Y.E. Ju, B. Marg, M. Osterfield, P.A. Janmey, Neurite branching on deformable substrates, Neuroreport 13(18) (2002) 2411-5.

[36] A.J. Engler, S. Sen, H.L. Sweeney, D.E. Discher, Matrix elasticity directs stem cell lineage specification, Cell 126(4) (2006) 677-89.

[37] P.C. Georges, W.J. Miller, D.F. Meaney, E.S. Sawyer, P.A. Janmey, Matrices with compliance comparable to that of brain tissue select neuronal over glial growth in mixed cortical cultures, Biophys J 90(8) (2006) 3012-8.

[38] K. Saha, A.J. Keung, E.F. Irwin, Y. Li, L. Little, D.V. Schaffer, K.E. Healy, Substrate modulus directs neural stem cell behavior, Biophys. J. 95(9) (2008) 4426-38.

[39] A. Banerjee, M. Arha, S. Choudhary, R.S. Ashton, S.R. Bhatia, D.V. Schaffer, R.S. Kane, The influence of hydrogel modulus on the proliferation and differentiation of encapsulated neural stem cells, Biomaterials 30(27) (2009) 4695-9.

[40] S.R. Hynes, M.F. Rauch, J.P. Bertram, E.B. Lavik, A library of tunable poly(ethylene glycol)/poly(L-lysine) hydrogels to investigate the material cues that influence neural stem cell differentiation, J Biomed Mater Res A 89(2) (2009) 499-509.

[41] T.L. Laundos, J. Silva, M. Assuncao, P. Quelhas, C. Monteiro, C. Oliveira, M.J. Oliveira, A.P. Pego, I.F. Amaral, Rotary orbital suspension culture of embryonic stem cell-derived neural stem/progenitor cells: impact of hydrodynamic culture on aggregate yield, morphology and cell phenotype, J Tissue Eng Regen Med 11(8) (2017) 2227-2240.

[42] A.R. Bento, P. Quelhas, M.J. Oliveira, A.P. Pego, I.F. Amaral, Three-dimensional culture of single embryonic stem-derived neural/stem progenitor cells in fibrin hydrogels: neuronal network formation and matrix remodelling, J Tissue Eng Regen Med 11(12) (2017) 3494-3507.

[43] N.J. Darling, Y.S. Hung, S. Sharma, T. Segura, Controlling the kinetics of thiol-maleimide Michael-type addition gelation kinetics for the generation of homogenous poly(ethylene glycol) hydrogels, Biomaterials 101 (2016) 199-206.

[44] K. Onuma, N. Kanzaki, Size Distribution and Intermolecular Interaction of Laminin-1 in Physiological Solutions, J. Phys. Chem. 107 (2003) 11799-11804.

[45] M. Hjort, M. Bauer, S. Gunnarsson, E. Marsell, A.A. Zakharov, G. Karlsson, E. Sanfins, C.N. Prinz, R. Wallenberg, T. Cedervall, A. Mikkelsen, Electron microscopy imaging of proteins on gallium phosphide semiconductor nanowires, Nanoscale 8(7) (2016) 3936-43.

[46] K.J. Lampe, R.G. Mooney, K.B. Bjugstad, M.J. Mahoney, Effect of macromer weight percent on neural cell growth in 2D and 3D nondegradable PEG hydrogel culture, J Biomed Mater Res A 94(4) (2010) 1162-71.

[47] L. Marquardt, R.K. Willits, Student award winner in the undergraduate's degree category for the Society for Biomaterials 35th Annual Meeting, Orlando, Florida, April 13-16, 2011. Neurite growth in PEG gels: effect of mechanical stiffness and laminin concentration, J Biomed Mater Res A 98(1) (2011) 1-6.

[48] I.O.f. Standardization, ISO 10993-5:2009 : Biological evaluation of medical devices Tests for in vitro cytotoxicity, 2009.

# CHAPTER VII

An Alternative Approach to Engineer Synthetic Hydrogels with Affinity-Bound Laminin

# An Alternative Approach to Engineer Synthetic Hydrogels with Affinity-Bound Laminin

Daniela Barros [1,2,3], Andrés J. García [4,5], Isabel F. Amaral [1,2,6], Ana P. Pêgo [1,2,3,6]

[1] i3S - Instituto de Investigação e Inovação em Saúde, Universidade do Porto (UPorto), Portugal

[2] INEB - Instituto de Engenharia Biomédica, UPorto, Portugal

[3] ICBAS - Instituto de Ciências Biomédicas Abel Salazar, UPorto, Portugal

[4] Parker H. Petit Institute for Bioengineering and Biosciences, Georgia Institute of Technology, Atlanta, Georgia, USA

[5] George W. Woodruff School of Mechanical Engineering, Georgia Institute of Technology, Atlanta, Georgia, USA

[6] FEUP - Faculdade de Engenharia, UPorto, Portugal

**Abstract**

Laminin-521 (Ln-521) has a key role on the modulation of neural cell behavior and have shown potential to be used as a robust substratum for the culture and renewal of human embryonic and pluripotent stem cells. Despite the potential of this laminin isoform, to the best of our knowledge, no study to date has explored the immobilization of Ln-521 for the development of three-dimensional (3D) matrices for the culture of human neural stem cells (hNSCs). In this regard, and envisaging the development of a defined and whole-human 3D cell-instructive platform, capable of supporting hNSC differentiation and function, in this study we describe the preparation of a degradable synthetic hydrogel functionalized with affinity-bound recombinant human Ln-521. The proposed methodology introduces some modifications to the previously described approach for laminin immobilization, aiming the improvement of laminin binding to NtA and its impact on NSC behavior. Specifically, a mono-PEGylated recombinant human N-terminal agrin (NtA) domain was incubated with laminin and the resultant conjugate (NtA-Ln-521) was subsequently tethered to a four-arm maleimide terminated poly(ethylene glycol) (PEG-4MAL) macromer. The hydrogels were formed, under physiological conditions, through the use of a mixture of protease degradable and non-degradable cross-linkers. Affinity-bound laminin PEG-4MAL hydrogels were shown to better preserve laminin bioactivity, as evidenced by the enhanced ability to support neurite outgrowth, when compared to unmodified hydrogels and hydrogels with equal amount of physically entrapped laminin. However, in the latter case, significant differences were not attained.

Overall, the results obtained show that the alternative approach herein proposed for laminin immobilization, can be used as an effective immobilization strategy for hydrogel biofunctionalization envisaging its use as defined platforms for hNSC culture.

Neural stem cells (NSCs) reside within a dynamic and complex microenvironment, the NSC niche, which provides a unique and specialized microenvironment, where cell-cell interactions and local microenvironmental cues, including those from extracellular matrix (ECM), soluble factors and cellular components, are key for the modulation of NSC function [1]. In this regard, in the last few years, there was an attempt to develop new platforms to allow the dissection of the role of individual or multiple components of the niche on the modulation of NSC function and fate.

Laminin constitutes one of the most important ECM effectors of NSC niches [2, 3], as it provides important biological cues to different biological processes, including cell adhesion and viability [4] and neuronal outgrowth and migration [5-7]. Furthermore, laminin has other key roles in CNS homeostasis, as contributing to synapse function and stability [8, 9]. Several studies have already explored the incorporation of this ECM protein into three-dimensional (3D) cell-instructive microenvironments [10-17], by taking advantage of different immobilization strategies. The latter include non-covalent incorporation or physical entrapment or, alternatively, non-specific covalent immobilization by taking advantage of functional groups present in multiple sites of the laminin structure such as amines [10-14] and thiols [15-17]. Although such strategies are rather efficient, their application to immobilize proteins might be limited due to the lack of control over protein conformation and orientation upon immobilization, which often results in a reduction or loss of bioactivity. In this regard, in recent years, affinity-binding strategies have been increasingly explored to mediate highly site- and conformation-specific reactions for protein and peptide immobilization [18]. Besides allowing the retention of protein bioactivity, the versatility of this approach allows the generation of dynamic biomimetic microenvironments. An important factor to take into consideration when applying such strategies is the appropriate selection of the binding pairs. In this regard, different “artificial” moieties, including streptavidin, biotin, protein A, among others, have been widely explored for the development of 3D matrices with a broad applicability and specificity [19, 20]. Alternatively, natural binding partners have become an attractive alternative, as strong non-covalent interactions can be achieved without the need of the protein of interest to be either recombinantly or chemically modified [21, 22].

Laminin-521 (Ln-521) has a key role on the modulation of neural cell behavior, including neuronal adhesion, viability and network formation [4, 23]. Moreover, this laminin isoform demonstrated great potential to be used as a xeno-free substratum for the culture and renewal of human embryonic [24] and pluripotent [4] stem cells. Despite the potential of this laminin isoform, to the best of our knowledge, no study to date, explored its immobilization for the development of defined 3D matrices for the culture of human NSCs (hNSCs). In this regard, and envisaging the development of a whole-human 3D cell-instructive microenvironment, to

support hNSC fate and function, in this study we propose the development of an affinity-bound recombinant human Ln-521 (rhLn-521) degradable synthetic hydrogel, using an immobilization strategy previously proposed [25-27]. The proposed approach takes advantage of the well described native high affinity interaction between laminin and the N-terminal agrin (NtA) domain [28, 29]. A four-arm maleimide terminated poly(ethylene glycol) (PEG-4MAL) macromer was used as the hydrogel base material (Fig. 1), due to its good biocompatibility, both *in vitro* and *in vivo* [30-32], and well characterized biochemical and biophysical properties [32-34]. To allow the site-selective immobilization of laminin on the PEG-4MAL hydrogel, a thiol-containing mono-PEGylated rhNtA (NtA) domain was produced and characterized, showing high affinity for rhLn-521 (dissociation constant ($K_D$) = 1.58 $\pm$ 0.41 nM) [25]. To enable the hNSC 3D culture that would span the time frame of hNSC proliferation and neuronal differentiation, a mix of protease degradable (cysteine-flanked matrix metalloproteinase 2 (MMP2)-sensitive peptide) [35] and non-degradable (PEG-dithiol) cross-linkers was used to mediate, under physiological conditions, the formation of a degradable hydrogel network (Fig. 1). The developed hydrogels were expected to allow the highly specific and orthogonal immobilization of laminin to form a cell-instructive microenvironment. Moreover, the versatility and dynamic nature of the proposed strategy can be further explored for the immobilization of different exogenous laminin isoforms, with application in distinct disease contexts, as well as to assess their exchangeability by endogenously secreted laminin.

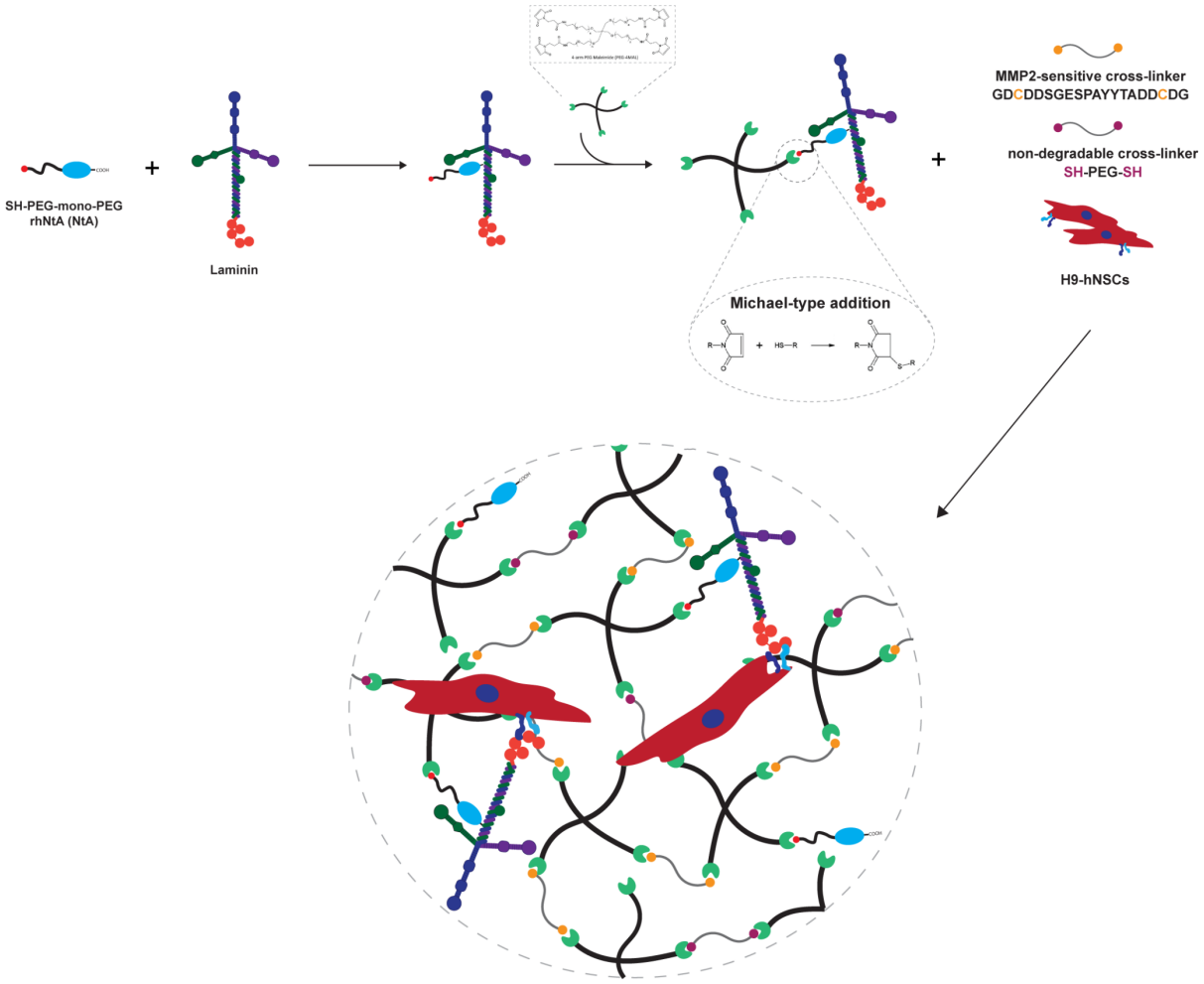


**Figure 1. Schematic representation of the preparation of cell-laden affinity-bound laminin PEG-4MAL hydrogels (not to scale).** A thiol-containing mono-PEGylated rhNtA (NtA) is firstly reacted with rhLn-521 and the formed conjugate subsequently tethered to a PEG-4MAL macromer. Functionalized PEG-4MAL is finally reacted with a mixture of protease degradable (MMP2-sensitive peptide) and non-degradable (PEG-dithiol) cross-linkers to allow the formation, under physiological conditions, of a hydrogel network in the presence of cells.

Preliminary studies, exploring the site-selective immobilization of rhLn-521 into a PEG-4MAL hydrogel, using a previously proposed approach [25-27], did not evidence a significant increase on hNSC neurite outgrowth, when compared to unmodified hydrogels and hydrogels with equal amount of physically entrapped laminin (Fig. S1, in Supplementary Data). In line with this outcome, we hypothesize that the lower bioactivity presented by the site-selective immobilized laminin could be related with the methodology explored for laminin incorporation into the hydrogel. Namely, in the previously reported immobilization scheme, a PEG-4MAL macromer is firstly functionalized with a thiol-containing mono-PEGylated rhNtA domain, which will then mediate the binding of laminin with high affinity. The hydrogel is subsequently

formed by cross-linking of the laminin functionalized PEG-4MAL. Therefore, in this work, we aimed to explore an alternative functionalization scheme. In the newly proposed approach the NtA domain is initially incubated with the rhLn-521 and the resultant conjugate tethered to a PEG-4MAL macromer (Fig. 1). This was proposed under the assumption that protein-protein interaction in solution would allow a more efficient and controlled immobilization of rhLn-521, even at lower concentrations. As maleimide groups efficiently react with thiol-containing moieties through Michael-type addition, one expects to have a finer control over the final conjugate incorporation. Different NtA concentrations (10, 50 and 100 μM) were initially used to determine the most suitable concentration allowing to have a finer control over the binding ligand (NtA) density/presentation and ultimately, over the amount of affinity-bound laminin.

To evaluate the tethering efficiency of the NtA-rhLn-521 conjugates to the PEG-4MAL macromer and their further incorporation into the final hydrogels, radiolabeling studies were conducted. For that, both NtA and laminin were labeled with $^{125}$I, as described elsewhere [36], and then used for hydrogel preparation. The amount of NtA or laminin retained in each hydrogel was determined after 1 and 7 days, by measuring the gamma activity of the hydrogel at each time point. NtA tethering efficiency (Fig. 2A) or laminin incorporation (Fig 2B) was expressed as a percentage of the initial gamma activity of the hydrogel, prior to incubation in buffer. NtA domain was tethered onto the PEG-4MAL macromers with yields below 50%, for all the concentrations tested (10, 50 and 100 μM; Fig. 2A and Table S1 in Supplementary Data). Affinity-bound laminin revealed a laminin incorporation of 60% at day 1, which decrease to 40-50% at day 7 (Fig. 2B and Table S1 in Supplementary Data). Site-selective immobilization of laminin using 10 μM NtA favors a significant higher protein incorporation compared to that observed when 100 μM NtA domain was used ($p$ = 0.0241, day 7). The same trend was also observed for hydrogels with physically entrapped laminin ($p$ = 0.0146 *vs.* Immob 100 μM NtA, day 7).

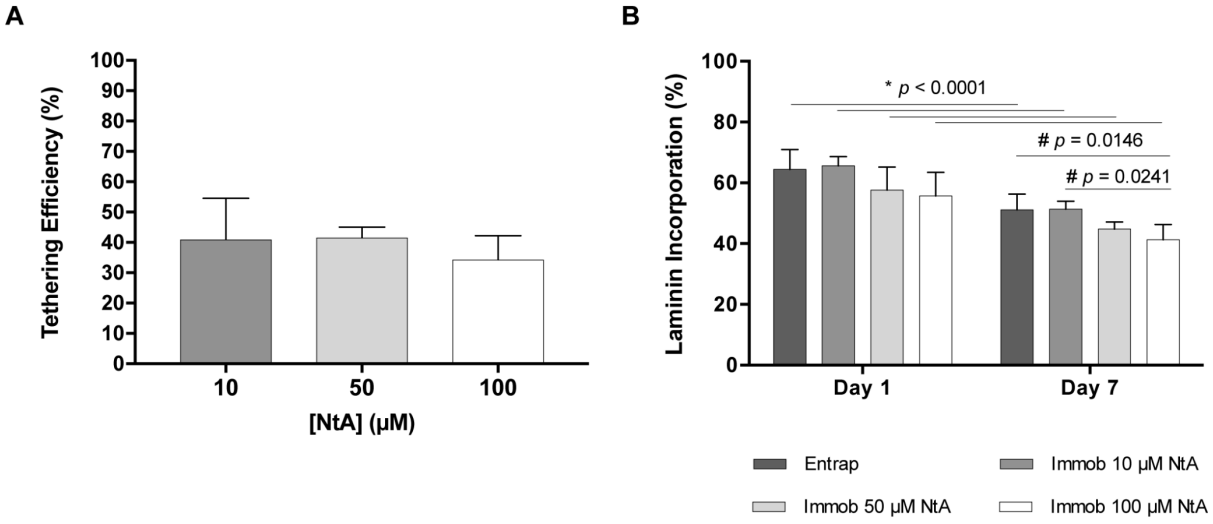


**Figure 2.** Effect of NtA concentration on the **A)** Efficiency of NtA covalent tethering to PEG-4Mal after 1 day of incubation in buffer; and **B)** Incorporation of affinity-bound laminin in PEG-4Mal hydrogels after 1 or 7 days of incubation in buffer, determined using $^{125}$I-labeled NtA or laminin. The incorporation of laminin through physical entrapment is also shown. Data represent mean ± standard deviation (SD) of three independent experiments performed in duplicate; * two-way repeated measures ANOVA followed by Sidak's test; # one-way ANOVA followed by Bonferroni's test.

The lower yields obtained were not expected and may be a consequence of steric effects resultant from the laminin high molecular weight (≅ 800 kDa). More specifically, it is possible that the initial conjugation of laminin to the NtA domain have prevented the reaction of the thiol group from mono-PEGylated NtA with maleimide groups. On the other hand, higher concentrations of NtA may have led to the formation of disulfide bridges, between thiol groups from mono-PEGylated NtA, contributing for the decrease observed in laminin incorporation when increasing concentrations of the binding ligand (NtA) were used. Despite of the similar levels of laminin incorporation when using 10 μM or 50 μM NtA (Fig. 2A and B), the use of 50 μM NtA concentration to selectively immobilize rhLn-521, resulted in a better biological outcome in terms of ability to support cellular outgrowth of hNSCs cultured within PEG-4MAL hydrogels (Fig. S2 in Supplementary Data). Therefore, all the studies from here on, were conducted using a 50 μM NtA concentration.

The effect of the incorporation of affinity-bound rhLn-521 on PEG-4Mal hydrogels mechanical properties and structure (mesh size) was assessed by rheological studies. All the prepared hydrogels presented storage modulus (G') > loss modulus (G'') (Table S2 in Supplementary Data), an indication that PEG-4MAL transitioned from a viscous liquid to a gelled state. Moreover, laminin incorporation either by entrapment or affinity binding led to an increase in the complex modulus of the gels (G*; Fig. 3A), resulting in the formation of a significantly

tighter polymer network, as evidenced by the significantly decrease in mesh size (Fig. 3B), when compared to unmodified hydrogels. Nevertheless, the G* values found for hydrogels containing affinity-bound laminin lie well within the range of those reported for human brain tissue (100 – 1000 Pa) and preferred for neurite extension and branching (200 – 400 Pa) [37-42].

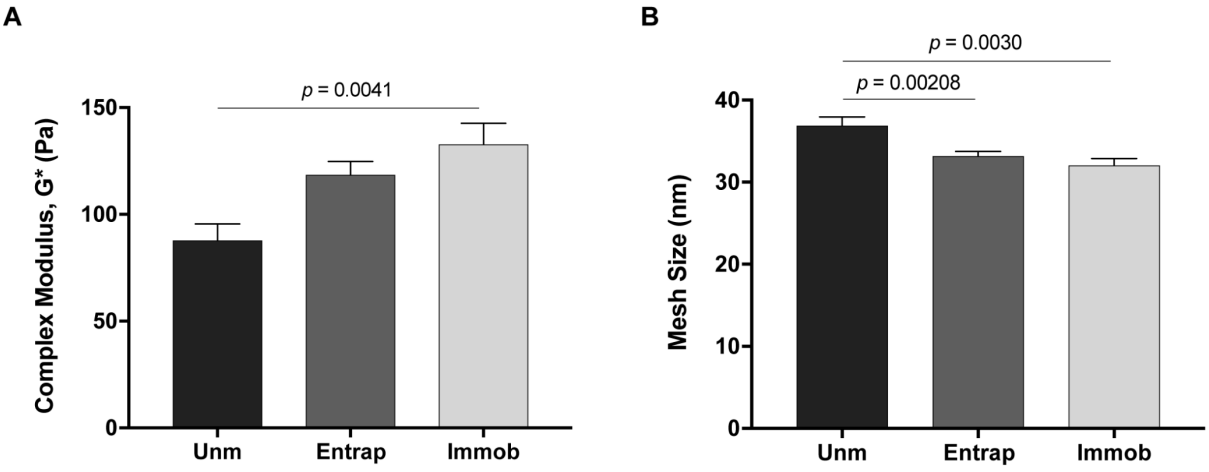


**Figure 3. Influence of affinity-bound laminin incorporation on PEG-4MAL hydrogel mechanical and structural properties. A)** Complex modulus (G*) of hydrogels determined by rheological analysis; and **B)** Estimation of hydrogels mesh size, based on the measured storage modulus (G'). Data represent mean ± standard error of the mean (SEM); n = 6; one-way ANOVA followed by Bonferroni's test.

The bioactivity of hydrogels with affinity-bound rhLn-521 was subsequently evaluated, and compared with the performance of hydrogels containing entrapped laminin. For this purpose, hNSCs were cultured within degradable PEG-4MAL hydrogels with either soluble or affinity-bound rhLn-521 (20 μg/mL) and cell viability and neurite outgrowth were assessed. Unmodified hydrogels were used as controls. The effect of the proposed strategy on hNSC survival was evaluated after 7 days of culture. Confocal analysis showed the presence of viable cells evenly distributed throughout the hydrogels, often growing as cellular spheroids, for all the conditions tested (Fig. 4A). The quantitative analysis of viable/unviable cells, assessed by flow cytometry upon cell isolation from hydrogels, showed fractions of viable cells greater than 75% for all the conditions tested, evidencing the good cytocompatibility of the proposed matrices (Fig. 4B) [43].

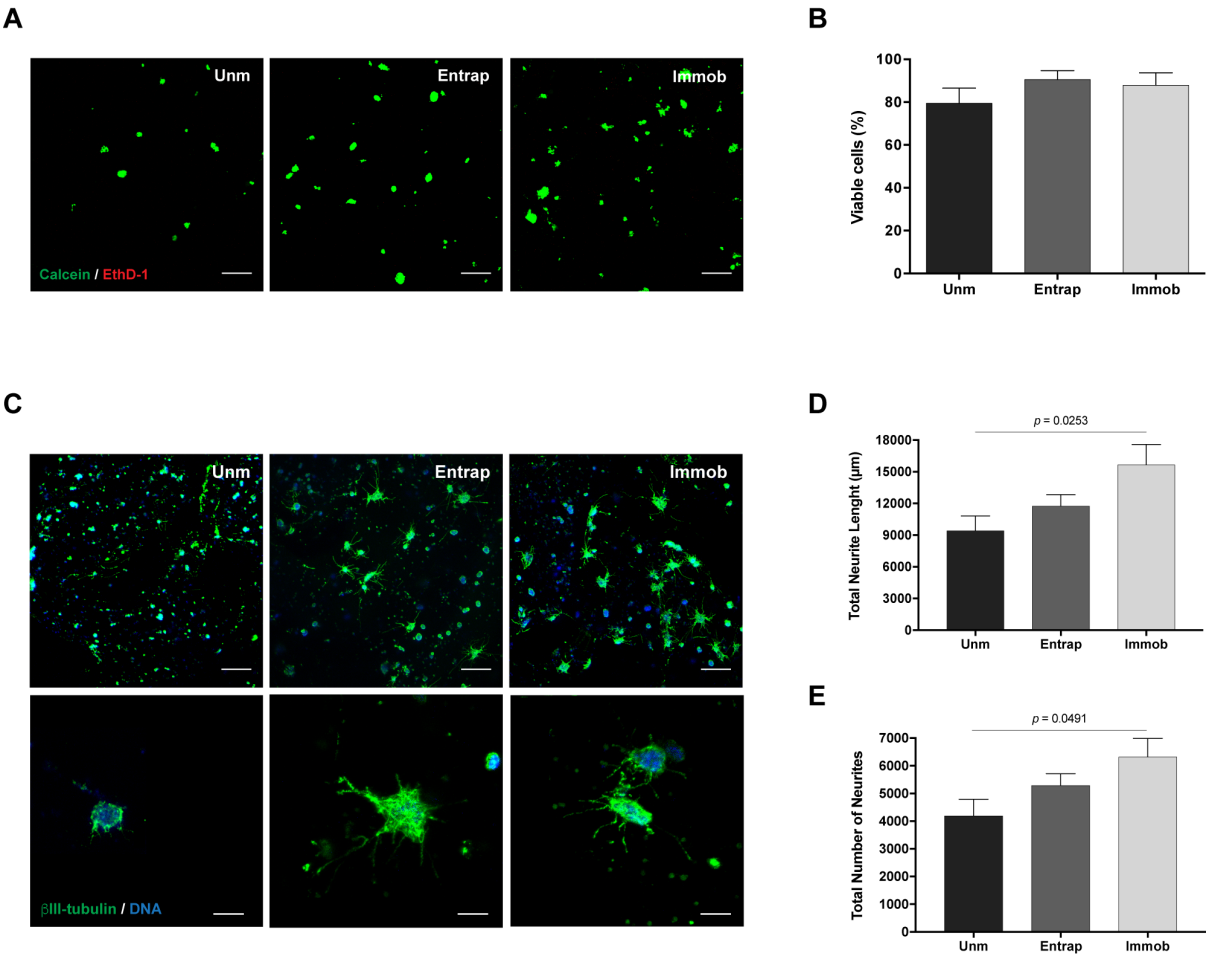


**Figure 4. Affinity-bound laminin PEG-4MAL hydrogels and its effect on hNSC viability and neurite outgrowth. A)** Distribution of viable (green) and dead (red) cells cultured within unmodified (Unm), laminin physically entrapped (Entrap) and NtA affinity-bound laminin (Immob) PEG-4MAL hydrogels was assessed at day 7 of cell culture, using a live/dead assay. Representative 2D projections of confocal laser scanning microscopy (CLSM) 3D stack images of cell-laden hydrogels covering a thickness of 200 μm, showing the distribution of live (green) and dead (red) cells. Scale bar = 200 μm. **B)** Quantitative analysis of live cells at day 7, as determined by flow cytometry. Data represent mean ± SD of three independent experiments. **C)** hNSCs cultured within unmodified (Unm), rhLn-521 physically entrapped (Entrap) and 50 μM NtA-affinity-bound rhLn-521 (Immob) PEG-4MAL hydrogels after 14 days of culture, under differentiation conditions. Images show 2D projections of CLSM 3D stack images of cells processed for immunofluorescence labeling of βIII-tubulin/DNA and covering a thickness of 200 μm (top images) and 100 μm (bottom images). Scale Bar = 200 μm (top images); 100 μm (bottom images). **D)** Total Neurite Length; and **E)** Total Number of Neurites determined by quantitative analysis of images acquired in CLSM. Data represent mean ± SD of 11-17 images analyzed per condition; one-way ANOVA followed by Bonferroni's test.

To investigate the effect of laminin site-selective immobilization on neurite outgrowth, hNSCs were cultured for 14 days under differentiation conditions, and then processed as whole-

mounts for βIII-tubulin and DNA staining (Fig. 4C). A population of differentiated neurons, expressing βIII-tubulin and starting to form a neuronal network, was observed for affinity-bound laminin PEG-4MAL hydrogels (Fig. 4C). Differences between the conditions tested were assessed by image process and quantitative analysis, using ImageJ/Fiji. More specifically, total neurite length (μm) and total number of neurites were quantified (Fig. 4D-F). A significant increase in neurite outgrowth was observed for the PEG-4MAL hydrogels with affinity-bound laminin, compared to unmodified hydrogels, as evidenced by the higher values of total neurite length (15663 ± 7951 μm; $p$ = 0.0253; Fig. 4D) and total number of neurites (6327 ± 2817; $p$ = 0.0491; Fig. 4E). Laminin entrapment also promoted neurite outgrowth in PEG-4MAL hydrogels but its impact was not significant. Despite the tendency for increased neurite outgrowth observed for hydrogels with affinity-bound laminin, no significant differences on total neurite length and total number of neurites were detected when compared to hydrogels containing laminin entrapped (Fig. 4D-E)

Overall, these results suggest that the alternative strategy explored in this work for laminin incorporation better preserves laminin bioactivity, thus assuring the hydrogel biofunctionality. Although this work represents a good starting point for the development of a whole-human 3D cell instructive matrix, future studies exploring approaches that better promote the tethering of NtA-bound laminin to PEG-4MAL with preservation of its bioactive domains, and/or allow an increase in rhLn-521 initial concentration (> 20 μg/mL) need to be conducted.

## Materials and Methods

### *Hydrogel components*

A four-arm maleimide terminated poly(ethylene glycol) (PEG-4MAL; 40 kDa, > 95% purity, >90% substitution, Jenkem USA) was chosen as the hydrogel base material. A macromer solution was prepared in 10 mM 4-(2-hydroxyethyl)piperazine-1-ethanesulfonic acid (HEPES) buffer (pH 7.4) at a final polymer concentration of 10% (w/v). Mono-PEGylated recombinant human N-terminal agrin (NtA) domain was produced as previously described [25]. Recombinant human laminin-521 (rhLn-521) was obtained from Biolamina. A cysteine-flanked matrix metalloproteinase-2 (MMP2)-sensitive peptide (Acetyl (Ac)-GD*C*DD**SGESPAY↓YTA**DD*C*DG-Amide ($NH_2$); 2.1 kDa, > 85% purity, GenScript) and a PEG-dithiol (3.5 kDa, ≥ 95% purity, Jenkem USA) were used as the degradable and non-degradable cross-linkers, respectively.

***Preparation of affinity-bound rhLn-521 PEG-4MAL hydrogels***

A schematic representation of affinity-bound laminin PEG-4MAL hydrogel preparation is presented in Fig. 1. Briefly, NtA (input concentration in the gel: 50 μM) was initially reacted with rhLn-521 (input concentration in the gel: 20 μg/mL) for 30 min at room temperature (RT) in 10 mM HEPES buffer (pH 7.4). PEG-4MAL was then functionalized with the previously formed conjugate (NtA – rhLn-521) for 15 min in 10 mM HEPES buffer (pH 7.4). Functionalized PEG-4MAL macromers were then cross-linked linked into a hydrogel by addition of a mix of a MMP2-sensitive peptide and a PEG-dithiol dissolved in 10 mM HEPES buffer (pH 6.5), at an 80:20 molar ratio (%). The cross-linkers were added at a 1:1 molar ratio of cysteine residues on the cross-linkers to remaining maleimide groups on NtA-rhLn521-functionalized PEG-4MAL. Hydrogels were polymerized at 37ºC, 5% $CO_2$ for 15 min. Unmodified PEG-4MAL gels and PEG-4MAL gels containing entrapped rhLn-521 (20 μg/mL) were also prepared and used as controls.

***$^{125}$I-radiolabeling – NtA and laminin incorporation efficiency***

To assess the incorporation efficiency of NtA and laminin into PEG-4MAL hydrogels, both proteins were first labeled with $^{125}$I as described elsewhere [36] and then used for hydrogel preparation. Briefly, NtA or laminin (5 μg) were labeled with 0.5 mCi of Na$^{125}$I (Perkin Elmer) using the Iodogen method [44], and further purified using a PD-10 Desalting Column packed with Sephadex $^{TM}$ G-25 Medium (GE Healthcare), to remove free $^{125}$I ions. Fractions with yield of $^{125}$I-labelling ≥ 98.8% were used. Functionalized hydrogels (10 μL) were prepared as described above in radioimmunoassay (RIA) tubes, using NtA or laminin spiked with $^{125}$I-labeled domain or protein, respectively, in order to achieve a final activity of $\approx 2.0 \times 10^5$ cpm/μg of NtA/laminin. Hydrogels containing $^{125}$I-labeled soluble laminin (20 μg/mL) were also prepared and used as controls. The gels were processed straight away for gamma activity counting γ-counter (CAPRAC® - t Wipe Test / Well Counter; Capintec, Inc.) and further incubated with 125 μL of phosphate buffered saline (PBS) buffer containing 2% (w/v) bovine serum albumin (BSA) at 37 ºC. The amount of NtA or laminin retained in each hydrogel was determined after 1 and 7 days. At each time point, the buffer solution was replaced by fresh buffer, the gamma activity of the hydrogel measured, and NtA or laminin incorporation was expressed as a percentage of the initial gamma activity of the hydrogel prior to incubation in buffer.

***Rheological properties and mesh size estimation of affinity-bound laminin PEG-4MAL hydrogels***

The viscoelastic properties of PEG-4MAL hydrogels were characterized using an MCR 302 stress-controlled rheometer (Anton Paar, Austria) with a 9 mm diameter, 2º cone angle (CP10-

2) and plate geometry. Hydrogels for each condition (∅ 8 mm) were prepared as previously described, and allowed to hydrate in PBS buffer at 37 ºC for 24h. The samples were then loaded between the cone and the plate, in a humidified environment at physiological temperature (37 ºC), and the measuring system was lowered to a 40 μm gap using TruGap™ system. Amplitude strain sweeps (0.001 – 1% at 10 rad/s) were initially performed for each condition to define the linear viscoelastic region (LVR). Frequency sweeps (0.1-100 rad/s at 0.01% strain) were then performed and the storage (G'), loss (G'') and complex (G*) modulus Determined within the LVR, by averaging all data points acquired from a 0.1 - 10 rad/s interval. The relative mesh size (nm) value was estimated using the following equation [45]:

$$\xi = \left(\frac{G'A}{RT}\right)^{-\frac{1}{3}}$$

where G' = storage modulus in Pa, A = Avogadro's constant ($6.022140857 \times 10^{23}$ $mol^{-1}$), R = gas constant (8.314 $m^3.Pa.mol^{-1}.K^{-1}$), T = temperature (37 ºC = 310.15 K) .

***Culture of human neural stem cells***

Human neural stem cells (hNSCs) derived from the NIH approved H9 (WA09) human embryonic stem cell line were purchased from Life Technologies (N7800-200). Cells were expanded according to the manufacturer's protocol on poly(ornithine)/laminin-111 from mouse Engelbreth-Holm-Swarm sarcoma (msLn-111; Sigma-Aldrich)-coated tissue coated polystyrene (TCPS) plates (Corning) in expansion medium - StemPro® NSC serum free medium (SFM; Life Technologies) supplemented with basic fibroblast growth factor (bFGF, 20 ng/mL; Life Technologies) and epidermal growth factor (EGF, 20 ng/mL; Life Technologies).

***Culture of hNSCs within affinity-bound rhLn-521 PEG-4MAL hydrogels***

hNSCs were dissociated into single cells using StemPro Accutase cell dissociation reagent (Life Technologies) and further suspended in the solution containing laminin-functionalized PEG-4MAL precursors (4 x $10^6$ viable cells/mL). Cell-laden hydrogels were formed by mixing the PEG-4MAL precursor solution containing cells with the MMP2-sensitive peptide and PEG-dithiol cross-linkers, dissolved in 10 mM HEPES (pH 6.5), at an 80:20 molar ratio (%), and subsequently incubating the polymerizing gels at 37 ºC, 5% $CO_2$ for 15 minutes. hNSCs were initially cultured in expansion medium and, at day 2 of culture, the medium was switched to the StemPro NSC SFM media-Neurobasal/B27 (Life Technologies) (1:1) mix, without growth factors. At day 8, half of the medium was replaced by the StemPro NSC SFM-Neurobasal/B27 (1:3) mix supplemented with 10 ng/mL of brain-derived neurotrophic factor (BDNF; Peprotech) and 500 μM of $N^6$, 2'-O-Dibutyryladenosine 3', 5'-cyclic monophosphate sodium salt (dibutyril cAMP; Sigma). Half of the medium was changed every other day, up to 14 days. hNSCs

cultured within unmodified and PEG-4MAL gels containing entrapped rhLn-521 (20 μg/mL) were herein used as controls.

***Cell viability***

The distribution of viable and dead cells within PEG hydrogels was assessed at day 7 of cell culture using a live/dead assay. Cell-hydrogel matrices were rinsed with warm PBS pH 7.4 and incubated with 4 μM calcein AM (Life Technologies) and 6 μM propidium iodide (PI; Life Technologies) at 37 ºC for 30 min, for detection of viable and dead cells, respectively. After incubation, the samples were rinsed twice with PBS pH 7.4, transferred to culture medium, and immediately observed under confocal laser scanning microscopy (CLSM, Leica TCS SP5). Quantitative analysis of live and dead cells was also conducted using immunocytometry (See Supplementary Materials and Methods).

***hNSC neurite outgrowth***

The effect of laminin site-selective immobilization on neurite outgrowth was assessed after 14 days of culture under neuronal differentiation conditions. Samples were processed as whole-mounts for βIII-tubulin/DNA staining as described in Supplementary Materials and Methods, and z-sections covering a thickness of 200 μm or 100 μm were acquired with the CLSM using an HC Plan APO CS 10× / 0.40 NA or HC Plan APO CS 20× / 0.70 NA objective, respectively. Neurite outgrowth was assessed in the projected two-dimensional (2D) images using a developed ImageJ script. Briefly, nuclei were segmented through an Otsu thresholding method, while neurites were segmented through subtraction of the previously identified nucleus, using a Huang thresholding method. Measurements were obtained for total neurite length (μm) and total number of neurites per image.

***Statistical Analysis***

Statistical analysis was performed using GraphPad Prism 6 software (San Diego). Sample distribution was initially tested for normality using the Kolmogorov-Smirnov test. Comparisons between three or more groups were performed with one-way ANOVA analysis, followed by the Bonferroni correction for pairwise comparisons. For all analysis, differences were considered significant at $p < 0.05$.

**Acknowledgments**

Radiolabeling studies were conducted at Serviço de Medicina Nuclear – IPO Porto, with the assistance of Dra. Carla Vaz, Dr. João Miranda dos Santos and Dr. Hugo Duarte. Confocal microscopy was conducted at the Bioimaging i3S Scientific Platform, member of the PPBI (PPBI-POCI-01-0145-FEDER-022122), with the assistance of Maria Lázaro. This work was

funded by projects NORTE-01-0145-FEDER-000008 and NORTE-01-0145-FEDER-000012, supported by Norte Portugal Regional Operational Programme (NORTE 2020), under the PORTUGAL 2020 Partnership Agreement, through the European Regional Development Fund (ERDF) and FEDER - Fundo Europeu de Desenvolvimento Regional funds through the COMPETE 2020 - Operacional Programme for Competitiveness and Internationalisation (POCI), Portugal 2020; by Portuguese funds through FCT/MCTES in the framework of the project "Institute for Research and Innovation in Health Sciences" (POCI-01-0145-FEDER-007274), and by Santa Casa da Misericordia de Lisboa through project COMBINE (Prémio Neurociências Melo e Castro 1068-2015).

D.B. was supported by FCT PhD Programs (PD/BD/105953/2014) and Programa Operacional Potencial Humano (POCH), in the scope of the BiotechHealth Program (Doctoral Program on Cellular and Molecular Biotechnology Applied to Health Sciences), Programa FLAD Healthcare 2020 and the project PARES (Prémio Albino Aroso).

# SUPPLEMENTARY DATA

## Supplementary Materials and Methods

*Cell viability - Immunocytometry*

Quantitative analysis of cell viability was conducted by immunocytometry performed in six-pooled hydrogels, after hydrogel dissociation. Briefly, the hydrogels were sequentially incubated with 1.25 mg/mL of collagenase type II (Gibco; 1h at 37 ºC) and StemPro accutase cell dissociation reagent (Life Technologies; 20 min at 37 ºC) under stirring (70 rpm). Cells were mechanically dissociated by pipetting, diluted in Glasgow Minimal Essential Medium (GMEM; Life Technologies) supplemented with 10% (v/v) inactivated fetal bovine serum (FBS) and centrifuged. For live/dead staining cells were then transferred to a round-bottomed 96-well plate and stained with calcein AM (67 nM, 20 min at 37 ºC) and propidium iodide (PI; 6 μM, 10 min at 37 ºC). Cells were finally washed trice and suspended in FACS buffer (PBS pH 7.4 supplemented with 2% (v/v) FBS) for flow cytometry analysis on BD FACSCanto™ II (BD Biosciences). Unlabeled cells were used to set the fluorescence gates and cells stained with calcein AM and PI only were used to establish the compensation settings. For each flow cytometry analysis, 10,000 events were acquired inside the respective gate.

*Neurite outgrowth - Immunohistochemistry*

The ability of hNSCs to extend neurites was assessed after 14 days of culture, under differentiation conditions, in samples processed as whole-mounts for βIII-tubulin/DNA staining. Cells/hydrogels were fixed in 3.7% (w/v) paraformaldehyde (PFA) solution diluted 1:1 in culture media (30 min; 37 ºC) and permeabilized with 0.2% (v/v) Triton X-100 in PBS (45 min; RT). Samples were then incubated with blocking buffer (5% (v/v) bovine serum albumin (BSA) in PBS) for 1 h at RT, followed by incubation with the primary antibody – mouse anti-βIII-tubulin (1:500; Biolegend, 801201), overnight at 4 ºC. To detect primary antibodies, samples were incubated with Alexa Fluor® 488 conjugated anti-mouse secondary antibody (1:1000; Life Technologies, A21202) ON at 4 ºC. The nuclei were counterstained with 0.1 μg/mL Hoechst 33342 (Life Technologies, H1399) for 20 min at RT. Samples were observed under confocal laser scanning microscopy (CLSM; TCS SP5II; Leica Mycrosystems).

## Supplementary Figures and Tables

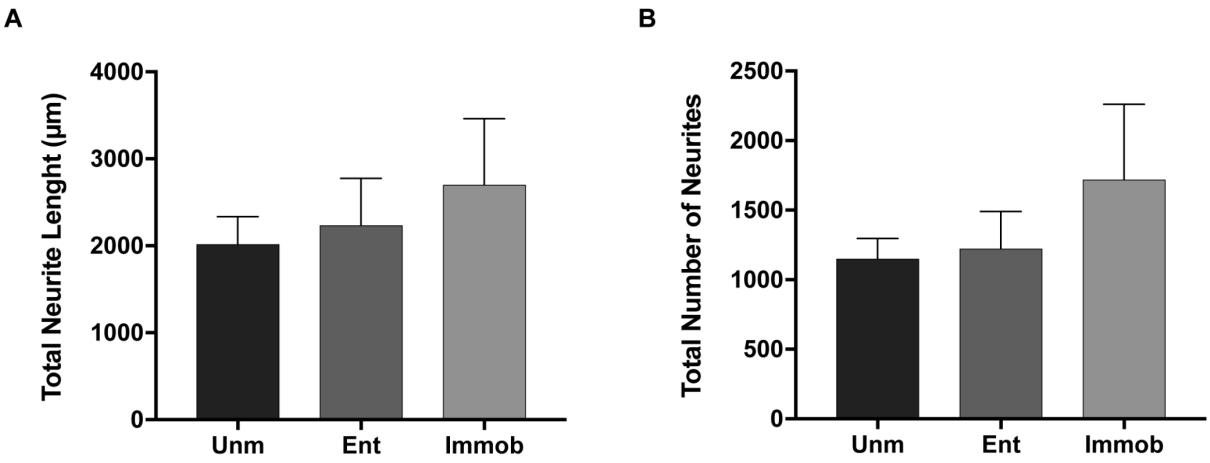


**Figure S1. Site-selective immobilization of rhLn-521 onto PEG-4MAL hydrogels and its effect on human neural stem cells (hNSC) neurite outgrowth. A)** Total neurite length; and **B)** Total number of neurites determined by quantitative analysis of images acquired in confocal laser scanning microscopy (CLSM). Data represent mean ± standard deviation (SD) of images analyzed from one representative experiment performed in triplicate. No significant differences were detected (one-way ANOVA followed by Bonferroni's test).

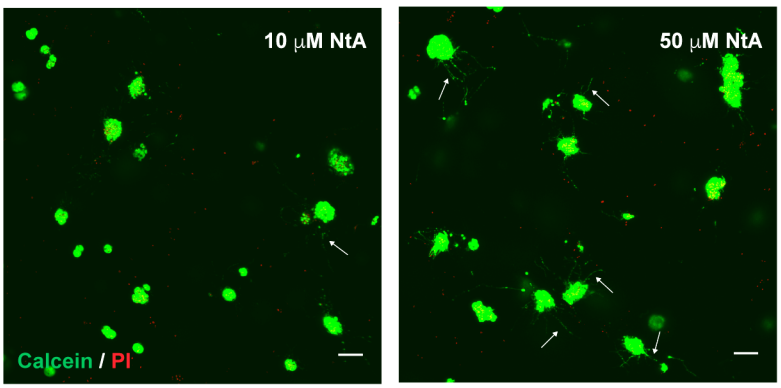


**Figure S2. Effect of NtA concentration on cell viability of hNSCs cultured within affinity-bound rhLn-521 PEG-4MAL hydrogels**. Representative two-dimensional (2D) projections of CLSM three-dimensional (3D) stack images of cell-laden hydrogels covering a thickness of 100 µm, showing the distribution of live (in green) and dead (in red) cells at day 14 of cell culture, under neuronal differentiation conditions. Arrows depict neurites protruding from neurospheres. Scale bar = 100 µm.

**Table S1.** Final amount of tethered NtA and laminin (msLn-111) incorporation into PEG-4MAL hydrogels, determined by radiolabeling analysis. Data represent mean ± SD of 3 independent experiments performed in duplicate.

| Input [NtA] (μM) | Tethered [NtA] (μM) | Laminin incorporation [msLn-111] (μg/mL) | |
|---|---|---|---|
| | | Day 1 | Day 7 |
| **0** | - | 12.9 ± 1.3 | 10.2 ± 1.0 |
| **10** | 4.1 ± 1.3 | 13.1 ± 0.6 | 10.3 ± 0.5 |
| **50** | 20.8 ± 1.7 | 11.5 ± 1.5 | 9.0 ± 0.5 |
| **100** | 34.3 ± 7.9 | 11.1 ± 1.5 | 8.3 ± 1.0 |

**Table S2.** Impact of rhLn-521 immobilization on the storage (G') and loss moduli (G'') of PEG-4MAL hydrogels, as determined by rheological analysis. Data represent mean ± standard error of the mean (SEM); n = 6; one-way ANOVA followed by Bonferroni's test; ** $p < 0.01$ (*vs.* unmodified).

| Hydrogel | Storage Modulus (G', Pa) | Loss Modulus (G'', Pa) |
|---|---|---|
| **Unmodified** | 87.5 ± 7.7 | 7.1 ± 0.7 |
| **Entrapped** | 118.2 ± 6.2 | 8.3 ± 0.5 |
| **Immobilized** | 132.5 ± 9.9 ** | 7.4 ± 0.3 |

## References

[1] S.W. Lane, D.A. Williams, F.M. Watt, Modulating the stem cell niche for tissue regeneration, Nat Biotechnol 32(8) (2014) 795-803.

[2] A. Kerever, J. Schnack, D. Vellinga, N. Ichikawa, C. Moon, E. Arikawa-Hirasawa, J.T. Efird, F. Mercier, Novel extracellular matrix structures in the neural stem cell niche capture the neurogenic factor fibroblast growth factor 2 from the extracellular milieu, Stem Cells 25(9) (2007) 2146-57.

[3] I. Kazanis, J.D. Lathia, T.J. Vadakkan, E. Raborn, R. Wan, M.R. Mughal, D.M. Eckley, T. Sasaki, B. Patton, M.P. Mattson, K.K. Hirschi, M.E. Dickinson, C. ffrench-Constant, Quiescence and activation of stem and precursor cell populations in the subependymal zone of the mammalian brain are associated with distinct cellular and extracellular matrix signals, J Neurosci 30(29) (2010) 9771-81.

[4] A. Hyysalo, M. Ristola, M.E. Makinen, S. Hayrynen, M. Nykter, S. Narkilahti, Laminin alpha5 substrates promote survival, network formation and functional development of human pluripotent stem cell-derived neurons in vitro, Stem Cell Res 24 (2017) 118-127.

[5] L. Luckenbill-Edds, Laminin and the mechanism of neuronal outgrowth, Brain Res Brain Res Rev 23(1-2) (1997) 1-27.

[6] S.K. Powell, H.K. Kleinman, Neuronal laminins and their cellular receptors, Int J Biochem Cell Biol 29(3) (1997) 401-14.

[7] S. Plantman, M. Patarroyo, K. Fried, A. Domogatskaya, K. Tryggvason, H. Hammarberg, S. Cullheim, Integrin-laminin interactions controlling neurite outgrowth from adult DRG neurons in vitro, Mol Cell Neurosci 39(1) (2008) 50-62.

[8] R.S. Rogers, H. Nishimune, The role of laminins in the organization and function of neuromuscular junctions, Matrix Biol 57-58 (2017) 86-105.

[9] H. Nishimune, G. Valdez, G. Jarad, C.L. Moulson, U. Muller, J.H. Miner, J.R. Sanes, Laminins promote postsynaptic maturation by an autocrine mechanism at the neuromuscular junction, J Cell Biol 182(6) (2008) 1201-15.

[10] S.E. Stabenfeldt, A.J. Garcia, M.C. LaPlaca, Thermoreversible laminin-functionalized hydrogel for neural tissue engineering, J Biomed Mater Res A 77(4) (2006) 718-25.

[11] S.E. Stabenfeldt, G. Munglani, A.J. Garcia, M.C. LaPlaca, Biomimetic microenvironment modulates neural stem cell survival, migration, and differentiation, Tissue Eng Part A 16(12) (2010) 3747-58.

[12] S.E. Stabenfeldt, M.C. LaPlaca, Variations in rigidity and ligand density influence neuronal response in methylcellulose-laminin hydrogels, Acta Biomater 7(12) (2011) 4102-8.

[13] A.T. Francisco, R.J. Mancino, R.D. Bowles, J.M. Brunger, D.M. Tainter, Y.T. Chen, W.J. Richardson, F. Guilak, L.A. Setton, Injectable laminin-functionalized hydrogel for nucleus pulposus regeneration, Biomaterials 34(30) (2013) 7381-8.
[14] A.T. Francisco, P.Y. Hwang, C.G. Jeong, L. Jing, J. Chen, L.A. Setton, Photocrosslinkable laminin-functionalized polyethylene glycol hydrogel for intervertebral disc regeneration, Acta Biomater 10(3) (2014) 1102-11.
[15] C.P. Addington, J.M. Heffernan, C.S. Millar-Haskell, E.W. Tucker, R.W. Sirianni, S.E. Stabenfeldt, Enhancing neural stem cell response to SDF-1alpha gradients through hyaluronic acid-laminin hydrogels, Biomaterials 72 (2015) 11-9.
[16] J. Arulmoli, H.J. Wright, D.T.T. Phan, U. Sheth, R.A. Que, G.A. Botten, M. Keating, E.L. Botvinick, M.M. Pathak, T.I. Zarembinski, D.S. Yanni, O.V. Razorenova, C.C.W. Hughes, L.A. Flanagan, Combination scaffolds of salmon fibrin, hyaluronic acid, and laminin for human neural stem cell and vascular tissue engineering, Acta Biomater 43 (2016) 122-138.
[17] C.P. Addington, S. Dharmawaj, J.M. Heffernan, R.W. Sirianni, S.E. Stabenfeldt, Hyaluronic acid-laminin hydrogels increase neural stem cell transplant retention and migratory response to SDF-1alpha, Matrix Biol 60-61 (2017) 206-216.
[18] S.A. Fisher, A.E.G. Baker, M.S. Shoichet, Designing Peptide and Protein Modified Hydrogels: Selecting the Optimal Conjugation Strategy, J Am Chem Soc 139(22) (2017) 7416-7427.
[19] C.C. Lin, K.S. Anseth, Controlling Affinity Binding with Peptide-Functionalized Poly(ethylene glycol) Hydrogels, Adv Funct Mater 19(14) (2009) 2325.
[20] J. Parker, N. Mitrousis, M.S. Shoichet, Hydrogel for Simultaneous Tunable Growth Factor Delivery and Enhanced Viability of Encapsulated Cells in Vitro, Biomacromolecules 17(2) (2016) 476-84.
[21] S.E. Sakiyama-Elbert, J.A. Hubbell, Controlled release of nerve growth factor from a heparin-containing fibrin-based cell ingrowth matrix, J Control Release 69(1) (2000) 149-58.
[22] S.E. Sakiyama-Elbert, J.A. Hubbell, Development of fibrin derivatives for controlled release of heparin-binding growth factors, J Control Release 65(3) (2000) 389-402.
[23] A. Bergeron, H. Sherman, P. Pardo, H. Gitschier, H. Nandivada, D. Saxena, Corning® rLaminin-521 (Human) for Expansion and Differentiation of Human Neural Stem Cells, Corning Incorporated | Application Note (2015).
[24] S. Rodin, L. Antonsson, C. Niaudet, O.E. Simonson, E. Salmela, E.M. Hansson, A. Domogatskaya, Z. Xiao, P. Damdimopoulou, M. Sheikhi, J. Inzunza, A.S. Nilsson, D. Baker, R. Kuiper, Y. Sun, E. Blennow, M. Nordenskjold, K.H. Grinnemo, J. Kere, C. Betsholtz, O. Hovatta, K. Tryggvason, Clonal culturing of human embryonic stem cells on laminin-521/E-cadherin matrix in defined and xeno-free environment, Nat Commun 5 (2014) 3195.

[25] D. Barros, P. Parreira, J. Furtado, F. Ferreira-da-Silva, E. Conde-Sousa, A.J. Garcia, M.C.L. Martins, I.F. Amaral, A.P. Pego, An affinity-based approach to engineer laminin-presenting cell instructive microenvironments, Biomaterials 192 (2019) 601-611.

[26] D. Barros, I.F. Amaral, A.P. Pego, Laminin immobilization, methods and uses thereof, Portuguese Provisional Patent Application no. 20181000074673, filled 2018/11/30.

[27] D. Barros, E. Conde-Sousa, A.J. Garcia, I.F. Amaral, A.P. Pego, Engineering hydrogels with affinity-bound laminin as 3D neural stem cell culture systems Manuscript in preparation (2019).

[28] J.B. Mascarenhas, M.A. Ruegg, U. Winzen, W. Halfter, J. Engel, J. Stetefeld, Mapping of the laminin-binding site of the N-terminal agrin domain (NtA), EMBO J 22(3) (2003) 529-36.

[29] A.J. Denzer, T. Schulthess, C. Fauser, B. Schumacher, R.A. Kammerer, J. Engel, M.A. Ruegg, Electron microscopic structure of agrin and mapping of its binding site in laminin-1, EMBO J 17(2) (1998) 335-43.

[30] J.D. Weaver, D.M. Headen, J. Aquart, C.T. Johnson, L.D. Shea, H. Shirwan, A.J. Garcia, Vasculogenic hydrogel enhances islet survival, engraftment, and function in leading extrahepatic sites, Sci Adv 3(6) (2017) e1700184.

[31] R. Cruz-Acuna, M. Quiros, A.E. Farkas, P.H. Dedhia, S. Huang, D. Siuda, V. Garcia-Hernandez, A.J. Miller, J.R. Spence, A. Nusrat, A.J. Garcia, Synthetic hydrogels for human intestinal organoid generation and colonic wound repair, Nat Cell Biol 19(11) (2017) 1326-1335.

[32] W.M. Han, S.E. Anderson, M. Mohiuddin, D. Barros, S.A. Nakhai, E. Shin, I.F. Amaral, A.P. Pego, A.J. Garcia, Y.C. Jang, Synthetic matrix enhances transplanted satellite cell engraftment in dystrophic and aged skeletal muscle with comorbid trauma, Sci Adv 4(8) (2018) eaar4008.

[33] E.A. Phelps, N.O. Enemchukwu, V.F. Fiore, J.C. Sy, N. Murthy, T.A. Sulchek, T.H. Barker, A.J. Garcia, Maleimide cross-linked bioactive PEG hydrogel exhibits improved reaction kinetics and cross-linking for cell encapsulation and in situ delivery, Adv Mater 24(1) (2012) 64-70, 2.

[34] N.O. Enemchukwu, R. Cruz-Acuna, T. Bongiorno, C.T. Johnson, J.R. Garcia, T. Sulchek, A.J. Garcia, Synthetic matrices reveal contributions of ECM biophysical and biochemical properties to epithelial morphogenesis, J Cell Biol 212(1) (2016) 113-24.

[35] J. Patterson, J.A. Hubbell, Enhanced proteolytic degradation of molecularly engineered PEG hydrogels in response to MMP-1 and MMP-2, Biomaterials 31(30) (2010) 7836-45.

[36] J. Silva, A.R. Bento, D. Barros, T.L. Laundos, S.R. Sousa, P. Quelhas, M.M. Sousa, A.P. Pego, I.F. Amaral, Fibrin functionalization with synthetic adhesive ligands interacting with alpha6beta1 integrin receptor enhance neurite outgrowth of embryonic stem cell-derived neural stem/progenitors, Acta Biomater 59 (2017) 243-256.

[37] L.A. Flanagan, Y.E. Ju, B. Marg, M. Osterfield, P.A. Janmey, Neurite branching on deformable substrates, Neuroreport 13(18) (2002) 2411-5.
[38] A.J. Engler, S. Sen, H.L. Sweeney, D.E. Discher, Matrix elasticity directs stem cell lineage specification, Cell 126(4) (2006) 677-89.
[39] P.C. Georges, W.J. Miller, D.F. Meaney, E.S. Sawyer, P.A. Janmey, Matrices with compliance comparable to that of brain tissue select neuronal over glial growth in mixed cortical cultures, Biophys J 90(8) (2006) 3012-8.
[40] K. Saha, A.J. Keung, E.F. Irwin, Y. Li, L. Little, D.V. Schaffer, K.E. Healy, Substrate modulus directs neural stem cell behavior, Biophys. J. 95(9) (2008) 4426-38.
[41] A. Banerjee, M. Arha, S. Choudhary, R.S. Ashton, S.R. Bhatia, D.V. Schaffer, R.S. Kane, The influence of hydrogel modulus on the proliferation and differentiation of encapsulated neural stem cells, Biomaterials 30(27) (2009) 4695-9.
[42] S.R. Hynes, M.F. Rauch, J.P. Bertram, E.B. Lavik, A library of tunable poly(ethylene glycol)/poly(L-lysine) hydrogels to investigate the material cues that influence neural stem cell differentiation, J Biomed Mater Res A 89(2) (2009) 499-509.
[43] I.O.f. Standardization, ISO 10993-5:2009 : Biological evaluation of medical devices Tests for in vitro cytotoxicity, 2009.
[44] Iodine-125, a guide to radioiodination techniques, A.L. Sciences (Ed.) Amersham International, Little Chalfont, Buckinghamshire, UK, 1993, p. p. 64.
[45] M. Rubinstein, R.H. Colby, Polymer physics, Oxford University Press, 2003.

# CHAPTER VIII

AG73-Functionalized Synthetic Hydrogels Support Neural Stem Cell Survival, Proliferation and Neurite Outgrowth

# AG73-Functionalized Synthetic Hydrogels Support Neural Stem Cell Survival, Proliferation and Neurite Outgrowth

Daniela Barros [1,2,3], Andrés J. García [4,5], Isabel Freitas Amaral [1,2,6], Ana Paula Pêgo [1,2,3,6]

[1] i3S - Instituto de Investigação e Inovação em Saúde, Universidade do Porto (UPorto), Portugal

[2] INEB - Instituto de Engenharia Biomédica, UPorto, Portugal

[3] ICBAS - Instituto de Ciências Biomédicas Abel Salazar, UPorto, Portugal

[4] Parker H. Petit Institute for Bioengineering and Biosciences, Georgia Institute of Technology, Atlanta, Georgia, USA

[5] George W. Woodruff School of Mechanical Engineering, Georgia Institute of Technology, Atlanta, Georgia, USA

[6] FEUP - Faculdade de Engenharia, UPorto, Portugal

**Abstract**

Synthetic-based hydrogels engineered to mimic some of the elements of the native extracellular matrix (ECM), constitute highly attractive platforms to study neural stem cell (NSC) biology and better understand the interactions with the surrounding microenvironment. By allowing a precise and independent control over the biochemical and biophysical properties of the matrix, these hydrogels enable the systematic study of their effects on cell behavior and function, thus addressing some of the main challenges associated with the design of well-defined matrices for three-dimensional (3D) cell culture systems. However, as these materials are usually bioinert, their modification with cell adhesive motifs / bioactive domains, found in proteins comprised in the native NSC niches, is highly desirable. Cell adhesive motifs interacting with syndecan receptors were showed to have a key role on the regulation of NSC fate lineage, and thus constitute a highly attractive option for the design of biomimetic matrices. Accordingly, in this work we proposed the tethering of the AG73 (RKRLQVQLSIRT) peptide sequence, from the LG4 globular domain of laminin $\alpha$1 chain, into a degradable synthetic-based hydrogel. A four-arm maleimide terminated poly(ethylene glycol) (PEG-4MAL) was chosen as the base material. The modular nature of the synthetic matrix used, allowed us to explore the effect of AG73 peptide density on cell behavior, independently of other hydrogel biophysical and biochemical properties. The tethering of AG73 peptide to PEG-4MAL hydrogels led to a significant improvement of cell viability, after 7 days in culture, independently of the input peptide concentration tested. The potential of this 3D culture system to support human NSC (hNSC) proliferation and neurite outgrowth was further evidenced at a higher input AG73 concentration (1 mM). This was demonstrated by the significant increase in cell proliferation ($p$ = 0.0012 *vs.* 0 mM) and neurite outgrowth ($p$ < 0001 *vs.* 0 mM) found after 14 days of culture, as well as by the neuronal network established at this same time point. These results highlight the potential of syndecan-binding adhesive motifs for the biofunctionalization of 3D synthetic hydrogel platforms designed for the culture of hNSC, and potentially for use as vehicles of neural stem/progenitor cells in the context of central nervous system (CNS) injury/regeneration, foreseeing a better efficacy of the available therapeutic strategies.

## 1. Introduction

Neural stem cells (NSCs) are multipotent cells that hold great potential for application in regenerative medicine and tissue engineering, namely for the treatment of central nervous system (CNS) disorders (*e.g.* traumatic brain and spinal cord injury and neurodegenerative diseases, such as Parkinson's and Alzheimer's disease) [1-3]. Nevertheless, the successful application of these cells in a regenerative context is still hampered by the lack of understanding of the regulatory role of the different niche components on the modulation of NSC behavior and fate. Therefore, the development of new three-dimensional (3D) platforms incorporating different physical and chemical elements of the native NSC niches is highly desirable. Ultimately, one expects these provide a better understanding into stem cell biology and interactions with the surrounding microenvironment and allow to overcome some of the main drawbacks limiting the efficacy of current stem cell-based therapies. The latter include, low cell survival, inability to control specific cell differentiation and functionality and poor cell engraftment within the host tissue upon transplantation [4]. In this regard, hydrogels have been widely explored, for the development of cell-instructive microenvironments, as they are well-defined and tunable matrices that share many key physical properties with native ECM/tissues (*e.g.* high-water content, good permeability and elasticity) [5, 6].

Matrix adhesiveness is a critical factor to take into consideration when designing cell-compatible hydrogels, as this will significantly impact the modulation of NSC function (*e.g.* viability, proliferation, outgrowth and differentiation). Therefore, several works have explored the incorporation of bioactive cell adhesive domains, found in the native NSC niche, to confer to hydrogels the ability to modulate cell function and fate. More specifically, synthetic adhesive peptides derived from fibronectin (RGD [7-10]) or laminin (YIGSR [7, 10-12], IKVAV [7, 10, 12-14], RNIAEIIKDI [7]) were used. These peptides can mediate cell interaction *via* integrin receptors, which play a key role in cell adhesion and outgrowth/migration [15]. Alternatively, the use of cell binding ligands interacting with transmembrane heparan sulfate proteoglycans (HSPGs) has become highly attractive to engineer biomimetic matrices, for application in advanced NSC-based therapies, as result of their key role in the regulation of NSC stemness [16]. Syndecans in particular, have a pivotal role on the modulation of all stages of stem cell maintenance and neurogenesis (*e.g.* proliferation, self-renewal, differentiation, migration and maturation), either through independent signaling or by working alongside with other receptors, such as integrins [17-19]. To date, four members of the syndecan family were identified in mammals (Syndecan-1, -2, -3 and -4) and their expression was found to differ among different cells and tissues [20]. More specifically, within the NSC niche, syndecan-1 is highly expressed during

neurogenesis being key to support NSC proliferation and progenitor cell maintenance [21, 22], while syndecan-4 constitutes a key marker of NSC differentiation [16]. Syndecan-3 [23], in turn, plays an essential role on the modulation of axon guidance [24, 25] and neurite outgrowth [26, 27], and, together with syndecan-4 [28], controls neuronal migration. Lastly, syndecan-2 expression is known to exert a remarkable effect in dendritic spine morphogenesis [29]. AG73 (RKRLQVQLSIRT), a synthetic peptide derived from the laminin globular 4 (LG4) module of laminin $\alpha$1 chain, interacts with syndecan-1 [30, 31] and -4 [32] promoting cell adhesion with membrane ruffling [33-35]. In addition, this peptide showed already great potential to enhance neurite outgrowth of PC12 neuronal cells when tethered onto alginate- [36], collagen- [37] or agarose- [38] based hydrogels, as well as onto chitosan membranes [35]. In a previous study from our lab, we also showed that functionalization of fibrin hydrogels with AG73 improves cell outgrowth of human NSCs (hNSCs) [39]. Despite the promising results obtained to date, the intrinsic bioactivity presented by natural-based polymers makes difficult to deconvolute the contribution of the syndecan-binding peptide to the final biological outcome. Synthetic-based polymers, in turn, are chemically-defined materials that allow a precise and independent control over the biochemical and biophysical properties of the matrix, thus allowing a systematic study of their effects on cell behavior/function [5]. Moreover, although these materials are usually biological inert, they can be easily engineered to include biological signals (*e.g.* adhesive cues, growth factors or protease-sensitive sequences) [5]. Therefore, they constitute a valuable resource when deciphering the intricate relationship between the matrix components and their possible individual influence on cell behavior. In this work, we aim to explore a synthetic-based hydrogel to assess the effect of the AG73 syndecan-binding peptide on the modulation of hNSC behavior. A hydrogel based on a four-arm maleimide terminated poly(ethylene glycol) (PEG-4MAL) macromer, previously optimized by our group [40], was herein explored (Fig. 1). The modular nature of these hydrogels allows an independent control over their mechanical and structural properties, cell-adhesive ligand type/density and protease-dependent degradation [41, 42], which enabled the testing of different AG73 densities, independently of other hydrogel parameters. PEG-4MAL macromer was first functionalized with different input AG73 peptide concentrations (Fig. 1). To allow a time frame of 3D culture sufficient for hNSCs proliferation and neuronal differentiation, a mix of protease degradable (cysteine-flanked matrix metalloproteinase 2 (MMP2)-sensitive peptide) [43] and non-degradable (PEG-dithiol) cross-linkers was used to mediate, under physiological conditions, the formation of a degradable hydrogel network (Fig. 1).

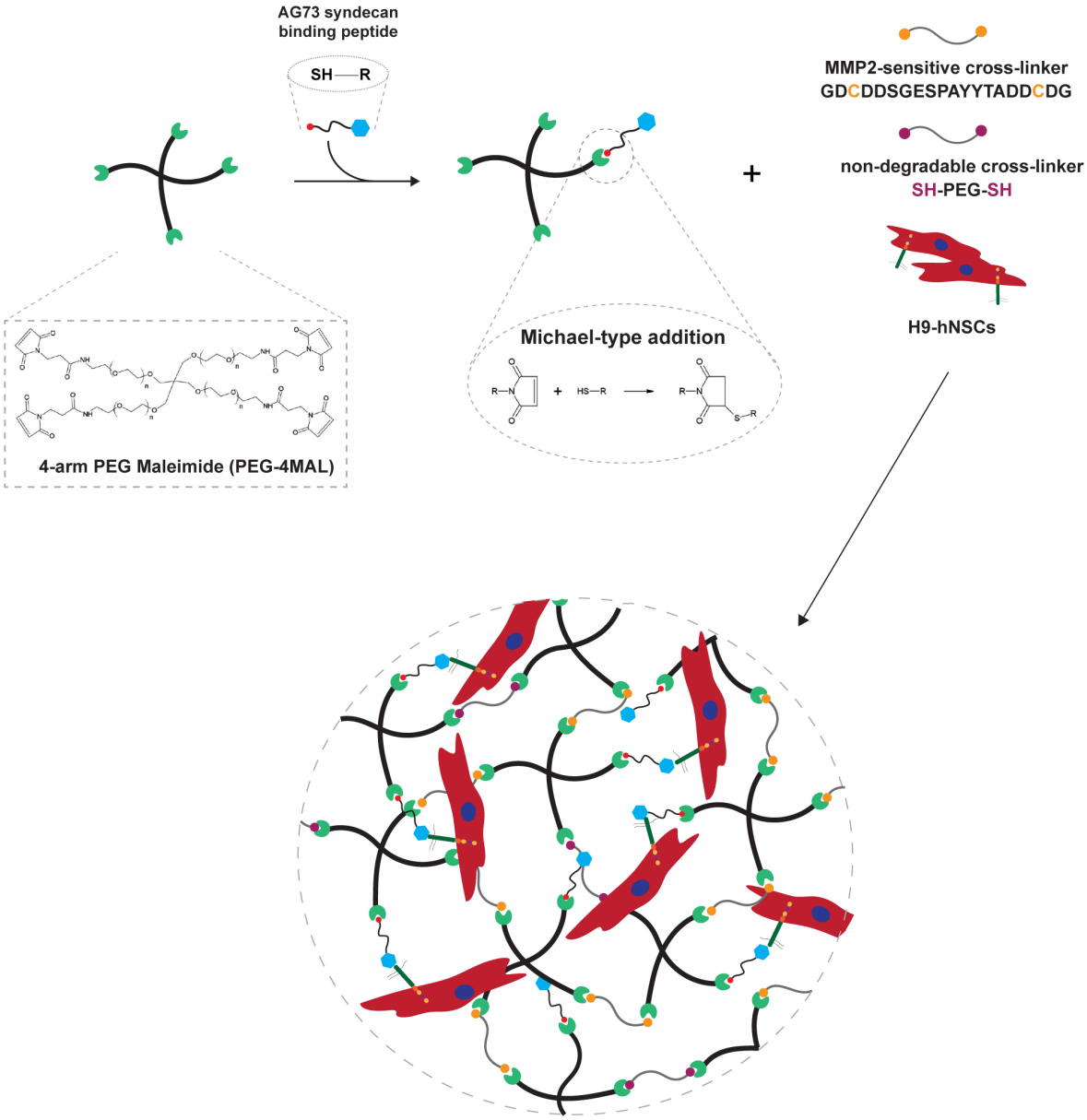


**Figure 1**. **Schematic representation of the preparation of cell-laden AG73-functionalized PEG-4MAL hydrogels (not to scale).** PEG-4MAL is firstly functionalized with a thiol-containing AG73 peptide. Functionalized PEG-4MAL is then reacted with a mixture of protease degradable (MMP2-sensitive peptide) and non-degradable (PEG-dithiol) cross-linkers to allow the formation, under physiological conditions, of a hydrogel network in the presence of cells.

The resultant hydrogel was characterized in terms of fragment density and the potential of different input concentrations of the syndecan-binding peptide to support hNSC viability, proliferation and neurite outgrowth was further assessed. A significant improvement in cell proliferation and neurite outgrowth, as well as the establishment of a neuronal network, were observed after 14 days of culture, for hydrogels modified with the higher input AG73

concentration (1 mM). In summary, this study evidences the potential of syndecan-binding adhesive motifs, for the design of 3D hydrogel platforms for the culture and transplantation of hNSCs.

## 2. Materials and Methods

### 2.1. Hydrogel components

A four-arm maleimide terminated poly(ethylene glycol) (PEG-4MAL; 40 kDa, > 95% purity, > 90% substitution, Jenkem USA) was chosen as the hydrogel base material. A macromer solution was prepared in 10 mM 4-(2-hydroxyethyl)piperazine-1-ethanesulfonic acid (HEPES) in phosphate buffered saline (PBS, pH 7.4) at a final polymer concentration of 10.0% (w/v). The syndecan-binding peptide AG73 (Acetyl (Ac)-*C*GG**RKRLQVQLSIRT**-Amide ($NH_2$), 1.7 kDa, > 90% purity) was obtained from GenScript. A cysteine-flanked matrix metalloproteinase-2 (MMP2)-sensitive peptide (Acetyl (Ac)-GD*C*DD**SGESPAY↓YTA**DD*C*DG-Amide ($NH_2$); 2.1 kDa, > 85% purity, GenScript) and a PEG-dithiol (3.5 kDa, ≥ 95% purity, Jenkem USA) were used as the degradable and non-degradable cross-linkers, respectively.

### 2.2. AG73 tethering efficiency

To determine the tethering efficiency of AG73 to PEG-4MAL, free/unreacted thiols in the reaction mixture were quantified using the Measure-iT thiol assay kit (Invitrogen) according to the manufacturer's instructions. Briefly, PEG-4MAL was functionalized with the syndecan-binding peptide AG73 (input AG73 concentration: 0.01, 0.1, 0.5 or 1 mM) for 15 min in 10 mM HEPES in PBS (pH 7.4). The samples were then mixed with thiol-quantitation reagent in a black 96-well plate and the fluorescence measured ($\lambda_{ex}$ = 494 nm; $\lambda_{em}$ = 517 nm) using a microwell plate reader (BioTek® Synergy™ Mx). A calibration curve of glutathione (0 – 55 μM) was used to calculate the concentration of free thiols.

### 2.3. Preparation of AG73-functionalized PEG-4MAL hydrogels

A schematic representation of AG73-functionalized PEG-4MAL hydrogel preparation is presented in Fig. 1. Briefly, PEG-4MAL was first functionalized with the syndecan-binding peptide AG73 for 15 min in 10 mM HEPES buffer (pH 7.4). Different AG73 input concentrations were used – 0.01, 0.1, 0.5 and 1 mM. Functionalized PEG-4MAL macromers were then cross-linked into a hydrogel by addition of a mix of a MMP2-sensitive peptide and a PEG-dithiol prepared in 10 mM HEPES in PBS (pH 6.5), at an 80:20 molar ratio (%). The cross-linkers were added at a 1:1 molar ratio of cysteine residues on the cross-linkers to remaining maleimide groups on PEG-4MAL macromer, following functionalization with

AG73. Hydrogels were polymerized at 37 ºC, 5% $CO_2$ for 15 min. Unmodified (0 mM) PEG-4MAL gels were also prepared and used as controls.

### 2.4. Culture of human neural stem cells

Human neural stem cells (hNSCs) derived from the NIH approved H9 (WA09) human embryonic stem cell line were purchased from Life Technologies (N7800-200). Cells were expanded according to the manufacturer's protocol on poly(ornithine)/laminin-111 from mouse Engelbreth-Holm-Swarm sarcoma (msLn-111)-coated tissue coated polystyrene (TCPS) plates (Corning) in expansion medium - StemPro® NSC serum-free medium (SFM) (Life Technologies) supplemented with basic fibroblast growth factor (bFGF, 20 ng/mL; Life Technologies) and epidermal growth factor (EGF, 20 ng/mL; Life Technologies).

### 2.5. Culture of hNSCs within AG73-functionalized hydrogels

hNSCs were dissociated into single cells using StemPro accutase cell dissociation reagent (Life Technologies) and further suspended in the solution containing AG73-functionalized PEG-4MAL precursors (4 x $10^6$ viable cells/mL). Cell-laden hydrogels were formed by mixing the PEG-4MAL precursor solution containing cells with the MMP2-sensitive peptide and PEG-dithiol cross-linkers, dissolved in 10 mM HEPES (pH 6.5), at an 80:20 molar ratio (%), and subsequently incubating the polymerizing gels at 37ºC, 5% $CO_2$ for 15 minutes. hNSCs were initially cultured in expansion medium and, at day 2 of culture, the medium was switched to the StemPro NSC SFM media-Neurobasal/B27 (Life Technologies) (1:1) mix, without growth factors. At day 8, half of the medium was replaced by the StemPro NSC SFM-Neurobasal/B27 (1:3) mix supplemented with 10 ng/mL of brain-derived neurotrophic factor (BDNF; Peprotech) and 500 μM of $N^6$, 2'-O-Dibutyryladenosine 3', 5'-cyclic monophosphate sodium salt (dibutyril cAMP; Sigma). Half of the medium was changed every other day, up to 14 days. hNSCs cultured within unmodified (0 mM) PEG-4MAL gels were herein used as controls.

### 2.6. Cell viability

The distribution of viable and dead cells within PEG-4MAL hydrogels was assessed at day 7 of cell culture using a live/dead assay. Cell-hydrogel matrices were rinsed with warm PBS pH 7.4 and incubated with 4 μM calcein AM (Life Technologies) and 6 μM propidium iodide (PI; Life Technologies) at 37 ºC for 30 min, for detection of viable and dead cells, respectively. After incubation, the samples were rinsed twice with PBS pH 7.4, transferred to culture medium, and immediately observed under confocal laser scanning microscopy (CLSM, Leica TCS SP5; Leica Mycrosystems). z-sections, covering a thickness of 300 μm, were acquired using an HC Plan APO CS 10× / 0.40 NA objective and subsequently

projected into 2D images. Quantitative analysis of cell viability was conducted by immunocytometry performed in six-pooled hydrogels, after hydrogel dissociation. Briefly, the hydrogels were sequentially incubated with 1.25 mg/mL of collagenase type II (Gibco; 1h at 37 ºC) and StemPro accutase cell dissociation reagent (Life Technologies; 20 min at 37 ºC, 70 rpm). Cells were mechanically dissociated by pipetting, diluted in Glasgow Minimal Essential Medium (GMEM; Life Technologies) supplemented with 10% (v/v) inactivated fetal bovine serum (FBS) and centrifuged. For live/dead staining, cells were then transferred to a round-bottomed 96-well plate and stained with calcein AM (67 nM, 20 min at 37 ºC) and PI (6 μM, 10 min at 37 ºC). Cells were finally washed trice and suspended in FACS buffer (PBS pH 7.4 supplemented with 2% (v/v) FBS) for flow cytometry analysis (BD FACSCanto™ II, BD Biosciences). Unlabeled cells were used to set the fluorescence gates and cells stained with calcein AM or PI were used to establish the compensation settings. For each flow cytometry analysis, 10,000 events were acquired.

### 2.7. DNA quantification

The growth of hNSCs cultured within PEG-4MAL hydrogels was estimated from total cell number after 7 days of cell culture, using the CyQUANT® cell proliferation assay kit (Life Technologies), according to manufacturer's instructions. Briefly, cells were extracted from the hydrogels, through sequential incubation with 1.25 mg/mL of collagenase type II (Gibco; 1 h at 37 ºC) and StemPro accutase cell dissociation reagent (Life Technologies; 20 min at 37 ºC) under stirring (70 rpm). Cells were mechanically dissociated by pipetting, diluted in GMEM (Life Technologies) supplemented with 10% (v/v) FBS, centrifuged and the cell pellet stored at -80 ºC. Cell pellet was then thawed at room temperature (RT) and incubated with CyQUANT® GR dye/cell lysis buffer. Fluorescence ($\lambda_{ex}$ = 480 nm; $\lambda_{em}$ = 520 nm) was measured, after mixing with CyQUANT GR dye, in a microwell plate reader (BioTek® Synergy™ Mx). The total number of cells for each condition was estimated from a standard curve generated with a known amount of hNSCs over a range of 50 to 250,000 cells. Cell samples used to generate the standard curve were measured in triplicate. For each condition, hydrogels without cells, cultured in parallel and processed similarly to those with cells, were used as blanks and their background fluorescence values subtracted.

### 2.8. hNSC neurite outgrowth

The effect of different input AG73 concentrations on neurite outgrowth was assessed after 14 days of culture, under neuronal differentiation conditions. Samples were processed as whole-mounts for βIII-tubulin/DNA staining. Cell-laden hydrogels were fixed in 3.7% (w/v) paraformaldehyde (PFA) solution diluted 1:1 in culture medium (30 min; 37 ºC) and permeabilized with 0.2% (v/v) Triton X-100 in PBS (45 min; RT). Samples were then

incubated with blocking buffer (5% (v/v) bovine serum albumin (BSA) in PBS) for 1 h at RT, followed by incubation with the primary antibody – mouse anti-βIII-tubulin (1:500; Biolegend, 801201), overnight (ON) at 4 ºC. To detect primary antibodies, samples were incubated with Alexa Fluor® 488 conjugated anti-mouse secondary antibody (1:1,000; Life Technologies, A21202) ON at 4 ºC. The nuclei were counterstained with 0.1 μg/mL Hoechst 33342 (Life Technologies, H1399) for 20 min at RT. z-sections, covering a thickness of 200 μm or 100 μm, were acquired with the CLSM using an HC Plan APO CS 10× / 0.40 NA objective with a zoom factor of 1 or 2, respectively, and subsequently projected into 2D images. Neurite outgrowth was assessed in the projected 2D images using a developed ImageJ script. Briefly, nuclei were segmented through an Otsu thresholding method, while neurites were segmented through subtraction of the previously identified nucleus, using a Huang thresholding method. Measurements were obtained for total neurite length (μm) and total number of neurites per image.

### 2.9. Statistical Analysis

Statistical analysis was performed using GraphPad Prism 6 software (San Diego). Sample distribution was initially tested for normality using the Kolmogorov-Smirnov test. Comparisons with control conditions were performed with one-way ANOVA analysis, followed by the Dunnett's two-tailed test. For all analysis, differences were considered significant at $p < 0.05$.

## 3. Results and Discussion

### 3.1. AG73 peptide is efficiently tethered to PEG-4MAL hydrogels

The key role of syndecans on the regulation of neural stem cell (NSC) fate lineage, make these heparan sulfate proteoglycans (HSPGs) highly attractive therapeutic targets when considering the biofunctionalization of synthetic matrices. As such, in this study we explored the functionalization of a bioinert degradable synthetic hydrogel with AG73 (RKRLQVQLSIRT), a synthetic peptide derived from the laminin globular 4 (LG4) module of laminin α1 chain that interacts with syndecan-1 and -4 [30-32]. For this purpose, an hydrogel platform based on a four-arm maleimide terminated poly(ethylene glycol) (PEG-4MAL) macromer (Fig.1) was selected as the base material for this work, due to its modular nature, excellent *in vitro* and *in vivo* biocompatibility with different cell types [40, 42, 44, 45] and well characterized biochemical and biophysical properties [41, 42, 46]. Maleimide groups in PEG-4MAL macromers efficiently react with thiol-containing peptides through Michael-type addition, enabling a fine tuning of ligand incorporation, and thus the formation of structurally defined matrices. To assess the effect of AG73 peptide density on the human

NSC (hNSC) biological response, PEG-4MAL macromers were covalently modified with different concentrations of this syndecan-binding peptide (0, 0.01, 0.1, 0.5 or 1mM) and the conjugation efficiency determined by measuring the amount of free/unreacted thiols in the reaction mixture. Free thiols were not detected (< 0.05 μM), the lower detection limit of the assay), indicating that AG73 was tethered onto the PEG-4MAL macromer with an immobilization efficiency higher than 96%, for all the concentrations tested.

### 3.2. AG73-presenting PEG-4MAL hydrogels support hNSC viability and proliferation

To get insight into the effect of AG73 density on hNSC survival and proliferation, cells were cultured for 7 days within degradable PEG-4MAL hydrogels functionalized with different AG73 concentrations (0, 0.01, 0.1, 0.5 and 1 mM). Confocal microscopy analysis showed, for all the conditions tested, the presence of live cells evenly distributed throughout the hydrogels, often growing as cellular spheroids (Fig. 2A). The quantitative analysis of live/dead cells, assessed by flow cytometry, showed values of average viability greater than 75% for all the conditions tested, evidencing the good cytocompatibility of the proposed matrices [47] (Fig. 2B). Interestingly, hydrogels functionalized with AG73 evidenced a significantly higher percentage of viable cells compared to plain hydrogels ($p < 0.0214$ *vs.* 0 mM; Fig. 2B).

The tethering of AG73 peptide enhanced the ability of PEG-4MAL hydrogels to support hNSC growth, as shown by the higher cell numbers found at day 7 of cell culture compared to those observed for unmodified hydrogels (Fig. 2C). This effect was significant for the highest input AG73 concentration tested (1 mM; $p = 0.0012$; *vs.* 0 mM), for which a 3.0-fold increase in cell number (*vs.* 0 mM) was observed.

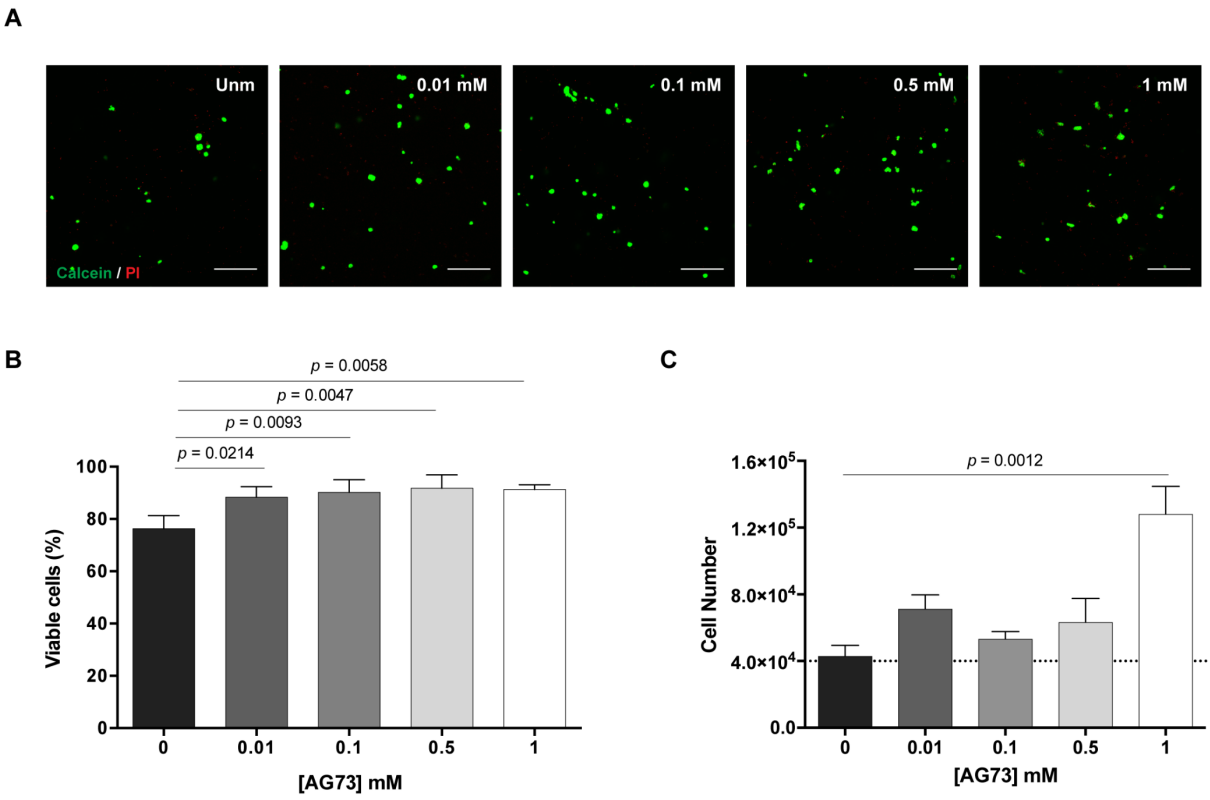


**Figure 2. hNSC viability and proliferation in AG73-functionalized PEG-4MAL hydrogels as a function of input peptide concentration. A)** Representative 2D projections of CLSM 3D stack images of cell-laden hydrogels covering a thickness of 300 μm, showing the distribution of live (in green) and dead (in red) cells at day 7 of cell culture. Scale bar = 300 μm. **B)** Quantitative analysis of live and dead cells at day 7, as determined by flow cytometry. Data represent mean ± SD of three independent experiments; one-way ANOVA followed by Dunnett's test (*vs.* 0 mM). **C)** Quantitative analysis of total cell number at day 7, as determined by CyQuant® Cell Proliferation kit. Data represent mean ± standard error of the mean (SEM) of three independent experiments performed in triplicate; one-way ANOVA followed by Dunnett's test (*vs.* 0 mM).

### 3.3. The tethering of 1 mM AG73 render PEG-4MAL hydrogels permissive to neurite outgrowth

To unveil the effect of AG73 concentration on neurite outgrowth, hNSCs were cultured for 14 days under differentiation conditions, and then processed as whole-mounts for βIII-tubulin and DNA staining (Fig. 3). Qualitative analysis of CLSM images (Fig. 3A) showed a population of differentiated neurons, expressing βIII-tubulin and starting to form a neuronal network in PEG-4MAL hydrogels functionalized with 1 mM of AG73. For lower input peptide concentrations, the establishment of a neuronal network was less evident (Fig. 3A). Differences between conditions were assessed by image processing and quantitative analysis, using ImageJ/Fiji. More specifically, total neurite length (μm) and total number of

neurites were quantified (Fig. 3B-D). A significant increase in the neurite outgrowth, relative to unmodified (0 mM) hydrogels, was observed for the input peptide concentration of 1 mM. In these AG73-derivatized hydrogels, total neurite length evidenced an 18.6-fold increase ($p < 0.0001$ *vs.* 0 mM; Fig. 3C) while that correspondent to the total number of neurites showed a 15.2-fold increase ($p < 0.0001$ *vs.* 0 mM; Fig. 3D). Previous studies from our group using fibrin hydrogels, showed that fibrin functionalization with low concentrations of AG73 (60 μM) was effective in promoting hNSC outgrowth [39]. Fibrinogen, one of the components of these natural-based hydrogels, has heparin-binding domains at its N-terminus with high affinity to syndecans [48, 49], which can potentiate the effect of AG73, even at low concentrations. PEG-4MAL hydrogels, in turn, due to the lack of integrin or heparin-binding motifs, as result of their bioinert nature, require higher peptide concentrations to exert similar effect.

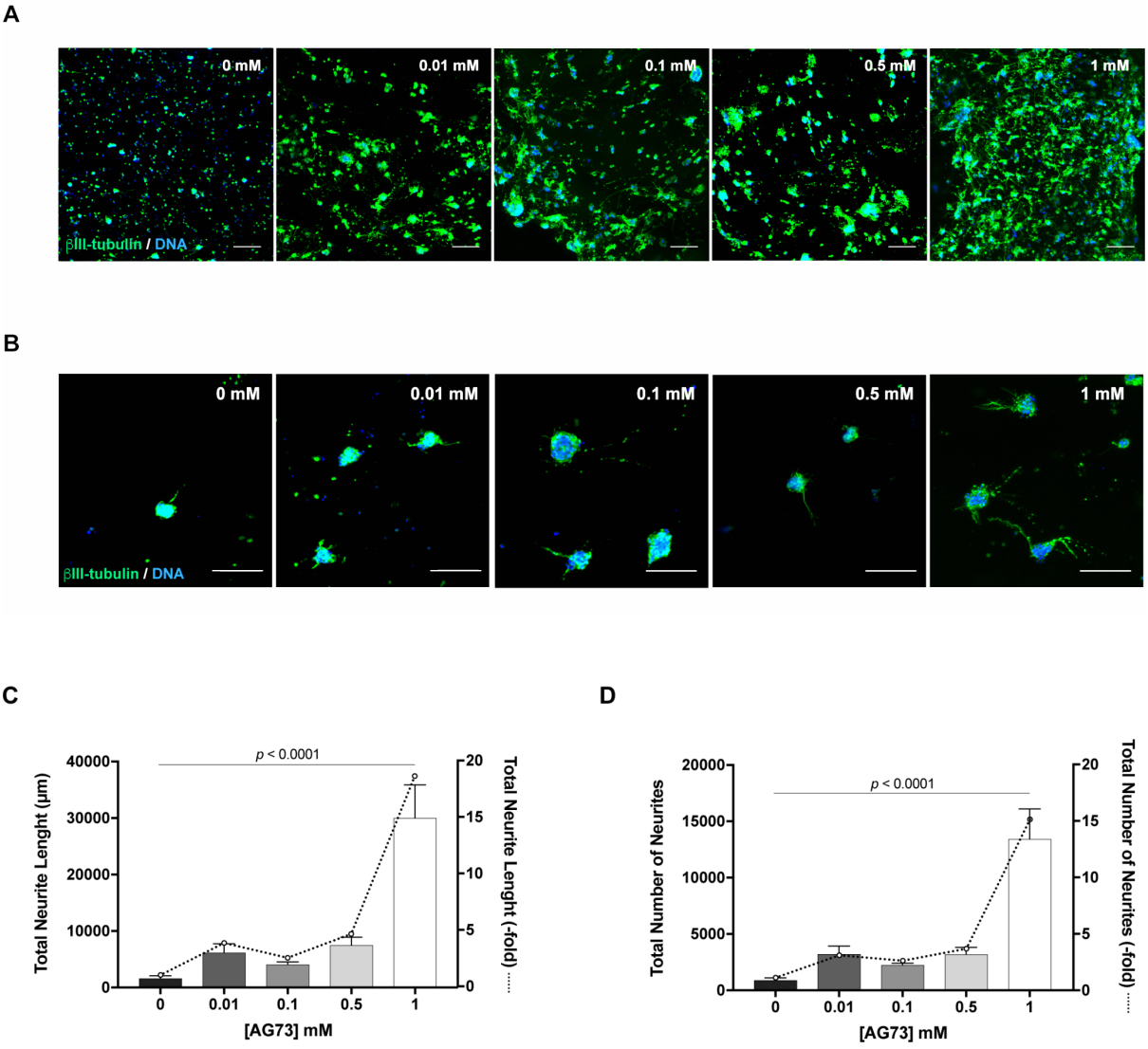


**Figure 3**. **Effect of AG73 input concentration on hNSC neurite outgrowth. A)** hNSCs cultured within unmodified (0 mM) and AG73-functionalized (0.01, 0.1, 0.5 and 1 mM) PEG-4MAL hydrogels

after 14 days of culture, under differentiation conditions. Images are representative of 2D projections of CLSM 3D stack images of cells processed for immunofluorescence labeling of βIII-tubulin/DNA, covering a thickness of 200 μm. Arrows depict neurites expressing βIII-tubulin protruding from neurospheres. Scale Bar = 200 μm. **B)** Representative 2D projections of CLSM 3D stack of hNSC outgrowth, covering a thickness of 200 μm, after 14 days of culture under differentiation conditions. Scale Bar = 100 μm. **C)** Total Neurite Length; and **D)** Total Number of Neurites determined by quantitative analysis of images acquired in CLSM. Absolute values (bars) and values normalized to outgrowth in 0 mM AG73 hydrogels (dotted line) are presented. Data represent mean ± SD of 10 images analyzed per condition; one-way ANOVA followed by Dunnett's test (*vs.* 0 mM).

Hydrogel mechanical and structural properties have a key role on the modulation of different cellular functions, including survival, proliferation and neurite outgrowth [41, 42, 46]. With this in mind, we hypothesize that the significant increase in cell number and neurite outgrowth observed for PEG-4MAL hydrogels functionalized with the highest input AG73 concentration (1 mM), may be also related with alterations in mechanical and structural properties of the hydrogel, resultant from the incorporation of a synthetic peptide. In a 3D microenvironment the processes involved on the modulation of different cell functions, including migration and neurite outgrowth, depend not only on the presence of cell adhesion domains but also on the ability of cells to degrade the surrounding matrix. Therefore, and although most of the studies published to date focus in understanding the independent contribution of each of these parameters for cell function, understanding how matrix bioactivity and mechanical properties influence each other and the impact of that concerted action on the modulation of cell behavior is highly desirable. Indeed, a study assessing the influence of cell-adhesive peptides (RGDS, IKVAV and YIGSR) on a PEG hydrogel physical and mechanical properties, showed that depending on the ligand type and concentration, the extent of their impact and whether a ligand increases or decreases a specific property, will be different [50]. Therefore, studies to understand how the AG73 tethering impacts PEG-4MAL hydrogel mechanical and structural properties, and how that correlates with the observed biological outcome, should be conducted.

To better recapitulate the biological activity of laminin chains, different studies proposed the combination of laminin-derived synthetic adhesive peptides targeting different cell receptors (*e.g.* integrins and syndecans). Indeed, the modification of chitosan membranes with a combination of syndecan- (AG73) and integrin- (A2G10, A99a or EF1zz) binding peptides, evidenced the synergistic ability of these peptides to enhance different cell functions, including PC12 cell adhesion and neurite outgrowth [51, 52]. Moreover, the characterization of the expression profile of integrins and syndecans in H9-derived NSCs, previously performed by our group, showed that 93% of the cells expressing syndecan-1 also

expressed the integrin $\alpha$6 subunit [53]. Considering all these evidences, future studies should address the functionalization of PEG-4MAL hydrogels with a combination of AG73 peptide and integrin-binding ligands, and its additive or synergistic effect on neurite outgrowth.

## 4. Conclusions

The present work demonstrates that a fine control over AG73-binding peptide density allows to maximize hNSC proliferation and neurite outgrowth, within PEG-4MAL hydrogels. However, and despite the promising results obtained, future studies need to be conducted to validate the observations presented in this work and better understand the role of AG73-syndecan-binding peptide on the modulation of hNSC behavior/function. Overall, the proposed hydrogels showed great potential to be used as 3D platforms for the *in vitro* culture of hNSCs and, potentially, as vehicles for cell transplantation in the context of nervous system regeneration/disorders.

## Acknowledgments

Confocal microscopy was conducted at the Bioimaging i3S Scientific Platform, member of the PPBI (PPBI-POCI-01-0145-FEDER-022122), with the assistance of Maria Lázaro. This work was funded by projects NORTE-01-0145-FEDER-000008 and NORTE-01-0145-FEDER-000012, supported by Norte Portugal Regional Operational Programme (NORTE 2020), under the PORTUGAL 2020 Partnership Agreement, through the European Regional Development Fund (ERDF) and FEDER - Fundo Europeu de Desenvolvimento Regional funds through the COMPETE 2020 - Operacional Programme for Competitiveness and Internationalisation (POCI), Portugal 2020; by Portuguese funds through FCT/MCTES in the framework of the project "Institute for Research and Innovation in Health Sciences" (POCI-01-0145-FEDER-007274), and by Santa Casa da Misericordia de Lisboa through project COMBINE (Prémio Neurociências Melo e Castro 1068-2015).
D.B. was supported by FCT PhD Programs (PD/BD/105953/2014) and Programa Operacional Potencial Humano (POCH), in the scope of the BiotechHealth Program (Doctoral Program on Cellular and Molecular Biotechnology Applied to Health Sciences), Programa FLAD Healthcare 2020 and the project PARES (Prémio Albino Aroso).

## References

[1] S. Pluchino, L. Zanotti, M. Deleidi, G. Martino, Neural stem cells and their use as therapeutic tool in neurological disorders, Brain Res Brain Res Rev 48(2) (2005) 211-9.

[2] C. Cossetti, C. Alfaro-Cervello, M. Donega, G. Tyzack, S. Pluchino, New perspectives of tissue remodelling with neural stem and progenitor cell-based therapies, Cell Tissue Res 349(1) (2012) 321-9.

[3] F.H. Gage, S. Temple, Neural stem cells: generating and regenerating the brain, Neuron 80(3) (2013) 588-601.

[4] M.H. Amer, F. Rose, K.M. Shakesheff, M. Modo, L.J. White, Translational considerations in injectable cell-based therapeutics for neurological applications: concepts, progress and challenges, NPJ Regen Med 2 (2017) 23.

[5] D. Barros, I.F. Amaral, A.P. Pego, Biomimetic synthetic self-assembled hydrogels for cell transplantation, Curr Top Med Chem 15(13) (2015) 1209-26.

[6] J.L. Wilson, T.C. McDevitt, Biofunctional Hydrogels for Three-Dimensional Stem Cell Culture, in: A. Vishwakarma, J.M. Karp (Eds.), Biology and Engineering of Stem Cell Niches, Elsevier2017.

[7] J.C. Schense, J. Bloch, P. Aebischer, J.A. Hubbell, Enzymatic incorporation of bioactive peptides into fibrin matrices enhances neurite extension, Nat Biotechnol 18(4) (2000) 415-9.

[8] J.C. Schense, J.A. Hubbell, Three-dimensional migration of neurites is mediated by adhesion site density and affinity, J Biol Chem 275(10) (2000) 6813-8.

[9] U. Freudenberg, A. Hermann, P.B. Welzel, K. Stirl, S.C. Schwarz, M. Grimmer, A. Zieris, W. Panyanuwat, S. Zschoche, D. Meinhold, A. Storch, C. Werner, A star-PEG-heparin hydrogel platform to aid cell replacement therapies for neurodegenerative diseases, Biomaterials 30(28) (2009) 5049-60.

[10] S.P. Zustiak, S. Pubill, A. Ribeiro, J.B. Leach, Hydrolytically degradable poly(ethylene glycol) hydrogel scaffolds as a cell delivery vehicle: characterization of PC12 cell response, Biotechnol Prog 29(5) (2013) 1255-64.

[11] R. Bellamkonda, J.P. Ranieri, P. Aebischer, Laminin oligopeptide derivatized agarose gels allow three-dimensional neurite extension in vitro, J Neurosci Res 41(4) (1995) 501-9.

[12] T. Zhao, D.L. Sellers, Y. Cheng, P.J. Horner, S.H. Pun, Tunable, Injectable Hydrogels Based on Peptide-Cross-Linked, Cyclized Polymer Nanoparticles for Neural Progenitor Cell Delivery, Biomacromolecules 18(9) (2017) 2723-2731.

[13] Y.T. Wei, W.M. Tian, X. Yu, F.Z. Cui, S.P. Hou, Q.Y. Xu, I.S. Lee, Hyaluronic acid hydrogels with IKVAV peptides for tissue repair and axonal regeneration in an injured rat brain, Biomed Mater 2(3) (2007) S142-6.

[14] W. Sun, T. Incitti, C. Migliaresi, A. Quattrone, S. Casarosa, A. Motta, Viability and neuronal differentiation of neural stem cells encapsulated in silk fibroin hydrogel functionalized with an IKVAV peptide, J Tissue Eng Regen Med 11(5) (2017) 1532-1541.
[15] L.A. Flanagan, L.M. Rebaza, S. Derzic, P.H. Schwartz, E.S. Monuki, Regulation of human neural precursor cells by laminin and integrins, J Neurosci Res 83(5) (2006) 845-56.
[16] L.E. Oikari, R.K. Okolicsanyi, A. Qin, C. Yu, L.R. Griffiths, L.M. Haupt, Cell surface heparan sulfate proteoglycans as novel markers of human neural stem cell fate determination, Stem Cell Res 16(1) (2016) 92-104.
[17] M. Ford-Perriss, K. Turner, S. Guimond, A. Apedaile, H.D. Haubeck, J. Turnbull, M. Murphy, Localisation of specific heparan sulfate proteoglycans during the proliferative phase of brain development, Dev Dyn 227(2) (2003) 170-84.
[18] Y. Choi, H. Chung, H. Jung, J.R. Couchman, E.S. Oh, Syndecans as cell surface receptors: Unique structure equates with functional diversity, Matrix Biol 30(2) (2011) 93-9.
[19] F.E. Poulain, H.J. Yost, Heparan sulfate proteoglycans: a sugar code for vertebrate development?, Development 142(20) (2015) 3456-67.
[20] X. Xian, S. Gopal, J.R. Couchman, Syndecans as receptors and organizers of the extracellular matrix, Cell Tissue Res 339(1) (2010) 31-46.
[21] Q. Wang, L. Yang, C. Alexander, S. Temple, The niche factor syndecan-1 regulates the maintenance and proliferation of neural progenitor cells during mammalian cortical development, PLoS One 7(8) (2012) e42883.
[22] L. Morizur, A. Chicheportiche, L.R. Gauthier, M. Daynac, F.D. Boussin, M.A. Mouthon, Distinct Molecular Signatures of Quiescent and Activated Adult Neural Stem Cells Reveal Specific Interactions with Their Microenvironment, Stem Cell Reports (2018).
[23] M.M. Bespalov, Y.A. Sidorova, S. Tumova, A. Ahonen-Bishopp, A.C. Magalhaes, E. Kulesskiy, M. Paveliev, C. Rivera, H. Rauvala, M. Saarma, Heparan sulfate proteoglycan syndecan-3 is a novel receptor for GDNF, neurturin, and artemin, J Cell Biol 192(1) (2011) 153-69.
[24] A. Kinnunen, T. Kinnunen, M. Kaksonen, R. Nolo, P. Panula, H. Rauvala, N-syndecan and HB-GAM (heparin-binding growth-associated molecule) associate with early axonal tracts in the rat brain, Eur J Neurosci 10(2) (1998) 635-48.
[25] A. Kinnunen, M. Niemi, T. Kinnunen, M. Kaksonen, R. Nolo, H. Rauvala, Heparan sulphate and HB-GAM (heparin-binding growth-associated molecule) in the development of the thalamocortical pathway of rat brain, Eur J Neurosci 11(2) (1999) 491-502.
[26] E. Raulo, M.A. Chernousov, D.J. Carey, R. Nolo, H. Rauvala, Isolation of a neuronal cell surface receptor of heparin binding growth-associated molecule (HB-GAM). Identification as N-syndecan (syndecan-3), J Biol Chem 269(17) (1994) 12999-3004.

[27] T. Kinnunen, E. Raulo, R. Nolo, M. Maccarana, U. Lindahl, H. Rauvala, Neurite outgrowth in brain neurons induced by heparin-binding growth-associated molecule (HB-GAM) depends on the specific interaction of HB-GAM with heparan sulfate at the cell surface, J Biol Chem 271(4) (1996) 2243-8.

[28] H.K. Matthews, L. Marchant, C. Carmona-Fontaine, S. Kuriyama, J. Larrain, M.R. Holt, M. Parsons, R. Mayor, Directional migration of neural crest cells in vivo is regulated by Syndecan-4/Rac1 and non-canonical Wnt signaling/RhoA, Development 135(10) (2008) 1771-80.

[29] I.M. Ethell, Y. Yamaguchi, Cell surface heparan sulfate proteoglycan syndecan-2 induces the maturation of dendritic spines in rat hippocampal neurons, J Cell Biol 144(3) (1999) 575-86.

[30] M.P. Hoffman, M. Nomizu, E. Roque, S. Lee, D.W. Jung, Y. Yamada, H.K. Kleinman, Laminin-1 and laminin-2 G-domain synthetic peptides bind syndecan-1 and are involved in acinar formation of a human submandibular gland cell line, J Biol Chem 273(44) (1998) 28633-41.

[31] L.N. Gama-de-Souza, E. Cyreno-Oliveira, V.M. Freitas, E.S. Melo, V.F. Vilas-Boas, A.S. Moriscot, R.G. Jaeger, Adhesion and protease activity in cell lines from human salivary gland tumors are regulated by the laminin-derived peptide AG73, syndecan-1 and beta1 integrin, Matrix Biol 27(5) (2008) 402-19.

[32] N. Suzuki, N. Ichikawa, S. Kasai, M. Yamada, N. Nishi, H. Morioka, H. Yamashita, Y. Kitagawa, A. Utani, M.P. Hoffman, M. Nomizu, Syndecan binding sites in the laminin alpha1 chain G domain, Biochemistry 42(43) (2003) 12625-33.

[33] M. Nomizu, W.H. Kim, K. Yamamura, A. Utani, S.Y. Song, A. Otaka, P.P. Roller, H.K. Kleinman, Y. Yamada, Identification of cell binding sites in the laminin alpha 1 chain carboxyl-terminal globular domain by systematic screening of synthetic peptides, J Biol Chem 270(35) (1995) 20583-90.

[34] K. Hozumi, N. Suzuki, P.K. Nielsen, M. Nomizu, Y. Yamada, Laminin alpha1 chain LG4 module promotes cell attachment through syndecans and cell spreading through integrin alpha2beta1, J Biol Chem 281(43) (2006) 32929-40.

[35] M. Mochizuki, Y. Kadoya, Y. Wakabayashi, K. Kato, I. Okazaki, M. Yamada, T. Sato, N. Sakairi, N. Nishi, M. Nomizu, Laminin-1 peptide-conjugated chitosan membranes as a novel approach for cell engineering, FASEB J 17(8) (2003) 875-7.

[36] Y. Yamada, K. Hozumi, F. Katagiri, Y. Kikkawa, M. Nomizu, Biological activity of laminin peptide-conjugated alginate and chitosan matrices, Biopolymers 94(6) (2010) 711-20.

[37] Y. Yamada, F. Katagiri, K. Hozumi, Y. Kikkawa, M. Nomizu, Cell behavior on protein matrices containing laminin alpha1 peptide AG73, Biomaterials 32(19) (2011) 4327-35.

[38] Y. Yamada, K. Hozumi, A. Aso, A. Hotta, K. Toma, F. Katagiri, Y. Kikkawa, M. Nomizu, Laminin active peptide/agarose matrices as multifunctional biomaterials for tissue engineering, Biomaterials 33(16) (2012) 4118-25.

[39] A.R. Bento, Improving neurite outgrowth in 3D hydrogel matrices by mimicking cell receptor-ECM interactions occurring in neurogenic niches: an engineering approach to develop more efficient neural stem cell hydrogel carriers, Faculdade de Engenharia, Universidade do Porto, 2018.

[40] D. Barros, E. Conde-Sousa, A.J. Garcia, I.F. Amaral, A.P. Pego, Engineering hydrogels with affinity-bound laminin as 3D neural stem cell culture systems Manuscript in preparation (2019).

[41] N.O. Enemchukwu, R. Cruz-Acuna, T. Bongiorno, C.T. Johnson, J.R. Garcia, T. Sulchek, A.J. Garcia, Synthetic matrices reveal contributions of ECM biophysical and biochemical properties to epithelial morphogenesis, J Cell Biol 212(1) (2016) 113-24.

[42] W.M. Han, S.E. Anderson, M. Mohiuddin, D. Barros, S.A. Nakhai, E. Shin, I.F. Amaral, A.P. Pego, A.J. Garcia, Y.C. Jang, Synthetic matrix enhances transplanted satellite cell engraftment in dystrophic and aged skeletal muscle with comorbid trauma, Sci Adv 4(8) (2018) eaar4008.

[43] J. Patterson, J.A. Hubbell, Enhanced proteolytic degradation of molecularly engineered PEG hydrogels in response to MMP-1 and MMP-2, Biomaterials 31(30) (2010) 7836-45.

[44] J.D. Weaver, D.M. Headen, J. Aquart, C.T. Johnson, L.D. Shea, H. Shirwan, A.J. Garcia, Vasculogenic hydrogel enhances islet survival, engraftment, and function in leading extrahepatic sites, Sci Adv 3(6) (2017) e1700184.

[45] R. Cruz-Acuna, M. Quiros, A.E. Farkas, P.H. Dedhia, S. Huang, D. Siuda, V. Garcia-Hernandez, A.J. Miller, J.R. Spence, A. Nusrat, A.J. Garcia, Synthetic hydrogels for human intestinal organoid generation and colonic wound repair, Nat Cell Biol 19(11) (2017) 1326-1335.

[46] E.A. Phelps, N.O. Enemchukwu, V.F. Fiore, J.C. Sy, N. Murthy, T.A. Sulchek, T.H. Barker, A.J. Garcia, Maleimide cross-linked bioactive PEG hydrogel exhibits improved reaction kinetics and cross-linking for cell encapsulation and in situ delivery, Adv Mater 24(1) (2012) 64-70, 2.

[47] I.O.f. Standardization, ISO 10993-5:2009 : Biological evaluation of medical devices Tests for in vitro cytotoxicity, 2009.

[48] M.M. Martino, P.S. Briquez, A. Ranga, M.P. Lutolf, J.A. Hubbell, Heparin-binding domain of fibrin(ogen) binds growth factors and promotes tissue repair when incorporated within a synthetic matrix, Proc Natl Acad Sci U S A 110(12) (2013) 4563-8.

[49] A.C. Brown, T.H. Barker, Fibrin-based biomaterials: modulation of macroscopic properties through rational design at the molecular level, Acta Biomater 10(4) (2014) 1502-14.

[50] S.P. Zustiak, R. Durbal, J.B. Leach, Influence of cell-adhesive peptide ligands on poly(ethylene glycol) hydrogel physical, mechanical and transport properties, Acta Biomater 6(9) (2010) 3404-14.

[51] K. Hozumi, A. Sasaki, Y. Yamada, D. Otagiri, K. Kobayashi, C. Fujimori, F. Katagiri, Y. Kikkawa, M. Nomizu, Reconstitution of laminin-111 biological activity using multiple peptide coupled to chitosan scaffolds, Biomaterials 33(17) (2012) 4241-50.

[52] D. Otagiri, Y. Yamada, K. Hozumi, F. Katagiri, Y. Kikkawa, M. Nomizu, Cell attachment and spreading activity of mixed laminin peptide-chitosan membranes, Biopolymers 100(6) (2013) 751-9.

[53] A.R. Bento, A.P. Pego, I.F. Amaral, Controlling the density of α6β1 integrin- or syndecan-binding motifs tethered to fibrin improve the outgrowth of hES-derived neural stem cells, 2018.

# CHAPTER IX

Concluding Remarks and Future Perspectives

The main aim of the work presented in this thesis was the design of biologically relevant matrices able to recapitulate the laminin-rich microenvironment of neural stem cell (NSC) niches. For that, we proposed the modification of a degradable synthetic hydrogel with full-length laminin. Additionally, a laminin-derived peptide interacting with syndecan receptors (AG73) was also explored. The developed matrices can be used to address the role of laminin on the modulation of NSC function and fate and, ultimately, contribute to the development of chemically-defined platforms for NSC culture and/or NSC delivery into the central nervous system (CNS) in the context of regenerative therapies.

Laminin is one of the most important and well described extracellular matrix (ECM) proteins within the neurogenic niches [1, 2], with a key role in the modulation of NSC maintenance [3], migration and differentiation [4-6]. Furthermore, laminin has other paramount roles in CNS homeostasis, as contributing to synapse function and stability [7, 8]. Therefore, this ECM protein constitutes a highly attractive option while considering the design of NSC niche microenvironments.

Full-length laminin immobilization into biological and synthetic matrices was already explored in different studies for the design of three-dimensional (3D) NSC niche microenvironments (see **Chapter III** for a review). Despite the promising results, a major caveat of the conventionally used immobilization strategies (based on non-covalent incorporation/physical entrapment or non-selective covalent immobilization), is the lack of control over the orientation and conformation of laminin, upon immobilization, which was proven to be crucial for the modulation of cellular behavior, function and fate [9]. As such, one of the specific aims of this thesis was to establish an affinity-based strategy to generate a highly versatile and dynamic system, expected to allow the site-selective immobilization of laminin, while controlling its orientation and bioactivity. For this purpose, in **Chapter V** we proposed a strategy that takes advantage of the native high affinity interaction (dissociation constant ($K_D$) = 5 nM) between laminin and the N-terminal agrin (NtA) domain [10, 11]. Studies conducted to date, characterizing this domain and its interaction with laminin, have used the NtA derived from chicken agrin [10-13]. In the work presented in this thesis, the recombinant human (rh) variant of the NtA domain was produced and, for the first time, its interaction with laminin characterized [9, 14]. This is particularly important since we envisage the application of the proposed strategy in platforms for human cell culture/delivery and human-disease modelling. The conjugation of a thiol-terminated poly(ethylene glycol) (PEG) at the NtA N-terminus - mono-PEGylated rhNtA, allowed us to establish an affinity-binding ligand suitable for laminin site-selective immobilization to two-dimensional (2D) and 3D matrices. In addition, the proposed ligand presents a high versatility, as evidenced by its high affinity for different laminin isoforms (in the context of this thesis assessed for mouse laminin-111 (msLn-111) and

recombinant human laminin-521 (rhLn-521)). This allows the use of the proposed strategy for the immobilization of different laminin isoforms, which can be of interest for particular cell types and for application in specific disease contexts. The biological effectiveness of the immobilization strategy was assessed using self-assembled monolayers (SAMs) of mono-PEGylated rhNtA on gold. Overall, the obtained data suggested that mono-PEGylated rhNtA works as an effective binding ligand for the site-selective immobilization of laminin, allowing the preservation of laminin ability to polymerize and mediate human NSC (hNSC) adhesion and spreading. In summary, in this work we provided a new affinity-based strategy that surpasses some of the main limitations associated with the current available laminin immobilization strategies (non-covalent incorporation/physical entrapment or non-selective covalent immobilization), assuring the exposure of laminin cell binding domains, as well as other distinct complementary domains that modulate important biological functions.

In the future, it would be interesting to perform further studies to establish this as an universal strategy of coating, allowing the controlled and oriented immobilization of laminin regardless of the 2D model surface (*e.g.* TCPS, Au, *etc.*). In addition, the potential of this strategy to immobilize different laminin isoforms and be used as 2D coating for the culture of different cell types should also be confirmed. Neural electrode-tissue interface research is facing an exponential growth in the last few years [15]. Despite the promising results obtained to date, the search for effective strategies to improve this interface is highly needed. In this regard, the affinity-based immobilization approach presented in this thesis can be advantageous for the development of engineered coatings for neural electrodes. This is expected to improve the interface electrode-tissue, achieve seamless integration between the implanted electrodes and neural tissue, and ultimately, boost neural electrode performance.

The application of the proposed affinity-based immobilization strategy was subsequently explored for the development of 3D cell-instructive microenvironments, with potential to support NSC proliferation and neuronal differentiation (**Chapter VI**). For that a degradable synthetic hydrogel based on a four-arm maleimide-end functionalized poly(ethylene glycol) (PEG-4MAL) macromer was selected as the base material. These hydrogels have been extensively used to support the culture and/or delivery of different cell types, within different regenerative contexts [16-19], and thus a high amount of information regarding the best way to modulate their biochemical and biophysical properties is currently available. Therefore, these hydrogels can be engineered to have the most suitable properties to support NSC culture and transplantation. In this work, we explored msLn-111, and we showed that the approach used for laminin incorporation (physical entrapment *vs.* affinity immobilization) significantly impact the hydrogel mechanical and structural properties. The tethering of NtA, which mediates laminin site-selective immobilization, reduces the number of maleimide-

terminated PEG chains available for cross-linking, thus reducing the number of cross-linking points and favoring a reduction in the complex modulus (G*). Affinity-bound laminin PEG-4MAL hydrogels showed great potential to be used as a dynamic biomimetic 3D platform enabling NSC proliferation and neurite outgrowth, when compared to currently available strategies for laminin immobilization, which include physical entrapment and non-selective covalent immobilization. Overall, this work provided evidence of the potential of the proposed engineered matrices to be used as defined 3D platforms, for the establishment of artificial NSC niches and as temporary mimetic microenvironments to support cell transplantation. To further consolidate the full potential of the developed 3D platform for the culture of hNSCs, studies assessing its ability to support cell differentiation and ECM remodeling, and the establishment of a functional neuronal network should be conducted.

The key role of rhLn-521 on the *in vitro* modulation of neural cell behavior [3, 20], led us to subsequently explore the preparation of a degradable PEG-4MAL hydrogel containing affinity-bound rhLn-521 (**Chapter VII**). This is of particular relevance when envisaging the development of a whole-human 3D cell-instructive microenvironment. Preliminary studies exploring the site-selective immobilization of rhLn-521 into a degradable PEG-4MAL hydrogel, using the strategy proposed in **Chapter VI,** did not evidence a significant impact on neurite outgrowth, when compared to unmodified hydrogels and hydrogels with equal amount of physically entrapped laminin. Therefore, some steps of the original immobilization protocol were altered, in an attempt to improve rLn-521 binding to NtA and its impact on NSC behavior. An improvement on neurite outgrowth was observed, compared to unmodified hydrogels and hydrogels with physically entrapped rhLn-521, although differences only reached statistical significance in the former case, suggesting an impact of such modifications on protein conformation and domain presentation to cells. Therefore, and although the data obtained represent a good start for the development of a whole-human 3D cell instructive matrix, further studies need to be conducted. More specifically, in the future the use of higher rhLn-521 concentrations (> 20 μg/mL) should be considered and its biological performance when immobilized through the strategy proposed in **Chapter VI** assessed. In addition, the look for alternatives to improve NtA-bound rhLn-521 tethering to PEG-4MAL is also highly desirable.

As previously pointed, the versatility and dynamic nature of the proposed strategy allows the immobilization of different laminin isoforms within 3D matrices, thus opening doors for future studies exploring cell-laminin interactions, occurring in different stem cell niches and disease contexts. In addition, studies assessing the exchangeability with endogenously secreted laminin could also be of interest. Direct evidence on the potential of the proposed immobilization strategy to preserve the exposure of key laminin bioactive epitopes is also critical to assess. For that, laminin peptide analogues known to mediate important laminin

functions, such as neuronal adhesion, neurite outgrowth and/or NSC migration can be used as competitive inhibitors. Alternatively, function blocking studies using antibodies against integrin or syndecan receptors interacting with specific laminin regions, can also be explored in this regard. The hydrogel proposed can be also of interest to provide a controlled niche with instructive cues to improve survival, engraftment and long-term function of transplanted stem cells. Accordingly, and to validate the developed affinity-bound laminin hydrogel as a cell-instructive microenvironment, in the future, *in vivo* studies using, for example, an experimental model of brain or spinal cord injury, should be conducted. One of the main caveats currently limiting the successful translation of stem cell therapies to clinic is the lack of effective cell expansion and biomanufacturing systems. In this regard, in the last few years the systems used for cell expansion have shifted towards the use of 3D platforms. These provide a defined environment for adherent stem cells and organoid culture (*e.g.* NSCs, induced pluripotent stem cells, *etc.*), while enabling the culture in large-scale bioreactor systems. Although, further studies assessing the ability of affinity-bound laminin PEG-4MAL hydrogels to support hNSC differentiation need to be conducted, their ability to support cell viability, proliferation and neurite outgrowth, suggest that these hydrogels constitute a highly attractive option to be used on the development of cell expansion and biomanufacturing systems.

Laminin-derived small adhesive sequences have also been explored, in alternative to the incorporation of full-length laminin, to confer bioactivity to 3D matrices (see **Chapter III** for a review). These small sequences can be chemically synthesized in large scale and are commonly incorporated at higher densities, for similar amounts of native protein, usually, with no significant impact on hydrogel biophysical properties [21]. In **Chapter VIII** we explored the functionalization of a degradable synthetic hydrogel with a syndecan-binding peptide (AG73 – RKRLQVQSIRT) with neurite-promoting activity, and already successfully explored to modify natural hydrogel matrices [22-25]. The tethering of AG73 peptide to PEG-4MAL hydrogels led to a significant improvement of cell viability, after 7 days in culture, independently of the input peptide concentration tested. In addition, we demonstrated that a higher input AG73 concentration (1 mM) better supports hNSC proliferation and neurite outgrowth. Despite the promising results obtained, future studies need to be conducted to validate the observations presented in this work. More specifically, to verify if the biological outcome observed for the different AG73 input concentrations could be related with differences in hydrogel mechanical and structural properties, rheological studies need to be conducted. In addition, for the defined optimal AG73 concentration (1 mM), future studies should assess the ability of the developed 3D platforms to support hNSC neuronal differentiation and maturation in long-term cultures. To get insight into the contribution of syndecan-1 and -4 receptors for the NSC response to immobilized AG73, silencing of the

syndecan receptor expression in hNSCs, by means of siRNA, can be performed. Envisaging the application of AG73-functionalized PEG-4MAL hydrogels in the CNS as vehicle for NSC transplantation, its impact on axonal extension growth should be assessed, using for instance organotypic cultures of sensory and motor neurons. To better recapitulate the biological activity of laminin chains, we propose to address, in future studies, the functionalization of PEG-4MAL hydrogels with a combination of AG73 peptide and integrin-binding ligands, and evaluate its additive or synergistic effect on neurite outgrowth.

In summary, the affinity-based strategy proposed in this thesis can be successfully used as an alternative to conventional immobilization approaches in a wide range of applications, including engineered coatings for neuroelectrodes and for 2D substrates for cell culture, as well as for the biofunctionalization of 3D matrices. Furthermore, the hydrogels developed exploring the proposed strategy, showed great potential to be used as chemically-defined 3D platforms for the *in vitro* culture of hNSCs and, potentially, as vehicles for hNSCs cell transplantation in the context of nervous system regeneration/disorders. In addition, the developed 3D matrices have potential to be successfully applied to study the molecular mechanisms implicated in neurogenesis, in a 3D microenvironment that better mimics the *in vivo* conditions. Alternatively, and envisaging the clinical translation of stem cell therapies, affinity-bound laminin hydrogels can be also explored for the development of tissue engineering constructs and biomanufacturing systems to expand stem cells. Ultimately, we strongly believe this work opens new avenues in the design of more efficient hydrogel matrices for application in NSC-based regenerative approaches for the treatment of traumatic CNS disorders or neurodegenerative diseases.

**References**

[1] A. Kerever, J. Schnack, D. Vellinga, N. Ichikawa, C. Moon, E. Arikawa-Hirasawa, J.T. Efird, F. Mercier, Novel extracellular matrix structures in the neural stem cell niche capture the neurogenic factor fibroblast growth factor 2 from the extracellular milieu, Stem Cells 25(9) (2007) 2146-57.

[2] I. Kazanis, J.D. Lathia, T.J. Vadakkan, E. Raborn, R. Wan, M.R. Mughal, D.M. Eckley, T. Sasaki, B. Patton, M.P. Mattson, K.K. Hirschi, M.E. Dickinson, C. ffrench-Constant, Quiescence and activation of stem and precursor cell populations in the subependymal zone of the mammalian brain are associated with distinct cellular and extracellular matrix signals, J Neurosci 30(29) (2010) 9771-81.

[3] A. Hyysalo, M. Ristola, M.E. Makinen, S. Hayrynen, M. Nykter, S. Narkilahti, Laminin alpha5 substrates promote survival, network formation and functional development of human pluripotent stem cell-derived neurons in vitro, Stem Cell Res 24 (2017) 118-127.

[4] L. Luckenbill-Edds, Laminin and the mechanism of neuronal outgrowth, Brain Res Brain Res Rev 23(1-2) (1997) 1-27.

[5] S.K. Powell, H.K. Kleinman, Neuronal laminins and their cellular receptors, Int J Biochem Cell Biol 29(3) (1997) 401-14.

[6] S. Plantman, M. Patarroyo, K. Fried, A. Domogatskaya, K. Tryggvason, H. Hammarberg, S. Cullheim, Integrin-laminin interactions controlling neurite outgrowth from adult DRG neurons in vitro, Mol Cell Neurosci 39(1) (2008) 50-62.

[7] R.S. Rogers, H. Nishimune, The role of laminins in the organization and function of neuromuscular junctions, Matrix Biol 57-58 (2017) 86-105.

[8] H. Nishimune, G. Valdez, G. Jarad, C.L. Moulson, U. Muller, J.H. Miner, J.R. Sanes, Laminins promote postsynaptic maturation by an autocrine mechanism at the neuromuscular junction, J Cell Biol 182(6) (2008) 1201-15.

[9] D D. Barros, P. Parreira, J. Furtado, F. Ferreira-da-Silva, E. Conde-Sousa, A.J. Garcia, M.C.L. Martins, I.F. Amaral, A.P. Pego, An affinity-based approach to engineer laminin-presenting cell instructive microenvironments, Biomaterials 192 (2019) 601-611.

[10] J.B. Mascarenhas, M.A. Ruegg, U. Winzen, W. Halfter, J. Engel, J. Stetefeld, Mapping of the laminin-binding site of the N-terminal agrin domain (NtA), EMBO J 22(3) (2003) 529-36.

[11] A.J. Denzer, T. Schulthess, C. Fauser, B. Schumacher, R.A. Kammerer, J. Engel, M.A. Ruegg, Electron microscopic structure of agrin and mapping of its binding site in laminin-1, EMBO J 17(2) (1998) 335-43.

[12] R.A. Kammerer, T. Schulthess, R. Landwehr, B. Schumacher, A. Lustig, P.D. Yurchenco, M.A. Ruegg, J. Engel, A.J. Denzer, Interaction of agrin with laminin requires a coiled-coil

conformation of the agrin-binding site within the laminin gamma1 chain, EMBO J 18(23) (1999) 6762-70.
[13] J. Stetefeld, M. Jenny, T. Schulthess, R. Landwehr, B. Schumacher, S. Frank, M.A. Ruegg, J. Engel, R.A. Kammerer, The laminin-binding domain of agrin is structurally related to N-TIMP-1, Nat Struct Biol 8(8) (2001) 705-9.
[14] D. Barros, I.F. Amaral, A.P. Pego, Laminin immobilization, methods and uses thereof, Portuguese Provisional Patent Application no. 20181000074673, filled 2018/11/30.
[15] K. Woeppel, Q. Yang, X.T. Cui, Recent Advances in Neural Electrode-Tissue Interfaces, Curr Opin Biomed Eng 4 (2017) 21-31.
[16] D. Barros, I.F. Amaral, A.P. Pego, Biomimetic synthetic self-assembled hydrogels for cell transplantation, Curr Top Med Chem 15(13) (2015) 1209-26.
[17] N.O. Enemchukwu, R. Cruz-Acuna, T. Bongiorno, C.T. Johnson, J.R. Garcia, T. Sulchek, A.J. Garcia, Synthetic matrices reveal contributions of ECM biophysical and biochemical properties to epithelial morphogenesis, J Cell Biol 212(1) (2016) 113-24.
[18] J.D. Weaver, D.M. Headen, J. Aquart, C.T. Johnson, L.D. Shea, H. Shirwan, A.J. Garcia, Vasculogenic hydrogel enhances islet survival, engraftment, and function in leading extrahepatic sites, Sci Adv 3(6) (2017) e1700184.
[19] W.M. Han, S.E. Anderson, M. Mohiuddin, D. Barros, S.A. Nakhai, E. Shin, I.F. Amaral, A.P. Pego, A.J. Garcia, Y.C. Jang, Synthetic matrix enhances transplanted satellite cell engraftment in dystrophic and aged skeletal muscle with comorbid trauma, Sci Adv 4(8) (2018) eaar4008.
[20] A. Bergeron, H. Sherman, P. Pardo, H. Gitschier, H. Nandivada, D. Saxena, Corning® rLaminin-521 (Human) for Expansion and Differentiation of Human Neural Stem Cells, Corning Incorporated | Application Note (2015).
[21] J.H. Collier, T. Segura, Evolving the use of peptides as components of biomaterials, Biomaterials 32(18) (2011) 4198-204.
[22] M. Mochizuki, Y. Kadoya, Y. Wakabayashi, K. Kato, I. Okazaki, M. Yamada, T. Sato, N. Sakairi, N. Nishi, M. Nomizu, Laminin-1 peptide-conjugated chitosan membranes as a novel approach for cell engineering, FASEB J 17(8) (2003) 875-7.
[23] Y. Yamada, K. Hozumi, F. Katagiri, Y. Kikkawa, M. Nomizu, Biological activity of laminin peptide-conjugated alginate and chitosan matrices, Biopolymers 94(6) (2010) 711-20.
[24] Y. Yamada, F. Katagiri, K. Hozumi, Y. Kikkawa, M. Nomizu, Cell behavior on protein matrices containing laminin alpha1 peptide AG73, Biomaterials 32(19) (2011) 4327-35.
[25] Y. Yamada, K. Hozumi, A. Aso, A. Hotta, K. Toma, F. Katagiri, Y. Kikkawa, M. Nomizu, Laminin active peptide/agarose matrices as multifunctional biomaterials for tissue engineering, Biomaterials 33(16) (2012) 4118-25.

# APPENDIX I

Laminin immobilization, methods and uses thereof

**APPENDIX I** – Laminin immobilization, methods and uses thereof

# Laminin immobilization, methods and uses thereof

Daniela Barros [1,2,3], Isabel Freitas Amaral [1,2,4], Ana Paula Pêgo [1,2,3,4]

[1] i3S - Instituto de Investigação e Inovação em Saúde, Universidade do Porto (UPorto), Portugal

[2] INEB - Instituto de Engenharia Biomédica, UPorto, Portugal

[3] ICBAS - Instituto de Ciências Biomédicas Abel Salazar, UPorto, Portugal

[4] FEUP - Faculdade de Engenharia, UPorto, Portugal

---

**Portuguese Provisional Patent Application no. 20181000074673, filled 2018/11/30**

## D E S C R I P T I O N

### LAMININ IMMOBILIZATION, METHODS AND USES THEREOF

#### Technical field

[0001] The present disclosure relates to an approach for site-specific laminin immobilization, methods and uses thereof. Namely the use of a composition for biofunctionalization of 2D and 3D substrates.

#### Background

[0002] In the framework of regenerative medicine and tissue engineering, much attention has been devoted towards the development of engineered matrices incorporating bioadhesive cues present in stem cell niches, to recapitulate the dynamic nature and biological complexity of these microenvironments, as well as to gain more insight into the function of specific extracellular matrix (ECM) components on stem cell behaviour. The ECM is an essential component of the stem cell niche, as it modulates important biological functions including proliferation, self-renewal and differentiation of stem cells. Among major ECM constituents, laminins play crucial and essential roles in many aspects of tissue physiology and function. These heterotrimeric glycoproteins comprise several bioactive domains involved in the modulation of different biological functions. The latter include the interaction with other ECM proteins (*e.g.* nidogen, netrin 4 and collagen VII) mediated by the laminin short arms (N-terminus), which contributes to the assembly and stability of basement membranes. These domains are also responsible for the laminin ability to polymerize, even in the absence of other basement membrane components, forming the molecular network that it is in contact with the cellular surface. In addition to its structural role, laminin comprises multiple bioactive domains that interact with growth factors and/or with cell surface receptors (*e.g.* integrins, dystroglycans, and syndecans), modulating different cell functions including cell adhesion, proliferation, migration and differentiation, as well as ECM deposition.

[0003] Laminin has been incorporated into both two-dimensional (2D) and three-dimensional (3D) cell-instructive microenvironments for applications in regenerative therapies or to get insights into the role of laminin on the modulation of cell behaviour. Strategies explored for laminin immobilization have relied either on its non-specific adsorption or entrapment or, alternatively, on its non-specific covalent immobilization to different substrates through the use of functional groups present in multiple sites of the laminin structure such as amines and thiols. One of the main caveats presented by these strategies is the inability to control orientation and conformation of laminin upon immobilization, which were proven to be crucial for the modulation of cellular behaviour. As such, the exposure of key laminin bioactive epitopes can be compromised. In an attempt to assure the control over the tethering of laminin, in recent years protein immobilization strategies have shifted toward site-specific conjugation, with special focus on biorthogonal chemical reactions (click chemistry), enzymatic ligation and affinity binding, using either unnatural amino acids or engineered site-selective amino acid sequences. These strategies are expected to provide a higher retention of bioactivity, by favouring the access to the active sites of immobilized proteins. To the best of our knowledge, to date, only one study reported the site-selective immobilization of laminin. To control the presentation of full-length ECM proteins without altering their bioactivity, Lee and co-workers explored click chemistry to anchor collagen, fibronectin and laminin onto polyacrylamide gels by their N-terminus. Nevertheless, despite guaranteeing the site-selective immobilization of the proteins, as result of the use of the N-terminus of laminin chains, this approach compromises one of laminin's hallmark features, which is its ability to polymerize. Affinity-binding has been increasingly explored for the site-specific and reversible conjugation of proteins and peptides, because of its versatility and ability to generate dynamic biomimetic systems. However, the successful implementation of this strategy is strongly dependent on the appropriate selection of the binding pairs. Binding systems using high affinity interactions, such as streptavidin and biotin, although often used, require the protein of interest to be either recombinantly or chemically modified. In contrast, the use of natural binding partners constitutes an attractive alternative, as strong non-covalent interactions can be achieved without the need for protein modification.

[0004] These facts are disclosed in order to illustrate the technical problem addressed by the present disclosure.

#### General Description

[0005] Laminin immobilization into diverse biological and synthetic matrices has been explored to replicate the microenvironment of stem cell niches and gain insight into the role of

extracellular matrix (ECM) on stem cell behaviour. However, the site-specific immobilization of this heterotrimeric glycoprotein and, consequently, control over its orientation and bioactivity has been a challenge that has limited many of the explored strategies to date. It An affinity-based approach that takes advantage of the native high affinity interaction between laminin and the human N-terminal agrin (hNtA) domain was established. This interaction was expected to promote the site-selective immobilization of laminin to a substrate, while preserving the exposure of its key bioactive epitopes. Recombinant hNtA (rhNtA) domain was produced with high purity (>90%) and successfully conjugated at its N-terminal with a thiol-terminated poly(ethylene glycol) (PEG) without affecting its affinity to laminin. Self-assembled monolayers (SAMs) of mono-PEGylated rhNtA on gold (mPEG rhNtA-SAMs) were then prepared to evaluate the effectiveness of this strategy. The site-specific immobilization of laminin onto mPEG rhNtA-SAMs was shown to better preserve protein bioactivity in comparison to laminin immobilized on SAMs of thiol-PEG-succinimidyl glutaramide, used for the non-selective covalent immobilization of laminin, as evidenced by its enhanced ability to efficiently self-polymerize and mediate cell adhesion and spreading of human neural stem cells. These results highlight the potential of this novel strategy to be used as an alternative to the conventional immobilization approaches in a wide range of applications, including engineered coatings for neuroelectrodes and cell culture, as well as biofunctionalization of 3D matrices.

[0006] In an embodiment, a strategy that explores the native high affinity interaction ($K_D$ = 5 nM) between laminin and the N-terminal agrin (NtA) domain is described. The agrin-binding site in laminin is localized in the central region of its coiled-coil domain and maps to a sequence of 20 conserved residues within the $\gamma$1 chain. Interestingly, this interaction requires a coiled-coil conformation of the agrin-binding site. In an embodiment, to assess the ability of this affinity-based approach to immobilize laminin with retention of bioactivity, recombinant human NtA (rhNtA) domain was produced and further conjugated at its N-terminus with a poly(ethylene glycol) (PEG), preferably with a thiol-terminated PEG, to enable the preparation of self-assembled monolayers (SAMs) of rhNtA on gold.

[0007] It is also disclosed the specific interactions between mono-PEGylated rhNTA-immobilized laminin and cells. For this purpose, SAMs of mono-PEGylated rhNTA on gold were used as proof-of-concept platforms, since they can be easily produced and specifically tailored to provide a chemically well-defined molecular monolayer. The binding ligand was characterized and its ability to mediate laminin immobilization through a high affinity interaction was shown by solid-binding assay, surface plasmon resonance (SPR) and quartz crystal microbalance with dissipation monitoring (QCM-D). The bioactivity of mono-PEGylated rhNtA-immobilized laminin was subsequently investigated by evaluating its ability to self-polymerize and modulate the behaviour of human neural stem cells (hNSCs). hNSCs were used due to the well described role of laminin on the modulation of neural cell behavior.

[0008] The present disclosure is a versatile approach for the site-selective immobilization of laminin, while preserving its bioactivity, and it is useful for the development of cell instructive microenvironments for tissue engineering and regenerative medicine.

[0009] An aspect of the present disclosure, composition for substrate functionalization comprising: a poly(ethylene glycol) - PEG - for binding to the substrate; an agrin domain comprising a sequence at least 95% identical to SEQ. ID NO: 1 bound to said PEG; a laminin able for binding to a bioactive agent; wherein the laminin is bound to the agrin domain. The composition for substrate functionalization comprising:; an agrin domain comprising a sequence at least 95% identical to SEQ. ID. NO: 1 conjugated at its N-terminus to an end-group functionalized poly(ethylene glycol) to allow the binding of the agrin domain to a substrate while assuring the exposure of the high-affinity laminin binding site of agrin, located on the C-terminal; laminin capable of interacting with a bioactive agent, wherein laminin is bound to the agrin domain by high affinity interaction.

[0010] The SEQ. ID. 1 is:
GPTCPERALERREEEANVVLTGTVEEILNVDPVQHTYSCKVRVWRYLKGKDLVARESLLDGGNKVVISGFGD
PLICDNQVSTGDTRIFFVNPAPPYLWPAHKNELMLNSSLMRITLRNLEEVEFCVEDKP.

[0011] Methods for the alignment of sequences for comparison are well known in the art, such methods include GAP, BESTFIT, BLAST, FASTA and TFASTA. GAP uses the algorithm of Needleman and Wunsch ((1970) J Mol Biol 48: 443-453) to find the global (over the whole the sequence) alignment of two sequences that maximizes the number of matches and minimizes the number of gaps. The BLAST algorithm (Altschul et al. (1990) J Mol Biol 215: 403-10) calculates percent sequence identity and performs a statistical analysis of the similarity between the two sequences. The software for performing BLAST analysis is publicly available through the National Centre for Biotechnology Information (NCBI). Global percentages of similarity and identity may

also be determined using one of the methods available in the MatGAT software package (Campanella et al., BMC Bioinformatics. 2003 Jul 10; 4:29. MatGAT: an application that generates similarity/identity matrices using protein or DNA sequences). Minor manual editing may be performed to optimise alignment between conserved motifs, as would be apparent to a person skilled in the art. The sequence identity values, which are indicated in the present subject matter as a percentage were determined over the entire amino acid sequence, using BLAST with the default parameters.

[0012] In an embodiment for better results, the agrin domain comprises a sequence at least 96% identical to SEQ. ID NO: 1, preferably at least 97% identical to SEQ. ID NO: 1, at least 98% identical to SEQ. ID NO: 1, at least 99% identical to SEQ. ID NO: 1.

[0013] In an embodiment for better results, the agrin domain comprises a sequence identical to SEQ. ID NO: 1.

[0014] In an embodiment for better results, the agrin domain is conjugated at its N-terminal with a thiol-terminated poly(ethylene glycol).

[0015] In an embodiment for better results, the bioactive agent is selected from a list consisting of: a biomolecule, an active ingredient, a growth factor, extracellular vesicle, a hormone, a cell, or mixtures thereof.

[0016] In an embodiment for better results, the biomolecule is another laminin, a different protein, a peptide, a drug, a polysaccharide, or mixtures thereof.

[0017] In an embodiment for better results; the cell is selected from: osteoblast, osteoclast, osteocyte, pericyte, endothelial cells, endothelial progenitor cells, hematopoietic progenitor cell, hematopoietic stem cell, neural progenitor cell, neural stem cell, neural cell, oligodendrocyte progenitor cell, oligodendrocytes, ependymal cells, mesenchymal stromal/stem cell, induced pluripotent stem cell, embryonic stem cell, perivascular stem cells, amniotic fluid stem cell, amniotic membrane stem cell, umbilical cord stem cell, genetically engineered cell, or mixtures thereof.

[0018] In an embodiment for better results, the poly(ethylene glycol) size varies between 2 and 40 KDa; preferably 3-20 KDa, more preferably 3.5-10 KDa.

[0019] Another aspect of the present disclosure is the use of the composition of the present disclosure in veterinary or human medicine. Namely, for use in the treatment of diseases that involve the regeneration or treatment of tissues, or for use in the prevention of tissue degeneration.

[0020] In an embodiment for better results, the substrate is a naturally-derived or purely synthetic polymer, a synthetically-derived biopolymer, a metal, or mixtures thereof.

[0021] Another aspect of the present disclosure is a hydrogel comprising the composition described in the present subject matter.

[0022] In an embodiment for better results, the hydrogel is selected from the following list: poly(ethylene glycol), poly(vinyl alcohol), chitosan, alginate, collagen, dextran, fibrin, hyaluronic acid, silk fibroin, cellulose, synthetically-derived biopolymers, or mixtures thereof.

[0023] Another aspect of the present disclosure is a substrate coating comprising the composition described in the present subject matter.

[0024] Another aspect of the present disclosure is a coated article comprising the coating composition of the in the present subject matter. In particular wherein the article is an electrode.

[0025] Another aspect of the present disclosure is a kit for screening therapeutic drugs, comprising the composition described in in the present subject matter.

**Brief Description of the Drawings**

[0026] The following figures provide preferred embodiments for illustrating the description and should not be seen as limiting the scope of invention.

[0027] **Figure 1** - **Recombinant human NtA (rhNtA) domain characterization. A)** Coomassie Blue stained 15% SDS-PAGE gel and **B)** Western-blot analysis of 10 µg of purified rhNtA. MW, Molecular Weight marker. **C)** MALDI-TOF MS spectra of purified rhNtA.

[0028] **Figure 2** – **rhNtA Bioactivity**. Solid-phase assay of rhNtA binding to immobilized msLn-111 (10 µg/mL). The results are shown as fitted curve of the mean ± standard deviation (SD) of three replicate samples from one experiment representative of three independent assays. Non-linear regression analysis revealed a $K_D$ value of rhNtA to msLn-111 of 5.85 ± 0.43 nM ($r^2$ = 0.99).

[0029] **Figure 3** – hNSC adhesion to rhNtA-immobilized msLn-111 (10 µg/mL) as a function of rhNtA concentration (0.1 – 40 µg/mL), evaluated performing a cell adhesion centrifugation assay. The number of adherent cells on wells coated with BSA (1% (w/v), negative control),

rhNtA (10 μg/mL) and 20 μg/mL poly(ornithine)/ 10 μg/mL msLn-111 (positive control), is also shown. Data represent mean ± SD of 10 to 18 replicates from two independent experiments; one-way ANOVA followed by Dunnett's test (*vs.* poly(ornithine)/msLn-111).

[0030] **Figure 4** – **Characterization of N-terminal PEGylated rhNtA. A)** Cation-exchange chromatogram of the conjugation mixture. The chromatogram was obtained by monitoring the eluent at 280 nm and using a HiTrap SP HP column (GE Healthcare); 1, di-PEGylated rhNtA; 2, mono-PEGylated rhNtA; 3, Native rhNtA. **B)** Coomassie Blue stained 4-12% Bis-Tris gel of native and PEGylated rhNtA after purification. M, MW marker; C, Conjugation mixture before cation-exchange chromatography; 1, di-PEGylated rhNtA band at around 36.5 kDa; 2, mono-PEGylated rhNtA band at around 28.8 kDa; 3, native rhNtA at around 14.9 kDa. **C)** MALDI-TOF MS spectra of native and PEGylated rhNtA. The presented molecular weight corresponds to the value obtained for the high intensity peak – Native rhNtA 14.8 kDa; mono-PEGylated rhNtA 18.4 kDa; di-PEGylated rhNtA 22.1 kDa.

[0031] **Figure 5** – **Assessment of the ability of site-selective immobilized laminin to self-polymerize**. **A)** Schematic representation of laminin self-polymerization (not to scale). Adapted from [57]. N-terminal domains of α, β and γ chains interact to form a polygonal network. The long arm is not involved in the network formation. **B)** mPEG rhNtA-SAM (left panel) or SGA-SAM (right panel) were incubated with msLn-111 (50 μg/mL) for 24 h, under neutral conditions (pH 7.0), and samples processed for immunofluorescence staining of laminin. Scale Bar = 50 μm. **C)** Number of aggregates; **D)** Average size ($\mu m^2$); **E)** Perimeter (μm); and **F)** Maximum Feret's diameter (μm) determined by image processing and quantitative analysis using ImageJ/Fiji and MATLAB® software, respectively. Data represent mean ± SD of 13-16 replicate samples from three independent assays; non-parametric Mann-Whitney U-test.

[0032] **Figure 6** – **Immobilization of rhLn-521 onto SAMs and its effect on hNSC adhesion and spreading. A)** Schematic representation of the prepared surfaces (not to scale) – Au surface (control surface), EG4-SAM (non-fouling surface), mPEG rhNtA-SAM (for site-selective immobilization of laminin) and SGA-SAM (for non-specific covalent immobilization of laminin). **B)** QCM-D analysis of rhLn-521 immobilization ($ng/cm^2$) on SAMs. Data represent mean ± SD of three independent experiments; one-way ANOVA followed by Bonferroni's test. **C)** Representative 2D projections of CLSM 3D stack images of adhered hNSCs, after 24h of culture. Scale Bar = 50 μm; **D)** Total number of adherent cells; and **E)** Average cell spreading area ($\mu m^2$) determined by quantitative analysis of images acquired with an IN Cell Analyzer 2000 imaging system. Data represent mean ± standard error of the mean (SEM) of four replicate samples from an experiment representative of three independent assays; one-way ANOVA followed by Bonferroni's test.

[0033] **Figure 7** – Amino acid sequence of recombinant human N-terminal agrin (rhNtA) domain after purification and N-terminal tag cleavage.

[0034] **Figure 8** – Solid-phase assay of Trx-$His_6$-hNtA binding to immobilized msLn-111 (10 μg/mL). The results are shown as fitted curve of the mean ± standard deviation (SD) of three replicate samples from one experiment representative of three independent assays. Non-linear regression analysis revealed a $K_D$ value of Trx-$His_6$-hNtA to msLn-111 of 6.49 ± 0.58 nM ($r^2$ = 0.98).

[0035] **Figure 9** – Isotherm of rhNtA adsorption determined using a direct ELISA assay. The results are shown as fitted curves of the mean ± SD of twelve replicate samples analysed from two independent experiments ($r^2$ = 0.94).

[0036] **Figure 10** – Position of conjugated PEG moiety on the purified mono-PEGylated rhNtA determined by peptide mapping. Positive mode MALDI-TOF/TOF identification of the fragments obtained upon digestion of native and mono-PEGylated rhNtA with trypsin. Two peaks correspondent to the N-terminus were identified on both native and mono-PEGylated rhNtA (arrows) – (**A**) F1 - GPTCPER [1-7] m/z 816.3677 and (**B**) F2 - GPTCPERALER [1-11] m/z 1285.6278.

[0037] **Figure 11** – Immobilization of rhLn-521 ($ng/cm^2$) onto mPEG rhNtA-SAMs, as a function of the mono-PEGylated rhNtA concentration. SAMs were prepared using a fixed concentration of EG4 (100.0 μM) and decreasing concentrations of mono-PEGylated rhNtA (2.5, 5.0 and 10.0 μM). rhLn-521 immobilization was monitored in real time by QCM-D analysis and data modeled with application of the Voigt model. Results represent mean ± SD of three independent experiments; one-way ANOVA followed by Bonferroni's test.

[0038] **Figure 12** – IRRAS spectra of mPEG rhNtA- and SGA- SAMs. EG4-SAMs and native rhNtA-adsorbed to Au surfaces were used as controls. A baseline correction and smoothing were applied to all the spectra. Two protein characteristic bands were identified – amide I (1690 ± 45 $cm^{-1}$) and II (1540 ± 60 $cm^{-1}$).

[0039] **Figure 13** – Representative 2D projections of CLSM 3D stack images of hNSCs adhered to TCPS and EG4- and SGA-SAMs. Images were acquired after 24h of culture. Scale Bar = 50 μm.

[0040] **Figure 14** – hNSC adhesion to SAMs determined measuring the average fluorescence intensity of Hoechst 33342 in samples processed for F-actin/DNA staining. Data represent mean ± SEM of four replicate samples from one experiment representative of three independent assays; one-way ANOVA followed by Bonferroni's test.

[0041] **Figure 15** – hNSCs average occupied area ($\mu m^2$) determined by quantitative analysis of images acquired in IN Cell Analyzer 2000 imaging system. Data represent mean ± SEM of four replicate samples of an experiment representative of three independent assays; one-way ANOVA followed by Bonferroni's test.

[0042] **Figure 16** – Oligonucleotide sequences used for PCR linearization of hNtA gene and pCoofy2 expression vector

[0043] **Figure 17** – Fragments obtained upon digestion of native- and mono-PEGylated rhNtA with trypsin. The N-terminus sequence of rhNtA fragment is depicted in bold.

**Detailed Description**

[0044] The present disclosure is also further described, in particular, using embodiments of the disclosure. Therefore, the disclosure is not limited to the descriptions and illustrations provided. These are used so that the disclosure is sufficiently detailed and comprehensive. Moreover, the intention of the drawings is for illustrative purposes and not for the purpose of limitation.

[0045] In this embodiment, the assays and resulting data of the present disclosure are described. In an embodiment, recombinant human N-terminal agrin (rhNtA) domain expression and purification are described. The NtA domain, comprising residues Thr 30 – Pro 157 of the human agrin protein (Uniprot reference O00468), was expressed in Escherichia coli (E. coli) strain BL21(DE3) using the pCoofy2 expression vector (gift from Sabine Suppmann – Addgene plasmid # 43981). pCoofy2 is a derivative of pETM22 vector that contains a thioredoxin-poly-His6 (6x Histidine residues) (Trx-His6) N-terminal tag followed by an HRV 3C recognition site located downstream of the N-terminal tag.

In an embodiment, details on cloning of human NtA gene and expression vector are disclosed. The fusion protein (Trx-His6-hNtA) was expressed by induction of log-phase cultures with 0.2 mM of isopropyl β-D-1-thiogalactopyranoside (IPTG; Sigma-Aldrich) at 20°C for 5h and purified by immobilized metal affinity chromatography using a HisTrap column (GE Healthcare). A concentration gradient of 0 to 500 mM of imidazole was applied to elute the fusion protein. The N-terminal Trx-His6 tag was then cleaved during dialysis using HRV 3C protease (kindly provided by Biochemical and Biophysical Technologies (B2Tech) Platform of i3S) in a protease:target protein ratio (unit/μg) of 1:10. Untagged recombinant human NtA (rhNtA) contains additional Gly and Pro residues at its N-terminus (Fig. 7). rhNtA was dialyzed against 10 mM phosphate buffered saline (PBS) pH 7.4, concentrated in a 10 kDa molecular weight cut-off (MWCO) ultrafiltration membrane (GE Healthcare) and stored at -80°C until further use. Final domain concentration was estimated by measuring the absorbance at 280 nm. The purity of the rhNtA domain was assessed by sodium dodecyl sulfate–polyacrylamide gel electrophoresis (SDS-PAGE) analysis and Western blotting using the anti-agrin antibody - rabbit polyclonal agrin antibody (1:5000; Abcam, ab85174). The rhNtA molecular weight was determined by mass spectrometry, as described in "Protein and PEGylated conjugate characterization by mass spectrometry".

[0046] In an embodiment, a solid-phase binding assay was described. Binding of rhNtA to immobilize laminin was assessed performing an enzyme-linked binding assay (ELISA). 96-well microtiter ELISA plates (BD Falcon) were coated with poly(D-lysine) (PDL; 20 μg/mL; Sigma-Aldrich) and then incubated with laminin-111 from mouse Engelbreth-Holm-Swarm sarcoma (msLn-111;10 μg/mL; Sigma-Aldrich) in 50 mM sodium bicarbonate buffer pH 9.6 (overnight, 4°C). After blocking with 2.5% (w/v) bovine serum albumin (BSA; Biowest; 1.5h, room temperature (RT)), wells were incubated with 2-fold serial dilutions of rhNtA (0.1 – 100 nM; 2h, 37°C). Plates were then washed with PBS/0.05% (v/v) Tween® 20 and incubated with rabbit polyclonal agrin antibody (1:5000; 2h, RT). A goat anti-rabbit IgG (H+L) coupled to horseradish peroxidase (HRP) (1:2000; Life Technologies, A16023) was used as secondary antibody, and colour was developed using 3,3',5,5' tetramethyl benzidine (TMB) as substrate (Biolegend; 30 min, RT). The reaction was stopped with 2 M $H_2SO_4$ and the absorbance measured at 450 nm (BioTek® Synergy™ Mx). The dissociation constant ($K_D$) value of rhNtA to msLn-111 was estimated by non-linear regression analysis using GraphPad Prism 6 software (San Diego).

[0047] In an embodiment, real-time interactions between rhNtA and immobilized laminin were detected by surface plasmon resonance (SPR) at 25°C using a BIACORE X100 (GE Healthcare). Laminin was immobilized on a CM5 sensor chip (GE Healthcare) using amine-coupling chemistry. Briefly, the flow cells surface was activated with a 1:1 mixture of 0.1 M N-hydroxysuccinimide (NHS; Sigma-Aldrich) and 0.4 M 3-(N,N-dimethylamino) propyl-N-ethylcarbodiimide (EDC; Sigma-Aldrich) at a flow rate of 10 μL/min. msLn-111 or recombinant human laminin-521 (rhLn-

521; Biolamina) (50 µg/mL in 10 mM sodium acetate pH 3.5) were immobilized at a density of 4000 resonance units. The reactive groups in excess were then deactivated with 1 M ethanolamine-HCl pH 8.5 (Sigma-Aldrich). For binding measurements, 5-fold serial dilutions of rhNtA (500 – 0.8 nM) were prepared in 10 mM 4-(2-hydroxyethyl)-1-piperazineethanesulfonic acid (HEPES; pH 7.4, containing 150 mM sodium chloride (NaCl; VWR), 3 mM Ethylenediamine tetra-acetic acid (Sigma-Aldrich) and 0.005% (v/v) surfactant P20 (GE Healthcare)) and flowed at 30 µL/min onto the flow cells. Proteins were allowed to associate and dissociate for 120 and 1600 s, respectively. Experimental results were fitted with Langmuir 1:1 binding kinetics within Biacore X100 Evaluation software version 2.0.1 (GE Healthcare).

[0048] Human neural stem cells (hNSCs) derived from the National Institutes of Health (NIH) approved H9 (WA09) human embryonic stem cells were purchased from Life Technologies (N7800-200). Cells were expanded according to the manufacturer's protocol in poly(ornithine)/msLn-111-coated tissue culture-treated plates in serum-free StemPro® NSC SFM growth medium (Life Technologies).

[0049] To evaluate the ability of rhNtA-immobilized msLn-111 to promote the adhesion of hNSCs, a centrifugation cell adhesion assay was performed. Here, controllable and reproducible detachment forces were applied to adherent cells, providing relative measurements of adhesion strength. 96-well tissue culture plates (Corning) were coated with increased concentrations of rhNtA (0 – 40 µg/mL) overnight at 4°C and blocked with 1% (w/v) BSA for 1h at RT to prevent non-specific adhesion to the substrate. msLn-111 was then added at a fixed concentration (10 µg/mL), the plate incubated for 2h at 37°C and hNSC adhesion assessed. Wells incubated with 1% (w/v) BSA or 20 µg/mL poly(ornithine) / 10 µg/mL msLn-111 were used as negative and positive control, respectively. To assess the effect of the domain per se on cell adhesion, wells incubated with 10 µg/mL rhNtA were used.

In an embodiment, N-terminal PEGylation of rhNtA was performed. A 5 mg/mL rhNtA solution in 0.1 M sodium phosphate ($NaH_2PO_4$) pH 6.5 was added to thiol-PEG-succinimidyl glutaramide (HS-PEG-SGA; 3.5 kDa; purity > 90%, Jenkem USA) at a protein:PEG molar ratio of 1:2. The reaction was allowed to proceed for 4h at 4°C and then quenched with 2 M hydroxylamine pH 7.4. The solution was diluted to a final protein concentration of 0.5 mg/mL with 1 mM HCl and the pH adjusted to 3.5 with 1 M HCl. The reaction mixture was then diluted (100×) with 20 mM sodium acetate pH 4.0 and loaded onto a HiTrap SP HP cation exchange column (GE Healthcare). A gradient of 0 to 1 M NaCl in 20 mM sodium acetate pH 4.0 was used to elute the different PEGylated fractions. The peak corresponding to the mono-N-terminal conjugate was dialyzed against 10 mM PBS pH 7.4, concentrated in a 10 kDa MWCO ultrafiltration membrane (GE Healthcare) and stored at -80°C until further use. Protein concentration was estimated by measuring the absorbance at 280 nm and the conjugate was characterized by SDS-PAGE and MALDI-TOF mass spectrometry (MALDI-TOF MS).

[0050] In an embodiment, rhNtA and the PEGylated conjugate were characterized by mass spectrometry. The native or mono-PEGylated rhNtA, as well as unmodified HS-PEG-SGA, were analysed by MALDI-TOF MS. Briefly, samples were diluted 1:4 (v/v) in MALDI matrix (sinapinic acid 10 mg/mL, 50% acetonitrile, 0.1% trifluoroacetic acid, all purchased from Sigma-Aldrich), spotted onto a target plate and analysed in linear positive mode. Mass spectra were internally calibrated with thioredoxin (m/z 11674) and apomyoglobin (m/z 16952). To characterize the site of PEG conjugation to rhNtA, peptide mapping of native and mono-PEGylated rhNtA was performed.

[0051] In an embodiment, self-assembled monolayers (SAMs) were prepared. Mixed SAMs of mono-PEGylated rhNtA (mPEG rhNtA-SAM) or HS-PEG-SGA (SGA-SAM) were prepared on gold-coated substrates (0.5 × 0.5 $cm^2$), obtained from Instituto de Engenharia de Sistemas e Computadores – Microsistemas e Nanotecnologias, Portugal (INESC-MN). Prior to use, gold surfaces were cleaned. Gold substrates were then incubated in ethanolic solutions (99.9%; Merck-Millipore) of either mono-PEGylated rhNtA (2.5, 5.0 or 10.0 µM), for laminin affinity binding; or HS-PEG-SGA (5.0 µM), for non-selective covalent immobilization of laminin. After 4h at RT and under inert conditions (glove chamber saturated with dry nitrogen), SAMs were rinsed with absolute ethanol to remove any physically adsorbed molecules. For proper monolayer packing mPEG rhNtA- and SGA- SAMs were subsequently incubated with a 100.0 µM absolute ethanolic solution of (11-mercaptoundecyl) tetraethylene glycol (EG4, SensoPath Technologies) for 16h at RT and under the inert conditions mentioned above. Afterwards, SAMs were thoroughly rinsed with absolute ethanol (99.9%; Merck-Millipore). EG4-SAMs, used as control surfaces, were prepared by immersing cleaned gold substrates in a 100.0 µM ethanolic solution of EG4 for 16h at RT and under inert conditions.

[0052] In an embodiment, laminin binding to SAMs was followed by Quartz crystal microbalance with dissipation monitoring (QCM-D)

[0053] Gold-coated QCM-D sensors (Biolin Scientific) were cleaned as previously described. Clean sensors were further modified. A QCM-D system (Q-Sense E4 instrument, Biolin Scientific)

was used to monitor in real time the frequency (Δf) and dissipation (ΔD) shifts related to laminin adsorption as described in the document. Data was modeled using the Voigt model in the QTools® V3 software. Results are presented as mass per surface area (ng/cm²).

[0054] In an embodiment, laminin self-polymerization was assessed. mPEG rhNtA- SAMs were equilibrated in 10 mM HEPES pH 7.4, to favour the affinity interaction with laminin, while SGA-SAMs were equilibrated in 100 mM sodium bicarbonate pH 8.5, to favour the non-selective covalent interaction with laminin amine groups, and then incubated with msLn-111 (20 µg/mL; 2h, RT). The substrates were then thoroughly washed, to remove any unbound laminin. To assess the ability of laminin to self-polymerize, an msLn-111 solution (50 µg/mL) in 20 mM Tris-HCl pH 7.0, containing 1 mM $CaCl_2$, was used. The laminin concentration used was below the critical protein concentration necessary to trigger laminin polymerization in neutral pH solution. Mixed SAMs with affinity- (mPEG rhNtA-SAMs) or covalent-bound (SGA-SAMs) msLn-111 were incubated with the laminin solution for 24h at 37°C. Finally, samples were processed for laminin immunostaining, and observed under confocal laser scanning microscopy (CLSM) (TCS SP5 II; Leica Mycrosystems), using a Plan-Apochromat 63×/1.4NA oil objective. A z-section of 15 µm was acquired and subsequently projected into a 2D image. Processing and quantitative analysis of the acquired images were performed in ImageJ/Fiji and MATLAB® software, respectively.

[0055] In an embodiment, cell adhesion and morphology were analysed to determine the impact of the immobilization approach on the cell adhesion-promoting activity of laminin, mPEG rhNtA- or SGA-SAMs were equilibrated in 10 mM HEPES pH 7.4 and then incubated for 2h at RT with rhLn-521 (20 µg/mL). After being washed with 10 mM HEPES pH 7.4 to remove unbound laminin, hNSCs (50,000 viable cells/cm²) were added to the substrates and incubated at 37°C with 5% $CO_2$ for 24h. Samples were processed for F-actin/DNA staining, as described in Supplementary Materials and Methods, and imaged with the IN Cell Analyzer 2000 imaging system (GE Healthcare) using a Nikon 20×/0.45 NA Plan Fluor objective. A z-section of 45 µm was acquired per field of view (FOV) and then projected into a 2D image. Images spanning a total area of 4.6 mm² were analyzed using CellProfiler image analysis software. Briefly, nuclei were segmented through an Otsu thresholding method from the 4',6-diamidino-2-phenylindole (DAPI) channel while cells cytoplasm was segmented from the actin channel through a propagation from the previously identified nucleus, using a minimum cross entropy threshold. Measurements were obtained for total number of adhered cells, average cell spreading area (µm²) and average occupied area (µm²) per FOV. Representative images for each condition were also obtained by CLSM using a Plan-Apochromat 63×/1.4NA oil objective. A z-section of 12 µm was acquired and subsequently projected into a 2D image.

[0056] Individual experiments with biological replicates were performed at least in duplicate and statistical analysis was performed using GraphPad Prism 6 software (San Diego). Statistically significant differences between two conditions were detected using a non-parametric Mann Whitney U-test. Comparisons between three or more groups were performed with one-way ANOVA analysis, followed by the Bonferroni correction for pairwise comparisons or the Dunnett's two-tailed test for comparisons with the control condition. For all analyses, differences were considered significant at $p < 0.05$.

[0057] In an embodiment, recombinant human N-terminal agrin (rhNtA) domain was produced. In contrast with most of reports published to date in which the NtA used was derived from chicken agrin, we produced the human variant of this domain because of its higher clinical relevance. This is of particular interest when envisaging the use of this domain in platforms for human-disease modelling, cell culture/delivery or engineered coatings for neuroelectrodes.

[0058] The produced fusion protein Trx-$His_6$-hNtA, revealed high affinity binding to msLn-111 with an equilibrium dissociation constant ($K_D$) of 6.49 ± 0.58 nM, as determined by solid-phase binding assay (Fig. 8), similar to that reported for chicken NtA - msLn-111 interaction ($K_D$ = 5 nM). Cleavage of the N-terminal tag was subsequently conducted to enable conjugation of a thiol-terminated PEG moiety to the domain N-terminal, for further immobilization of rhNtA to the selected substrate. This immobilization approach was chosen to assure the exposure of the high-affinity laminin binding site of rhNtA, located on the C-terminal. Untagged rhNtA domain was produced with a high purity (> 90%) and with the expected MW 14.5 kDa, as evidenced by Coomassie blue staining (Fig. 1A) and Western blot analysis (Fig. 1B). Molecular weight was further confirmed by MALDI-TOF MS (MW 14.8 kDa) (Fig. 1C).

[0059] rhNtA was shown to mediate a high affinity interaction with msLn-111 ($K_D$ = 5.85 ± 0.43 nM), as evidenced by solid-phase binding assay (Fig. 2). To monitor in real time the interaction between rhNtA and immobilized msLn-111 or rhLn-521, SPR was conducted (Table 1). Native rhNtA was found to interact with high affinity with both msLn-111 and rhLn-521 ($K_D$ = 0.98 ± 0.02 and 0.54 ± 0.14 nM, respectively; Table 1), showing that binding affinity towards laminin was retained independently of the laminin isoform. Results from both techniques indicate that the laminin binding site of the produced rhNtA domain preserved its bioactivity, namely the ability to interact with high affinity with laminin.

[0060] **Table 1.** Kinetic parameters ($k_a$, association rate constant; $k_d$, dissociation rate constant) and affinity constant ($K_D$, dissociation constant) of rhNtA to immobilized msLn-111 or rhLn-521, estimated by SPR. Data represent mean ± SD of three independent experiments.

| | $k_a$ ($x10^5$) $M^{-1}.s^{-1}$ | $k_d$ ($x10^{-4}$) $s^{-1}$ | $K_D$ (nM) |
|---|---|---|---|
| **msLn-111** | 5.25 ± 1.83 | 5.12 ± 1.71 | 0.98 ± 0.02 |
| **rhLn-521** | 4.86 ± 1.55 | 2.52 ± 0.43 | 0.54 ± 0.14 |

[0061] In an embodiment, rhNtA-immobilized laminin was shown to mediate cell adhesion of human neural stem cells. Laminin mediates integrin- and non-integrin-dependent adhesion of neural stem cell (NSCs), being commonly used as a surface coating for NSC culture. As the site-specific immobilization of laminin should preserve exposure of its multiple bioactive domains interacting with cell adhesion receptors and, therefore, its cell adhesion-promoting activity, we assessed the ability of rhNtA-immobilized msLn-111 to mediate cell adhesion of hNSCs. These cells were seeded on cell culture wells coated with rhNtA-immobilized msLn-111 and cell adhesion quantified, as a function of rhNtA concentration, using a centrifugation adhesion assay (Fig. 3). The application of a constant centrifugal force revealed an increase in cell adhesion with the increase of the rhNtA concentration from 0.1 to 10 μg/mL (Fig. 3), at which the levels of cell adhesion observed on rhNtA-immobilized msLn-111 reached values similar to those on the msLn-111 positive control (Fig. 3). This suggests that under these conditions, the amount of affinity-immobilized msLn-111 attained a plateau, which is in agreement with the isotherm of rhNtA adsorption (Fig. 9) that shows a saturation plateau at domain concentrations ≥ 2.5 μg /mL. The cell adhesion levels observed in the absence of rhNtA (0 μg/mL rhNtA) are most likely due to the competitive displacement of adsorbed BSA by laminin, an effect also known as the Vroman effect. Cell adhesion to wells incubated only with rhNtA (10 μg/mL) was comparable to that observed on the negative control (BSA; Fig. 3), due to the absence in the rhNtA of bioactive cell adhesion domains. These results demonstrate that, when immobilized through rhNtA, laminin retains its ability to mediate cell adhesion, suggesting the correct exposure of laminin's main bioactive sites interacting with cell surface receptors.

[0062] In an embodiment, rhNtA was shown to be selectively PEGylated at the N-terminal. The rhNtA sequence comprises seven primary amines, including the α-amine of Gly1 and the ε-amine of six Lys residues (Fig. 7), which can theoretically react with HS-PEG-SGA, more specifically with the SGA group. The site-specific addition of the PEG moiety at the N-terminal domain (α-amine) of rhNtA can be controlled by adjusting the pH at which the PEGylation reaction occurs and by adjusting the protein:PEG molar ratio. The conjugation reaction was performed at pH 6.5 and using a protein:PEG molar ratio of 1:2. The slightly acidic pH directs the PEGylation reaction to the α-amino group at the N-terminal of rhNtA, by taking advantage of the differences in pKa values of the α-amino group (pKa 7.8) *versus* that of the ε-amino groups (pKa 10.1) on the side chains of Lys residues. These conditions favour the protonation of the ε-amino groups of Lys, while assuring the availability of the α-amino group at the N-terminal as nucleophile. The cation-exchange chromatogram of the conjugation mixture (Fig. 4A) showed three different fractions, which correspond, as evidenced by molecular weight estimation from SDS-PAGE analysis (Fig. 4B), to rhNtA PEG conjugates containing either a double (MW ≈ 36.5 kDa; di-PEGylated rhNtA, peak 1) or single (MW ≈ 28.8 kDa; mono-PEGylated rhNtA, peak 2) PEG molecule and native rhNtA (MW ≈ 14.5 kDa, peak 3). The efficiency of the PEGylation reaction was determined based on the SDS-PAGE analysis (Fig. 4B). A PEGylation yield of 47% was obtained, from which 94% corresponds to mono-PEGylated rhNtA and the remaining 6% to di-PEGylated rhNtA. Since the large hydrodynamic volume of PEGylated proteins retards their mobility on SDS-PAGE gels, resulting in higher molecular weight estimates, PEGylation reaction products were further analysed by MALDI-TOF MS for an absolute estimation of their molecular weight. The MALDI-TOF MS spectra of native and PEGylated rhNtA (Fig. 4C) indicate a molecular weight centred at 18.4 and 22.1 kDa for mono- and di-PEGylated rhNtA, respectively (the MW of native rhNtA was found to be 14.8 kDa, confirming the previously determined value (Figure 1C)).

[0063] The position of the conjugated PEG moiety on the purified mono-PEGylated rhNtA conjugate was further determined by peptide mapping, comparing the fingerprint of native- and PEGylated rhNtA. The majority of the theoretical fragments, as well as the rhNtA N-terminus were experimentally detected in both samples (Figure 14). Also, their molecular masses, which were experimentally determined by MALDI-TOF MS, are very similar to the predicted values obtained in web.expasy.org/peptide_mass (Fig. 17). Two peaks corresponding to the N-terminus of rhNtA domain were identified in both native and mono-PEGylated rhNtA – GPTCPER (F1) [1-7] m/z 816.3677 (Fig. 17, Fig. 10A) and GPTCPERALER (F2) [1-11] m/z 1285.6278 uj nm rfc (Fig. 17, Fig. 10B). In the conjugated sample, a significant decrease in the signal-to-noise ratio was observed for F1, while the peak correspondent to F2 was not detected.

[0064] In an embodiment, N-terminal PEGylated rhNtA was shown to bind with high affinity to laminin. SPR analysis was conducted to evaluate the impact of N-terminal PEGylation on rhNtA laminin binding ability. N-terminal PEGylation led to a decrease of the binding affinity for both msLn-111 ($K_D$ = 3.36 ± 0.11 nM) and rhLn-521 ($K_D$ = 1.58 ± 0.41 nM) (Table 2), estimated as a 3.4- and 2.9- fold decrease, respectively, compared to native rhNtA (Table 1). This shows that PEG conjugation to rhNtA slowed down the rate of domain association ($k_a$) towards immobilized laminin, while the dissociation rate ($k_d$) was not affected (Table 2). Interestingly, the affinity of both native (Table 1) and mono-PEGylated rhNtA (Table 2) for rhLn-521 was found to be slightly higher than that determined for msLn-111. Moreover, the complex formed with this laminin isoform is more stable, as evidenced by higher $k_d$ values (Table 1 and 2). The affinity between NtA and laminin is regulated by laminin chain composition, and that although the agrin binding site is located within the γ1 chain, α and β laminin chains may also contribute to the binding, even though to a lesser extent. Therefore, the differences observed in the binding affinity of native and mono-PEGylated rhNtA to msLn-111 and rhLn-521 can be related to the chain composition of the laminin isoforms tested.

[0065] **Table 2.** Kinetic parameters ($k_a$ and $k_d$) and affinity constant ($K_D$) of mono-PEGylated rhNtA to immobilized msLn-111 or rhLn-521, estimated by SPR. Data represent mean ± SD of three independent experiments.

| | $k_a$ ($x10^5$) $M^{-1}.s^{-1}$ | $k_d$ ($x10^{-4}$) $s^{-1}$ | $K_D$ (nM) |
|---|---|---|---|
| **msLn-111** | 1.38 ± 0.05 | 4.64 ± 0.31 | 3.36 ± 0.11 |
| **rhLn-521** | 1.66 ± 0.63 | 2.47 ± 0.40 | 1.58 ± 0.41 |

[0066] In an embodiment, N-terminal PEGylated rhNtA is used for the site-selective immobilization of laminin with retention of bioactivity. The potential of mono-PEGylated rhNtA to promote the site-selective immobilization of laminin onto substrates was assessed by using mixed SAMs of mono-PEGylated rhNtA and (11-mercaptoundecyl) tetraethylene glycol (EG4) (mPEG rhNtA-SAMs) as a model surface. EG4 was used to prevent nonspecific protein immobilization and thus guarantee signal specificity and maximum bioactivity of the immobilized biomolecules, while also enhancing the correct monolayer packing. Mixed SAMs of HS-PEG-SGA and EG4 (SGA-SAMs) were also prepared to promote the non-selective covalent immobilization of laminin through the reaction with protein amine groups present in multiple locations within the laminin structure.

[0067] To avoid steric effects and have a finer control over the binding ligand surface density, which ultimately would determine the amount of affinity-bound laminin, an initial screening was conducted to determine the most suitable mono-PEGylated rhNtA domain concentration. QCM-D analysis was conducted with different mono-PEGylated rhNtA concentrations (2.5, 5.0 and 10.0 μM) while keeping that of EG4 constant (100.0 μM), to evaluate laminin immobilization (Fig. 11). Results show a more effective laminin immobilization when an intermediate concentration of mono-PEGylated rhNtA (5.0 μM) was used (638 ± 29 ng/$cm^2$, compared to the 146 ± 115 and 445 ± 57 ng/$cm^2$, obtained for 2.5 and 10.0 μM mono-PEGylated rhNtA, respectively) (Fig. 11). Based on these results, mixed SAMs were prepared using an intermediate concentration (5.0 μM) of either mono-PEGylated rhNtA or HS-PEG-SGA.

[0068] Infrared reflection absorption spectroscopy (IRRAS) analysis was performed to characterize the prepared mixed mPEG rhNtA- and SGA-SAMs, using Au surfaces as background. EG4-SAMs and adsorbed native rhNtA to Au surfaces were used as controls. The presence of rhNtA domain was confirmed by the detection of the two protein characteristic absorption bands correspondent to amide I (1690 ± 45 $cm^{-1}$), which is mainly associated with C=O stretching vibration and is directly related to the backbone conformation, and amide II (1540 ± 60 $cm^{-1}$), which results from the N-H and C-N vibration that were observed on both native rhNtA and mPEG rhNtA spectra (Fig. 12).

[0069] In an embodiment, site-selective immobilized laminin was shown to retain its ability to self-polymerize. Laminin polymerization is a key process to direct basement membrane assembly and organization and occurs by a thermally reversible process dependent on the presence of calcium ions. Previous studies exploring this hallmark feature of laminin demonstrated that this ECM protein is able to spontaneously self-polymerize in solution at neutral pH, requiring a minimal protein concentration of approximately 60 nM. The three-arm interaction model has been proposed by Cheng and co-workers (Fig. 5A) to explain the mechanism of laminin polymerization. This model proposes that the three laminin N-terminal short arms are able to interact with the globular N-terminal domains of other laminins to form a polygonal network, contributing to the basement membrane architecture. The long arm of the laminin heterotrimer, in turn, is predicted not to be involved in the network formation, being free to interact with cells out of the plan of the polymer. Based on this evidence, we evaluated

the ability of laminin to self-polymerize when immobilized onto mPEG rhNtA-SAMs (Fig. 5B, left panel) or SGA-SAMs (Fig. 5B, right panel). Differences between the two conditions were assessed by image processing and quantitative analysis, using ImageJ/Fiji and MATLAB® software, respectively. Four different variables were measured, including number of aggregates (Fig. 5C), aggregates average size (Fig. 5D), perimeter (Fig. 5E) and maximum Feret's diameter (Fig. 5F). More information about the specific meaning of each measured variable can be found in https://imagej.nih.gov/ij/docs/menus/analyze.html. The relation between the number of aggregates, the aggregates average size and the perimeter give us an indication about laminin ability to form larger organized polygonal-shape structures versus several small unstructured aggregates, while maximum Feret's diameter are good indicators of network organization. An organized polygonal network consisting mainly of lamellar aggregates was consistently observed when laminin was selectively immobilized onto mPEG rhNtA-SAMs (Fig. 5B, left panel). Data from image quantitative analysis (Fig. 5C-F) support this observation, as a higher tendency for the formation of larger polygonal-based (Fig. 5C-E) and organized (Fig. 5F) structures is evident as result of laminin polymerization. Moreover, the formed homogeneous matrix presents a fractal-like organization (Fig. 5B, left panel) and resembles the pattern of the networks reported in literature. On the other hand, the non-selective covalent immobilization of laminin onto SGA-SAMs, led to the formation of a matrix consisting mainly of several smaller aggregates (Fig. 5C-E), which are extended over several focal plans with no observable formation of polygon-based structures (Fig. 5B, right panel). The inability to form a more organized structure is evidenced by the lower values of maximum Feret's diameter (Fig. 5F). The 3D structures of the different formed laminin matrices can be better appreciated in the animation movies presented as Movie S1 – S2 in Supporting Information. The combination of the three independent variables (average size, perimeter and maximum Feret's diameter) and its analysis using the Fisher's combined probability test [56], also revealed statistically significant differences ($p < 0.0001$) on laminin self-polymerization between mPEG rhNtA- and SGA-SAMs. Overall, the results obtained showed that depending on the binding ligand (mono-PEGylated rhNtA vs. HS-PEG-SGA), structural distinct matrices can be formed. Moreover, we clearly demonstrate that only when we promote the site-selective immobilization of laminin (mPEG rhNtA-SAMs), one retains its natural/intrinsic ability to self-polymerize.

[0070] In an embodiment, site-selective immobilized rhLn-521 supports hNSC adhesion and spreading. rhLn-521 has a key role in the modulation of neural cell behaviour, including neuronal adhesion, viability and network formation. Indeed, documents show the potential of this laminin isoform to be used as a robust substratum for the culture and renewal of human embryonic and pluripotent stem cells. To assess laminin ability to mediate hNSC adhesion and spreading upon its binding to mPEG rhNtA-SAMs, rhLn-521was used. QCM-D analysis was first conducted to follow the kinetics of rhLn-521 immobilization onto SAMs (Fig. 6 A-B). Then, to characterize whether the proposed strategy favoured the exposure of rhLn-521 cell-adhesive domains, hNSC adhesion and spreading was assessed (Fig. 6 C-E).

[0071] In an embodiment, QCM-D monitoring of rhLn-521 immobilization onto mPEG rhNtA-SAMs indicated a protein immobilization (638 ± 29 ng/cm$^2$, Fig. 6B), with mass per surface area values close to the theoretical value calculated for laminin immobilization under these conditions (952 ng/cm$^2$). This suggests that the immobilized mono-PEGylated rhNtA retained a 3D conformation that allowed the selective interaction with laminin. Moreover, mPEG rhNtA SAMs led to an immobilization degree statistically similar to that observed for uncoated Au surfaces (1130 ± 348 ng/cm$^2$), in which laminin may randomly adsorb over the entire surface. SGA-SAMs, in contrast, presented lower amounts of immobilized rhLn-521 (342 ± 44 ng/cm$^2$) (Figure 6B), when compared to mPEG rhNtA-SAMs. As HS-PEG-SGA moieties can randomly interact with different amine groups within a single laminin molecule, these results suggest that the conformation of covalently-bound laminin and its spatial arrangement at the surface were distinct from that of affinity-bound laminin, leaving less area for the immobilization of other laminin molecules. As expected, the amount of adsorbed rhLn-521 on EG4-SAMs, was very low (20 ± 1 ng/cm$^2$) (Fig. 6B).

[0072] In an embodiment, site-selective immobilization of laminin onto mPEG rhNtA-SAMs led to hNSC adhesion comparable to that observed on rhLn-521-coated Au surfaces, used here as a control surface for hNSC adhesion (Fig. 6D and Fig. 14). After 24 h of culture, cells were well-spread (Fig. 6E and Fig. 15), exhibiting a morphology (Fig. 6C) comparable to that observed for cells seeded on rhLn-521-coated Au surfaces surfaces (Fig. 6C). Moreover, cells adhered to mPEG rhNtA-SAMs exhibit an average spreading area of 2812 ± 89 µm$^2$ (Fig. 6E), comparable to that observed for cells cultured on rhLn-521-coated Au (3089 ± 101 µm$^2$; Figure 6E). TCPS surfaces, which are conventional used in adhesion studies, were used herein as additional control surfaces. The morphology of cells seeded on rhLn-521- site-selective immobilized on SAMs or -coated on Au surfaces is comparable to that observed on rhLn-521-modified TCPS surfaces (Fig. 13). In addition, the average cell spreading area in these conditions is similar/equivalent to that observed in TCPS surfaces (3496 ± 483 µm$^2$). The non-selective immobilization of laminin onto SGA-SAMs, in turn, resulted in a significantly lower cell adhesion ($p = 0.0191$; Fig. 6D and Fig. 14)

and average spreading area (1430 ± 161 $\mu m^2$; *p < 0.0001*; Fig. 6E and Fig. 15) when compared to mPEG rhNtA-SAMs. Moreover, cells with both spread (Fig. 6C) and round (Fig. Fig. 13) morphology were observed. These results suggest that the non-selective nature of the immobilization process partially compromises the exposure of laminin cell binding domains, despite the considerable amount of rhLn-521 bound to SGA-SAMs (342.3 ± 43.6 $ng/cm^2$) (Fig. 6B). As expected, on EG4-SAMs, the few adherent cells (Fig. 6D and Fig. 14) presented mainly a round morphology (Fig. 6C and Fig. 13), as evidenced by the low average cell spreading area (881 ± 70 $\mu m^2$, Fig. 6E). Overall, these results clearly demonstrate that site-specific immobilization of laminin through the use of mono-PEGylated rhNtA better preserved laminin bioactivity in terms of ability to self-polymerize and to mediate hNSC adhesion and spreading, when compared to non-selective covalent immobilization approaches.

[0073] The present disclosure demonstrates the potential of mono-PEGylated rhNtA as an effective natural affinity binding ligand for site-selective immobilization of laminin, allowing the preservation of laminin ability to self-polymerize and mediate cell adhesion and spreading. This affinity binding strategy overcomes several drawbacks associated with the currently available strategies for laminin immobilization. Moreover, this approach is highly versatile, as result of the ability of NtA to bind the different laminin isoforms that comprise the γ1 chain, which represent more than 50% of the isoforms identified to date, with variations in affinity imposed by α and β chains. Therefore, this strategy enables the immobilization of different laminin isoforms, which can be of interest for particular cell types and for application in specific disease contexts. Overall, the proposed strategy is important for a broad range of applications, including 2D coatings for cell culture, functionalization of 3D matrices for cell and/or drug delivery, engineered coatings for neuroelectrodes, among others.

[0074] In an embodiment, the human N-terminal agrin (hNtA) domain gene was synthesized by GenScript (Piscataway, NJ, USA) – Clone ID: B25738, from the protein sequence with the Uniprot reference O00468 (Thr 30 – Pro 157). A gene of 395bp length was produced in pUC57 cloning vector and the conditions for expression in *Escherichia coli (E. coli)* optimized. A high-throughput expression screening was conducted to select, among the several pCoofy expression vectors available [37], the most suitable for the expression of the soluble protein. pCoofy2 expression vector – 6080 bp (gift from Sabine Suppmann – Addgene plasmid # 43981) was the one selected. Both hNtA gene and pCoofy2 expression vector were polymerase chain reaction (PCR) linearized using specific-designed primers and LP1 forward and LP2 reverse primers, respectively (Fig. 16). Following PCR amplification, the hNtA gene was sub-cloned into the pCoofy2 expression vector using a sequence and ligation independent cloning (SLIC) reaction. The efficiency of DNA insert incorporation into the expression vector was confirmed by colony PCR and DNA sequencing (Macrogen).

[0075] In an embodiment, ten micrograms of rhNtA was resolved in a 15% SDS-PAGE gel and transferred onto a nitrocellulose membrane (0.45 µm, GE Healthcare). Unspecific binding was prevented by incubating the membrane with blocking solution (5% (w/v) BSA in Tris-buffered saline – 0.1% Tween® 20 (TBS-T) for 2h at RT. The membrane was then incubated with the primary antibody - rabbit polyclonal agrin antibody (1:1000; Abcam, ab85174), overnight at 4°C. After washing with PBS/0.05% (v/v) Tween® 20, the membrane was incubated with the goat anti-rabbit IgG (H+L) coupled to horseradish peroxidase (HRP) secondary antibody (1:2000; Life Technologies, A16023) for 1h at RT. The membrane was finally washed three times with PBS/0.05% (v/v) Tween® 20 and the blots developed with HRP-reactive chemiluminescence reagents (GE Healthcare).

[0076] In nan embodiment, 96-well microtiter ELISA plates (BD Falcon) were coated with 2-fold serial dilution of rhNtA (0 – 40 µg/mL; overnight, 4°C) and blocked with 1% (w/v) BSA to prevent non-specific adhesion to substrate. The wells were then incubated with the primary antibody - rabbit polyclonal agrin antibody (1:5000; 2h, RT). Goat anti-rabbit IgG (H+L) coupled to HRP secondary antibody (1:2000) was incubated for 1,5 h at RT. The color was developed using 3, 3', 5, 5' tetramethyl benzidine (TMB) substrate (Biolegend), incubated for 30 min at RT. The reaction was stopped using 2 M $H_2SO_4$ and the absorbance measured at 450 nm (BioTek® Synergy™ Mx).

[0077] In an embodiment, hNSCs were fluorescently-labelled with 2 µM of Calcein AM (Molecular Probes, 10 min, 37°C), suspended in StemPro® NSC SFM medium (Life Technologies) and transferred to rhNtA-immobilized msLn-111-adsorbed surfaces at $3\times10^5$ viable cells/$cm^2$. Cells were allowed to adhere for 5 h and before subjecting the cells to centrifugation, initial fluorescence intensity was measured using a microwell plate reader (BioTek® Synergy™ Mx). After overfilling the wells with 10 mM PBS pH 7.4, until a positive meniscus was observed, the plates were sealed with transparent tape, inverted, and spun at 50 RCF for 5 min. Following cell detachment, the medium was changed, and the wells filled with fresh medium for measurement of final fluorescence. For each well, the adherent cell fraction was determined as the ratio of post-spin (final) to pre-spin (initial) fluorescence readings ($\lambda_{ex}$ = 485 nm; $\lambda_{em}$ = 535 nm).

[0078] In an embodiment, protein bands correspondent to native or mono-PEGylated rhNtA were cut from the gel, washed with ultrapure water and de-stained with 50% (v/v) acetonitrile (ACN) in 50 mM ammonium bicarbonate. The samples were then reduced with 50 mM dithiothreitol (20 min, 56°C) and alkylated with 55 mM iodoacetamide, (20 min, RT in the dark). Next, protein *in gel* enzymatic digestion was performed by the addition of 20 ng of trypsin for 3 h at 37°C in the presence of 0.01% surfactant (ProteaseMAX™, Promega). Resulting peptides were extracted from gel plugs with 2.5% trifluoroacetic acid (TFA; 15 min at 1400 rpm), dried under vacuum and resuspended in 0.1% TFA.

[0079] Protein identification was performed by a MALDI-TOF/TOF mass spectrometer (4800 Plus, SCIEX). Protein digests were purified by reversed-phase C18 chromatography (ZipTips®, Millipore) following the manufacturer's instructions and eluted in the MALDI sample plate using the MALDI matrix *alpha-Cyano-4-hydroxycinnamic acid* (CHCA) elution solution at 8 mg/mL in 50% ACN, 0.1% TFA, 6 mM ammonium phosphate. Peptide mass spectra were acquired in positive MS reflector mode in the mass range of *m/z* 700-5000 and internally calibrated with trypsin autolysis peaks. Individual peptides from both native and mono-PEGylated rhNtA were identified by peptide mass fingerprint (PMF) approach using MS-Bridge software version 5.16.1 (ProteinProspector, University of California, San Francisco, CA) and the protein sequence data (Figure S1). The protein search settings were: cysteine carbamidomethylation (constant modification), methionine oxidation (variable modification), up to two missed trypsin cleavages, minimum and maximum digest fragment mass of 500 and 4000 Da, respectively, and a minimum digest fragment length of five amino acids. To estimate the location of the PEG moiety in the conjugate, experimental ion peaks obtained in the peptide map of purified mono-PEGylated rhNtA conjugate were compared to the peptide content of native rhNtA. In addition, an indirect estimation of PEG moiety position in the rhNtA sequence was performed by comparing the mass difference between the conjugated and unmodified PEG molecule.

[0080] In an embodiment, for Quartz crystal microbalance with dissipation monitoring (QCM-D) real-time monitoring of laminin immobilization, sensors were pre-incubated with 10 mM HEPES pH 7.4 for 15 min at a constant flow rate of 0.1 µL/min followed by an additional 15 min incubation, under static conditions, to establish the baseline. Then, 300 µL/sensor of rhLn-521 (20 µg/mL) in 10 mM HEPES pH 7.4 was injected at a constant flow rate of 0.1 µL/min, followed by 1 h incubation in static conditions. After, the system was flushed with 10 mM HEPES pH 7.4 during 30 min at a constant flow rate of 0.1 µL/min. All the experiments were conducted at 25°C. The total amount of immobilized laminin was calculated with application of the Voigt model, which takes into account the viscoelastic contributions of the hydrated layer. The fluid density and viscosity of rhLn-521 solution were established at 1000 kg/m$^3$ and 0.001 kg/m·s, respectively and data from the 5$^{th}$ harmonic was used in the analysis.

[0081] In an embodiment, infrared reflection absorption spectroscopy (IRRAS) spectra were obtained using a Perkin Elmer FTIR spectrophotometer, model 2000, coupled with a VeeMax II Accessory (PIKE) and a liquid-nitrogen-cooled MTC detector. To avoid water vapor adsorption, instrument was purged with dry nitrogen for 5 min before and during each sample analysis. Au substrates were here used as a background. Incident light was p-polarized and spectra were collected using the 80° grazing angle reflection mode. The analysis of each sample was performed through the acquisition of 100 scans with 4 cm$^{-1}$ resolution.

[0082] In an embodiment, mPEG rhNtA- or SGA-SAMs incubated with msLn-111 were fixed with 3.7% (w/v) paraformaldehyde (PFA) for 20 min at RT and washed 3× with 10 mM PBS pH 7.4. Samples were then incubated with blocking buffer (5% (w/v) BSA in PBS for 30 min at RT), followed by incubation with the primary antibody – rabbit polyclonal laminin antibody (1:30; Sigma-Aldrich, L9393), overnight at 4°C. Samples were washed 3× with 10 mM PBS pH 7.4 and incubated with Alexa Fluor® 488 conjugated anti-rabbit secondary antibody (1:300; Life Technologies, A11034), for 1h at RT. Samples were observed under confocal laser scanning microscopy (CLSM, Leica TCS SP5II) using a Plan-Apochromat 63×/1.4NA oil objective and acquired z-sections of 15 µm were processed using the ImageJ/Fiji software. Briefly, the rolling ball algorithm was first applied to maximum intensity projection 3D images, to fix uneven background and followed by the application of a Gaussian blur with $\sigma = 1$ to reduce noise. Aggregates were segmented through an Otsu thresholding method and a morphological filter was then used to unify structures distanced by less than 1 µm. Lastly, all the structures with an area below 10 µm$^2$ were removed/rejected. For each resulting image, measurements were obtained for number of aggregates, aggregates average size (µm$^2$), perimeter (µm) and maximum Feret's diameter (µm). To evaluate differences on the data resultant from both conditions, statistical analysis of the different variables was conducted on MATLAB® software (R2018a) using the non-parametric Mann-Whitney U-test. Moreover, differences resultant from the combination of the different variables measured were determined by application of the Fisher's combined probability test and an overall *p*-value determined. This test is applied under the assumption that variables should be independent from each other. As the count is not

independent from the other variables, for the Fisher's combined probability test, only average size, perimeter and maximum Feret's diameter of aggregates were considered.

[0083] In an embodiment, cell adhesion and morphology – F-actin/DNA staining was performed. hNSC adhesion and morphology was assessed, after 24 h of culture, in samples processed for F-actin/DNA staining. Cells were fixed with 2% (w/v) PFA for 20 min at RT, permeabilized with 0.5% (v/v) Triton X-100 (Sigma-Aldrich) for 10 min at RT and stained with Alexa Fluor® 647 phalloidin (1:50; Biolegend, 424205) for 20 min at RT. The nuclei were counterstained with 0.1 μg/mL of Hoechst 33342 (Life Technologies, H1399) for 20 min at RT. Samples were imaged with the IN Cell Analyzer 2000 imaging system (GE Healthcare) using a Nikon 20×/0.45 NA Plan Fluor objective and CLSM (TCS SP5 II; Leica Mycrosystems) using a Plan-Apochromat 63×/1.4NA oil objective.

[0084] In an embodiment, cell adhesion was also estimated from Hoechst 33342 average fluorescence intensity of samples processed for F-actin/DNA staining. Briefly, samples were transferred to the wells of black 24-well plates (ibidi) and the fluorescence of each surface measured ($\lambda_{ex}$ = 350 nm; $\lambda_{em}$ = 461 nm) using a microwell plate reader (BioTek® Synergy™ Mx). The measurement was performed using the area scan mode with the optics position set to the bottom. The fluorescence intensity (FI) of unseeded SAMs, processed in parallel, was subtracted and the average FI determined.

[0085] Where singular forms of elements or features are used in the specification of the claims, the plural form is also included, and vice versa, if not specifically excluded. For example, the term "a polysaccharide" or "the polysaccharide" also includes the plural forms "polysaccharides" or "the polysaccharides," and vice versa. In the claims articles such as "a," "an," and "the" may mean one or more than one unless indicated to the contrary or otherwise evident from the context. Claims or descriptions that include "or" between one or more members of a group are considered satisfied if one, more than one, or all of the group members are present in, employed in, or otherwise relevant to a given product or process unless indicated to the contrary or otherwise evident from the context. The invention includes embodiments in which exactly one member of the group is present in, employed in, or otherwise relevant to a given product or process. The invention also includes embodiments in which more than one, or all of the group members are present in, employed in, or otherwise relevant to a given product or process.

[0086] Furthermore, it is to be understood that the invention encompasses all variations, combinations, and permutations in which one or more limitations, elements, clauses, descriptive terms, etc., from one or more of the claims or from relevant portions of the description is introduced into another claim. For example, any claim that is dependent on another claim can be modified to include one or more limitations found in any other claim that is dependent on the same base claim.

[0087] Furthermore, where the claims recite a composition, it is to be understood that methods of using the composition for any of the purposes disclosed herein are included, and methods of making the composition according to any of the methods of making disclosed herein or other methods known in the art are included, unless otherwise indicated or unless it would be evident to one of ordinary skill in the art that a contradiction or inconsistency would arise.

[0088] Where ranges are given, endpoints are included. Furthermore, it is to be understood that unless otherwise indicated or otherwise evident from the context and/or the understanding of one of ordinary skill in the art, values that are expressed as ranges can assume any specific value within the stated ranges in different embodiments of the invention, to the tenth of the unit of the lower limit of the range, unless the context clearly dictates otherwise. It is also to be understood that unless otherwise indicated or otherwise evident from the context and/or the understanding of one of ordinary skill in the art, values expressed as ranges can assume any subrange within the given range, wherein the endpoints of the subrange are expressed to the same degree of accuracy as the tenth of the unit of the lower limit of the range.

[0089] The disclosure should not be seen in any way restricted to the embodiments described and a person with ordinary skill in the art will foresee many possibilities to modifications thereof.

[0090] The above described embodiments are combinable.

[0091] The following claims further set out particular embodiments of the disclosure.

REFERENCES

1. Aumailley, M., The laminin family. Cell Adh Migr, 2013. 7(1): p. 48-55
2. Taylor, A.C., et al., Surface functionalisation of nanodiamonds for human neural stem cell adhesion and proliferation. Sci Rep, 2017. 7(1): p. 7307.

3. Stabenfeldt, S.E., A.J. Garcia, and M.C. LaPlaca, Thermoreversible lamininfunctionalized hydrogel for neural tissue engineering. J Biomed Mater Res A, 2006. 77(4): p. 718-25.

4. Lee, J.P., et al., N-terminal specific conjugation of extracellular matrix proteins to 2-pyridinecarboxaldehyde functionalized polyacrylamide hydrogels. Biomaterials, 2016. 102: p. 268-76

5. Mascarenhas, J.B., et al., Mapping of the laminin-binding site of the N-terminal agrin domain (NtA). EMBO J, 2003. 22(3): p. 529-36.

6. Denzer, A.J., et al., Electron microscopic structure of agrin and mapping of its binding site in laminin-1. EMBO J, 1998. 17(2): p. 335-43.

## C L A I M S

1. A composition for substrate functionalization comprising:

   a poly(ethylene glycol) - PEG - for binding to the substrate;
   an agrin domain comprising a sequence at least 95% identical to SEQ. ID NO: 1 bound to said PEG;
   a laminin able for binding to a bioactive agent;
   wherein the laminin is bound to the agrin domain.

2. The composition according to any of the previous claim wherein the agrin domain comprises a sequence at least 96% identical to SEQ. ID NO: 1, preferably at least 97% identical to SEQ. ID NO: 1, at least 98% identical to SEQ. ID NO: 1, at least 99% identical to SEQ. ID NO: 1.

3. The composition according to any of the previous claim wherein the agrin domain comprises a sequence identical to SEQ. ID NO: 1.

4. The composition according to any of the previous claims wherein the agrin domain is conjugated at its N-terminal with an end-group functionalized poly(ethylene glycol).

5. The composition according to any of the previous claims wherein the bioactive agent is selected from a list consisting of: a biomolecule, an active ingredient, a growth factor, extracellular vesicle, a hormone, a cell, or mixtures thereof.

6. The composition according to any of the previous claims wherein the biomolecule is another laminin, a different protein, a peptide, a drug, a polysaccharide, or mixtures thereof.

7. The composition according to any of the previous claims wherein the cell is selected from: osteoblast, osteoclast, osteocyte, pericyte, endothelial cells, endothelial progenitor cells, hematopoietic progenitor cell, hematopoietic stem cell, neural progenitor cell, neural stem cell, neural cell, oligodendrocyte progenitor cell, oligodendrocytes, ependymal cells, mesenchymal stromal/stem cell, induced pluripotent stem cell, embryonic stem cell, perivascular stem cells, amniotic fluid stem cell, amniotic membrane stem cell, umbilical cord stem cell, genetically engineered cell, or mixtures thereof.

8. The composition according to any of the previous claims wherein the poly(ethylene glycol) size varies between 2 and 40 KDa; preferably 3-20 KDa, more preferably 3.5-10 KDa .
9. The composition according to any of the previous claims for use in veterinary or human medicine.
10. The composition according to any of the previous claims, for use in the treatment of diseases that involve the regeneration or treatment of tissues, or for use in the prevention of tissue degeneration.
11. The composition according to any of the previous claims, wherein the substrate is a naturally-derived or purely synthetic polymer, a synthetically-derived biopolymer, a metal, or combinations thereof.
12. A hydrogel comprising the composition described in any of the previous claims.
13. The hydrogel of the previous claim wherein the hydrogel is selected from the following list: poly(ethylene glycol), poly(vinyl alcohol), chitosan, collagen, alginate, dextran, fibrin, hyaluronic acid, silk fibroin, cellulose, synthetically-derived biopolymers, or mixtures thereof.
14. A substrate coating comprising the composition described in any of the previous claims.
15. A coated article comprising the coating of the previous claim.
16. The coated article of the previous claim wherein the article is an electrode.
17. A kit for screening therapeutic drugs comprising the composition described in any of the previous claims.

**A B S T R A C T**

**LAMININ IMMOBILIZATION, METHODS AND USES THEREOF**

Laminin immobilization into diverse biological and synthetic matrices has been explored to replicate the microenvironment of stem cell niches and gain insight into the role of extracellular matrix (ECM) on stem cell behaviour. However, the site-specific immobilization of this heterotrimeric glycoprotein and, consequently, control over its orientation and bioactivity has been a challenge that has limited many of the explored strategies to date. It was established an affinity-based approach that takes advantage of the native high affinity interaction between laminin and the human N-terminal agrin (hNtA) domain.

D R A W I N G S

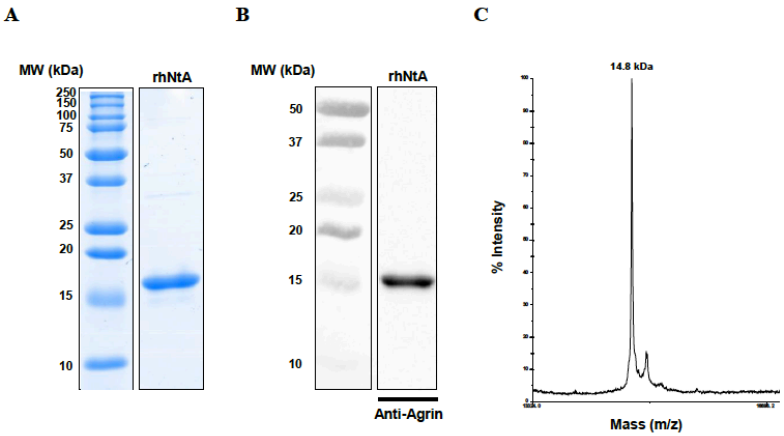


Fig. 1

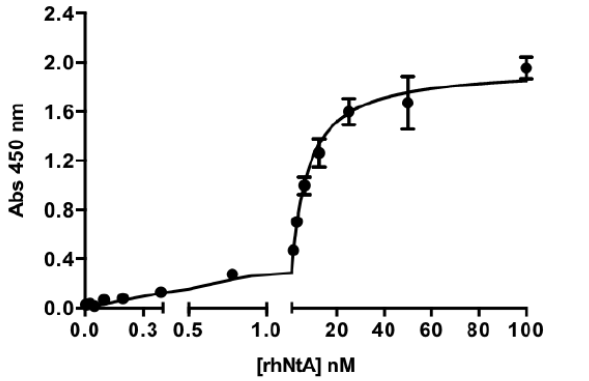


Fig. 2

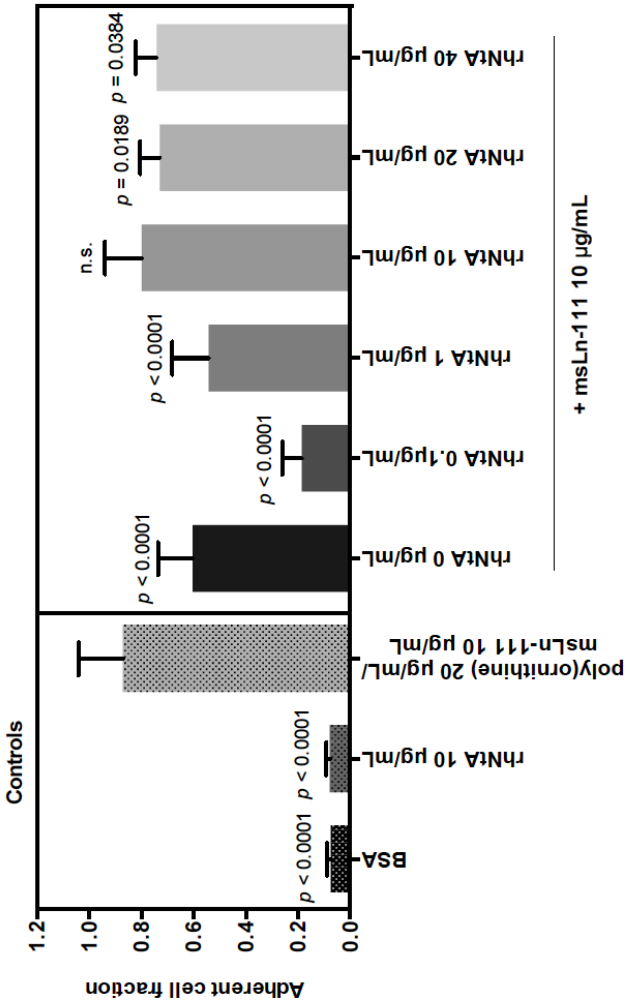


Fig. 3

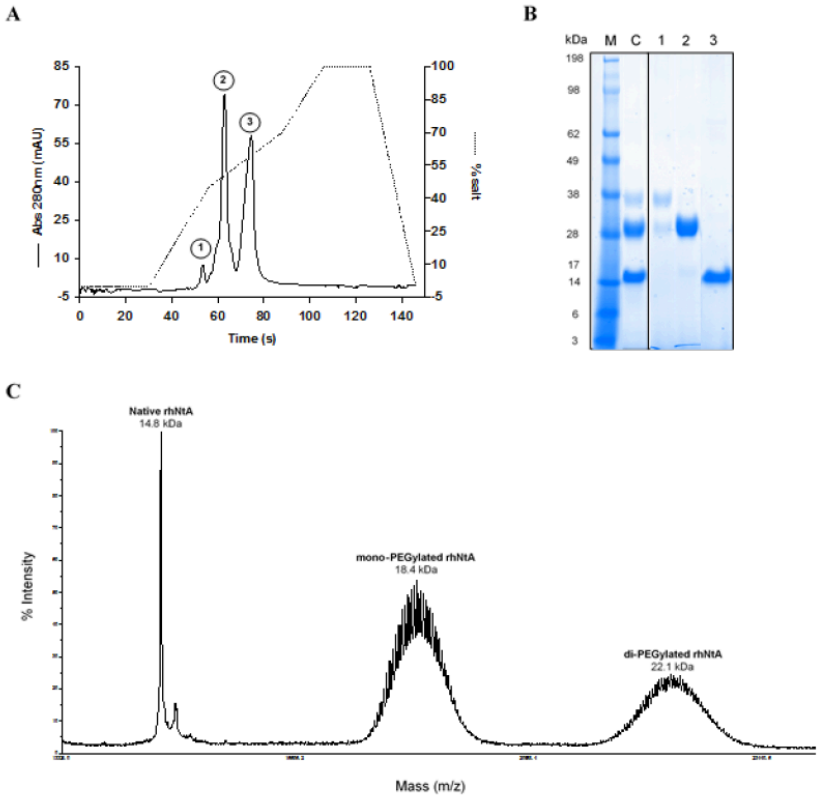
A
B
C
Abs 280nm (mAU)
% salt
Time (s)
kDa
M
C
1
2
3
Native rhNtA
14.8 kDa
mono-PEGylated rhNtA
18.4 kDa
di-PEGylated rhNtA
22.1 kDa
% Intensity
Mass (m/z)

Fig. 4

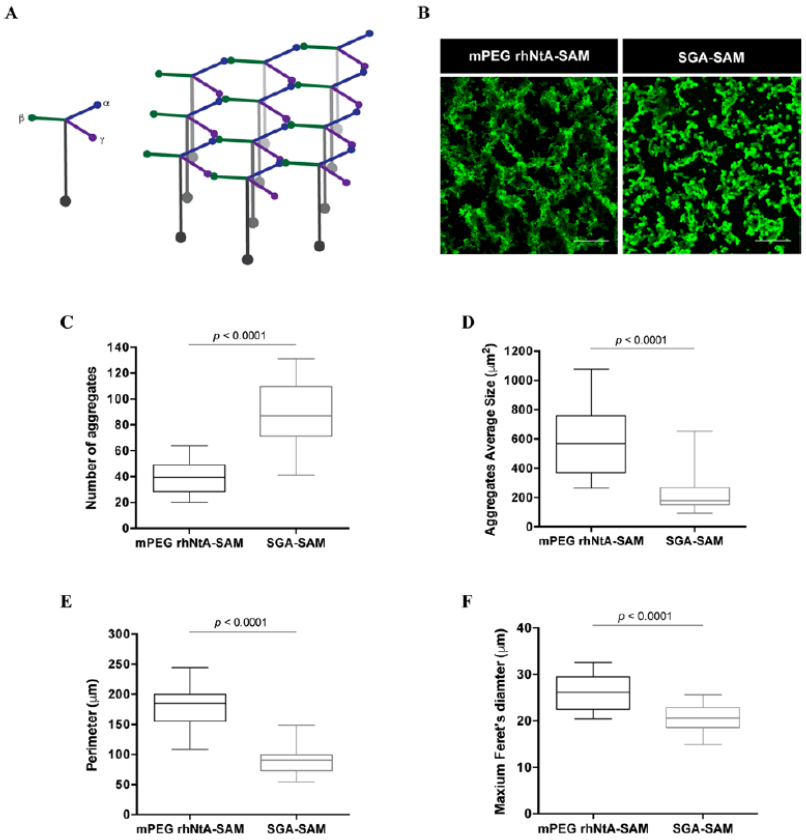
A
B
mPEG rhNtA-SAM
SGA-SAM
C
D
E
F
p < 0.0001
Number of aggregates
Aggregates Average Size (μm²)
Perimeter (μm)
Maxium Feret's diamter (μm)
mPEG rhNtA-SAM
SGA-SAM

Fig. 5

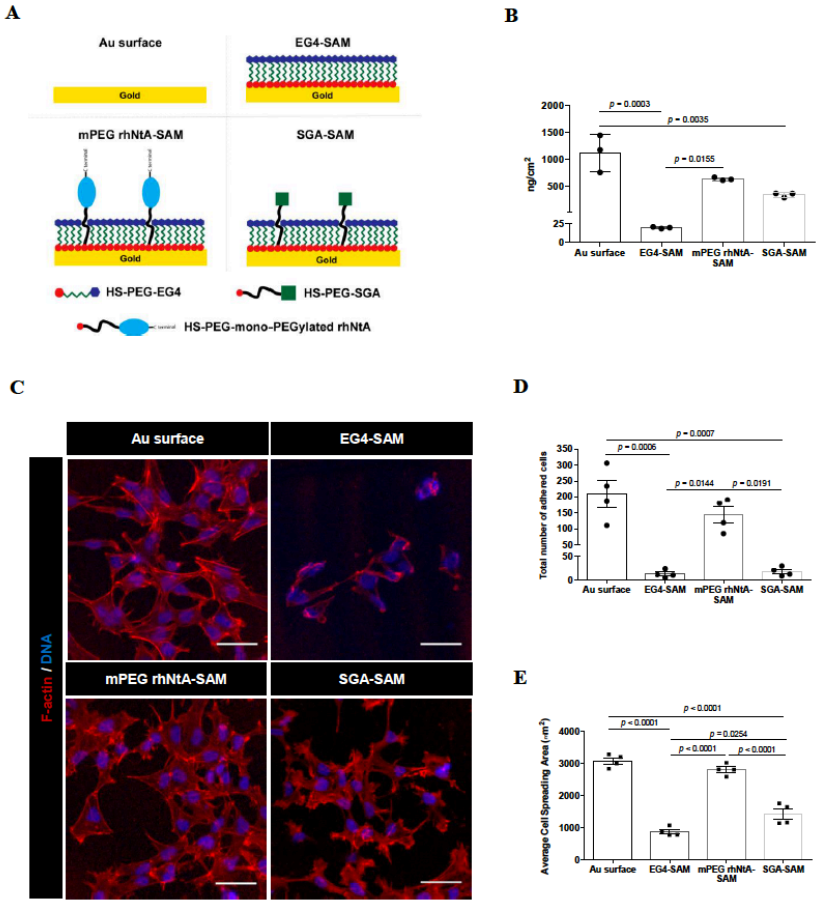


Fig. 6

GPTCPERALERREEEANVVLTGTVEEILNVDPVQHTYSCKVRVWRYLKGKDLVARESLLDGGNKVVISGFGD
PLICDNQVSTGDTRIFFVNPAPPYLWPAHKNELMLNSSLMRITLRNLEEVEFCVEDKP

Fig. 7

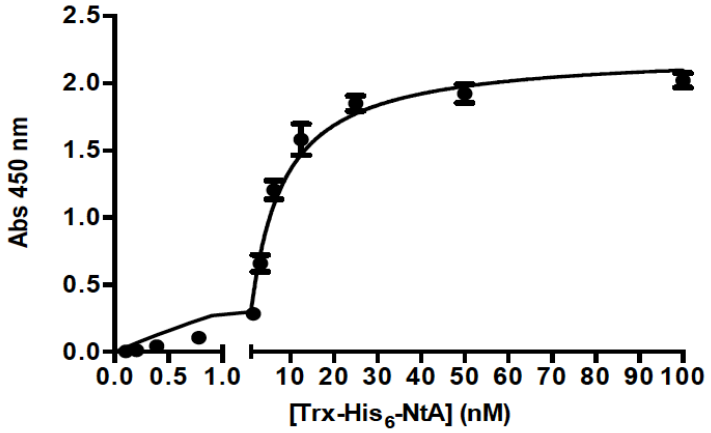


Fig. 8

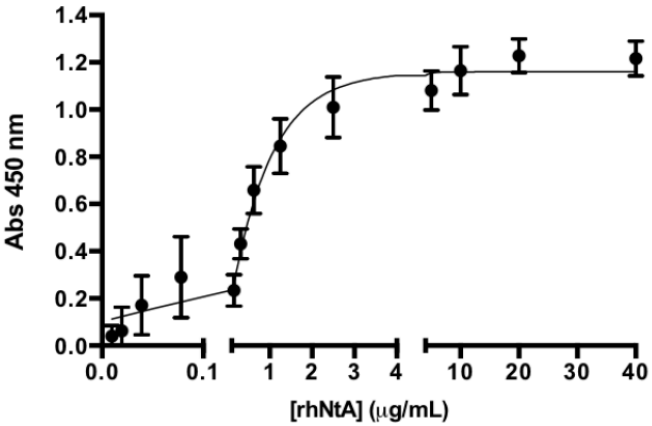
Abs 450 nm
1.4
1.2
1.0
0.8
0.6
0.4
0.2
0.0
0.0
0.1
1
2
3
4
10
20
30
40
[rhNtA] (μg/mL)

Fig. 9

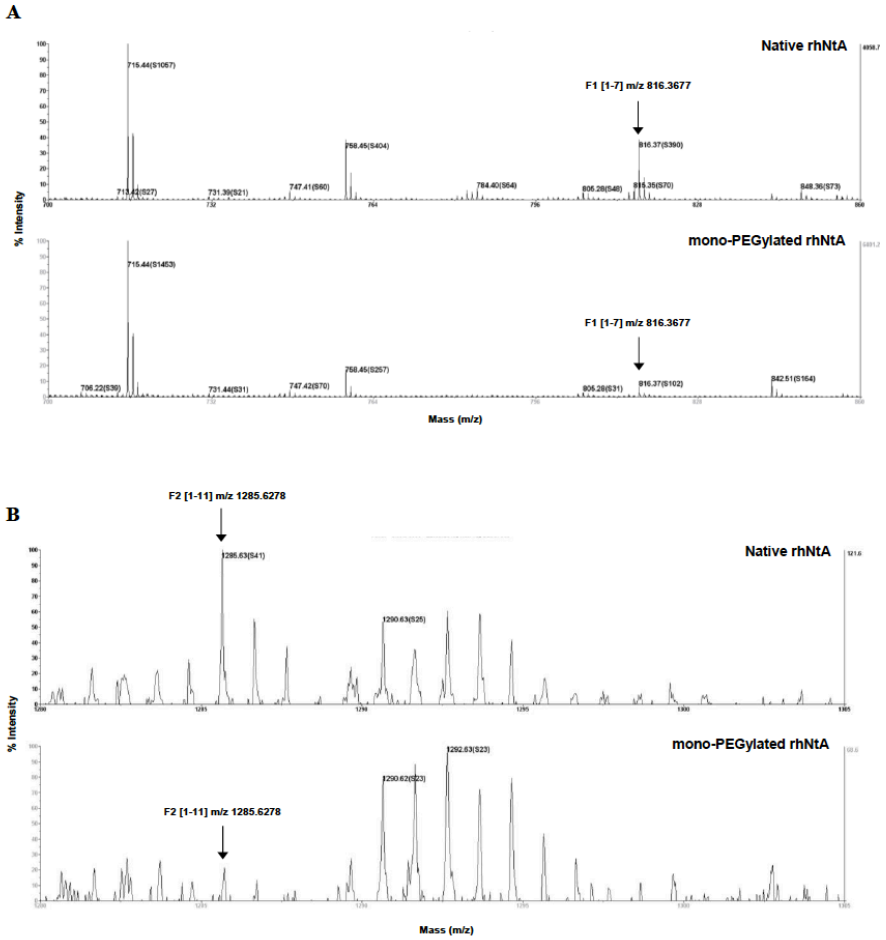
A
Native rhNtA
F1 [1-7] m/z 816.3677
% Intensity
mono-PEGylated rhNtA
F1 [1-7] m/z 816.3677
Mass (m/z)
B
F2 [1-11] m/z 1285.6278
Native rhNtA
% Intensity
mono-PEGylated rhNtA
F2 [1-11] m/z 1285.6278
Mass (m/z)

Fig. 10

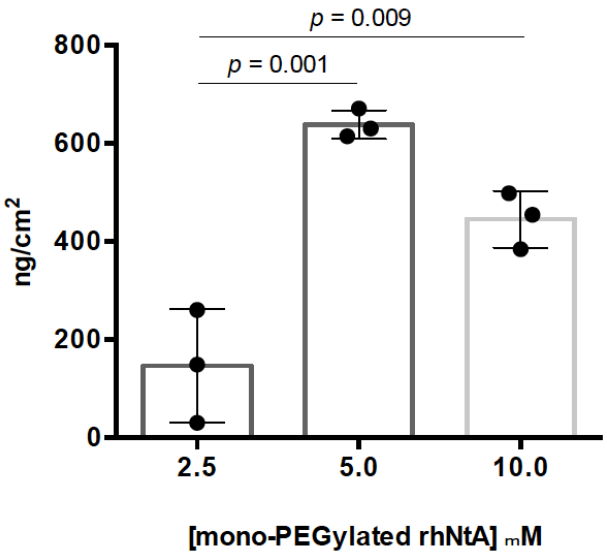
p = 0.009
p = 0.001
800
600
400
200
0
ng/cm2
2.5
5.0
10.0
[mono-PEGylated rhNtA] mM

Fig. 11

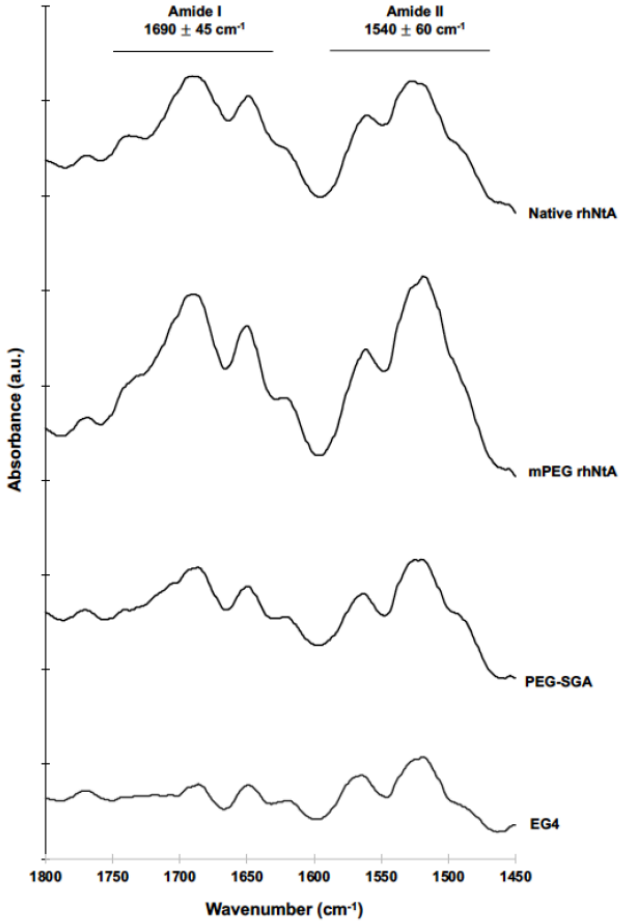
Amide I
1690 ± 45 cm-1
Amide II
1540 ± 60 cm-1
Native rhNtA
mPEG rhNtA
PEG-SGA
EG4
Absorbance (a.u.)
1800
1750
1700
1650
1600
1550
1500
1450
Wavenumber (cm-1)

Fig. 12

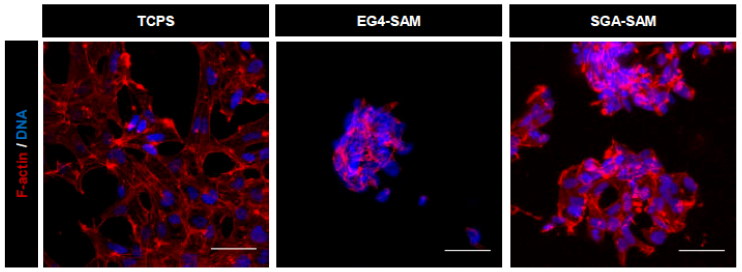


Fig. 13

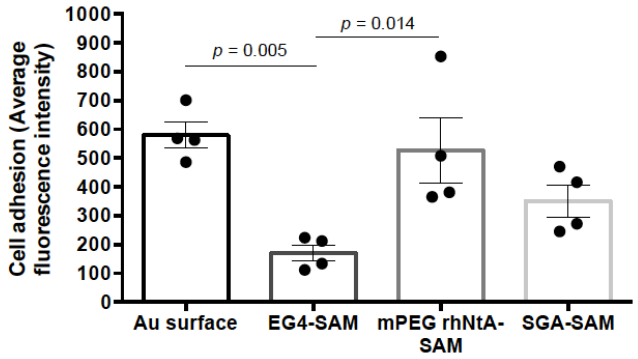


Fig. 14

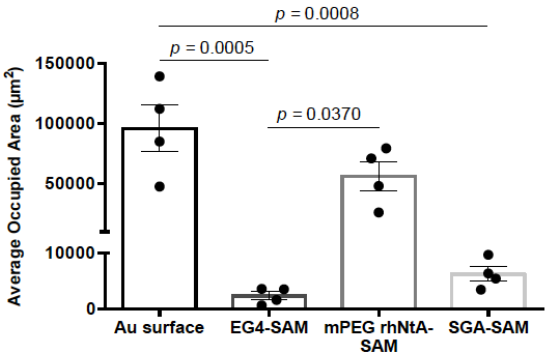


Fig. 15

| Primer | Sequence 5′ – 3′ |
|---|---|
| **3C - LP1 forward vector primer** [a] | 5' AAGTTCTGTTCCAGGGGCCC 3′ |
| **ccdB - LP2 reverse vector primer** [a] | 5' CCCCAGAACATCAGGTTAATGGCG 3′ |
| **hNtA forward primer (3C)** [b] | 5' AAGTTCTGTTCCAGGGGCCCGGCACCTGTCCGGAACGCGC 3′ |
| **hNtA reverse primer (ccdB)** [b] | 5′CCCCAGAACATCAGGTTAATGGCGTTACGGTTTATCTTCAACGCAAAATTC 3′ |

[a] Primers for vector amplification were obtained from [37].

[b] Primers used for hNtA gene amplification were specifically designed to have gene specific sequences plus 15 to 25 bp extensions complementary to LP1 and LP2 vector primers.

**Fig. 16**

| Sample | Fragments | Sequence | Molecular Mass (Da) | |
|---|---|---|---|---|
| | | | Calculated[a] | Experimental[b] |
| rhNtA mono-PEG rhNtA | **1-7** | **GPTCPER** | **816.3668** | **816.3677**<br>**816.3736** |
| rhNtA mono-PEG rhNtA | **1-11** | **GPTCPERALER** | **1285.6317** | **1285.6278**<br>***c*** |
| rhNtA mono-PEG rhNtA | 8-40 | ALERREEEANVVLTGTVEEI LNVDPVQHTYSCK | 3741.8752 | 3798.9145<br>3798.9299 |
| rhNtA mono-PEG rhNtA | 12-40 | REEEANVVLTGTVEEILNVD PVQHTYSCK | 3329.6317 | 3329.6360<br>3329.6489 |
| rhNtA mono-PEG rhNtA | 13-40 | EEEANVVLTGTVEEILNVDP VQHTYSCK | 3173.5306 | 3173.5747<br>3173.5818 |
| rhNtA mono-PEG rhNtA | 41-45 | VRVWR | 715.4362 | 715.4423<br>715.4426 |
| rhNtA mono-PEG rhNtA | 46-55 | YLKGKDLVAR | 1162.6930 | *c*<br>1162.6930 |
| rhNtA mono-PEG rhNtA | 49-55 | GKDLVAR | 758.4519 | 758.4529<br>758.4524 |
| rhNtA mono-PEG rhNtA | 56-64 | ESLLDGGNK | 932.4745 | *c*<br>932.4745 |
| rhNtA mono-PEG rhNtA | 56-86 | ESLLDGGNKVVISGFGDPLI CDNQVSTGDTR | 3263.5848 | 3263.5940<br>3263.6089 |
| rhNtA mono-PEG rhNtA | 65-86 | VVISGFGDPLICDNQVSTGD TR | 2350.1343 | 2350.1294<br>2350.1355 |
| rhNtA mono-PEG rhNtA | 87-102 | IFFVNPAPPYLWPAHK | 1897.0159 | 1897.0105<br>1897.0167 |
| rhNtA | 87-113 | | 3217.6325 | 3217.6418 |

| | | | | |
|---|---|---|---|---|
| mono-PEG rhNtA | | IFFVNPAPPILWPAHKNEL MLNSSLMR | | 3217.6716 |
| rhNtA | | | 1339.6344 | 1339.6328 |
| mono-PEG rhNtA | 103-113 | NELMLNSSLMR | | 1339.6374 |
| rhNtA | | | 2091.0426 | 2091.0317 |
| mono-PEG rhNtA | 114-130 | ITLRNLEEVEFCVEDKP | | 2091.0422 |
| rhNtA | | | 1607.7257 | 1607.7244 |
| mono-PEG rhNtA | 118-130 | NLEEVEFCVEDKP | | 1607.7286 |

[a] Theoretical molecular mass of the fragments calculated in *web.expasy.org/peptide_mass*. [b] Experimental molecular masses determined by MALDI-TOF MS. [c] Fragment not found.

**Fig. 17**